University of Sussex

Augmenting NNLL resummations with event-generators and multi-jets

Augmenting ***ARES***

Luke Arpino

Submitted for the degree of Doctor of Philosophy

University of Sussex

September 2019

Declaration

The contents of Chapters 4 and 5 are based on work done in collaboration with Andrea Banfi and Basem Kamal El-Menoufi, resulting in the publication of ref. [1]. The contents of Chapter 6 are based on work done in collaboration with Andrea Banfi, Nikolas Kauer and Sebastian Jäger, resulting in the publication of ref. [2].

I hereby declare that this thesis has not been and will not be submitted in whole or in part to another University for the award of any other degree.

Signature:

Luke Arpino

UNIVERSITY OF SUSSEX

Luke Arpino, Doctor of Philosophy

Augmenting NNLL resummations with event-generators and multi-jets

Augmenting ARES

Summary

This work extends the ARES framework for NNLL resummations: automating calculations via the use of fixed-order event generators, and, extending the ARES method to multi-jet observables. We extend the ARES method to multi-jet observables in electron-positron annihilation, and we use this extension to perform the first NNLL resummation of the D-parameter, a three-jet event-shape.We introduce a new method to interface resummations to fixed-order event generators. Utilising this new method we interface jet-veto resummations with the fixed-order code MCFM. The result is a new code capable of resumming jet-veto effects in all processes that proceed via a colour-singlet, and completely differential in leptonic final states. We use the code to resum jet-veto effects in WW final states at the Large Hadron Collider, and place constraints on the unique dimension-six operator coupling gluons to the Higgs field.

Acknowledgements

First, I would like to thank my supervisor Andrea Banfi for all of his support and guidance, without which this thesis would not have been possible. To all the members of the Sussex TPP group, thank you for making my time at Sussex enjoyable. Thank you to all of my friends, in Brighton and beyond, for your help along the way.

And finally, but most importantly, I am very grateful to my family for their constant support.

Contents

List of Tables

List of Figures

Chapter 1

Introduction

The story of elementary particle physics is one of remarkable success. Our knowledge of elementary particles has grown from the discovery of the first subatomic particle (the electron) in 1897, to a theory that is capable of explaining the electromagnetic force, the strong nuclear force and the weak nuclear force—three of the four fundamental forces—to incredible experimental precision. To describe the interactions between elementary particles at such high levels of precision we must use the language of quantum field theory (QFT), a unification of quantum mechanics and special relativity. In the language of QFT, elementary particles are described in terms of quantum fields, and their dynamics via the interaction of these quantum fields. QFTs are the basis for theories that attempt to describe interactions at the smallest possible length scales.

Our best description of elementary particles is encoded in the Standard Model (SM) of particle physics. The SM is a renormalisable gauge QFT, that is invariant under the action of the local product group $SU(3)_c \times SU(2)_L \times U(1)_Y$. The gauge groups in the SM encode different forces, the $SU(3)_c$ gauge group describes the strong force, and the product group $SU(2)_L \times U(1)_Y$ described the electroweak force. The $SU(2)_L \times U(1)_Y$ symmetry is spontaneously broken according to the Higgs mechanism, giving rise to the electromagnetic and weak nuclear forces. In this thesis we will only concern ourselves with the $SU(N_c)$ sector, the dynamics of which are described by the theory of *quantum chromodynamics* (QCD).

The phenomena of QCD are rich and varied across many different energy scales. At low energies QCD is responsible for the hadrons (bound states of quarks and gluons) and the existence of the atomic nucleus. At high energies QCD is the dominant mechanism of interactions at colliders. In this thesis we will only consider QCD at high energies. At high energies QCD behaves like a free theory and is will described by *perturbation theory*,

where the strong coupling constant acts as a small parameter. The *fixed-order*[1] perturbative treatment of QCD is remarkably successful, and, broadly, agrees very well with experimental data. However in certain kinematic regimes these predictions can become unreliable. Problems arise when particle dynamics occur at multiple scales. For reliable predictions it is thus essential that we take into account these multi-scale dynamics. This is usually done by performing an *all-orders*[2] resummation.

The main subject of this thesis is the resummation of final-state observables in QCD. Considering only a particular (although still rather generic) class of hadronic observable, a general method for their resummation can be devised. At next-to-leading-logarithmic (NLL) accuracy this exists in the form of `CAESAR` [3] a framework and a computer program. And at next-to-next-to-leading-logarithmic (NNLL) accuracy this exists in the form of `ARES` [4], also a framework and a computer program. Within the scope of `CAESAR` and `ARES` are many observables that can be resummed, for example most event shape variables including: Thrust, the C-parameter and the D-parameter.

There is always more phenomenology that is of considerable interest that we can study, one such case is that of three-jet events. There is a wealth of three-jet data from the Large Electron-Positron (LEP) collider, for which more accurate predictions are necessary for good agreement between theory and experiment. Another such case is the need for differential distributions. Such distributions provide far more information than simple rate calculations, and are necessary for accurate measurements of certain parameters, such as the coupling of the Higgs field. In this thesis we extend the `ARES` framework to cover these cases, paving the way for new phenomenological studies.

In chapter 2 we review the kinematic details necessary for the calculation of cross sections in scattering experiments. Along the way we will introduce some of the notation that will be used throughout the thesis, remaining as general as possible in our considerations. We will then introduce QCD, concerning ourselves only with perturbative QCD (pQCD). We cannot possibly give a complete review of pQCD, so we will review some of the important aspects of pQCD in the infrared regime: the class of observables that can be reliably calculated in pQCD and the factorisation of QCD matrix elements in the soft and/or collinear limit. In chapter 3 we introduce jets, and, the intimately related, jet observables. Such observables can be used to probe every aspects of QCD and the SM of particle physics.

In chapter 4 we come to the original work that I have carried out. We extend the `ARES`

[1] By fixed-order we mean that we consider only a fixed number of terms in the perturbative series.

[2] By all-orders we mean that we consider all orders in the strong coupling constant.

method of resummation to three-jet event shapes in e^+e^- annihilation at NNLL accuracy. Careful consideration of all possible contributions is necessary, and we find many new and interesting features not present in the two-jet case. Following this in chapter 5 we apply the new `ARES` method to resum the D-parameter in near-to-planar three-jet events at NNLL accuracy, the first such resummation at this accuracy.

Finally, in chapter 6 again we extend the `ARES` method, so as to produce predictions that are differential in the kinematics of the final-state. We focus on the production of a colour-singlet in the presence of a jet veto. We then examine the phenomenology of WW production in the presence of a jet veto, and use the differential production cross section to put constraints on a simple Beyond the Standard Model (BSM) operator.

Chapter 2

Quantum Chromodynamics

Before we begin our incursion into the realms of Quantum Field Theory (QFT) and Quantum Chromodynamics (QCD), we will first briefly review how to calculate measurable quantities in QFT.

2.1 The cross section

The experiments that probe the behaviour of elementary particles, especially in the relativistic regime are scattering experiments. In scattering experiments we either collide two beams of particles together or we smash a single beam of particles into a fixed target. We measure the resulting final state particles to understand the dynamics of the underlying collision. The likelihood of a particular final state can be expressed in terms of the *cross section*, a quantity that is intrinsic to the colliding particles and independent of the experimental setup. It is the cross section that allows us to compare measurements taken from different experimental configurations to one another.

Considering two bunches of particles of type a and b, with length ℓ_a, ℓ_b, density ρ_a, ρ_b and a cross-sectional area A that is common to the two bunches, we can define the cross section as

$$\sigma \equiv \frac{\text{Number of scattering events}}{\rho_a \, \ell_a \, \rho_b \, \ell_b \, A} \,. \tag{2.1}$$

We are usually interested in more than just counting the number of particles, we would like to measure the momenta of the final state particles. We can still use the cross section definition of Eq. (2.1) to do this, only now by specifying the exact momenta the cross section is infinitesimal. The solution to this is to define a *differential cross section* $\mathrm{d}\sigma/(\mathrm{d}^3 p_1 \ldots \mathrm{d}^3 p_m)$, which is infinitesimal in the momenta of the final state particles. Integrating the differential cross section over the momenta of the final state particles we

recover the total cross section.

Usually as physicists we are interested only in specific combinations of momenta that define an *observable*, a quantity with a specific kinematic dependence on the final state momenta. The differential cross section for a completely general observable (or set of observables) is given by the following expression

$$\mathrm{d}\sigma = \frac{1}{F}\sum_{\{m\}}\frac{1}{S_{\{m\}}}\,\mathrm{d}\Phi_m(p_1,\ldots,p_m)\,|\mathcal{M}_m(p_a,p_b\to p_1,\ldots,p_m)|^2 F_J^{(m)}(p_1,\ldots,p_m)\,, \quad (2.2)$$

where working from left to right the new terms in Eq. (2.2) are

- The flux factor F, which takes care of the correct normalisation with respect to the incoming particles in accordance with Eq. (2.1).
- The sum $\sum_{\{m\}}$, which denotes the sum over all the configurations with m particles in the final state.
- The Bose symmetry factor $S_{\{m\}}$, which ensures that contributions due to indistinguishable final states are not double counted.
- The phase space for m final state particles $\mathrm{d}\Phi_m$.
- The squared matrix element for a $2\to m$ scattering $|\mathcal{M}_m(p_a,p_b\to p_1,\ldots,p_n)|^2$. The squared matrix element contains all of the dynamics of the theory, and encodes the transition probability for any given scattering process.
- A phase space weight function $F_J^{(m)}$, called a *jet function*, which defines the measurement. Inside the jet function we can include phase space cuts (encoded as Θ-functions of the final state momenta), or observable definitions (encoded as δ-functions). The jet function can be made up of many different terms encoding simultaneous distributions in many observables taken over complicated phase space cuts. The simplest example of a jet function is $F_J^{(m)}=1$, in which case Eq. (2.2) reduces to the total cross section. There are some technical limitations on the kinds of observables that can be included in the jet function, and we will come to these restrictions later.

To calculate cross sections we need to understand *both* the kinematics and dynamics of the scattering process. The dynamics are encoded in the square matrix elements of Eq. (2.2), and to calculate these we must specify a QFT. We will dedicate the rest of this chapter to a review of QCD, taking our time to walk through the elements that are most important for the resummations that we will perform in Chapters. 4, 5 and 6.

2.2 QCD: The theory of the strong force

Before we can write down the QCD Lagrangian density we must specify the field content of the theory. The dynamical degrees of freedom in QCD are those of quarks and gluons, these can be written in the language of fields as

- Quark fields, which are spin-$\frac{1}{2}$ Dirac fields $\Psi^{\alpha}_{a,f}$ with the indices α, a and f corresponding respectively to a Dirac *spinor* index, a *colour* index in the fundamental representation of the gauge group and a *flavour* index. Generically we will consider a theory with n_F different quark flavours—in the SM there are six different flavours of quarks.

- Gluon fields, which are spin-1 bosonic fields A^{A}_{μ} with the indices μ and A corresponding respectively to a *Lorentz* vector index and a *colour* index in the adjoint representation of the gauge group.

In defining the degrees of freedom in terms of fields we have mentioned a gauge symmetry without pinning down a specific group. The dynamics of the strong interaction are in fact governed by the non-Abelian gauge group $SU(N_c)$, where in the SM $N_c = 3$ [5–7]. We report the details of the $SU(N_c)$ Lie algebra in appendix A.

Now that we understand the field content and the gauge group structure of the theory, we can write the standard Lagrangian density for a generic Yang-Mills theory [8] with minimally coupled matter fields

$$\mathcal{L}_{\text{QCD}} = -\frac{1}{4} G^{A}_{\mu\nu} G^{A,\mu\nu} + \sum_{f=1}^{n_F} \bar{\Psi}_a (i\not{D} - m)_{ab} \Psi_b \,, \tag{2.3}$$

where on the gluon side we have $G^{A}_{\mu\nu}$, which represents the field strength tensor, defined as

$$G^{A}_{\mu\nu} = \partial_\mu A^{A}_{\nu} - \partial_\nu A^{A}_{\mu} - g_s f^{ABC} A^{A}_{\mu} A^{B}_{\nu} \,, \tag{2.4}$$

where g_s is the strong coupling constant. On the quark side we have the four-component Dirac spinor Ψ[1]. Finally we have introduced the Feynman slashed shorthand to denote contraction with the γ-matrices and the covariant derivative, which is defined as

$$(D_\mu)_{ab} = \partial_\mu \delta_{ab} + i g_s \left(A^{A}_{\mu} t^{A} \right)_{ab} \,. \tag{2.5}$$

[1] We have omitted the explicit flavour index f, because it is always possible to diagonalise the mass matrix of the quarks in flavour space [9, 10]

The QCD Lagrangian Eq. (2.3) is invariant under the local gauge transformation

$$\begin{aligned}\Psi(x) &\to \Psi'(x) = \mathbf{U}(x)\Psi(x) \\ \mathbf{A}_\mu(x) &\to \mathbf{A}'_\mu(x) = \mathbf{U}(x)\mathbf{A}_\mu(x)\mathbf{U}^{-1}(x) + \frac{i}{g_s}(\partial_\mu \mathbf{U}(x))\mathbf{U}^{-1}(x)\,,\end{aligned} \tag{2.6}$$

where $\mathbf{U}(x) = \exp\left(i\theta^A(x)t^A\right)$ and $\mathbf{A}_\mu = A^A_\mu t^A$.

The Lagrangian Eq. (2.3) allows us to specify a generating functional for the theory in terms of the path integral

$$\begin{aligned}\mathcal{Z}_{\rm QCD}[J,\eta,\bar\eta] = \int \mathcal{D}\mathbf{A}_\mu\,\mathcal{D}\Psi\,\mathcal{D}\bar\Psi \times \\ \times \exp\left[i\int \mathrm{d}^4x\left(\mathcal{L}_{\rm QCD} + \mathbf{A}_\mu\mathbf{J}^\mu + \bar\Psi\eta + \bar\eta\Psi\right)\right]\,,\end{aligned} \tag{2.7}$$

from which we can calculate Green's functions of the theory[2]:

$$\langle\Omega|\,T\left\{\mathscr{F}[\mathbf{A}_\mu,\Psi,\bar\Psi]\right\}|\Omega\rangle = \mathcal{N}\int \mathcal{D}\mathbf{A}_\mu\,\mathcal{D}\Psi\,\mathcal{D}\bar\Psi\,\mathscr{F}[\mathbf{A}_\mu,\Psi,\bar\Psi]\,e^{iS_{\rm QCD}[\mathbf{A}_\mu,\Psi,\bar\Psi]}\,, \tag{2.8}$$

where $S_{\rm QCD}$ is the QCD action

$$S_{\rm QCD}[\mathbf{A}_\mu,\Psi,\bar\Psi] \equiv \int \mathrm{d}^4x\,\mathcal{L}_{\rm QCD}[\mathbf{A}_\mu,\Psi,\bar\Psi]\,, \tag{2.9}$$

$\mathscr{F}[\mathbf{A}_\mu,\Psi,\bar\Psi]$ is a functional of the fields, T denotes the time-ordering of the quantum fields, $|\Omega\rangle$ is the vacuum state of the full interacting theory and $\mathcal{N}$ is a normalisation factor, fixed by demanding that $\langle\Omega|\Omega\rangle = 1$. From the Green's functions of Eq. (2.8) we can compute the S-matrix elements, and, subsequently other measurable quantities by making use of the Lehmann-Symanzik-Zimmermann (LSZ) reduction formula [11, 12], which relates S-matrix elements to scattering amplitudes.

By construction, the action Eq. (2.9) is invariant under the local gauge transformation Eq. (2.6), this poses a problem to the path integral formulation of the Green's functions as defined by Eq. (2.8), in the path integral we sum over physically equivalent field configurations. This redundancy can be removed by the addition of a suitable gauge fixing term [13] to the Lagrangian Eq. (2.3). A particularly convenient choice for calculations is the family of *covariant gauges* defined by

$$\mathcal{L}_{\rm GF} = -\frac{1}{2\xi}\left(\partial^\mu A^A_\mu\right)^2\,, \tag{2.10}$$

this gauge fixing term must be accompanied by a ghost Lagrangian to preserve unitarity[3]

$$\mathcal{L}_{\rm Ghost} = \left(\partial^\mu\chi^A\right)^\dagger\left(D^{AB}_\mu\chi^B\right)\,, \tag{2.11}$$

[2] To be pedantic Green's functions are vacuum expectation values of time-ordered products of fields.

[3] The Ghost fields serve as negative degrees of freedom that cancel the effect of unphysical gluon polarisations that emerge from the gauge fixing procedure.

where χ^A is a ghost fields, a complex scalar field that obeys Fermi-Dirac statistics—the field is anti-commuting. ξ is a free parameter called the *gauge parameter*, it defines which of the family of covariant gauges that we use. Now that we have specified the renormalised QCD Lagrangian complete with gauge fixing and ghost terms we can determine the Feynman rules of QCD, we report them in our conventions in appendix. B.

2.3 The ultraviolet structure of QCD

Beyond leading order in perturbation theory, the Lagrangian in Eq. (2.3) does not by itself allow us to compute physical quantities. A problem arises when we wish to compute radiative corrections to processes involving particles charged under $SU(N_c)$. When we compute virtual (loop) corrections to a process involving particles charged under $SU(N_c)$, we encounter divergences when the momenta of the particles running in the loop become arbitrarily large. For example consider the one-loop two-point diagram given by

$I =$ 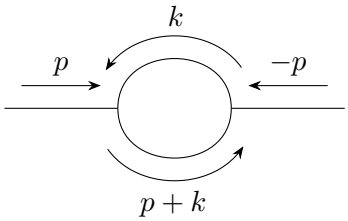

$$I = \int \frac{\mathrm{d}^4k}{(2\pi)^4} \frac{1}{(k+p)^2k^2} \sim \lim_{\Lambda\to\infty} \int_0^\Lambda \mathrm{d}k\, k^3 \frac{1}{(k^2)^2} \sim \lim_{\Lambda\to\infty} \int_0^\Lambda \frac{\mathrm{d}k}{k} \sim \lim_{\Lambda\to\infty} \log\Lambda\,. \tag{2.12}$$

Singularities of this form are called ultraviolet (UV) divergences, and are built into the formulation of QFT: we must sum over all possible momentum values of this virtual particle. This amounts to saying that we consider the quantum field theory to be valid up to an arbitrarily high energy scale. Naturally we do not believe this is true, and we expect that at some high energy scale the QFT will cease to be predictive[4].

In a renormalisable theory UV divergences can be absorbed in a redefinition of the parameters (the strong coupling constant, gauge fixing parameter and quark masses) and fields of the Lagrangian. we must construct a new *renormalised Lagrangian* replacing the fields and parameters by their new renormalised counterparts. The values of the redefined parameters are then set by comparing the theory to experimental measurements. In practice it is usually much simpler in massless QCD, where we only have two parameters: the coupling constant and the gauge fixing parameter. When considering only gauge invariant quantities we only have one parameter left: the coupling constant. The renormalised

[4]In fact one can consider QFTs to be low energy effective field theories (EFTs) of some currently unknown high energy theory.

coupling constant and fields are the only new ingredients necessary to perform calculations in massless QCD.

Before we can absorb the divergences into the renormalised quantities, we must isolate them. A particularly convenient and elegant way to do this is to make use of Conventional Dimensional Regularisation (CDR)[14–16], a regularisation scheme that preserves both Lorentz and gauge invariance. Throughout this thesis we will work with CDR in $d = 4-2\epsilon$ dimensions. In the context of CDR, divergences appear as poles in the parameter ϵ. By making use of CDR we are able to isolate the UV divergences. Considering again the integral in Eq. (2.12) we regulate using CDR and keep only the leading divergent terms

$$I = \int \frac{\mathrm{d}^d k}{(2\pi)^d} \frac{1}{(p+k)^2} \frac{1}{k^2} = \frac{i}{16\pi^2} \frac{1}{\epsilon} + \mathcal{O}(1)\,, \tag{2.13}$$

we see the expected single pole structure that corresponds to a UV divergence.

Next we must supplement the regularisation procedure with a *renormalisation condition*. In QCD there is no physically motivated renormalisation scheme, this is in stark contrast to Quantum Electrodynamics (QED) where the on-shell scheme emerges quite naturally as the renormalisation condition. This freedom leads us to choose a renormalisation scheme that is convenient for performing calculations, the modified minimal subtraction scheme ($\overline{\text{MS}}$). In the $\overline{\text{MS}}$ scheme the counterterms are chosen such that they contain only the poles and some universal terms that appear due to the use of CDR ($\log 4\pi$ and γ_E terms). Really the $\overline{\text{MS}}$ scheme is a family of renormalisation conditions depending on an arbitrary scale μ at which the subtraction of the UV divergences is performed— the scale μ has dimensions of mass and is introduced due to our use of CDR.

Renormalising the bare coupling constant α_s^0 in the $\overline{\text{MS}}$ scheme with the subtraction taking place at a scale μ leads to

$$\alpha_s^0 \mu_0^{2\epsilon} S_\epsilon = \alpha_s(\mu^2)\mu^{2\epsilon} \left[1 - \alpha_s(\mu^2)\frac{\beta_0}{\epsilon} + \alpha_s^2(\mu^2)\left(\frac{\beta_0^2}{\epsilon^2} - \frac{\beta_1}{2\epsilon}\right) + \mathcal{O}\big(\alpha_s^3(\mu^2)\big)\right], \tag{2.14}$$

where the coupling constant α_s is related to coupling g_s in Eq. (2.4) by the relation

$$\alpha_s = \frac{g_s^2}{4\pi}\,, \tag{2.15}$$

$S_\epsilon = (4\pi)^\epsilon e^{-\epsilon\gamma_E}$, the typical phase space factor of CDR and μ_0^2 is a mass parameter introduced in CDR to ensure that the coupling constant of the Lagrangian remains dimensionless. The coefficients β_0 and β_1 are the first two coefficients of the QCD β-function. We report their expressions in Eqs. (C.2) and (C.3). We can write the relation between the bare and renormalised coupling parameter Eq. (2.14) more compactly as

$$\alpha_s^0 = Z_{\alpha_s}(\mu^2)\alpha_s(\mu^2)\,, \tag{2.16}$$

where Z_{α_s} is the coupling renormalisation factor. We know that the bare parameters of the theory are independent of μ, they cannot depend on the arbitrary scale that we introduced for the purposes of renormalisation

$$\mu^2 \frac{\mathrm{d}}{\mathrm{d}\mu^2} \alpha_s^0 = 0 \,. \tag{2.17}$$

From the μ independence of the bare coupling parameter we can derive the QCD β-function

$$\frac{\mathrm{d}\alpha_s(\mu^2)}{\mathrm{d}\log\mu^2} = \beta(\alpha_s(\mu^2)) \equiv -\alpha_s(\mu^2) \frac{1}{Z_{\alpha_s}(\mu^2)} \frac{\mathrm{d}Z_{\alpha_s}(\mu^2)}{\mathrm{d}\log\mu^2} \,. \tag{2.18}$$

The β-function describes the dependence of the renormalised coupling parameter on the arbitrary subtraction scale μ. The β-function can be expanded as a perturbative series in the coupling constant

$$\beta(\alpha_s) = -\epsilon\alpha_s(\mu^2) - \alpha_s^2(\mu^2) \sum_{n=0}^{\infty} \beta_n \alpha_s^n(\mu^2) \,, \tag{2.19}$$

usually we are only interested in the $d = 4$ part of the β-function, the second term on the right hand side of Eq. (2.19). The running of the coupling constant Eq. (2.18) can be solved in the perturbative regime, and at lowest order we find

$$\alpha_s(\mu^2) = \frac{\alpha_s(\mu'^2)}{1 + \alpha_s\beta_0 \log\frac{\mu^2}{\mu'^2}} \,, \tag{2.20}$$

where μ' is an initial scale at which the coupling is known. We will now call the scale μ by its conventional name, the renormalisation scale. Looking at Eq. (2.20) we can determine the behaviour of the coupling constant as we vary the renormalisation scale:

1. *Asymptotic freedom*: $\mu \to \infty$

   At high energies QCD becomes more weakly interacting and tends towards a free theory in the very high energy limit. This means that for processes characterised by very high momentum transfer, perturbation theory provides an excellent approximation to the full theory.

2. *Confinement*: $\mu \to 0$

   At low energies QCD becomes strongly interacting, and perturbation theory fails.

This behaviour is a consequence of the sign of the QCD β-function, which is turn is due to the field content of QCD.

2.4 The infrared structure of pQCD

In calculating QCD cross sections we encounter not only UV divergences, but also infrared (IR) divergences. These singularities differ from those of UV origin in that they cannot be renormalised away as parameters in our Lagrangian.

We can trace physical origin of IR divergences by considering a simple $2 \to 2$ scattering process with an outgoing quark-antiquark pair and then allowing the outgoing quark to emit a further gluon. Such a process is shown in Fig. 2.1 where p_q, $p_{\bar{q}}$ and p_g are the

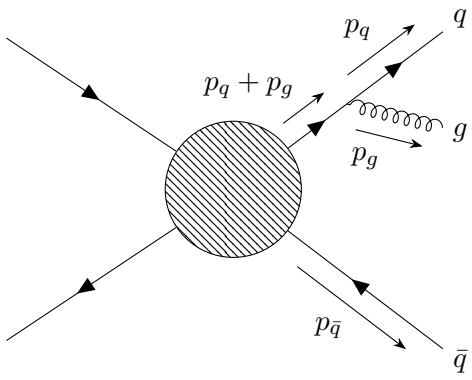

Figure 2.1: Feynman diagram for a generic scattering and a $q\bar{q}g$ final state.

momenta of the quark, antiquark and gluon respectively. Let us examine the amplitude for the gluon emission, to do this we consider the fermion propagator before the emission of the gluon, expanding the denominator in terms of energies and angles we find

$$\frac{1}{(p_q + p_g)^2} = \frac{1}{2E_q E_g(1 - \cos\theta_{qg})} \,. \tag{2.21}$$

We see that if either the energy of the gluon E_g, or the angle of the emission between the quark and gluon θ_{qg} goes to zero the propagator diverges. We refer to the $E_g \to 0$ limit as soft, and the $\theta_{qg} \to 0$ limit as collinear, these are the two types of IR singularities. We may also be concerned that the $E_q \to 0$ limit also gives rise to a singularity. This is not the case however, if we take into account the spinor of the outgoing quark we find that the limit $E_q \to 0$ gives rise only to an integrable singularity.

The IR singularities are related to long-distance physics, outside the realms of standard perturbation theory. We can see this by examining the fermion propagator further. The propagator is off-shell by an amount $\Delta E^2 \sim 2p_q \cdot p_g$. This small off-shell contribution means that the virtual quark is long lived, surviving for a time $\Delta t \sim 1/(2p_q \cdot p_g)$[5] before the gluon is radiated, this longevity corresponds to long distance effects. The virtual quark is able to travel an arbitrary distance if the radiated gluon is sufficiently soft and/or collinear.

The origin of IR singularities is intrinsic to the construction of QFT. We assumed that we could construct asymptotic states that are free of all interactions, this is not justified if a particle can propagate an infinite distance before radiating soft particles. It may seem

[5]Including the boost to take into account the motion of the quark-gluon system gives us this contribution.

like all is lost and we will be unable to compute anything observable in pQCD, but we are saved by the theorem of Kinoshita, Lee and Nauenberg (KLN) [17, 18] which states:

> *Observable transition probabilities are free of IRC singularities, provided that we sum over all indistinguishable configurations.*

In the context of scattering amplitudes in pQCD this means that when we sum over all possible configurations, the IRC singularities from the virtual corrections exactly cancel against those of the real corrections. This holds at every order in perturbation theory, ensuring that we have an observable prediction that is finite at any order.

2.5 Hadronic cross section in e^+e^- annihilation

Having considered the IR behaviour of QCD it is instructive to carry out a simple calculation to see how it works in practice. Electron-positron annihilation into hadrons is a process with a long history, it is a cornerstone of QCD phenomenology and is perhaps the simplest process that can be described using pQCD. The simplicity arises from two particular features:

1. The initial state particles have well defined energies

   In a lepton collider we can prepare initial states electrons with energies fixed by the experimental configuration, this allows us to determine the centre of mass energy of the event at a very high level of accuracy. In contrast at a collider involving hadrons we can prepare the energy state of the hadrons as in a lepton collider however the centre of mass energies of the hard scattering process depend on the the energies of the quarks and gluons – referred to as *partons* in the context of collider physics – that make up the hadrons and as a result the centre of mass energy varies between collisions depending on the momentum fraction of the reacting partons.

2. The interaction proceeds via an s-channel electroweak interaction

   Processes mediated by electroweak interactions provide a "clean" final state environment to study QCD effects. All of the measured partons must belong to the final state of the event, the incoming leptons do not radiate any partons. Again contrast this with collisions involving initial-state hadrons, where we may see partons due to initial state radiation, hadron remnants or due to secondary interactions between remnants of the initial hadrons.

2.5.1 Leading order

To begin we will first compute the leading order contribution to $e^+e^- \to$ hadrons, this is due to the process $e^+e^- \to q\bar{q}$. The Feynman diagram and kinematics for this process is shown in Fig. 2.2. Where, for simplicity, we will neglected the contribution due to the

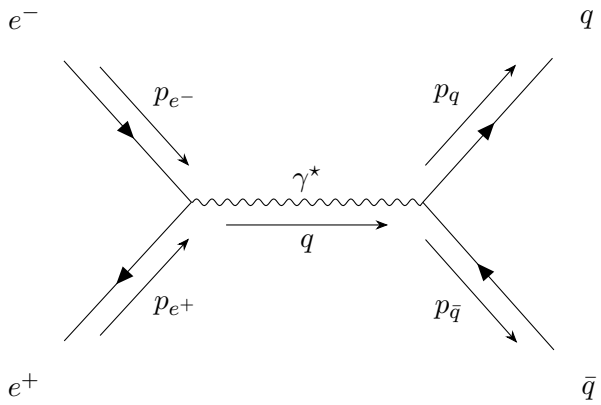

Figure 2.2: Feynman diagram for $e^+e^- \to q\bar{q}$.

Z boson in our calculation. Using Eq. (2.2) we can write down the cross section of the leading order process

$$\sigma_{\text{had},0}(s) = \frac{1}{2s}\int \mathrm{d}\Phi_2 \, \frac{1}{4}\sum_{\text{spins.}} \left|\mathcal{M}(e^+e^- \to q\bar{q})\right|^2 , \tag{2.22}$$

where we sum over the final spin states of the quarks and averaging over the initial spin states of the leptons and include the flux factor $1/2s$.

The squared amplitude summed over final state spins, colours and quark flavour and averaged over initial state spins can be factorised into a tensor describing the leptonic part $L^{\mu\nu}$ and a tensor describing the hadronic part $H_{\mu\nu}$

$$\frac{1}{4}\sum_{\text{spins.}} |\mathcal{M}|^2 = L^{\mu\nu}\frac{1}{s^2}H_{\mu\nu} , \tag{2.23}$$

where s is given by

$$s = q^2 = (p_{e^-} + p_{e^+})^2 = 2p_{e^-}\cdot p_{e^+} = (p_q + p_{\bar{q}})^2 = 2p_q \cdot p_{\bar{q}} , \tag{2.24}$$

where all of the fermions are assumed to be massless.

The leptonic tensor corresponds to the square of the leptonic part of the Feynman diagram in Fig. 2.2 and is given explicitly by the cut diagram

$$L^{\mu\nu} = \frac{1}{4}$$ 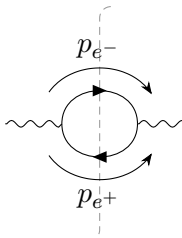 $$= e^2\left(p^\mu_{e^-}p^\nu_{e^+} + p^\mu_{e^+}p^\nu_{e^-} - p_{e^-}\cdot p_{e^+}\, g^{\mu\nu}\right) . \tag{2.25}$$

The expression for $H_{\mu\nu}$ is very similar to $L^{\mu\nu}$ except with momenta p_q, $p_{\bar{q}}$ replacing p_{e^-}, p_{e^+}, an additional prefactor taking into account the different electric charges of the different quark flavours Q_f and the number of colours N_c. Taking these into account the hadronic tensor is

$$H^{\mu\nu} = 4N_c e^2 \sum_f Q_f^2 \left(p_q^\mu p_{\bar{q}}^\nu + p_{\bar{q}}^\mu p_q^\nu - p_q \cdot p_{\bar{q}}\, g^{\mu\nu}\right). \tag{2.26}$$

Further both of these tensors satisfy

$$q_\mu L^{\mu\nu} = q^\mu H_{\mu\nu} = 0\,, \tag{2.27}$$

as a consequence of gauge invariance.

We can now write down an expression for the squared matrix element. But first we must decide on which variables to use. In the following we adopt Mandelstam variables, defined for $2 \to 2$ scattering kinematics as follows

$$s = (p_{e^-} + p_{e^+})^2\,, \quad t = (p_{e^-} - p_q)^2\,, \quad u = (p_{e^-} - p_{\bar{q}})\,. \tag{2.28}$$

The Mandelstam variables have some convenient properties: they are Lorentz invariant, which allows us to keep the expression for the squared matrix element as general as possible. At no point did we have to specify a reference frame. Further to this the Mandelstam variables satisfy the following sum

$$s + t + u = 0\,. \tag{2.29}$$

In terms of the Mandelstam variables we find the squared matrix element is

$$\frac{1}{4}\sum_{\text{spins.}} \left|\mathcal{M}(e^+e^- \to q\bar{q})\right|^2 = 2e^4 N_c \sum_f Q_f^2 \frac{t^2 + u^2 - \epsilon s^2}{s^2}\,. \tag{2.30}$$

This is a compact expression of the squared matrix element and is Lorentz invariant by virtue of our choice of Mandelstam variables. However Eq. (2.30) includes more information than we need for this calculation. In fact Eq. (2.30) contains information on the spin correlations between the initial and final states (this is referred to as the *event orientation*). The observables that we will study in this thesis will not depend on the event orientation and so we should find a way to remove it and simplify our calculations.

To remove the event orientation we first consider the more general cross section for $e^+e^- \to X$, where X is a final state containing only quarks and gluons. In d-dimensions this cross section can be written as follows

$$\sigma_X^d = \frac{1}{2s} L_{\mu\nu} \frac{1}{s^2} \int \mathrm{d}\Phi_X H_X^{\mu\nu}\,, \tag{2.31}$$

where we note that only the hadronic tensor depends on the momenta of the final state particles. In Eq. (2.31) we integrate over the momenta of the final state particles, following this integration the only remaining free variable is $q^2(=s)$, and the only available quantities to carry the Lorentz indices of $H_X^{\mu\nu}$ are $g^{\mu\nu}$ and q^μ. Hence the most general result of this integration must be of the form

$$\int \mathrm{d}\Phi_X \, H_X^{\mu\nu} = H_1(q^2) g^{\mu\nu} + H_2(q^2) q^\mu q^\nu \,. \tag{2.32}$$

To make further progress we contract Eq. (2.32) with q^μ and impose gauge invariance using Eq. (2.27), the result is as follows

$$q_\mu \int \mathrm{d}\Phi_X \, H_X^{\mu\nu} = \left(H_1(q^2) + q^2 H_2(q^2)\right) q^\nu = 0 \,. \tag{2.33}$$

In general $q^\nu \neq 0$ and thus the only way to satisfy Eq. (2.33) is relate H_1 and H_2 according to $H_1(q^2) = -q^2 H_2(q^2)$. Now we must isolate H_1 so that we can cast it into an explicit form, from which we can calculate it. To do this we contract Eq. (2.32) with negative of the metric tensor

$$-g_{\mu\nu} \int \mathrm{d}\Phi_X \, H_X^{\mu\nu} = -g_{\mu\nu} \left(g^{\mu\nu} - \frac{q^\mu q^\nu}{q^2}\right) H_1(q^2) = -(d-1) H_1(q^2) \,, \tag{2.34}$$

for convenience we define $H_X(q^2) = -H_1(q^2)/(d-1)$, and rewrite Eq. (2.32) as

$$\int \mathrm{d}\Phi_X \, H_X^{\mu\nu} = \frac{1}{d-1} \left(-g^{\mu\nu} + \frac{q^\mu q^\nu}{q^2}\right) H_X(q^2) \,. \tag{2.35}$$

Combining Eq. (2.32) with $H_X(q^2)$ defined in Eq. (2.35) we can isolate $H_X(q^2)$ and find

$$H_X(q^2) = -g_{\mu\nu} \int \mathrm{d}\Phi_X \, H_X^{\mu\nu} \,. \tag{2.36}$$

We are now in a position to write down the orientation averaged cross section. We replace the Hadronic tensor in Eq. (2.31) with the averaged version from Eq. (2.35) to find

$$\begin{aligned} \sigma_X^d &= \frac{1}{2s} \left(-g^{\mu\nu} L_{\mu\nu}\right) \frac{1}{s^2} H_X(q^2) \\ &= \frac{1}{2s} e^2 \frac{1}{2} \frac{d-2}{d-1} \frac{1}{s} H_X(q^2) \,. \end{aligned} \tag{2.37}$$

Finally we can drop the integration over the final state momenta in Eq. (2.37) and work at the level of the matrix elements. Returning to the case of $e^+e^- \to q\bar{q}$ we can write the orientation averaged matrix element as follows

$$\begin{aligned} \left\langle \frac{1}{4} \sum_{\text{spins.}} \left|\mathcal{M}(e^+e^- \to q\bar{q})\right|^2 \right\rangle &= e^2 \mu^{4-d} \frac{1}{2} \frac{d-2}{d-1} \frac{1}{s} (-g^{\mu\nu} H_{\mu\nu}) \\ &= e^4 \mu^{2(4-d)} \frac{(d-2)^2}{d-1} N_c \sum_f Q_f^2 \,. \end{aligned} \tag{2.38}$$

What is particularly striking about this matrix element is that it has no dependence on the external momenta, it is a constant. And so we are free to integrate inclusively over the two-particle phase space to determine the leading order cross section

$$\sigma^{d}_{\text{had},0} = \sigma_{\text{had},0}\,\mu^{2(4-d)}\left(\frac{4\pi}{s}\right)^{\frac{4-d}{2}}\frac{3\sqrt{\pi}(d-2)^2}{2^d\Gamma\left(\frac{d+1}{2}\right)}\,, \tag{2.39}$$

where $\sigma_{\text{had},0}$ is the cross section in $d=4$, and is given by

$$\sigma_{\text{had},0} = \frac{4\pi\alpha^2}{3s}N_c\sum_f Q_f^2\,. \tag{2.40}$$

2.5.2 Next-to-leading order

To compute the next-to-leading order (NLO) corrections we must include all possible diagrams that give rise to squared matrix elements that are $\mathcal{O}(\alpha_s)$ in the strong coupling constant: there are two such contributions.

1. The real correction:

   Due to the emission of an extra particle, the square of the real matrix element is $\mathcal{O}(\alpha_s)$.

2. The virtual correction:

   Due to the inclusion of a loop, the interference of the virtual matrix element and the LO matrix element is $\mathcal{O}(\alpha_s)$.

The real correction

First let us consider the real correction due to the emission of an additional particle. There is only one process with an extra parton that is compatible with QCD, which is $e^+e^- \to q\bar{q}g$. There are two Feynman diagrams for this process as the gluon can be emitted from either the quark or the anti-quark. These Feynman diagrams are shown in Fig. 2.3.

As before we appeal to Eq. (2.2) to write the cross section of the real process

$$\sigma^{R}_{\text{had},1} = \frac{1}{2s}\int \mathrm{d}\Phi_3\,\frac{1}{4}\sum_{\text{spins.}}\left|\mathcal{M}(e^+e^-\to q\bar{q}g)\right|^2\,, \tag{2.41}$$

notice that we are now integrating over a three-particle phase space due to extra emission. And once again we are able to decompose the squared matrix element into a leptonic tensor (the same tensor as before) and a hadronic tensor (different to the previous tensor). Considering the orientation averaged squared matrix element we have

$$\frac{1}{4}\sum_{\text{spins.}}\left|\mathcal{M}(e^+e^-\to q\bar{q}g)\right|^2 = \frac{e^2}{s}\frac{1}{2}\frac{d-2}{d-1}\sum_{\text{spins.}}\left|\mathcal{M}(\gamma^\star\to q\bar{q}g)\right|^2\,, \tag{2.42}$$

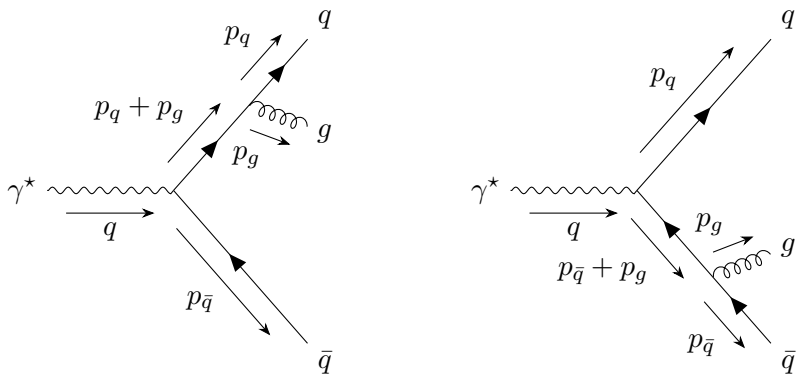

Figure 2.3: Feynman diagrams for $e^+e^- \to q\bar{q}g$.

where we only need to calculate the hadronic tensor by considering the decay matrix element $\gamma^\star \to q\bar{q}g$. The calculation is a straightforward exercise in γ-matrix algebra and we find the following result in d dimensions

$$\sum_{\text{spins.}} |\mathcal{M}(\gamma^\star \to q\bar{q}g)|^2 = 32\pi\alpha_s\mu_R^{2\epsilon}C_F e^2 N_c \sum_f Q_f^2 \times \left[\frac{(1-\epsilon)s_{\bar{q}g}}{s_{qg}} + \frac{(1-\epsilon)s_{qg}}{s_{\bar{q}g}} + \frac{2\left[s_{q\bar{q}}\left(s_{q\bar{q}}+s_{qg}+s_{\bar{q}g}\right) - \epsilon s_{qg}s_{\bar{q}g}\right]}{s_{qg}s_{\bar{q}g}}\right] . \quad (2.43)$$

Three particle final states containing no information on event orientation can be parametrised in a very convenient way in terms of energy fractions defined as follows

$$x_i = \frac{2q\cdot p_i}{q^2}\,, \quad i = q, \bar{q}, g\,, \quad (2.44)$$

where we consider only the final state particles in the determination of the energy fractions and we label them according to their flavour, further in the centre of mass frame the energy fractions adopt the particularly simple form $x_i = 2E_i/\sqrt{s}$. From the definition we are able to derive some constraints on the energy fractions. To begin we compute the sum of all the energy fractions

$$\sum_i x_i = \frac{2q\cdot(p_q + p_{\bar{q}} + p_g)}{s} = \frac{2}{\sqrt{s}}(E_q + E_{\bar{q}} + E_g) = 2\,. \quad (2.45)$$

Making use of energy-momentum conservation the x_i satisfy

$$0 \le x_i \le 1\,, \quad x_i + x_j \ge 1\,, \quad \text{with} \quad i \ne j\,, \text{and} \quad i,j = q,\bar{q},g\,. \quad (2.46)$$

These properties are sufficient to determine the matrix element and phase space in terms of x_i. The real cross section takes the form

$$\sigma^R_{\text{had},1} = \sigma_{\text{had},0}\, C_F \frac{\alpha_s}{2\pi}\int_0^1 \mathrm{d}x_q \int_{1-x_q}^1 \mathrm{d}x_{\bar{q}}\, \frac{x_q^2 + x_{\bar{q}}^2}{(1-x_q)(1-x_{\bar{q}})}\,. \quad (2.47)$$

Notice that in Eq. (2.47) we have the usual IR divergences of massless pQCD:

- $x_q \to 1$,

  corresponds to the antiquark and gluon becoming collinear.

- $x_{\bar{q}} \to 1$,

  corresponds to the quark and the gluon becoming collinear.

- $x_q \to 1$ and $x_{\bar{q}} \to 1$,

  corresponds to the emission of a soft gluon.

The virtual correction

Next we consider the virtual correction due to a loop.

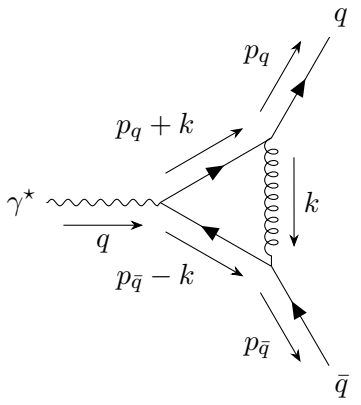

Figure 2.4: Feynman diagram for the one loop correction to $\gamma^\star \to q\bar{q}$.

Again we start from the symbolic expression for the cross section of the virtual correction, which is given by

$$\sigma^V_{\text{had},1} = \frac{1}{2s}\int \mathrm{d}\Phi_2 \, \frac{1}{4}\sum_{\text{spins.}} 2\,\mathrm{Re}\left[\mathcal{M}^{(0)\star}(e^+e^- \to q\bar{q})\mathcal{M}^{(1)}(e^+e^- \to q\bar{q})\right] , \tag{2.48}$$

notice that we are integrating over a two particle phase space, there are no extra resolved emissions in this integral. We also see that the matrix element structure is a bit different to what we have encountered so far. The virtual correction is determined by interfering the one loop correction with the tree level. Rather than computing the matrix element

$$\frac{1}{4}\sum_{\text{spins.}} 2\,\mathrm{Re}\left[\mathcal{M}^{(0)\star}(e^+e^- \to q\bar{q})\mathcal{M}^{(1)}(e^+e^- \to q\bar{q})\right] \tag{2.49}$$

directly, it's easier to consider the one loop QCD correction to the QED vertex instead. This is determined from the integral

$$\bar{u}(p_q)\Gamma^\mu v(p_{\bar{q}}) = -ig_s^2\mu^{2\epsilon}C_F \int \frac{\mathrm{d}^d k}{(2\pi)^d} \frac{\bar{u}(p_q)\gamma^\rho(\not{p}_q + \not{k})\gamma^\mu(\not{k} - \not{p}_{\bar{q}})\gamma_\rho v(p_{\bar{q}})}{[(p_q+k)^2 + i\epsilon][(k-p_{\bar{q}})^2 + i\epsilon][k^2 + i\epsilon]} , \tag{2.50}$$

from which we can easily determine the virtual corrections using the technique of Feynman parameters to evaluate this integral.

The total correction

Carrying out the evaluation of equations (2.41) and (2.48) in CDR we find respectively

$$\sigma^{R}_{\text{had},1} = \sigma_{\text{had},0} C_F \frac{\alpha_s}{2\pi} \frac{1}{\Gamma(1-\epsilon)} \left(\frac{4\pi\mu_R^2}{s}\right)^{\epsilon} \left[\frac{2}{\epsilon^2} + \frac{3}{\epsilon} - \pi^2 + \frac{19}{2} + \mathcal{O}(\epsilon)\right] , \tag{2.51}$$

$$\sigma^{V}_{\text{had},1} = \sigma_{\text{had},0} C_F \frac{\alpha_s}{2\pi} \frac{1}{\Gamma(1-\epsilon)} \left(\frac{4\pi\mu_R^2}{s}\right)^{\epsilon} \left[-\frac{2}{\epsilon^2} - \frac{3}{\epsilon} + \pi^2 - 8 + \mathcal{O}(\epsilon)\right] . \tag{2.52}$$

Both contributions to the NLO cross section contain IR divergences. Summing them to obtain the NLO correction to the cross section we find

$$\sigma_{\text{had},1} = \sigma^{R}_{\text{had},1} + \sigma^{V}_{\text{had},1} = \sigma_{\text{had},0} C_F \frac{\alpha_s(\mu^2)}{2\pi} \frac{1}{\Gamma(1-\epsilon)} \left(\frac{4\pi\mu^2}{s}\right)^{\epsilon} \left[\frac{3}{2} + \mathcal{O}(\epsilon)\right] , \tag{2.53}$$

which is *finite*—as we had anticipated due to the KLN theorem. We can now safely take the $\epsilon \to 0$ limit and add the LO cross section to find the prediction for the total cross section at NLO accuracy

$$\sigma_{\text{had}}(s) = \sigma_{\text{had},0} \left(1 + \frac{3}{2} C_F \frac{\alpha_s}{2\pi} + \mathcal{O}\left(\alpha_s^2\right)\right) . \tag{2.54}$$

2.6 Matrix element factorisation

Now that we have performed a simple calculation in pQCD it is essential to consider the IR limits with more generality. In doing so we can determine systematically where they will occur. Understanding these limits will allow us to determine the singular structure of QCD amplitudes at *all-orders* in α_s. It is this factorisation that allows us to compute resummations in QCD, which is the core subject of this thesis. For now we will systematically identify the IR limits of QCD squared matrix elements. Computations in pQCD are technically quite involved and thus good organisation of our calculations is essential. To that end we must introduce some rather abstract notation. Such notation is necessary to determine the limits of QCD in the generality that we desire.

We consider renormalised matrix elements with m coloured particles in the final state. Any number of non-coloured particles may also be present, but any notion of these particles will be suppressed in our notation. We will label resolved partons with $i, j, k, \ldots$ and unresolved ones by r and s.

The colour indices of the partons are denoted by c_i, and span $A = 1, \ldots, N_c^2 - 1$ for gluons and $a = 1, \ldots, N_c$ for quarks and anti-quarks. Spin indices are denoted by s_i, and span $\mu = 1, \ldots, d$ for gluons and $s = 1, 2$ for massless fermions. We introduce an orthogonal basis of unit vectors $|c_1, \ldots, c_m\rangle \otimes |s_1, \ldots, s_m\rangle$ in the space of colour and spin,

in such a way that the amplitude of a process involving m external partons, $\mathcal{M}_m^{\{c_I,s_I\}}(\{p_I\})$ with definite colour, spin and momenta $\{p_I\}$ can be written as

$$\mathcal{M}_m^{c_1\dots c_m;s_1\dots s_m}(p_1,\dots,p_m) \equiv \big(\langle c_1\dots c_m| \otimes \langle s_1\dots s_m|\big)\,|\mathcal{M}_m(p_1,\dots,p_m)\rangle\,. \tag{2.55}$$

Thus $|\mathcal{M}_m\rangle$ is an abstract vector in colour and spin space and its normalisation is fixed such that the squared amplitude summed over colours and spins is

$$\sum_{\text{colour.}}\sum_{\text{spin.}} |\mathcal{M}_m^{c_1\dots c_m;s_1\dots s_m}(p_1,\dots,p_m)|^2 = \langle \mathcal{M}_m(p_1,\dots,p_m)|\mathcal{M}_m(p_1,\dots,p_m)\rangle \tag{2.56}$$

The matrix element has the following loop expansion:

$$|\mathcal{M}_m\rangle = |\mathcal{M}_m^{(0)}\rangle + |\mathcal{M}_m^{(1)}\rangle + \dots\,, \tag{2.57}$$

where $|\mathcal{M}_m^{(0)}\rangle$ denotes the tree-level contribution, $|\mathcal{M}_m^{(1)}\rangle$ the one-loop contribution, and so on.

As for the colour structure, it is convenient to associate a colour charge $\mathbf{T}_i$ with the emission of a gluon from each parton i. If the emitted gluon has colour index c, the colour-charge operator is:

$$\mathbf{T}_i \equiv T_i^c\,|c\rangle \tag{2.58}$$

and its action onto the colour space is defined by

$$\langle c_1,\dots,c_i,\dots,c_m|\,T_i^c\,|b_1,\dots,b_i,\dots,b_m\rangle = \delta_{c_1b_1}\dots T^c_{c_ib_i}\dots\delta_{c_mb_m} \tag{2.59}$$

where $T^c_{a_ib_i}$ is the colour-charge matrix in the representation of the final state particle i, i.e. $T^A_{BC} = -if_{ABC}$ (or equivalently $T^A_{CB} = if_{CAB}$) if the emitting particle i is a gluon and $T^A_{ab} = (t^A)_{ab}$ if the emitting particle i is a quark (in the case of an emitting anti-quark $T^A_{ab} = (\bar{t}^A)_{ab} = -(t^A)_{ab}$).

The colour-charge algebra is:

$$\mathbf{T}_i\cdot\mathbf{T}_j = \mathbf{T}_j\cdot\mathbf{T}_i \quad \text{if} \quad i\neq j\,; \qquad \mathbf{T}_i^2 = C_i \tag{2.60}$$

where C_i is the Casimir operator, i.e. $C_i = C_A$ if i is a gluon and $C_i = C_F$ if i is a quark or antiquark.

Note that by definition, each vector $|\mathcal{M}_m\rangle$ is a colour-singlet state. Therefore colour conservation is simply

$$\left(\sum_{i=1}^{m}\mathbf{T}_i\right)|\mathcal{M}_m\rangle = 0\,. \tag{2.61}$$

A more complete review of this notation and the colour-space formalism can be found in Refs. [19–22].

Now that we have set up our notation we can set about determining the behaviour of a general QCD matrix element when a single parton becomes soft and/or collinear.

2.6.1 Collinear factorisation

In general for a single parton becoming collinear, this behaviour is captured in the universal collinear factorisation formula

$$\mathbf{C}_{ir}|\mathcal{M}^{(0)}_{m+1}| = 8\pi\alpha_s\mu^{2\epsilon}\frac{1}{s_{ir}}\langle\mathcal{M}^{(0)}_m|\,\hat{P}^{(0)}_{(ir)\to i+r}\,|\mathcal{M}^{(0)}_m\rangle\,, \tag{2.62}$$

where $\hat{P}^{(0)}_{(ir)\to i+r}$ is the unregulated leading-order Altarelli-Parisi (AP) splitting function describing the process of a particle of flavour (ir) splitting into two particles of flavours i and r. We will derive explicit expressions for these functions in this section. $\mathbf{C}_{ir}$ is an operator that takes the collinear limit of the particles i and r keeping only the most singular term.

The limit where the momenta p_i and p_r become collinear can be precisely defined by letting $k_\perp \to 0$ in the Sudakov parametrisation of the momenta

$$p_i^\mu = z_i p^\mu + k_\perp^\mu - \frac{k_\perp^2}{z_i}\frac{n^\mu}{s_{pn}} \tag{2.63}$$

$$p_r^\mu = z_r p^\mu - k_\perp^\mu - \frac{k_\perp^2}{z_r}\frac{n^\mu}{s_{pn}} \tag{2.64}$$

where $z_i + z_r = 1$, the momentum p denotes the collinear direction and n is an auxiliary vector required to specify the transverse component $k_\perp$. The following relations hold for massless partons in this parametrisation

$$p^2 = n^2 = p_i^2 = p_r^2 = 0\,, \quad k_\perp\cdot p = k_\perp\cdot n = 0\,, \quad k_\perp^2 < 0\,, \tag{2.65}$$

notice that by construction p, n, p_i and p_r are light-like and $k_\perp$ is space-like. There is one further identity that we observe in the collinear limit that will be necessary for our analysis

$$s_{ir} = -\frac{k_\perp^2}{z_i z_r}\,, \quad k_\perp \to 0\,. \tag{2.66}$$

Through the Sudakov decomposition we have a notion of collinearity. To determine which diagrams we must compute we appeal to the following theorems:

1. *The leading collinear singularities are due to the collinear splitting of an external parton*
2. *In a physical gauge, the interference Feynman diagrams obtained from the squared matrix element* $|\mathcal{M}^{(0)}_{m+1}|^2$ *in Eq. (2.62) are collinearly suppressed* [23–25].

Making use of this theorem we need only to consider the cut graphs that account for the splitting of a single external parton. There are three distinct cases that must be considered,

we will now treat them each in turn. To make the notation more tractable we will adopt the following shorthands. We denote the spin dependant part of the gluon propagator by

$$d_{\mu\nu}(p,n) = -g_{\mu\nu} + \frac{p_\mu n_\nu + n_\mu p_\nu}{p\cdot n}\,, \tag{2.67}$$

where p is the gluon momentum and n is an auxiliary light-like vector, and we will denote all of the momenta $p_i, p_r, \ldots$ by their Latin subscripts $i, r, \ldots$.

Collinear $q \to q + g$ splitting

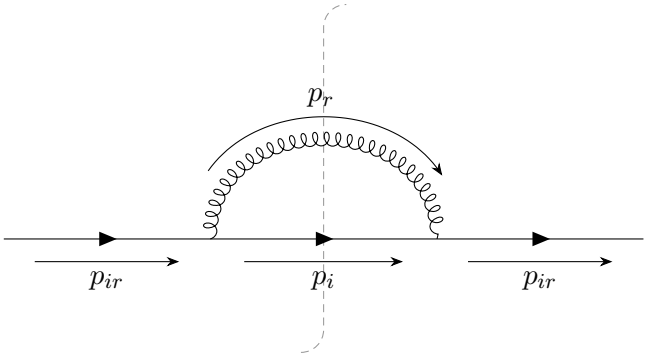

Figure 2.5: Cut diagram for the process $q \to q + g$

In the case of a quark splitting into a quark and a gluon, we must compute the cut diagram in Fig. 2.5. From this diagram we derive the squared matrix element

$$\begin{aligned}
\mathcal{C}_{q\to qg} &= C_F g_s^2 \mu^{2\epsilon} \frac{\not{l} + \not{r}}{s_{ir}} \gamma^\mu \not{l} \gamma^\nu d_{\mu\nu}(r,n) \frac{\not{l} + \not{r}}{s_{ir}} \\
&= C_F g_s^2 \mu^{2\epsilon} \frac{\not{l} + \not{r}}{s_{ir}} \gamma^\mu \not{l} \gamma^\nu \left[-g_{\mu\nu} + \frac{r_\mu n_\nu + n_\mu r_\nu}{r\cdot n} \right] \frac{\not{l} + \not{r}}{s_{ir}} \\
&= 4\pi\alpha_s \mu^{2\epsilon} C_F \frac{\not{l} + \not{r}}{s_{ir}} \left[-\gamma^\mu \not{l} \gamma_\mu + \frac{\not{r}\not{l}\not{n} + \not{n}\not{l}\not{r}}{r\cdot n} \right] \frac{\not{l} + \not{r}}{s_{ir}}\,,
\end{aligned} \tag{2.68}$$

where we have included the propagator of the quark with momentum $p_{ir} = p_i + p_r$ as this is necessary to compute the full $m+1$ parton matrix element. Some straightforward Dirac algebra yields

$$\mathcal{C}_{q\to qg} = 4\pi\alpha_s \mu^{2\epsilon} C_F \frac{1}{s_{ir}} \left[(d-2)\not{r} + \frac{2}{s_{rn}} \left(2 s_{in} \not{l} + s_{in} \not{r} + s_{rn} \not{l} - s_{ir} \not{n} \right) \right]. \tag{2.69}$$

We now insert the Sudakov parametrisation of Eq. (2.63) to expose the collinear limit

$$\begin{aligned}
\mathcal{C}_{q\to qg} &= 4\pi\alpha_s \mu^{2\epsilon} C_F \frac{1}{s_{ir}} \left[(d-2) z_r + \frac{1}{z_r} (2 z_i^2 + z_i z_r + z_r z_i) \right] \not{p} + \mathcal{O}\big(k_\perp^{-1}\big) \\
&= 8\pi\alpha_s \mu^{2\epsilon} \frac{1}{s_{ir}} C_F \left[\frac{1 + z_i^2}{z_r} - \epsilon z_r \right] \not{p} + \mathcal{O}\big(k_\perp^{-1}\big)\,.
\end{aligned} \tag{2.70}$$

We have kept only the most singular terms, those scaling as $\mathcal{O}\big(k_\perp^{-2}\big)$. And from Eq. (2.70) we can extract the LO AP splitting kernel which is a matrix in the spin state of the

unresolved parton. We insert a complete set of spin states into Eq. (2.62) and find

$$\mathbf{C}_{ir}|\mathcal{M}^{(0)}_{m+1}| = 8\pi\alpha_s\mu^{2\epsilon}\frac{1}{s_{ir}}\sum_{s,s'}\langle\mathcal{M}^{(0)}_m|s\rangle\,\langle s|\,\hat{P}^{(0)}_{q\to qg}\,|s'\rangle\,\langle s'|\mathcal{M}^{(0)}_m\rangle\,. \tag{2.71}$$

The $m+1$ parton matrix element is factorised into an m parton matrix element and a universal collinear splitting function. The collinear splitting function has a universal prefactor $8\pi\alpha_s\mu^{2\epsilon}/s_{ir}$ and a spin dependent piece given by the AP splitting kernel. Comparing to Eq. (2.70) we see that the AP splitting kernel takes the form

$$\langle s|\,\hat{P}^{(0)}_{q\to qg}(z_i,z_r,k_\perp;\epsilon)\,|s'\rangle = C_F\left[\frac{1+z_i^2}{z_r}-\epsilon z_r\right]\delta_{ss'}\,, \tag{2.72}$$

which is diagonal in the spin state of the unresolved parton[6]. We have dropped the factor $\not{p}$ that appears in Eq. (2.70) as it belongs to the m parton matrix element. This is because in our computation we included the quark propagators, which take into account the external spinors. These spinors belong to the m parton matrix element and thus are not a part of the AP splitting kernel.

Collinear $g \to q + \bar{q}$ splitting

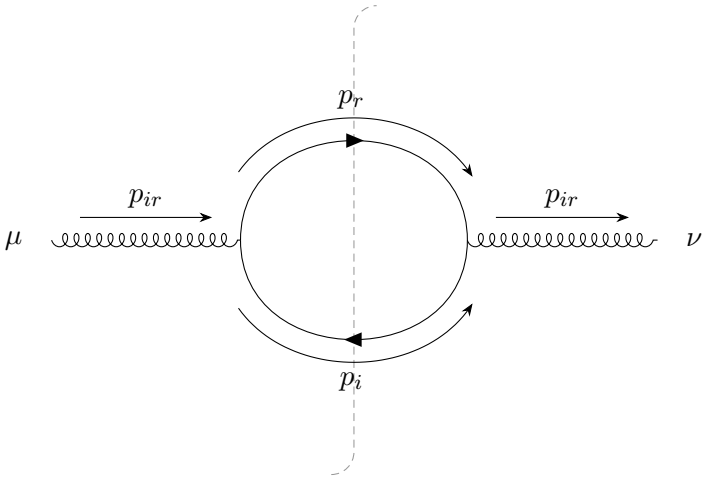

Figure 2.6: Cut diagram for the process $g \to q + \bar{q}$

In the case of a gluon splitting into a quark and an antiquark, we must compute the

[6]The $q \to q + g$ splitting function is diagonal in spin space due to helicity conservation which is a consequence of the vector nature of the quark-gluon vertex.

cut diagram in Fig. 2.6. From this diagram we derive the squared matrix element

$$\begin{aligned}\mathcal{C}^{\mu\nu}_{g\to q\bar{q}} &= 4\pi\alpha_s\mu^{2\epsilon}T_R\frac{d^{\mu\rho}(i+r,n)}{s_{ir}}\,\mathrm{Tr}\,\gamma_\rho \not{i}\gamma_\sigma \not{r}\frac{d^{\sigma\nu}(i+r,n)}{s_{ir}} \\ &= 16\pi\alpha_s\mu^{2\epsilon}\frac{1}{s_{ir}^2}T_R\left[-g^{\mu\rho}+2\frac{(i+r)^\mu n^\rho+n^\mu(i+r)^\rho}{s_{(ir)n}}\right] \\ &\quad\times\left[i^\rho r^\sigma+r^\rho i^\sigma-\frac{1}{2}g^{\rho\sigma}s_{ir}\right]\left[-g^{\sigma\nu}+2\frac{(i+r)^\sigma n^\nu+n^\sigma(i+r)^\nu}{s_{(ir)n}}\right] \\ &= 16\pi\alpha_s\mu^{2\epsilon}\frac{1}{s_{ir}^2}T_R\left[F_0^{\mu\nu}+F_1^{\mu\nu}+F_1^{\nu\mu}+F_2^{\mu\nu}\right]\end{aligned} \tag{2.73}$$

where the functions $F_p^{\mu\nu}$ are defined according to the power of $s_{(ir)n} = s_{in} + s_{rn}$ in the denominator. These functions take the explicit form

$$F_0^{\mu\nu} = i^\mu r^\nu + r^\mu i^\nu - \frac{1}{2}g^{\mu\nu}s_{ir} \tag{2.74}$$

$$F_1^{\mu\nu} = \frac{1}{s_{(ir)n}}\left[-i^\mu(i+r)^\nu s_{rn} - r^\mu(i+r)^\nu s_{in} + n^\mu(i+r)^\nu s_{ir}\right] \tag{2.75}$$

$$F_2^{\mu\nu} = \frac{1}{s_{(ir)n}^2}\left[2(i+r)^\mu(i+r)^\nu s_{in}s_{rn}\right]. \tag{2.76}$$

We now insert the Sudakov parametrisation of Eq. (2.63) to expose the collinear limit

$$\begin{aligned}F_0^{\mu\nu} &= 2z_iz_rp^\mu p^\nu + (z_r+z_i)(k_\perp^\mu p^\nu + p^\mu k_\perp^\nu) - 2k_\perp^\mu k_\perp^\nu \\ &\quad + \frac{s_{ir}}{s_{pn}}(z_i^2+z_r^2)(p^\mu n^\nu + n^\mu p^\nu)\frac{1}{2}g^{\mu\nu}s_{ir} + \mathcal{O}\big(k_\perp^{-3}\big),\end{aligned} \tag{2.77}$$

$$F_1^{\mu\nu} + F_1^{\nu\mu} = -4z_iz_rp^\mu p^\nu + (z_i - z_r)\left(k_\perp^\mu p^\nu + p^\mu k_\perp^\nu\right) + \mathcal{O}\big(k_\perp^{-3}\big), \tag{2.78}$$

$$F_2^{\mu\nu} = 2z_iz_rp^\mu p^\nu + 2z_iz_r\frac{s_{ir}}{s_{pn}}\left(p^\mu n^\nu + n^\mu p^\nu\right) + \mathcal{O}\big(k_\perp^{-3}\big). \tag{2.79}$$

Inserting these pieces back into the expression for $\mathcal{C}_{g\to q\bar{q}}$ we find

$$\begin{aligned}\mathcal{C}^{\mu\nu}_{g\to q\bar{q}} &= 16\pi\alpha_s\mu^{2\epsilon}\frac{1}{s_{ir}^2}T_R\left[-\frac{1}{2}g^{\mu\nu}s_{ir} - 2k_\perp^\mu k_\perp^\nu + \frac{s_{ir}}{s_{pn}}\left(p^\mu n^\nu + n^\mu p^\nu\right)\right] + \mathcal{O}\big(k_\perp^{-1}\big) \\ &= 8\pi\alpha_s\mu^{2\epsilon}\frac{1}{s_{ir}}T_R\left[-g^{\mu\nu} + 4z_iz_r\frac{k_\perp^\mu k_\perp^\nu}{k_\perp^2} + \frac{p^\mu n^\nu + n^\mu p^\nu}{p\cdot n}\right] + \mathcal{O}\big(k_\perp^{-1}\big).\end{aligned} \tag{2.80}$$

This expression contains gauge dependent terms in the form of n^μ dependence. Due to gauge invariance these terms must vanish when the collinear splitting term is contracted with the full squared matrix element, and so we drop it from our explicit form of the AP splitting kernel. Again we insert a complete set of spin states, onto this for the unresolved gluon into Eq. (2.62) and this time we find

$$\mathbf{C}_{ir}|\mathcal{M}^{(0)}_{m+1}| = 8\pi\alpha_s\mu^{2\epsilon}\frac{1}{s_{ir}}\sum_{\mu,\nu}\langle\mathcal{M}^{(0)}_m|\mu\rangle\,\langle\mu|\,\hat{P}^{(0)}_{g\to q\bar{q}}\,|\nu\rangle\,\langle\nu|\mathcal{M}^{(0)}_m\rangle\,. \tag{2.81}$$

Comparing this to Eq. (2.80) we see that AP splitting kernel takes the form

$$\langle\mu|\,\hat{P}^{(0)}_{g\to q\bar{q}}(z_i,z_r,k_\perp;\epsilon)\,|\nu\rangle = T_R\left[-g^{\mu\nu} + 4z_iz_r\frac{k_\perp^\mu k_\perp^\nu}{k_\perp^2}\right], \tag{2.82}$$

which is not diagonal in the spin state of the unresolved gluon. In this case we see that Eq. (2.80) does not contain explicit forms of the external polarisation vectors ϵ^{μ} and $\epsilon^{\nu\star}$. This is because

$$\mathcal{C}^{\mu\nu}_{g\to qq} = d_{\mu\sigma}(i+r)\mathcal{C}^{\sigma\lambda}_{g\to qq}d_{\nu\lambda}(i+r)\,, \tag{2.83}$$

we see that the factors for the external gluons are present but hidden, recalling that $d_{\mu\nu}(p) = \epsilon_{\mu}(p)\epsilon^{\star}_{\nu}(p)$.

Collinear $g \to g + g$ splitting

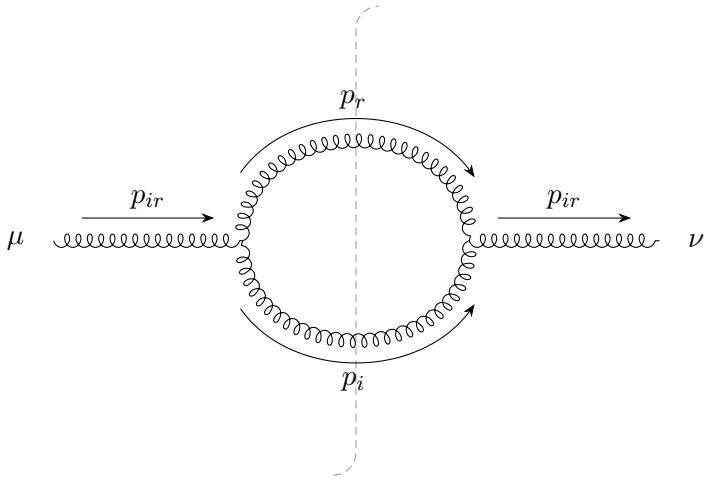

Figure 2.7: Cut diagram for the process $g \to g + g$

In the case of a gluon splitting into a pair of gluons, we must compute the cut diagram in Fig. 2.7. From this diagram we derive the squared matrix element

$$\begin{aligned}\mathcal{C}^{\mu\nu}_{g\to gg} &= 4\pi\alpha_s\mu^{2\epsilon}C_A\frac{d^{\mu\rho}(i+r,n)}{s_{ir}}V_{\rho\alpha\beta}(i+r,-i,-r)d^{\alpha\gamma}(i,n)V_{\sigma\gamma\delta}(-i-r,i,r)d^{\beta\delta}(r,n)\frac{d^{\sigma\nu}(i+r,n)}{s_{ir}}\\ &= 4\pi\alpha_s\mu^{2\epsilon}\frac{1}{s^2_{ir}}C_A\left[F_0^{\mu\nu}+F_0^{\nu\mu}+F_1^{\mu\nu}+F_1^{\nu\mu}+F_2^{\mu\nu}\right]\end{aligned} \tag{2.84}$$

where we again define functions $F_p^{\mu\nu}$ in terms of the power of $s_{(ir)n}$ in the denominator.

This time the functions take the explicit form

$$\begin{aligned}
F_0^{\mu\nu} &= -(1-\epsilon)(i+r)^\mu(i+r)^\nu - 4i^\mu r^\nu + 2i^\mu r^\nu \frac{s_{rn}}{s_{in}} + 2r^\mu r^\nu \frac{s_{in}}{s_{rn}} \\
&\quad + \frac{4s_{ir}}{s_{in}s_{rn}}\left(s_{rn}r^\mu n^\nu + s_{in}i^\mu n^\nu - s_{ir}n^\mu n^\nu\right) \\
&\quad + 2\left(\frac{s_{rn}}{s_{in}} + \frac{s_{in}}{s_{rn}}\right)\left(i^\mu r^\nu + (i+r)^\mu n^\nu - g^{\mu\nu}s_{ir}\right) , \qquad (2.85) \\
F_1^{\mu\nu} &= \frac{2}{s_{(ir)n}}\left[i^\mu(i+r)^\nu(1-2\epsilon)(s_{in}-s_{rn}) + (i+r)^\mu(i+r)^\nu(1-\epsilon)\right. \\
&\quad + n^\mu(i+r)^\nu s_{ir} + \frac{s_{in}^2}{s_{rn}}(i+r)^\mu(i+r)^\nu \\
&\quad \left. - \left(\frac{s_{rn}}{s_{in}} + \frac{s_{in}}{s_{rn}}\right)\left(i^\mu(i+r)^\nu s_{in} + n^\mu(i+r)^\nu s_{ir}\right)\right] , \qquad (2.86) \\
F_2^{\mu\nu} &= -\frac{2}{s_{(ir)n}}\left[2(1-\epsilon)(i+r)^\mu(i+r)^\nu(s_{in}+s_{rn})^2\right] . \qquad (2.87)
\end{aligned}$$

We simplify these expression using straightforward algebra, add together all of the terms, insert the Sudakov parametrisation and keep only the leading singular pieces to find

$$\begin{aligned}
\mathcal{C}_{g\to gg}^{\mu\nu} &= 4\pi\alpha_s\mu^{2\epsilon}C_A\left[\frac{4s_{ir}}{z_iz_r}g^{\mu\nu}(1-2z_iz_r) - 8(1-\epsilon)(z_ir^\mu - z_ri^\mu)(z_ir^\nu + z_ri^\nu)\right. \\
&\quad \left. + \frac{s_{ir}}{s_{pn}}\frac{4}{z_iz_r}\Big((i^\mu n^\nu + n^\mu i^\nu)(z_r - z_i) + ((i+r)^\mu n^\nu + n^\mu(i+r)^\nu)((3-2z_i)z_i - 2)\Big)\right] \\
&\quad + \mathcal{O}\big(k_\perp^{-1}\big) .
\end{aligned} \qquad (2.88)$$

We cast the expression into its more conventional form by extracting the universal singular term $1/s_{ir}$ and find

$$\begin{aligned}
\mathcal{C}_{g\to gg}^{\mu\nu} &= 4\pi\alpha_s\mu^{2\epsilon}C_A\frac{1}{s_{ir}^2}\left[8(1-\epsilon)k_\perp^\mu k_\perp^\nu - 4\left(\frac{z_i}{z_r} + \frac{z_r}{z_i}\right)g^{\mu\nu}s_{ir}\right. \\
&\quad \left. -4\left(\frac{z_i}{z_r} - \frac{z_r}{z_i}\right)s_{ir}\frac{n^\mu p^\nu + p^\mu p^\nu}{s_{pn}}\right] + \mathcal{O}\big(k_\perp^{-1}\big) \\
&= 8\pi\alpha_s\mu^{2\epsilon}\frac{1}{s_{ir}}2C_A\left[-g^{\mu\nu}\left(\frac{z_i}{z_r} + \frac{z_r}{z_i}\right) - 2(1-\epsilon)z_iz_r\frac{k_\perp^\mu k_\perp^\nu}{k_\perp^2}\right. \\
&\quad \left. - \left(\frac{z_i}{z_r} + \frac{z_r}{z_i}\right)\frac{n^\mu p^\nu + p^\mu n^\nu}{p\cdot n}\right] + \mathcal{O}\big(k_\perp^{-1}\big) .
\end{aligned} \qquad (2.89)$$

From Eq. (2.89) we find the LO AP splitting kernel

$$\langle\mu|\,\hat{P}_{g\to gg}^{(0)}(z_i,z_r,k_\perp;\epsilon)\,|\nu\rangle = 2C_A\left[-g^{\mu\nu}\left(\frac{z_i}{z_r} + \frac{z_r}{z_i}\right) - 2(1-\epsilon)z_iz_r\frac{k_\perp^\mu k_\perp^\nu}{k_\perp^2}\right] . \qquad (2.90)$$

Again the factors from the external gluons are not explicitly present.

Spin averaged splitting kernels

Equations (2.72), (2.82) and (2.90) lead to the more familiar form of the d-dimensional splitting functions after averaging over the polarisations of the unresolved parton (ir).

The d-dimensional average is obtained by means of the factors

$$\frac{1}{2}\delta_{ss'} \tag{2.91}$$

for a fermion, and (the gauge terms are proportional either to p^μ or to p^ν)

$$\frac{1}{d-2}d_{\mu\nu}(p) = \frac{1}{2(1-\epsilon)}(-g_{\mu\nu} + \text{gauge terms})\,, \tag{2.92}$$

with

$$-\,g^{\mu\nu}d_{\mu\nu}(p) = d-2\,, \quad p^\mu d_{\mu\nu}(p) = 0\,, \tag{2.93}$$

for a gluon with on-shell momentum p. Denoting by $\left\langle \hat{P}^{(0)}_{(ir)\to i+r} \right\rangle$ the average of $\hat{P}^{(0)}_{(ir)\to i+r}$ over the polarisations of the parton (ir), we find

$$\left\langle \hat{P}^{(0)}_{q\to qg}(z_i,z_r;\epsilon) \right\rangle = C_F\left[\frac{1+z_i^2}{z_r} - \epsilon z_r\right]\,, \tag{2.94}$$

$$\left\langle \hat{P}^{(0)}_{q\to gq}(z_i,z_r;\epsilon) \right\rangle = C_F\left[\frac{1+z_r^2}{z_i} - \epsilon z_i\right]\,, \tag{2.95}$$

$$\left\langle \hat{P}^{(0)}_{g\to q\bar{q}}(z_i,z_r;\epsilon) \right\rangle = T_R\left[1 - \frac{2z_iz_r}{1-\epsilon}\right]\,, \tag{2.96}$$

$$\left\langle \hat{P}^{(0)}_{g\to gg}(z_i,z_r;\epsilon) \right\rangle = 2C_A\left[\frac{z_i}{z_r} + \frac{z_r}{z_i} + z_iz_r\right]\,. \tag{2.97}$$

2.6.2 Soft factorisation

In the soft limit a gluon can be emitted from any of the external legs, and as a result we cannot use cut graphs, instead we must factorise at the level of the amplitude. We introduce the operator

$$\mathbf{S}_s\,\langle c_s|\mathcal{M}^{(0)}_{m+1}\rangle = g_s\epsilon^\lambda_\mu(s)\mathbf{J}^\mu(s)\,|\mathcal{M}^{(0)}_m\rangle\,, \tag{2.98}$$

which takes the soft limit of the amplitude, keeping only the most singular term. The factor $\mathbf{J}$ is the soft gluon current and c_s is the colour of the soft gluon. For the squared matrix element this implies the following factorisation

$$\begin{aligned}\mathbf{S}_s|\mathcal{M}^{(0)}_{m+1}|^2 &= 4\pi\alpha_s\mu^{2\epsilon}\epsilon^\lambda_\mu(s)\epsilon^{\lambda\star}_\nu(s)\,\langle\mathcal{M}^{(0)}_m|\,\mathbf{J}^\mu(s)\mathbf{J}^\nu(s)\,|\mathcal{M}^{(0)}_m\rangle \\ &= -8\pi\alpha_s\mu^{2\epsilon}\sum_{i,j=1}^{m}\mathcal{S}_{ij}(s)\,\langle\mathcal{M}^{(0)}_m|\,\mathbf{T}_i\cdot\mathbf{T}_j\,|\mathcal{M}^{(0)}_m\rangle \\ &\qquad + \text{gauge terms}\,,\end{aligned} \tag{2.99}$$

where we have used $\epsilon^\lambda_\mu(s)\epsilon^\lambda_\nu(s) = d_{\mu\nu}(s)$ and we have defined $\mathcal{S}_{ij}(k)$ as

$$\mathcal{S}_{ij}(s) = \frac{s_{ij}}{s_{is}s_{js}}\,. \tag{2.100}$$

$\mathcal{S}_{ij}(s)$ is the so called eikonal factor.

In the case of a soft gluon emission we have the following theorem:

1. *The leading soft singularities are due to the emission of soft gluons off external, or, in general, nearly on-shell partons* [25, 26].

Soft gluon emission from a quark

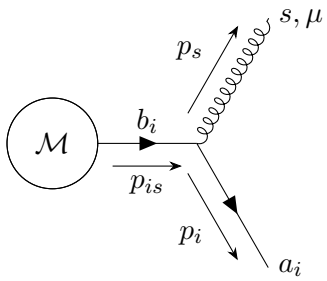

Figure 2.8: soft gluon emission from a quark

For the case of a soft gluon emission from a quark line, we must compute the diagram in Fig. 2.8. From this diagram we derive the amplitude

$$\mathcal{M}^{\lambda}_{m+1} = g_s \mu^{\epsilon} (t^s)_{a_i b_i} \bar{u}(i) \gamma^{\mu} \frac{\not{l} + \not{s}}{s_{is}} \epsilon^{\lambda}_{\mu}(s) \widetilde{\mathcal{M}}_m \,. \tag{2.101}$$

Inserting the parametrisation $s = \lambda q$ and keeping only the most singular terms we find

$$\begin{aligned} \mathcal{M}^{\lambda}_{m+1} &= g_s \mu^{\epsilon} (t^s)_{a_i b_i} \frac{1}{s_{is}} \bar{u}(i) \gamma^{\mu} \not{l} \epsilon^{\lambda}_{\mu}(s) \widetilde{\mathcal{M}}_m + \mathcal{O}\big(\lambda^0\big) \\ &= -g_s \mu^{\epsilon} (t^s)_{a_i b_i} \bar{u}(i) \not{l} \gamma^{\mu} \epsilon^{\lambda}_{\mu}(s) \widetilde{\mathcal{M}}_m + 2 g_s \mu^{\epsilon} (t^s)_{a_i b_i} \frac{1}{s_{is}} \bar{u}(i) i^{\mu} \epsilon^{\lambda}_{\mu}(s) \widetilde{\mathcal{M}}_m + \mathcal{O}\big(\lambda^0\big) \\ &= g_s \mu^{\epsilon} (t^s)_{a_i b_i} \frac{i^{\mu}}{i \cdot s} \epsilon^{\lambda}_{\mu}(s) \mathcal{M}_m + \mathcal{O}\big(\lambda^0\big) \end{aligned} \tag{2.102}$$

where we have used the Dirac equation $\bar{u}(i) \not{l} = 0$.

Soft gluon emission from a gluon

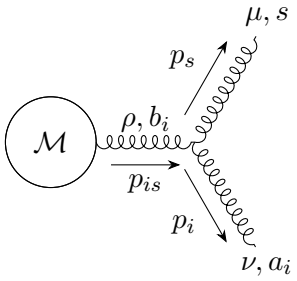

Figure 2.9: soft gluon emission from a gluon

For the case of a soft gluon emission from a gluon line, we must compute the diagram in Fig. 2.9. From this diagram we derive the amplitude

$$\mathcal{M}_{m+1}^{\lambda\lambda'} = \mu^{\epsilon} \frac{i\, d^{\rho\rho'}(i+s,n)}{s_{is}} \Gamma^{a_i s\, b_i}_{\nu\mu\rho'}(-i,-s,i+s)\epsilon_{\mu}^{\lambda}(s,n)\epsilon_{\nu}^{\lambda'}(i,n)\widetilde{\mathcal{M}}_m\,, \tag{2.103}$$

where in the soft limit the three-gluon vertex takes the form

$$\begin{aligned} V^{\nu\mu\rho}(-i,-s,i+s) &= -(i+2s)^{\nu} g^{\mu\rho} + (2i+s)^{\mu} g^{\nu\rho} - (i-s)^{\rho} g^{\mu\nu} \\ &= 2i^{\mu} g^{\nu\rho} + [-(i+s)^{\rho} g^{\mu\nu} - i^{\nu} g^{\mu\rho}] + [s^{\mu} g^{\nu\rho} + 2s^{\rho} g^{\mu\nu} - 2s^{\nu} g^{\mu\rho}] \\ &\simeq 2i^{\mu} g^{\nu\rho} - [(i+s)^{\rho} g^{\mu\nu} + i^{\nu} g^{\mu\rho}]\,. \end{aligned} \tag{2.104}$$

We use $d^{\rho\rho'}(i+s,n)(i+s)_{\rho} = 0$ and $\epsilon^{\nu}(i,n) i_{\nu} = 0$, to derive

$$\begin{aligned} i\, d^{\rho\rho'}(i+s,n)\Gamma^{a_i s\, b_i}_{\nu\mu\rho'}(-i,-s,i+s)\epsilon_{\nu}^{\lambda}(i,n) &= g_s(-if^{a_i s\, b_i}) 2i^{\mu} \left[d^{\rho\rho'}(i,n) g^{\nu\rho'} \epsilon_{\nu}^{\lambda}(i,n) \right] \\ &= -g_s(-if^{a_i s\, b_i}) 2i^{\mu} \epsilon_{\nu}^{\lambda}(i,n) \\ &= g_s(if^{a_i s\, b_i}) 2i^{\mu} \epsilon_{\nu}^{\lambda}(i,n)\,. \end{aligned} \tag{2.105}$$

Using this we find the final result

$$\mathcal{M}_{m+1}^{\lambda\lambda'} = g_s \mu^{\epsilon} (if^{a_i s\, b_i}) \frac{i^{\mu}}{i\cdot s} \epsilon_{\mu}^{\lambda}(s,n)\, \mathcal{M}_m^{\lambda'} + \mathcal{O}\big(\lambda^0\big)\,. \tag{2.106}$$

We see that in the soft limit we have the same kinematic factor but a different colour structure. These can be combined together into the soft gluon current, making use of the abstract colour operator $\mathbf{T}_i$ as defined in Eq. (2.58) and Eq. (2.59)

$$\mathbf{J}^{\mu}(s) = \sum_{i=1}^{m} \mathbf{T}_i \frac{i^{\mu}}{i\cdot s}\,. \tag{2.107}$$

The soft gluon can be emitted from any of the external legs, therefore the sum in the previous formula runs over all the external partons. And colour conservation in Eq. (2.61) implies that the current $\mathbf{J}^{\mu}(s)$ is conserved

$$s_{\mu}\mathbf{J}^{\mu}(s)\,|\mathcal{M}_m^{(0)}\rangle = \sum_{i=1}^{m} \mathbf{T}_i\,|\mathcal{M}_m^{(0)}\rangle = 0\,. \tag{2.108}$$

2.6.3 Soft-collinear overlap

There is a region of phase space in which the soft and collinear singularities overlap. Physically his corresponds to a soft gluon becoming collinear with its emitter. Such a situation provides the most singular IR contribution to the squared matrix element in

QCD. To determine the form of the soft-collinear matrix element we must determine the action of the collinear operator $\mathbf{C}$ on the soft operator $\mathbf{S}$ or more precisely

$$\mathbf{C}_{ir}\mathbf{S}_r|\mathcal{M}^{(0)}_{m+1}|^2 . \tag{2.109}$$

When the soft gluon (r) becomes collinear to its emitter (i) we can simplify the eikonal factor by noting that in the collinear limit $s_{ik} \to z_i s_{pk}$ and $s_{kr} = z_r s_{pk}$

$$\mathcal{S}_{ij} = \frac{s_{ij}}{s_{ir}s_{jr}} \to \frac{z_i}{z_r}\frac{1}{s_{ir}} . \tag{2.110}$$

So that we can write the soft and collinear limit as

$$\mathbf{C}_{ir}\mathbf{S}_r|\mathcal{M}^{(0)}_{m+1}|^2 = -8\pi\alpha_s\mu^{2\epsilon}\frac{2}{s_{ir}}\sum_{j\neq i}\frac{z_i}{z_r}\langle\mathcal{M}^{(0)}_m|\,\mathbf{T}_i\cdot\mathbf{T}_j\,|\mathcal{M}^{(0)}_m\rangle . \tag{2.111}$$

Making use of colour conservation Eq. (2.61) we can simplify further to find

$$\mathbf{C}_{ir}\mathbf{S}_r|\mathcal{M}^{(0)}_{m+1}|^2 = 8\pi\alpha_s\mu^{2\epsilon}\frac{2}{s_{ir}}\frac{z_i}{z_r}\mathbf{T}_i^2|\mathcal{M}^{(0)}_m|^2 , \tag{2.112}$$

where we note there are no longer colour-correlations between the partons emitting and absorbing the soft gluon. One further thing is that as we are in the soft limit $z_r \simeq 0$ which implies $z_i = 1 - z_r \simeq 1$, so we can simplify further to find

$$\mathbf{C}_{ir}\mathbf{S}_r|\mathcal{M}^{(0)}_{m+1}|^2 = 8\pi\alpha_s\mu^{2\epsilon}\frac{2}{s_{ir}}\frac{1}{z_r}\mathbf{T}_i^2|\mathcal{M}^{(0)}_m|^2 . \tag{2.113}$$

We can also consider taking the limit the other way around, first considering a collinear emission and then taking the soft limit. The algebra is much the same as before, and we find

$$\mathbf{S}_r\mathbf{C}_{ir}|\mathcal{M}^{(0)}_{m+1}|^2 = 8\pi\alpha_s\mu^{2\epsilon}\frac{2}{s_{ir}}\frac{1}{z_r}\mathbf{T}_i^2|\mathcal{M}^{(0)}_m|^2 . \tag{2.114}$$

We find that for a single soft and/or collinear emission the soft and collinear operators commute

$$[\mathbf{S}_r, \mathbf{C}_{ir}]|\mathcal{M}^{(0)}_{m+1}|^2 = 0 . \tag{2.115}$$

2.7 Infrared and collinear safety

So far we have examined how the cross-section can be calculated in QCD, the cross-section is a special kind of observable, called an *inclusive observable*. An inclusive observable is one where the phase space weight function F_J in Eq. (2.2) is set equal to 1. This is to be contrasted with *exclusive observables* where F_J can be a generic function with some important restrictions that we will come to shortly. We have also studied how QCD matrix

elements behave in the soft and/or collinear limits, with this knowledge of the soft and collinear behaviour of QCD matrix elements we can analyse the more general question: how do we compute exclusive quantities.

To see what happens we will return to the case of $e^+e^- \to$ hadrons (where we average over the event orientation), only this time we will consider an exclusive measurement. We parametrise the measurement using a jet function. We will do the calculation in the soft and collinear limits to see the properties that our observable must satisfy to be calculable within pQCD. In the soft (and optionally collinear) limit

$$\left|\mathcal{M}(e^+e^- \to q\bar{q}g)\right|^2 = \left|\mathcal{M}(e^+e^- \to q\bar{q})\right| 16\pi\alpha_s C_F \frac{s_{q\bar{q}}}{s_{qg}s_{\bar{q}g}} \tag{2.116}$$

The soft approximation can be applied also to the loop amplitude. In this limit we can in general neglect powers of the loop momentum q in the numerator if $q^\mu \ll \sqrt{Q^2}$, furthermore in the denominator we can use the fact that $q^2 \ll k_i \cdot q$. The loop correction to quark-antiquark pair production is therefore proportional to

$$\begin{aligned}\bar{u}(p_q)\Gamma^\mu v(p_{\bar{q}}) &= -ig_s^2\mu^{2\epsilon}C_F \int \frac{\mathrm{d}^d k}{(2\pi)^d} \frac{\bar{u}(p_q)\gamma^\rho(\not{p}_q + \not{k})\gamma^\mu(\not{k} - \not{p}_{\bar{q}})\gamma_\rho v(p_{\bar{q}})}{[(p_q+k)^2+i\epsilon][(k-p_{\bar{q}})^2+i\epsilon][k^2+i\epsilon]} \\ &= [\bar{u}(p_q)\gamma^\mu v(p_{\bar{q}})] I_s(p_q, p_{\bar{q}})\,,\end{aligned} \tag{2.117}$$

where

$$I_s(p_q, p_{\bar{q}}) = -ig_s^2\mu^{2\epsilon}2C_F \int \frac{\mathrm{d}^d k}{(2\pi)^d} \frac{(2p_q \cdot p_{\bar{q}})}{[2p_q\cdot k + i\epsilon][-2k\cdot p_{\bar{q}} + i\epsilon][k^2+i\epsilon]}\,. \tag{2.118}$$

The result in $d = 4$ can be evaluated in the centre of mass frame of the q and $\bar{q}$ partons with

$$p_q^\mu = E_q\,(1,0,0,1)\;, \quad p_{\bar{q}}^\mu = E_{\bar{q}}\,(1,0,0,-1)\;, \quad k^\mu = (k_0, \vec{k}) \text{ with } \vec{k} = (\vec{k}_\perp, k_z)\,, \tag{2.119}$$

where $\vec{k}_\perp$ is the vectorial transverse momentum and we define $k_\perp \equiv |\vec{k}_\perp|$. With this parametrisation we can recast Eq. (2.118) into the following form

$$I_s = -ig_s^2\mu^{2\epsilon}2C_F \int \frac{\mathrm{d}^3 k}{(2\pi)^4} \frac{2\,\mathrm{d}k_0}{[k_0 - k_z + i\epsilon][-k_0 - k_z + i\epsilon][k_0^2 - k_z^2 - k_\perp^2 + i\epsilon]}\,. \tag{2.120}$$

Eq. (2.120) has four poles in the complex k_0 plane at

$$k_0 = k_z - i\epsilon, \qquad k_0 = -k_z + i\epsilon, \qquad k_0 = \pm(|\vec{k}| + i\epsilon)\,, \tag{2.121}$$

closing the contour from below we find

$$I_s = -g_s^2\mu^{2\epsilon}2C_F \int \frac{\mathrm{d}^3 k}{(2\pi)^3} \left[\frac{1}{2|\vec{k}|}\frac{(2p_q\cdot p_{\bar{q}})}{(2p_q\cdot k)(2p_{\bar{q}}\cdot k)} + \frac{1}{2}\frac{1}{(k_z - i\epsilon)(k_\perp^2)}\right]\,, \tag{2.122}$$

where the second integral is a pure phase

$$\int \frac{\mathrm{d}k_z \mathrm{d}^2 k_\perp}{(2\pi)^3} \frac{1}{(k_z - i\epsilon)(k_\perp^2)} = -\int \mathrm{d}k_z \frac{k_z + i\epsilon}{k_z^2 + i\epsilon} \int \frac{\mathrm{d}k_\perp}{(2\pi)^2} \frac{1}{k_\perp} = -\frac{(i\pi)}{(2\pi)^2} \int \frac{\mathrm{d}k_\perp}{k_\perp} . \tag{2.123}$$

This phase term is referred to as a *Coulomb phase*. When considering physical observables this phase term is often zero, however in the presence of many hard coloured legs this term can give a measurable effect. For the observables considered in this thesis the Coulomb phase will always cancel, and so we shall not discuss this term any further.

We can now combine everything together. Once again we use Eq. (2.2) to write down the cross-section, we take the real contribution from Eq. (2.116) and the virtual contribution from the first term in Eq. (2.122). In $d = 4$ we have

$$\begin{aligned} \sigma_{F_J} =& \frac{1}{2s} \int \mathrm{d}\Phi_2 \frac{1}{4} \sum_{\text{spins.}} |\mathcal{M}(e^+e^- \to q\bar{q})|^2 F_J^{(2)}(p_q, p_{\bar{q}}) + \\ & \frac{1}{2s} \int \mathrm{d}\Phi_2 \frac{1}{4} \sum_{\text{spins.}} |\mathcal{M}(e^+e^- \to q\bar{q})|^2 16\pi\alpha_s C_F \int \frac{\mathrm{d}^3 k}{(2\pi)^3} \frac{1}{2|\vec{k}|} \frac{s_{q\bar{q}}}{s_{qg} s_{\bar{q}g}} \\ & \times \left[F_J^{(3)}(p_q, p_{\bar{q}}, k) - F_J^{(2)}(p_q, p_{\bar{q}}) \right] . \end{aligned} \tag{2.124}$$

- To ensure that the IRC poles cancel between the real and the virtual contributions the observable must be infrared and collinear safe [27]. Formally this means that the jet functions F_J must satisfy the following properties

$$F_J^{(n+1)}(\dots, p_i, \dots) \to F_J^{(n)}(\dots, p_{i-1}, p_{i+1}, \dots) \qquad \text{if } p_i \to 0 , \tag{2.125}$$

$$F_J^{(n+1)}(\dots, p_i, p_j, \dots) \to F_J^{(n)}(\dots, p_i + p_j, \dots) \qquad \text{if } p_i \parallel p_j . \tag{2.126}$$

  for all $n \geq m$, and

$$F_J^{(m)}(p_1, \dots, p_m) \to 0 \quad \text{if } p_i \cdot p_j \to 0 . \tag{2.127}$$

  Equations (2.125) and (2.126) respectively guarantee that the observable is infrared and collinear safe for any number of n final-state partons to any order in pQCD. The n-parton jet function $F_J^{(n)}$ on the right hand side of Eq. (2.125) is obtained from the original $F_J^{(n+1)}$ by removing the soft parton p_i, and that on the right-hand side of Eq. (2.126) by replacing the collinear partons $\{p_i, p_j\}$ by $p_i + p_j$. The final condition, Eq. (2.127) defines the leading order cross section and ensures that the Born level cross section is finite in $d = 4$.

  These limits must hold not only for a single particle, but also for an ensemble of partons becoming soft and/or collinear.

- In the case of inclusive observables, for which $F_J^{(m)}(p_1, \dots, p_m) = 1$ for all m, as was the case in our computation of $e^+e^- \to$ hadrons. We see that for an inclusive

observable in the IR limit the cancellation between the real and virtual is complete. This tells us that the total cross section is unchanged by the emission of soft particles.

- In the case of an exclusive, IRC safe observable, the singularities cancel, but the kinematic dependence of the observable can cause an imbalance in the cancellation of the real and virtual corrections. In such cases the emission of soft and/or collinear radiation can have a substantial impact on the observable. These remnants of the imbalance in the cancellation of the real and virtual manifest as logarithms to all orders in perturbation theory.

Chapter 3

Jet observables

In our discussion of QCD we have performed some simple calculations in the perturbative regime. This is not the full story, QCD is characterised by the phenomena of asymptotic freedom and confinement. Asymptotic freedom tells us that at high energies the dynamics of QCD are those of quarks and gluons, yet confinement tells us that we do not observe quarks and gluons, at low energies they exist only as bound states in the form of hadrons. In the SM this peculiar feature is unique to QCD[1] and it means that what we measure in a detector are final states consisting of hadrons, leptons and photons, not quarks and gluons. Between the hard scattering event (that we can compute in pQCD) and the measured final state the formation of hadrons will take place via the mechanism of *hadronisation*. Hadronisation is an entirely non-perturbative phenomenon and as a result cannot be calculated within the framework of pQCD. In order to retain the predictivity of our pQCD calculations we must find observables that are independent of the nature of the final state particles.

The mechanisms between the hard scattering and the measurement of final state particles are represented pictorially in Fig. 3.1 and can be qualitatively described as follows.

- Hard scattering event between the most energetic incoming partons taking place at an energy of the order of the centre of mass energy Q, so that the coupling $\alpha_s(Q) \ll 1$. These are the red circles in Fig. 3.1.

- High energy partons radiate many further real emissions of considerable energy, each of these emissions has a scale of the order of the transverse momentum of the emission k_t. These are emitted such that $\alpha_s(Q) \ll \alpha_s(k_t) < 1$. These are the red

[1] Confinement is a property of any theory with a negative β-function.

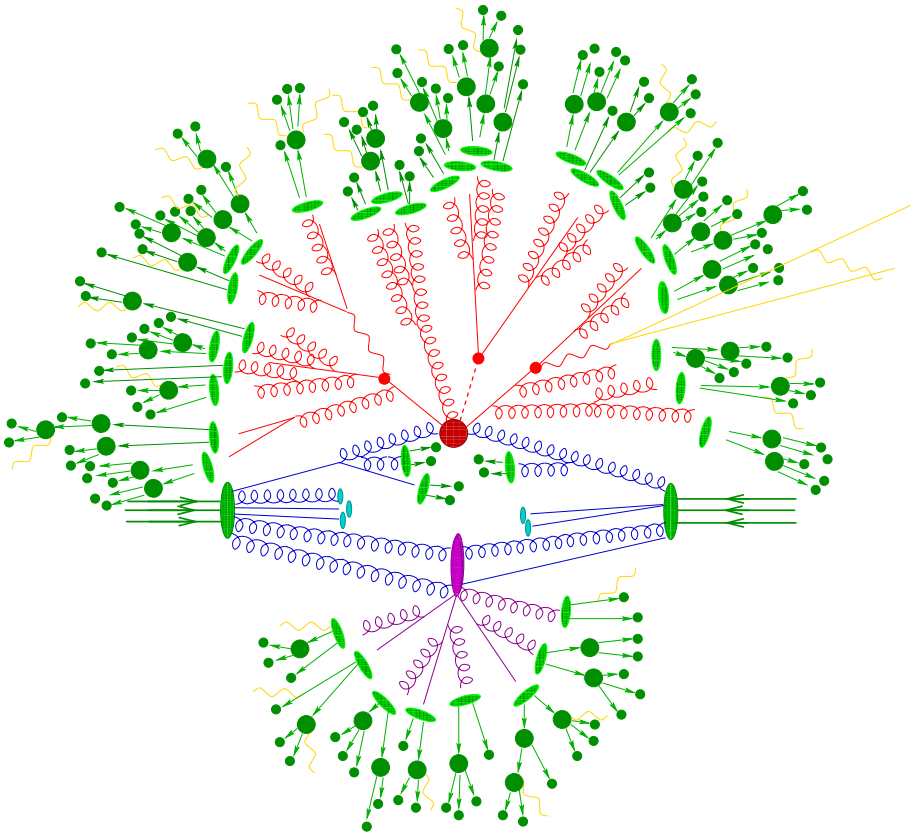

Figure 3.1: Pictorial representation of a $t\bar{t}h$ event [28].

lines immediately attached to the small red circles in Fig. 3.1.

- The partons continue to radiate, as the energy of the partons becomes smaller the emission of soft and/or collinear partons becomes highly probable, owing to the singular structure of the QCD matrix elements. Again these emissions have a scale of the order of the transverse momentum of the emission k_t. However due to the small k_t of these emissions even though the coupling remains perturbative the integral over the phase space and matrix element squared

$$\int \frac{\mathrm{d}z}{z}\frac{\mathrm{d}k_t}{k_t}\alpha_s(k_t) \gg 1\,, \tag{3.1}$$

can become very large. This emission of many soft and collinear partons can be modelled via the so called *parton shower*. The showering is approximately unitary, meaning that the momenta of partons is shuffled around as further partons are radiated but the rate remains constant. The couple ensemble of partons continue to shower until they have energies around the scale Λ_{QCD}. These are the red gluons and quark antiquark pairs attached to the red lines and the the blue gluons and quark antiquark pairs before the the central hard scattering in Fig. 3.1.

- Hadronisation takes place at scales of the order Λ_{QCD}, turning our collimated sprays of partons into colourless hadrons. This means that the coupling $\alpha_s(k_t) \simeq 1$. These are the green ovals at the end of the red lines in Fig. 3.1, the green circles following the green ovals are the final state hadrons that we see in the detector after the primary hadrons decay.

- The purple lines and oval are *multi-parton interactions* (MPI), also referred to as the *underlying event* (UE). The underlying event consists of all the secondary interactions that are less energetic than the hard scattering event. In general the UE mostly contributes a constant soft background of hadrons to each event.

- The light blue ovals are beam remnants, fragments of the colliding protons that did not take part in the interaction. These fragments make up part of the UE.

This is the essence of what goes on at a hadron collider. Let us consider the structure of the matrix elements further, the collinear singularities originate from $k_\perp \to 0$, this indicates that the most probable course of the shower is to generate very collinear partons. Rather than trying to consider these huge final states we consider instead clustering hadrons that are close by in terms of $k_\perp$ together into so called *jets*. The idea being that for a suitably defined jet we are able to capture the dynamics of the hard event in such a way that hadronisation does not have a large impact on predictions made at the parton level. A priori there is no reason to believe that the effect of hadronisation should be small, fortunately studies at high energies have shown that these corrections are indeed small, provided suitable observables are used.

The study of jets is important for measuring many aspects of QCD. Jets have become a way to compare theoretical calculations at the parton level and experimentally measured quantities in hadronic final states.

3.1 What is a jet

Having talked through some properties of QCD and the behaviours we would like in a jet we must set about the topic with more formality. A formal definition of a jet is through a *jet definition*, which consists of three elements:

1. A *jet algorithm*—a set of rules to recombine particles into a jet.

2. The *parameters* of the algorithm

3. A *recombination scheme*—a rule on how to define the four momentum of the jet.

A good jet definition, as agreed upon by the scientific community, must meet some basic requirements, this is outlined in a document known as the "Snowmass accord" [29]. The requirements of a good jet definition are as follows

1. Simple to implement in an experimental analysis
2. Simple to implement in a theoretical calculation
3. Defined at any order of perturbation theory
4. Yields finite cross section at any order of perturbation theory
5. Yields a cross section that is relatively insensitive to hadronisation

These requirements ensure that jets are well defined and consistent regardless of the representation of the hard scattering event that we choose to work with. By choosing a jet definition that is insensitive to hadronisation we can treat jets as objects composed of either hadrons or partons. Practically this allows us to directly compare the results of experiments to the predictions of Monte Carlo event generators and theoretical calculations performed at the parton level.

There are many different jet algorithms in the literature, however they can be divided into two broad classes:

- *cone algorithms*, which take a "top down" approach to clustering. We look for stable cone-like structures in the event.
- *sequential recombination algorithms*, which take a "bottom up" approach to clustering. We iteratively recombine the two particles closest to one another according to a distance measure.

We will only be working with algorithms of the sequential recombination variety, so we will briefly review the features of the most common sequential recombination algorithms, discussing their relevant characteristics. A more comprehensive review on the topic of jets can be found in Ref. [30].

Before we consider the sequential recombination algorithms we must first define a suitable recombination scheme. The simplest, and the most commonly used, example of such scheme is the so called E-scheme. In the E-scheme the four momentum of a jet is given by the sum of the four momentum of each constituent. Whilst there are other possible recombination schemes that are used in e.g. jet substructure, in this thesis we will only consider jets defined using the E-scheme.

3.2 Sequential recombination algorithms

One of the first sequential recombination algorithms is the *Jade algorithm* [31], proposed by the JADE collaboration in the context of e^+e^- collisions. It depends on a single parameter y_{cut}. The algorithm proceeds as follows

1. For each pair of particles i, j compute the distance measure

$$y_{ij}^{\text{Jade}} = \frac{2E_iE_j(1-\cos\theta_{ij})}{Q^2} = \frac{m_{ij}^2}{Q^2}\,, \tag{3.2}$$

   where Q is the total energy in the event, θ_{ij} is the angle between particles i and j, and E_i is the energy of the particle i.

2. Find the minimum y_{min} of all the possible y_{ij}^{Jade},

   (a) If $y_{\text{min}} < y_{\text{cut}}$, merge the particles i and j into a single new particle (or pseudo-jet) k making use of the chosen recombination scheme to combine their momenta, replace the particles i and j by the new particle k. Iterate from step 1.

   (b) If $y_{\text{min}} > y_{\text{cut}}$ declare that all of the remaining particles are jets and terminate the iteration.

Unfortunately the Jade algorithm suffers from an undesirable feature due to the use of the invariant mass as a distance measure. In the early stages of clustering two very soft particles travelling in opposite directions may be recombined into a single jet owing to the invariant mass term in the measure, an example of such a configuration is shown in Fig. 3.2.

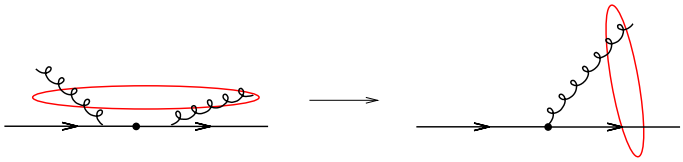

Figure 3.2: An example of a configuration where the Jade algorithm does not recombine child emissions with their correct parent [32].

The problems with the Jade algorithm can be overcome by a simple redefinition of the distance measure, defining a new algorithm the k_t *algorithm* or *Durham algorithm* [33]. The Durham algorithm uses the distance measure

$$y_{ij}^{\text{Durham}} = \frac{2\min(E_i^2, E_j^2)(1-\cos\theta_{ij})}{Q^2}\,, \tag{3.3}$$

which at small angles between the partons becomes the relative transverse momentum, which alleviates the problems with the Jade algorithm. This new distance measure is closely related to the singular structure of QCD matrix elements, and the clustering proceeds roughly in the inverse order in which the partons were emitted.

In defining jets at hadron colliders there are new technicalities that we must address. The first is that in e^+e^- collisions we have made use of a dimensionless distance measure, however in hadron collisions it is difficult to determine the total energy of the event. To avoid this issue we can introduce a dimensional variant of the Durham measure [34, 35], and, changing the variables such that they are invariant under longitudinal boosts

$$d_{ij}^{k_t} = \min(p_{ti}^2, p_{tj}^2)\frac{\Delta R_{ij}^2}{R^2}\,, \tag{3.4}$$

where p_{ti} is the transverse momentum of the constituent i, R is a parameter relating to the radius of the jet and ΔR_{ij} is the distance between the constituents i and j,

$$\Delta R_{ij}^2 = (y_i - y_j)^2 + (\phi_i - \phi_j)^2\,, \tag{3.5}$$

where y_i is the rapidity and ϕ_i is the azimuthal angle of parton i.

The second technicality is that in hadronic collisions we can have interactions between the outgoing partons and the incoming beam, which can lead to extra emissions in the detector. The *inclusive-k_t algorithm* [35] was introduced to address these additional effects. We introduce the notion of a particle beam distance

$$d_{iB}^{k_t} = p_{ti}^2\,. \tag{3.6}$$

The algorithm then proceeds as follows

1. For each subjet and pair of subjets determine $d_{ij}^{k_t}$ and $d_{iB}^{k_t}$
2. Find the minimum among all distances $d_{ij}^{k_t}$ and $d_{iB}^{k_t}$
   (a) If it is a distance between subjets $d_{ij}^{k_t}$, merge i and j into a new subjet
   (b) Otherwise, if it is a "beam distance" $d_{iB}^{k_t}$, i is a final state jet and it is removed from the list
3. Return to step 1 until there are no more subjets, then stop

We can extend the inclusive k_t algorithm by introducing an additional angular parameter p that defines the *generalised-k_t algorithm* with a distance measure

$$d_{ij}^{\mathrm{gen}-k_t} = \min(p_{ti}^{2p}, p_{tj}^{2p})\frac{\Delta R_{ij}^2}{R^2}\,, \quad d_{iB}^{\mathrm{gen}-k_t} = p_{ti}^{2p}\,, \tag{3.7}$$

from which we recover the inclusive-k_t algorithm by setting $p = 1$. Setting $p = 0$ we have the *Cambridge/Aachen algorithm* (C/A) [36], one of the standard algorithms. A particularly important case of the generalised-k_t algorithm is that of $p = -1$, this defines the *anti-k_t algorithm* [37], with the distance measure given explicitly by

$$d_{ij}^{\text{anti}-k_t} = \min\left(\frac{1}{p_{ti}^2}, \frac{1}{p_{tj}^2}\right)\frac{\Delta R_{ij}^2}{R^2}\,, \quad d_{iB}^{\text{anti}-k_t} = \frac{1}{p_{ti}^2}\,. \tag{3.8}$$

The distance measure of the anti-k_t algorithm is such that the hardest particles in a jet are clustered first, this makes the jets formed by the anti-k_t algorithm very stable, and has the interesting consequence that the jets formed are (almost) perfect cones. In some sense the anti-k_t algorithm is in fact the perfect cone algorithm. For these reasons the anti-k_t algorithm is the most used algorithm at hadron colliders.

3.3 Jet-rates and Jet-vetoes

With our jet definitions we can proceed to create observables that characterise specific properties of the final-state jets in an event. The simplest such observables are jet cross sections and the closely related jet-rate. The n-jet cross section is defined simply as the cross section for the production of n final-state jets, i.e. we just count the number of jets. The jet cross section clearly depends on our choice of jet algorithm and on the parameters of the algorithm. Jet-rates are simply the fraction of events classified with a given number of jets, i.e. the jet cross section normalised to the total hadronic cross section. For example the three-jet rate can be written as

$$\Sigma_3(y_{\text{cut}}) = \frac{\sigma_{3-\text{jets}}(y_{\text{cut}})}{\sigma}\,, \tag{3.9}$$

where $\sigma_{3-\text{jets}}$ is the three-jet cross section, σ is the total hadronic cross section and y_{cut} is the cut-off used in the jet algorithm.

Another jet observable is the transverse momentum of the *leading jet*. We can define the cumulative distribution of the leading jet transverse momentum as follows

$$\Sigma(p_t^J) = \sum_{n=0}^{\infty}\int \mathrm{d}\Phi_n \frac{\mathrm{d}\sigma_n}{\mathrm{d}\Phi_n}\,\Theta\left(p_t^J - \max(\{p_{ti}\})\right)\,, \tag{3.10}$$

where p_{ti} denotes the transverse momentum of the final-state jets $\{p_{t1}, p_{t2}, \dots\}$, and, we note that we can have an arbitrary number of jets in the final-state, provided they all satisfy the constraint due to the measurement function. The transverse momentum of the leading jet can be measured directly from the hadronic final states in the event or final state jets following the application of a jet algorithm.

The transverse momentum of the leading jet is very closely related to an important phase space cut that is of particular phenomenological relevance, the *jet-veto*. A jet-veto is a cut placed on the kinematics of final-state jets in an event, and a veto on the maximum transverse momentum of the leading jet is important for the study of Higgs production at the LHC. This will be the subject of Chapter. 6.

3.4 Event shapes

Event shape variables are another, more granular, way in which we can probe the jet-like characteristics of hadronic final states. The idea is to define a quantity that smoothly parametrises the energy-momentum flow in an event. For example is the distribution of the hadrons in the event pencil-like, planar, spherical and other such "shapes". Event shapes were originally designed to test QCD at electron-positron colliders, however they have subsequently been generalised so that they can be measured at hadron-lepton and hadron-hadron colliders.

Event-shape distributions are normalised to the total hadronic cross section, σ, so as to be dimensionless and independent of the production cross section and so that the value of the event shape v falls between $[0, 1]$. To ensure that the event shape variables we construct are IRC safe, we must build them from *linear* sums of momenta.

3.5 Classical Event Shape variables

We will briefly give the definitions of the event shape variables that we will make use of in this thesis. These are all classical event shapes and have been studied in the literature for some time.

- **Thrust**: T [38] is defined with a unit vector $\vec{n}_T$, called the thrust axis, which maximises the following quantity

$$T = \max_{\vec{n}_T} \frac{\sum_i |\vec{p}_i \cdot \vec{n}|}{\sum_i |\vec{p}_i|}, \quad \tau = 1 - T, \tag{3.11}$$

  where the sum runs over all the final state particles i in the event. It is conventional to define a new quantity τ (also referred to as the thrust), so that the two-jet limit of the thrust is at $\tau = 0$.

- **Spherocity**: S [39–41] is defined in terms of all the eigenvalues of the linearised energy-momentum tensor

$$S = \frac{3}{2}(\lambda_2 + \lambda_3), \tag{3.12}$$

where the linearised energy-momentum tensor is given by

$$\Theta^{\alpha\beta} = \frac{1}{\sum_i |\vec{p}_i|} \sum_i \frac{p_i^\alpha p_i^\beta}{|\vec{p}_i|}\,, \tag{3.13}$$

where the index i runs over all the final state momenta $\vec{p}_i$. This tensor has three eigenvalues λ_j, $j = 1, 2, 3$ satisfying

$$0 \leq \lambda_j \leq 1\,, \quad \sum_j \lambda_j\,,$$

and we order these eigenvalues $\lambda_1 \geq \lambda_2 \geq \lambda_3$.

- C**-parameter**: C [40, 41] is defined in terms of the eigenvalues of the linearised energy-momentum tensor

$$C = 3(\lambda_1\lambda_2 + \lambda_2\lambda_3 + \lambda_3\lambda_1)\,. \tag{3.14}$$

- D**-parameter**: D [40–42] is defined in terms of the eigenvalues of the linearised energy-momentum tensor

$$D = 27\lambda_1\lambda_2\lambda_3\,. \tag{3.15}$$

The D-parameter will be the subject of Chapter 5.

Chapter 4

NNLL resummation

We saw in Chapter 2 that whilst IRC safe observables can be calculated in pQCD, we noted that for non-inclusive observables there may be large contributions from the emission of soft and collinear radiation. This radiation may lead to the development of large logarithms that can spoil the convergence of the fixed-order perturbative expansion. To restore predictivity we must *resum* these logarithms to all-orders in the coupling constant. Namely we must determine all the diagrams that produce a certain class of logarithm and treat them all simultaneously. To perform an all-orders calculation we must make use of the singular limits of QCD matrix elements, which will allow us to treat the emissions of an arbitrary number of emissions.

The traditional methods of resummation are observable-dependent, and consist of determining a *factorisation theorem* for the specific observable under consideration. This approach has been very successful yielding many interesting results [43–56]. However there exist observables of considerable interest that do yet admit any such factorisation theorem.

Recently a framework for performing resummation in *direct space*[1] was developed in the form of `CAESAR` [3, 57]. The `CAESAR` framework made the study of jet rate resummation possible for the first time, and other difficult observables, such as those at hadron colliders. Resummation in direct space is considerably different to the traditional factorisation based approach. We consider only the scaling properties of the observable, and for a wide class of observables—those that are *continuously global* and *recursively* infrared and collinear safe—we are able to resum them at next-to-leading-logarithmic (NLL) accuracy.

In this chapter we will work with the `ARES` framework to provide a general resummation

[1] i.e. without using any integral transforms, and only relying on the factorisation properties of QCD matrix elements in the soft and/or collinear limit.

of events containing three final-state jets in e^+e^- annihilation.

4.1 Introduction to resummation

Before we dive into state-of-the-art resummation let us review some of the common features of resummation calculations. We will look at an additional property of QCD that is important and then we will consider the resummation of the thrust. We will be deliberately light on the details and notation to try and emphasise the concepts. The rest of this chapter will be dedicated to filling in the gaps.

First we look at an additional property of QCD. We saw that in eq. (2.113) that in the soft *and* collinear limit the colour charge of an emission depends only on the leg it was emitted from. That is to say that in the collinear limit the colour correlations that are present in the soft case due to the interference of emissions between the different emitters vanish. We say that the radiation is emitted *coherently*, this is a manifestation of the phenomenon of *colour coherence*. In fact, this coherence phenomenon is actually a feature that is common to all gauge theories. It tells us that radiated particles can only resolve the effective colour charge of the emitter and cannot resolve the details of interactions that take place at shorter distance scales and wider angles. When we generate emissions in a parton shower we do so iteratively, inserting emissions one-by-one. To enforce the colour coherence property of squared matrix elements we must generate emissions that are ordered in angle. This is referred to as *angular ordering* and is common to parton shower type simulations. Fig. 4.1 shows angular ordering diagrammatically for both QED and QCD.

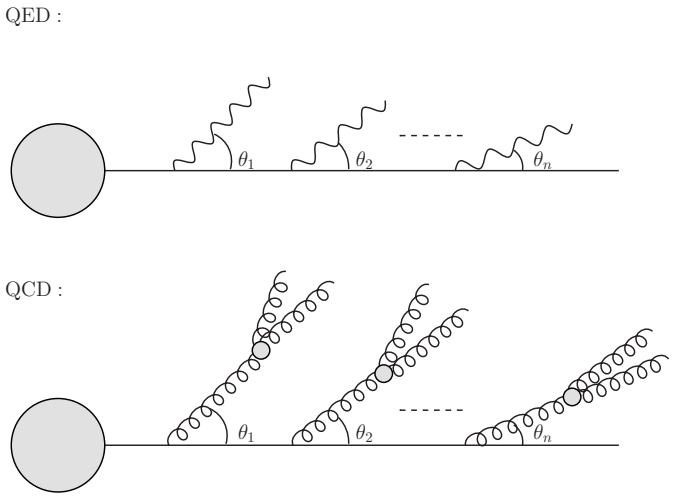

Figure 4.1: Angular ordering in QED and QCD [58]

Now we come to resummation. The first things to consider is which terms give rise to logarithmic enhancement in the fixed-order perturbative series—the problem terms. Each extra emission can contribute at most two logarithms, due to the two possible IR singularities, there is one from the angular integration and one from the transverse momentum integration. Terms that are double logarithmically enhanced are the most singular terms and are thus the terms that we should consider first. To calculate these *leading logarithms* (LL) we need only to consider emissions that are strongly ordered in energy and angle, these are the terms that give rise to the most logarithms. Taking just the double logarithmically enhanced terms is referred to as the *double logarithmic approximation* (DLA), this is the simplest approximation that we can make, but it captures the dominant terms. The LL terms are much like the LO terms in the fixed-order expansion, they typically contribute the largest contribution to the quantity under consideration and are the easiest terms to calculate.

Let us see how this works in practice with a specific observable, the *thrust*, τ, as we defined in eq. (3.11). The thrust is the canonical variable to resum owing to its simplicity. In the soft and collinear limit the thrust takes on the following simple form

$$\tau \simeq \sum_i \frac{k_{ti}^2}{z_i Q^2} = \sum_i \frac{k_{ti}}{Q} e^{-|\eta_i|} + \text{less singular terms.} \quad , \tag{4.1}$$

where k_t and η are the transverse momentum and rapidity with respect to the *emitter*. We can now compute the Thrust cumulant in the soft and collinear approximation

$$\Sigma_{\text{had},0}(\tau) = 1 \tag{4.2}$$

$$\begin{aligned}\Sigma_{\text{had},1}(\tau) &= 2C_F \frac{\alpha_s^{\overline{\text{MS}}}(Q)}{2\pi} \int \frac{\mathrm{d}k_t^2}{k_t^2} \int \mathrm{d}\eta \left(\Theta\left(\tau - \frac{k_t}{Q} e^{-|\eta|}\right) - 1\right) \Theta\left(\log \frac{Q}{k_t} - |\eta|\right) \\ &= -2C_F \frac{\alpha_s^{\overline{\text{MS}}}(Q)}{2\pi} \log^2 \frac{1}{\tau} \qquad (4.3) \\ &\equiv -2C_F \frac{\alpha_s^{\overline{\text{MS}}}(Q)}{2\pi} L^2 \,. \qquad (4.4)\end{aligned}$$

where we have defined $L = \log \frac{1}{\tau}$. Combining these the various orders together we arrive at the full NLO accurate result for the thrust cumulant

$$\Sigma_{\text{tot.}}(\tau) = 1 - 2C_F \frac{\alpha_s^{\overline{\text{MS}}}(Q)}{2\pi} \log^2 \frac{1}{\tau} + \mathcal{O}\big(\alpha_s^2\big) \,. \tag{4.5}$$

We can immediately see problems in the fixed-order perturbative approach. First we see that as the thrust becomes small, the logarithmic terms become increasingly large. When $\alpha_s L \sim 1$ the higher order terms are no longer small, in fact they are *enhanced* with respect to the leading order contribution, spoiling the convergence of the perturbative series. In

fact we can see that as $\tau \to 0$ the cumulant actually becomes *negative*, which is completely unphysical. The solution to this problem is to *resum* the logarithmically enhanced terms. To do this we must reorganise the perturbative series so that we resum different classes of logarithm.

There are different ways to classify the logarithms that we wish to resum, however for simplicity we will focus on the method that is used in the case of the thrust and the other event shape type observables that are considered in this thesis. The thrust is an example of an observable with an extra property, *exponentiation*. That is to say that all of the leading logarithms can be placed inside an exponent, summing up the LL contributions to *all-orders* in the strong coupling. With this setup we can define the classes of logarithms that we resum at the level of the exponent. In this case we define the LL contribution as terms of order $\alpha_s^n L^{n+1}$, NLL as terms of order $\alpha_s^n L^n$ and so on. This builds a tower of logarithms that are resummed in analogy to the successive orders of α_s that are included in fixed-order calculations. For the case of non-exponentiating observables we must define a different method to classify the logarithms that we resum, however that is beyond the scope of what we will consider in this thesis.

So far we have only considered fixed-order pQCD. To perform the calculation to all-order we must find the squared matrix element for the emission of an arbitrary number of soft and collinear partons. Figure. 4.1 is rather suggestive, in the QED case we can factorise the emission of n soft and collinear photons into a single emission raised to the power n with an appropriate Bose symmetry factor, symbolically

$$(n - \text{emissions}) = \frac{1}{n!} (1 - \text{emission})^n \ . \tag{4.6}$$

However, unlike QED, we cannot simply factorise the emissions of QCD due to the non-abelian nature of the theory. Gluons carry colour charge and are able to emit further secondary gluons and soft quark anti-quark pairs. However it is possible to find a QED type factorisation by redefining the coupling to include the subsequent branchings from the primary emission [59]. This new coupling scheme is referred to in the literature as the Monte Carlo or CMW scheme, but we will refer to it as the *physical* scheme. The relationship between the physical coupling $\alpha_s^{\text{phys.}}$ and the usual $\alpha_s^{\overline{\text{MS}}}$ coupling can be computed in perturbation theory. To recap, in QCD we can factorise an arbitrary number of soft and collinear emissions into a product of single emissions by using the physical coupling to absorb the contribution of secondary emissions.

Now we have all the necessary ingredients to perform a resummation. To get the leading logs correct we need only to include the most singular terms, that is the virtual

corrections and the unresolved real emissions. In the ARES formalism we can exponentiate the unresolved real terms up to power corrections given by $\delta^p v$, where p is a positive number and δ is a "resolution" at which we split the real emissions into resolved and unresolved. All the resolved radiation contributes to higher order terms in the resummation (NLL and beyond), and so can be neglected from our calculation of the leading singular behaviour.

$$\Sigma(\tau) = \exp\left[2C_F \int \frac{\mathrm{d}k_t^2}{k_t^2} \frac{\alpha_s^{\text{phys.}}(k_t^2)}{2\pi} \int \mathrm{d}\eta\, \Theta\left(\frac{k_t}{Q} e^{-|\eta|} - \tau\right) \Theta\left(\log\frac{Q}{k_t} - |\eta|\right)\right] \tag{4.7}$$

$$\simeq \exp\left[-2C_F \frac{\alpha_s^{\overline{\text{MS}}}(Q)}{2\pi} \log^2\frac{1}{\tau}\right], \tag{4.8}$$

where have made DLA to evaluate the integral and leave just the dominant terms. We see that by expanding the exponent in powers of α_s we can exactly reproduce the singular behaviour that was present in the fixed-order approach. However the exponent generates *all* of the leading logarithmic terms at every order in α_s. We can see also observe some of the characteristic properties of resummations: the leading logarithms are exponentiated and the negative value of cumulant has been replaced by an exponential suppression factor that is well behaved in the limit $\tau \to 0$.

This introduction has been fairly brief and we have left out a lot of the details about the objects involved in these calculations. We will address all of this in the following material. A more detailed, pedagogical, exposition to the properties of QCD, including colour coherence and angular ordering, can be found in Ref. [58, 60].

4.2 Problem specification

In the ARES framework we consider an observable, $V(q_1, q_2, \dots)$, that is a non-negative function of final-state momenta $q_1, q_2, \dots$. We specialise to the case of e^+e^- annihilation, although similar considerations can be made for hadron colliders. The observable under consideration, V, must be IRC safe, and, there exists some positive integer number n such that the observable goes smoothly to zero for momentum configurations that approach the limit of n narrow jets. We will call this an $(n+1)$-jet observable.

To begin we must introduce a procedure that selects for us events with n or more hard jets. This will usually be done through a jet algorithm that counts the number of hard, well separated, jets in the event; or through a cut on a secondary, n-jet, observable[2]. We can express this procedure in terms of an event selection function $\mathcal{H}(q_1, q_2, \dots)$ that is 1

[2]For example, when we resum the the D-parameter, a 4-jet observable, we will select 3-jet events by putting a cut on the Durham jet resolution parameter.

for events that pass the selection cuts, and zero for those that do not. From this we can define a hard n-jet cross section,

$$\sigma_{\mathcal{H}} \equiv \sum_{N=n}^{\infty} \int \mathrm{d}\Phi_N \frac{\mathrm{d}\sigma_N}{\mathrm{d}\Phi_N} \mathcal{H}(q_1, \ldots, q_N)\,, \tag{4.9}$$

where $\mathrm{d}\sigma_N/\mathrm{d}\Phi_N$ is the normalised differential cross section for producing N final-state particles.

We consider the integrated cross section, $\Sigma_{\mathcal{H}}(v)$, for events satisfying the hard n-jet cut, $\mathcal{H}$, for which, the observable, V is smaller than some value v,

$$\Sigma_{\mathcal{H}}(v) \equiv \frac{1}{\sigma_{\mathcal{H}}} \sum_{N=n}^{\infty} \int \mathrm{d}\Phi_N \frac{\mathrm{d}\sigma_N}{\mathrm{d}\Phi_N} \mathcal{H}(q_1, \ldots, q_N)\, \Theta(v - V(q_1, \ldots, q_n))\,, \tag{4.10}$$

from Eq. (4.10) we can obtain $1/\sigma_{\mathcal{H}}\, \mathrm{d}\Sigma_{\mathcal{H}}(v)/\mathrm{d}v$, the differential distribution for the observable.

In the case of n hard jets accompanied by an ensemble of soft and/or collinear radiation we can factorise Eq. (4.10) into a hard n-jet differential cross-section and a term containing the contribution of the soft and/or collinear radiation

$$\Sigma_{\mathcal{H}}(v) \equiv \frac{1}{\sigma_{\mathcal{H}}} \int \mathrm{d}\Phi_{\mathcal{B}}\, \frac{\mathrm{d}\sigma_n}{\mathrm{d}\Phi_{\mathcal{B}}}\, \Sigma_{\mathcal{B}}(\Phi_{\mathcal{B}}; v)\, \mathcal{H}(\Phi_{\mathcal{B}})\,. \tag{4.11}$$

The form of Eq. (4.11) involves the differential cross section $\mathrm{d}\sigma_n/\mathrm{d}\Phi_{\mathcal{B}}$ for producing an event with "Born kinematics", that consists of n outgoing hard momenta and an "observable dependent" function $\Sigma_{\mathcal{B}}(\Phi_{\mathcal{B}}; v)$, roughly telling us the number of events for which the value of the observable, V, is smaller than v.[3] When $v \ll 1$, the function $\Sigma_{\mathcal{B}}(\Phi_{\mathcal{B}}; v)$ develops large logarithms in v, which we will resum to all orders up to a given logarithmic accuracy.

4.3 Conditions for resummation

We outlined at the beginning of this chapter that observables that can be resummed in the `ARES` framework are those that are continuously global and recursively infrared and collinear (rIRC) safe. We will address each of these properties in turn.

An observable is said to be *global* if it is sensitive to all of the emissions in an event. Examples of global observables include the Thrust and all of the other event shapes described in Chapter 3. Non-global observables are those that are only sensitive to emissions

[3] Actually we can always write $\Sigma_{\mathcal{H}}(v)$ in the form of Eqs. (4.11), for any value of v. However the factorisation property of these equations, namely that $\Sigma_{\mathcal{B}}(\Phi_{\mathcal{B}}; v)$ is independent of the procedure used to select n-jet events, holds only in the limit of small v and for global observables.

in a certain region of phase space, for example the hemisphere jet-mass. *Continuous globalness* is the additional statement that the scaling of the observable with respect to the energy of an emission is the same everywhere in phase space. This condition ensures that (to all orders) there are no *non-global* logarithms.

In order to perform the all-orders resummation we need to know the exact behaviour of the observable in the presence of an arbitrary number of soft and/or collinear emissions. We consider only observables with the property of rIRC safety, rIRC safety encodes the requirement that the observable should be insensitive to additional soft and/or collinear emissions at widely separated scales. Further to this, the rIRC safety property ensures that the leading logarithms of an observable exponentiate.

We will briefly review the key aspects of rIRC safety, we follow the presentation in Section 2.2.4 of Ref. [3]. We begin by defining a momentum function $k_i = k_i(\zeta)$ such that $V(\{\tilde{p}\}, k_i(\zeta)) = \zeta$. A real emissions is fully determined by three variables η_i^0, ξ_i and ϕ_i, as well as the leg index ℓ_i,

$$\eta_i(\zeta) = \eta_i^0 - \frac{\xi_i \log \zeta}{a + b_{\ell_i}}, \quad k_{ti}(\zeta) = \left(\frac{\zeta e^{b_{\ell_i} \eta_i(\zeta)}}{d_{\ell_i} g_{\ell_i}(\phi_i)} \right)^{\frac{1}{a}}, \quad \phi_i(\zeta) = \phi_i \,, \tag{4.12}$$

We require that in the presence of multiple emissions the observable scales in the same fashion as it would for a single emission. We require that for any m such momentum functions, the following limit,

$$\lim_{\bar{v} \to 0} \frac{1}{\bar{v}} V(\{\tilde{p}\}, k_1(\bar{v}\zeta_1), \ldots, k_m(\bar{v}\zeta_m)) \,, \tag{4.13}$$

be well-defined and non-zero, for any choice of (non-zero) values of the ζ_i. Here $\bar{v}$ is a parameter that we vary to probe the observable's properties. The above condition guarantees that in the limit of small $\bar{v}$, any set of emissions close to the boundary $V(\{\tilde{p}\}, k) = \bar{v}$ will give a value of the observable that is of order $\bar{v}$.

For regular IRC safety, given an ensemble of partons, any additional soft and/or collinear splitting of one or more of these partons must not change the value of the observable by more than a positive power of the softness/collinearity of the splittings, normalised to the hard scale of the event Q.

In the context of resummations we have two relevant scales: the scale set by the event Q and the scale set by the boundary $V(\{\tilde{p}\}, k) = v$. We require that, for sufficiently small v, there exists some $\delta \ll v$, that can be chosen *independently* of v, such that we can neglect any splitting that is at a smaller scale than that defined by δv. Such splittings will change the value of the observable by an amount $\delta^p v$, where p is a positive power. The crucial property is that δ can be chosen independently of v.

In terms of the momentum functions $k_i(\zeta_i)$, IRC safety can be expressed with the requirement

$$\lim_{\zeta_{m+1}\to 0} V(\{\tilde{p}\}, k_1(\bar{v}\zeta_1), \ldots, k_m(\bar{v}\zeta_m), k_{m+1}(\bar{v}\zeta_{m+1})) = V(\{\tilde{p}\}, k_1(\bar{v}\zeta_1), \ldots, k_m(\bar{v}\zeta_m))\,. \tag{4.14}$$

The analogous requirement for rIRC safety is expressed by the double limit

$$\begin{aligned}\lim_{\zeta_{m+1}\to 0}\lim_{\bar{v}\to 0}\frac{1}{\bar{v}} V(\{\tilde{p}\}, k_1(\bar{v}\zeta_1), \ldots, k_m(\bar{v}\zeta_m), k_{m+1}(\bar{v}\zeta_{m+1})) \\ = \frac{1}{\bar{v}} V(\{\tilde{p}\}, k_1(\bar{v}\zeta_1), \ldots, k_m(\bar{v}\zeta_m))\,.\end{aligned} \tag{4.15}$$

The order of the limits on the left-hand-side is essential to the definition of rIRC safety: if the softness/collinearity ζ_{m+1} at which the $(m+1)^{\text{th}}$ emission becomes irrelevant depends on $\bar{v}$ (i.e. it scales as a power of $\bar{v}$), then even for arbitrarily small $\bar{v}$ the $(m+1)^{\text{th}}$ emission will never become irrelevant and the equality in Eq. (4.15) will never be satisfied. We can combine Eqs. (4.14) and (4.15) to obtain an alternative statement of the rIRC safety condition in terms of the commutator of the limits:

$$\left[\lim_{\zeta_{m+1}\to 0}, \lim_{\bar{v}\to 0}\right] \frac{1}{\bar{v}} V(\{\tilde{p}\}, k_1(\bar{v}\zeta_1), \ldots, k_m(\bar{v}\zeta_m), k_{m+1}(\bar{v}\zeta_{m+1})) = 0\,. \tag{4.16}$$

In addition to the limit where an extra emission is made soft/collinear to a hard leg, we also need to consider the situation where one or more existing emissions split softly and/or collinearly. We represent the collinear splitting of an existing emission with the notation $k_i(\zeta) \to \{k_{i_a}, k_{i_b}\}(\zeta, \mu)$ such that $\mu^2 = (k_{i_a} + k_{i_b})^2/k_{ti}^2$ and $\lim_{\mu\to 0}(k_{i_a} + k_{i_b}) = k_i$. We then require

$$\begin{aligned}\lim_{\mu\to 0}\lim_{\bar{v}\to 0}\frac{1}{\bar{v}} V(\{\tilde{p}\}, k_1(\bar{v}\zeta_1), \ldots, \{k_{i_a}, k_{i_b}\}(\bar{v}\zeta_i, \mu), \ldots, k_m(\bar{v}\zeta_m)) \\ = \frac{1}{\bar{v}} V(\{\tilde{p}\}, k_1(\bar{v}\zeta_1), \ldots, k_i(\bar{v}\zeta_i), \ldots, k_m(\bar{v}\zeta_m))\,.\end{aligned} \tag{4.17}$$

regardless of how the limit is taken—whether at fixed relative energy fractions for k_{i_a}, k_{i_b} or with one of them simultaneously becoming softer than the other. Again we can express Eq. (4.17) in terms of the commutator of the limits:

$$\left[\lim_{\mu\to 0}, \lim_{\bar{v}\to 0}\right] \frac{1}{\bar{v}} V(\{\tilde{p}\}, k_1(\bar{v}\zeta_1), \ldots, \{k_{i_a}, k_{i_b}\}(\bar{v}\zeta_i, \mu), \ldots, k_m(\bar{v}\zeta_m)) = 0\,. \tag{4.18}$$

Eqs. (4.16) and (4.18), together with the condition that (4.13) encode the conditions for an observable to be considered rIRC safe. The rIRC safety conditions ensure that the observable has the same scaling behaviour for any number of soft and collinear emissions. In addition the observable is insensitive to emissions that take place below a certain scale,

which lets us split the emissions into a set that are *resolved* and a set that are *unresolved*. rIRC safety allows us to place constraints on each emission individually:

$$V(\{\tilde{p}\}, k_1, \ldots, k_n) < v \implies \delta v \lesssim V(\{\tilde{p}\}, k_i) \lesssim v\,, \tag{4.19}$$

where δ satisfies

$$v \ll \delta \ll 1\,. \tag{4.20}$$

The rIRC safety conditions imply that the leading-logarithms will *exponentiate* and that the region in which resolved real radiation exists is next-to-leading logarithmic.

4.4 Kinematics and notation

All the considerations we have made so far have been completely general. We will now specialise to three-jet, rIRC safe, observables. At Born level, a three-jet event in e^+e^- annihilation is made up of a quark of momentum p_1, an antiquark p_2 and a gluon p_3, we choose without loss of generality to define their momenta as

$$p_1 = E_1(1,0,0,1)\,, \qquad p_2 = E_2(1,0,\sin\theta_{12},\cos\theta_{12})\,, \qquad p_3 = E_3(1,0,-\sin\theta_{13},\cos\theta_{13})\,, \tag{4.21}$$

with θ_{12} and θ_{13} the angles between p_1 and p_2, and p_1 and p_3 respectively. The relation between these angles and energies and the variables that are typically used to describe three-jet events is reported in Appendix. C.5.

We consider event shapes that vanish in the three-jet limit, i.e. $V(\{\tilde{p}\}) = 0$, where $\{\tilde{p}\}$ denotes the set $\{\tilde{p}_1, \tilde{p}_2, \tilde{p}_3\}$, the actual final-state momenta, which coincide with (p_1, p_2, p_3) in Eq. (4.21) at Born level. After many soft-collinear emissions $(k_1, \ldots, k_n)$ the three hard partons will recoil, and $\{\tilde{p}\}$ are the actual final-state momenta after recoil. In order to parametrise the radiation momenta, k_i, we introduce a so called Sudakov decomposition. In the case of three-jet kinematics there is not a single natural choice for Sudakov decomposition. So we adopt a different decomposition for the emission of soft (and optionally collinear) radiation and the emission of hard-collinear radiation. The decomposition serves to make the following calculations as simple as possible.

The soft radiation has a *dipole* structure that we shall come to shortly. As a result of this structure a convenient decomposition for a single emission k is along any pair of Born momenta $\{p_i, p_j\}$, which we shall call the (ij) dipole. This is done as follows

$$k = z^{(i)} p_i + z^{(j)} p_j + \kappa^{(ij)} \cos\phi\, n_{\text{in}}^{(ij)} + \kappa^{(ij)} \sin\phi\, n_{\text{out}}^{(ij)}\,. \tag{4.22}$$

where $n_{\rm in}^{(ij)}$ and $n_{\rm out}^{(ij)}$ are two space-like vectors that satisfy $(n_{\rm in}^{(ij)})^2 = (n_{\rm out}^{(ij)})^2 = -1$, given by

$$n_{\rm in}^{(ij)} = \left(\cot\frac{\theta_{ij}}{2}, \frac{\vec{n}_i + \vec{n}_j}{\sin\theta_{ij}}\right), \qquad n_{\rm out}^{(ij)} = \left(0, \frac{\vec{n}_i \times \vec{n}_j}{\sin\theta_{ij}}\right), \quad \vec{n}_\ell \equiv \frac{\vec{p}_\ell}{E_\ell}, \quad \ell = i, j\,. \tag{4.23}$$

We have introduced the invariant transverse momentum with respect to the (ij) dipole

$$\left(\kappa^{(ij)}\right)^2 = \frac{(2p_i k)(2p_j k)}{(2p_i p_j)}\,, \tag{4.24}$$

where $(p_i p_j)$ is short-hand notation for the Lorentz-invariant product $p_i \cdot p_j$.

On the other hand, for hard-collinear radiation we can choose to decompose the emission k along a single Born leg p_ℓ. This is done by defining the light-like momentum $\bar{p}_\ell = (E_\ell, -\vec{p}_\ell)$. Explicitly,

$$k = x^{(\ell)} p_\ell^\mu + \bar{x}^{(\ell)} \bar{p}_\ell^\mu + \kappa^{(\ell)}\,, \tag{4.25}$$

where $\kappa^{(\ell)}$ is a two-dimensional space-like vector lying in the transverse plane to leg p_ℓ, and whose magnitude reads

$$-\left(\kappa^{(\ell)}\right)^2 = \frac{(2p_\ell k)(2\bar{p}_\ell k)}{(2p_\ell \bar{p}_\ell)} \equiv \left(k_t^{(\ell)}\right)^2\,. \tag{4.26}$$

Note that, if k is collinear to the leg p_ℓ, we have $\kappa^{(ij)} \to k_t^{(\ell)}$.

We now introduce the rapidity $\eta^{(ij)}$ with respect to a dipole and its counterpart, $\eta^{(\ell)}$, with respect to leg p_ℓ

$$\eta^{(ij)} \equiv \frac{1}{2}\log\frac{z^{(i)}}{z^{(j)}}\,, \qquad \eta^{(\ell)} = \frac{1}{2}\log\frac{x^{(\ell)}}{\bar{x}^{(\ell)}}\,. \tag{4.27}$$

For an emission k collinear to p_i or p_j, the rapidities $\eta^{(ij)}, \eta^{(i)}, \eta^{(j)}$ are related as follows

$$\eta^{(i)} \simeq \eta^{(ij)} + \log\frac{2E_i}{Q_{ij}}\,, \qquad \eta^{(j)} \simeq -\eta^{(ij)} + \log\frac{2E_j}{Q_{ij}}\,, \qquad Q_{ij}^2 = 2(p_i p_j)\,. \tag{4.28}$$

From $z^{(i)}, z^{(j)}, x^{(\ell)}, \bar{x}^{(\ell)} < 1$, for a light-like vector k we obtain the rapidity bounds

$$|\eta^{(ij)}| < \log\frac{Q_{ij}}{\kappa^{(ij)}}\,, \qquad \eta^{(\ell)} < \log\frac{2E_\ell}{k_t^{(\ell)}}\,. \tag{4.29}$$

Last, we denote with $\phi^{(\ell)}$ the azimuthal angle of $\kappa^{(\ell)}$. We adopt the convention $\phi^{(ij)} = \phi^{(\ell)} = 0$ when an emission is in the plane formed by p_1, p_2, p_3. Comparing the expressions of the component of k outside the event plane in the Sudakov decompositions in Eqs. (4.22) and (4.25), we have that, for an emission k collinear to p_ℓ, $\phi^{(ij)} \simeq \phi^{(\ell)}$.

We note that for two-jet events the dipole Sudakov decomposition Eq. (4.22) and Eq. (4.25) coincide. From the dipole perspective two-jet events are simple events consisting of a single dipole.

A last remark is in order. When dealing with multiple soft-collinear emissions, using as reference vector the Born momenta p_1, p_2, p_3 can lead to cumbersome, observable dependent multiple-emission matrix elements. This is because, in the presence of multiple emissions, an emission might be collinear to one of the final state partons $\{\tilde{p}\}$ without being collinear to the corresponding Born momentum. Therefore, the reference light-cone vectors required to perform Sudakov decompositions might need to be redefined after each emission. There is no unique way to redefine reference vecors. The prescription we adopt here is explained in Appendix C. of ref. [3] and recalled in ref. [61].

4.5 General structure of NNLL resummation

We will now outline the considerations needed to perform at NNLL resummation of three-jet observables in the `ARES` framework. We closely follow the structure and discussions of Ref. [61]. We will attempt to stress as much as possible the new features that appear when considering three-jet observables.

Any rIRC safe observable $V(\{\tilde{p}\}, \{k_i\})$, can be parametrised in the following way for a single soft and collinear emission k collinear to leg ℓ

$$V(\{\tilde{p}\}, k) \simeq V_{\rm sc}(k) \equiv d_\ell \left(\frac{k_t^{(\ell)}}{Q}\right)^a e^{-b_\ell \eta^{(\ell)}} g_\ell(\phi^{(\ell)}) \,, \tag{4.30}$$

where $k_t^{(\ell)}, \eta^{(\ell)}, \phi^{(\ell)}$ are the transverse momentum, rapidity and azimuth of k with respect to the emitter p_ℓ, and a, b_ℓ, d_ℓ are constants.[4] The scale Q represents a typical hard scale of the process, in our case the centre-of-mass energy of the e^+e^- collision. The parametrisation of a single emission in eq. (4.30) may seem unduly limiting, however it turns out that a great number of observables can be parametrised in this way in the soft and collinear limit. This includes all of those observables discussed in chap. 3. The reason for this is for these observables it is only the *scaling* properties with respect to the transverse momentum and rapidity (captured in the a and b_ℓ coefficients) that are needed to capture the leading logarithmic behaviour. The remaining terms d_ℓ and $g_\ell(\phi^{(\ell)})$ are simply to appropriately normalise the observable and are necessary for computing corrections beyond LL accuracy.

We will also make use of a dipole based version of Eq. (4.30) which we define as follows:

$$V_{\rm sc}^{(ij)}(\{\tilde{p}\}, k) = d_\ell^{(ij)} \left(\frac{\kappa^{(ij)}}{Q_{ij}}\right)^a e^{-b_\ell \eta^{(ij)}} g_\ell(\phi^{(ij)}) \,, \tag{4.31}$$

[4] IRC safety implies $a > 0$ and $b_\ell > -a$. While b_ℓ, d_ℓ and g_ℓ can be different for each leg, continuous globalness implies a has to be the same for all legs.

where

$$d_\ell^{(ij)} = d_\ell \left(\frac{Q}{2E_\ell}\right)^{b_\ell} \cdot \left(\frac{Q_{ij}}{Q}\right)^{a+b_\ell}, \tag{4.32}$$

this is defined such that Eq. (4.30) and Eq. (4.31) are identical. Each expressing the behaviour of the observable most transparently for the leg and dipole based structure respectively.

Our aim is to resum large logarithms in the cumulative distribution $\Sigma_{\mathcal{B}}(\Phi_{\mathcal{B}}; v)$, the fraction of events for which $V(\{\tilde{p}\}, \{k_i\}) < v$, in the region $v \ll 1$. This is given by

$$\widetilde{\Sigma}_{\mathcal{B}}(\Phi_{\mathcal{B}}; v) \equiv \mathcal{V}(\Phi_{\mathcal{B}}) \sum_{n=0}^{\infty} S(n) \int \prod_{i=1}^{n} [\mathrm{d}k_i] \left|\mathcal{M}^2(\{\tilde{p}\}, k_1, \ldots, k_n)\right|^2 \Theta(v - V(\{\tilde{p}\}, k_1, \ldots, k_n)), \tag{4.33}$$

where $\mathcal{V}(\Phi_{\mathcal{B}})$ is a form factor that includes all virtual corrections to the Born process, $\left|\mathcal{M}(\{\tilde{p}\}, k_1, \ldots, k_n)\right|^2$ is the squared matrix element for n real emissions off of the three-jet Born antenna and the factor $S(n)$ represents the multiplicity coefficient for each final state (quarks or gluons). For instance, n identical gluons have a multiplicity factor $S(n) = 1/n!$. The Lorentz-invariant phase-space in $d = 4 - 2\epsilon$ dimensions is denoted by $[\mathrm{d}k]$ and defined as

$$[\mathrm{d}k] \equiv \frac{\mathrm{d}^d k}{(2\pi)^{d-1}} \delta(k^2)\Theta(k^0). \tag{4.34}$$

Given the Sudakov decomposition of any four-momentum k of (squared) invariant mass $k^2 = m^2$ as in Eq. (4.22), the measure $\mathrm{d}^d k$ can be expressed as

$$\mathrm{d}^d k = (p_i p_j)\mathrm{d}z^{(i)}\mathrm{d}z^{(j)}\mathrm{d}^{2-2\epsilon}\kappa^{(ij)} = \frac{\mathrm{d}y^{(ij)}}{2}\mathrm{d}m^2\mathrm{d}^{2-2\epsilon}\kappa^{(ij)}, \qquad y^{(ij)} \equiv \frac{1}{2}\log\left(\frac{z^{(i)}}{z^{(j)}}\right). \tag{4.35}$$

The variable $y^{(ij)}$ is the rapidity of k (with respect to some reference light-like directions p_i and p_j), and for real emissions ($k^2 = 0$) it is bounded by

$$\left|y^{(ij)}\right| < \log\left(\frac{Q_{ij}}{\kappa^{(ij)}}\right), \tag{4.36}$$

where $Q_{ij} = (2p_i p_j)$. It is immediate to link y to the rapidity of a massless emission k with respect to a given leg ℓ. In fact, $\eta^{(i)} = y^{(ij)}$ for $y^{(ij)} > 0$, and $\eta^{(j)} = -y^{(ij)}$ for $y^{(ij)} < 0$. This implies that the phase space $[\mathrm{d}k]$ in Eq. (4.34) of a single dipole can be written as follows

$$[\mathrm{d}k] = \sum_{\ell=1}^{2} \frac{\mathrm{d}\eta^{(\ell)}}{2}\Theta(\eta^{(\ell)})\frac{\mathrm{d}^{2-2\epsilon}\kappa^{(ij)}}{(2\pi)^{3-2\epsilon}}. \tag{4.37}$$

We have considered all of the momenta to be in d-dimensions, because dimensional regularisation is needed to regulate the IRC divergences present both in $\mathcal{V}(\Phi_{\mathcal{B}})$ and in the real radiation.

4.5.1 The structure of the virtual corrections

The virtual corrections $\mathcal{V}(\Phi_{\mathcal{B}})$ can be expressed in the following factorised form

$$\begin{aligned}\mathcal{V}(\Phi_{\mathcal{B}}) = H(\Phi_{\mathcal{B}}, \alpha_s(Q))\times \\ \times \exp\left\{\sum_{(ij)} C_{(ij)} \int \frac{\mathrm{d}^d k}{(2\pi)^d}\, w(m^2, (\kappa^{(ij)})^2 + m^2; \epsilon)\times \right. \\ \left. \times\Theta\left(\frac{1}{2}\log\left(\frac{Q_{ij}^2}{(\kappa^{(ij)})^2 + m^2}\right) - |y^{(ij)}|\right)\Theta(Q_{ij} - \kappa^{(ij)}\right\}\times \\ \times \exp\left\{-\sum_{\ell=1}^{3}\int^{Q^2}\frac{\mathrm{d}k^2}{k^2}\gamma_\ell(\alpha_s(k,\epsilon))\right\}.\end{aligned} \tag{4.38}$$

Such a factorisation is possible because at all orders there are three physical principles that apply to any hard scattering amplitude such as Eq. (4.38)

1. Soft gluons decouple from hard virtual partons (at leading power in the hard scale).

2. Virtual hard partons collinear to an external hard parton decouple from the remaining hard subdiagram, these hard collinear partons are insensitive to the energy and spin of hard partons that it is not collinear to.

3. Soft gluons decouple from jets, their long wavelength does not allow them to probe the details of a narrow jet beyond its overall colour and direction.

For the details of the factorisation see [62, 63] as the references therein.

The virtual corrections are parametrised in terms of three objects:

1. The *soft function*

   The first exponential in Eq. (4.38) represents the sum over all of the possible (ij) dipoles, where there is a soft web associated with each dipole. We extract the dipole colour factor $C_{(ij)}$ from each web so that $w(m^2, (\kappa^{(ij)})^2 + m^2; \epsilon)$ denotes the colour-stripped *soft web* [64, 65] of total momentum k and squared invariant mass m^2, in $d = 4 - 2\epsilon$ dimensions. In our representation of $\mathcal{V}(\Phi_{\mathcal{B}})$, the integration boundaries depend on which (ij) dipole we are considering. The upper integration bound for the $\kappa^{(ij)}$-integral of the web is set by the centre-of-mass energy of the dipole, Q_{ij}, and the upper bound for the rapidity integral to, $|y^{(ij)}| < \log\left(Q_{ij}/\sqrt{(\kappa^{(ij)})^2 + m^2}\right)$.

2. The *jet functions*

   The second exponential in Eq. (4.38) is the sum over all of the possible legs ℓ, where the function $\gamma_\ell(\alpha_s(k,\epsilon))$ coincides, up to an overall sign change, with the

coefficient of the $\delta(1-x)$ term of the regularised splitting functions $P_{q\to qg}(x)$ and $P_{g\to gg}(x)$, according to whether leg ℓ is a quark or a gluon, respectively. The strong coupling $\alpha_s(k,\epsilon)$ is defined as the solution of the d-dimensional renormalisation group equation:

$$\mu_R^2 \frac{\mathrm{d}\alpha_s}{\mathrm{d}\mu_R^2} = -\epsilon\,\alpha_s + \beta^{(\mathrm{d}=4)}(\alpha_s), \tag{4.39}$$

where $\beta^{(\mathrm{d}=4)}$ is the β-function in four dimensions, given by the following expansion

$$\beta^{(\mathrm{d}=4)}(\alpha_s) = -\alpha_s^2 \sum_{n=0}^{\infty} \beta_n \alpha_s^n\,, \tag{4.40}$$

namely the usual β-function.

3. The *Hard function*

   The overall quantity $H(\Phi_{\mathcal{B}}, \alpha_s(Q))$ is a multiplicative constant that is obtained by matching Eq. (4.38) at each order in perturbation theory to the quark or gluon form factor computed in the $\overline{\mathrm{MS}}$ scheme.

We take a brief interlude to explain the dipole structure that will be omnipresent throughout our considerations of the soft radiation. The dipole structure emerges naturally for the emission of soft gluons as we saw in Eq. (2.99). Generally the factorisation of soft radiation includes an eikonal factor and a colour correlation matrix. In the case of three-jet events we can compute the colour factors explicitly, and they are scalars rather than matrices—a special case for 2 and 3-jet events only. In our notation we define $C_{(ij)} = -\mathbf{T}_i \cdot \mathbf{T}_j$. In the three-jet case this leads us to $C_{(q\bar{q})} = C_F - \frac{C_A}{2}$ and $C_{(qg)} = C_{(\bar{q}g)} = \frac{C_A}{2}$. We stress again that the same structure is present in the two-jet case, only it is greatly simplified as there is only a single dipole to consider.

In order to proceed, we must devise a way to cancel the IRC singularities in Eq. (4.38) against those in the real emissions. We do this via the introduction of a *resolution parameter*. The resolution parameter is engineered so as to divide the real radiation into a *resolved* set and an *unresolved* set. The idea behind this division is to handle the unresolved part of the radiation analytically, and cancel these divergences against those of the virtual corrections. The cancellation is performed in a way that the contribution of the resolved set of radiation can subsequently be computed numerically in $d = 4$ dimensions. The resolution parameter is defined through its action on the soft and/or hard-collinear contributions to the squared matrix element, as we shall outline shortly.

4.5.2 Cancellation of soft singularities

We start by considering the contribution of soft radiation. The soft squared matrix element for n emissions off a hard antenna is denoted as $|\mathcal{M}(\{\tilde{p}\}, k_1, \ldots, k_n)|^2$. Soft radiation from such a hard antenna can be expressed as a sum over emissions off of all of the possible dipole antennas that make up the hard antenna. This result holds to all orders in QCD for any number of emissions. Schematically, this means that we can write

$$|\mathcal{M}(\Phi_{\mathcal{B}}, k_1, \ldots, k_n)|^2 = |\mathcal{M}(\Phi_{\mathcal{B}})|^2 \, |\mathcal{M}_{\mathrm{s}}(k_1, \ldots, k_n)|^2 . \tag{4.41}$$

Note that in general $|\mathcal{M}_{\mathrm{s}}(k_1, \ldots, k_n)|^2$ will be a matrix in colour space. For concreteness we reproduce the explicit expression for emissions off of a three-jet event. A single emission can be written as

$$|\mathcal{M}(\Phi_{\mathcal{B}}, k)|^2 = |\mathcal{M}(\Phi_{\mathcal{B}})|^2 \sum_{(ij)} 16\pi\mu_R^{2\epsilon}\alpha_s(\mu_R)\, C_{(ij)}\, \mathcal{S}_{ij}(k) \,, \tag{4.42}$$

and for two emissions we can write

$$\begin{aligned} |\mathcal{M}(\Phi_{\mathcal{B}}, k_1, k_2)|^2 = |\mathcal{M}(\Phi_{\mathcal{B}})|^2 (4\pi\mu_R^{2\epsilon}\alpha_s(\mu_R))^2 \Bigg[\left(\sum_{(ij)} 2C_{(ij)}\, \mathcal{S}_{ij}(k_1) \right) \left(\sum_{(ij)} 2C_{(kl)}\, \mathcal{S}_{kl}(k_2) \right) \\ + C_A \sum_{(ij)} C_{(ij)} \left[2\mathcal{S}_{ij} - \mathcal{S}_{ii} - \mathcal{S}_{jj} \right] - T_R n_F \sum_{(ij)} C_{(ij)} \left[2\mathcal{I}_{ij} - \mathcal{I}_{ii} - \mathcal{I}_{jj} \right] \Bigg] \,, \end{aligned} \tag{4.43}$$

where $\mathcal{S}_{ij}$, $\mathcal{S}_{ii}$ and $\mathcal{S}_{jj}$ account for the emission of two soft gluons and $\mathcal{I}_{ij}$, $\mathcal{I}_{ii}$ and $\mathcal{I}_{jj}$ account for the emission of a soft $q\bar{q}$ pair. Explicit expression for each of these terms can be found in Ref. [25].

Recalling Eq. (4.41), we denote squared matrix element for n soft emissions as $|\mathcal{M}_{\mathrm{s}}(k_1, \ldots, k_n)|^2$, which we can iteratively reorganised as follows

$$\begin{aligned} |\mathcal{M}_{\mathrm{s}}(k_1)|^2 &\equiv |\widetilde{\mathcal{M}}_{\mathrm{s}}(k_1)|^2 \\ |\mathcal{M}_{\mathrm{s}}(k_1, k_2)|^2 &= |\widetilde{\mathcal{M}}_{\mathrm{s}}(k_1)|^2 |\widetilde{\mathcal{M}}_{\mathrm{s}}(k_2)|^2 + |\widetilde{\mathcal{M}}_{\mathrm{s}}(k_1, k_2)|^2 \\ |\mathcal{M}_{\mathrm{s}}(k_1, k_2, k_3)|^2 &= |\widetilde{\mathcal{M}}_{\mathrm{s}}(k_1)|^2 |\widetilde{\mathcal{M}}_{\mathrm{s}}(k_2)|^2 |\widetilde{\mathcal{M}}_{\mathrm{s}}(k_3)|^2 + \left(|\widetilde{\mathcal{M}}_{\mathrm{s}}(k_1)|^2 |\widetilde{\mathcal{M}}_{\mathrm{s}}(k_2, k_3)|^2 + \text{perm.} \right) \\ &\quad + |\widetilde{\mathcal{M}}_{\mathrm{s}}(k_1, k_2, k_3)|^2 \\ &\vdots \end{aligned} \tag{4.44}$$

where it is understood that each $|\widetilde{\mathcal{M}}_{\mathrm{s}}(k_1, \ldots, k_n)|^2$ term takes the form of a sum over dipoles. The quantities $|\widetilde{\mathcal{M}}_{\mathrm{s}}(k_1, \ldots, k_n)|^2$ represent the correlated portion of the n-emission

soft squared matrix element, together with its virtual corrections.[5] The correlated portion of the squared matrix element is strongly suppressed unless all emissions $k_1, \ldots, k_n$ are close in angle. We refer to the $|\widetilde{\mathcal{M}}_{\rm s}(k_1, \ldots, k_n)|^2$ terms as *soft correlated blocks*, they are the building blocks of the *soft webs*, which in turn we will use to construct the Sudakov radiator. Each correlated block admits a perturbative expansion in α_s due to the virtual corrections, hence

$$|\widetilde{\mathcal{M}}_{\rm s}(k_1, \ldots, k_n)|^2 = |\widetilde{\mathcal{M}}_{\rm s,0}(k_1, \ldots, k_n)|^2 + \frac{\alpha_s(\mu_R)}{2\pi}|\widetilde{\mathcal{M}}_{\rm s,1}(k_1, \ldots, k_n)|^2 + \ldots \tag{4.45}$$

At tree level, the squared matrix element for the emission of a single soft gluon is given by

$$|\widetilde{\mathcal{M}}_{\rm s}(k)|^2 \simeq |\widetilde{\mathcal{M}}_{\rm s,0}(k)|^2 = \sum_{(ij)} 16\pi\, C_{(ij)}\, \mu_R^{2\epsilon} \alpha_s(\mu_R)\, \mathcal{S}_{ij}(k), \tag{4.46}$$

while at one-loop order we have [66]

$$|\widetilde{\mathcal{M}}_{\rm s,1}(k)|^2 = -\sum_{(ij)} 16\pi\, C_{(ij)}\, \mu_R^{2\epsilon} \alpha_s(\mu_R)\, \mathcal{S}_{ij}(k)\, C_A \frac{1}{\epsilon^2} \frac{\Gamma^4(1-\epsilon)\Gamma^3(1+\epsilon)}{\Gamma^2(1-2\epsilon)\Gamma(1+2\epsilon)} \left[4\pi\mu_R^2\, \mathcal{S}_{ij}(k)\right]^{\epsilon}. \tag{4.47}$$

In the following we will always renormalise the coupling in the $\overline{\rm MS}$ scheme, i.e. we replace

$$\mu_R^{2\epsilon}\alpha_s(\mu_R) \to \mu_R^{2\epsilon}\alpha_s(\mu_R)\frac{e^{\epsilon\gamma_E}}{(4\pi)^\epsilon}\left(1 - \frac{\beta_0}{\epsilon}\alpha_s(\mu_R) + \ldots\right), \tag{4.48}$$

where β_0 is the first coefficient of the beta function in four dimensions of Eq. (4.40). The tree-level correlated block with two emissions $|\widetilde{\mathcal{M}}_{\rm s,0}(k_1, k_2)|^2$ is reported in Appendix C.4, and will be useful later. This decomposition is particularly convenient as it allows us to define a logarithmic counting. Each soft correlated block $|\widetilde{\mathcal{M}}_{\rm s}(k_1, \ldots, k_n)|^2$ will contribute to $\log \Sigma_{\mathcal{B}}(\Phi_{\mathcal{B}}; v)$ with at most with a factor $\alpha_s^n \log^{n+1}(v)$, with n powers of $\log(v)$ coming from the soft singularities and an extra power from the only collinear singularity.

Rather than defining the resolution parameter as in Ref. [61], where it acts on the full correlated squared matrix element, we will instead define it to act separately on each dipole contribution. This will allow us to exponentiate the contribution of each dipole separately. Following the same approach as Ref. [61] we begin by defining a *clustering algorithm* that combines together the momenta of all particles emitted according to each correlated dipole block $|\widetilde{\mathcal{M}}_{\rm s}(k_1, \ldots, k_n)|^2$. In the simple case of two emissions, we cluster as follows

$$|\mathcal{M}_{\rm s}(k_1, k_2)|^2 = \underbrace{|\widetilde{\mathcal{M}}_{\rm s}(k_1)|^2\, |\widetilde{\mathcal{M}}_{\rm s}(k_2)|^2}_{\text{two clusters } (k_1, k_2)} + \underbrace{|\widetilde{\mathcal{M}}_{\rm s}(k_1, k_2)|^2}_{\text{a single cluster } k_{\rm clust.} = k_1 + k_2}. \tag{4.49}$$

[5] Note that the $|\widetilde{\mathcal{M}}_{\rm s}(k_1, \ldots, k_n)|^2$ are not in general positive definite, they are defined as differences of squared matrix elements.

rIRC safety [3] ensures that all particles in a cluster are both close in angle and have commensurate transverse momenta. This allows us to evaluate the QCD running coupling of each cluster at the transverse momenta of the corresponding emissions. This procedure allows us to absorb all logarithms of $\mu_R/\kappa_i^{(ij)}$ into the running of the coupling. As a consequence of this procedure, for rIRC safe observables, using the decomposition (4.44), every correlated block $|\widetilde{\mathcal{M}}_{\rm s}(k_1,\ldots,k_n)|^2$ (when combined with the corresponding virtual corrections) will contribute to $\log\Sigma_{\mathcal{B}}(\Phi_{\mathcal{B}};v)$ with terms of order $\alpha_s^m\log^{m+2-n}(v)$ for $m\geq n$. This allows us to build a logarithmic counting at the level of the squared matrix element, which defines which contributions must be considered at a given logarithmic order.

In order to proceed with the calculation of $\Sigma_{\mathcal{B}}(\Phi_{\mathcal{B}};v)$, we then choose a resolution parameter $\delta\ll 1$ such that all clusters of total momentum $k_{\rm clust.}$ satisfying

$$V_{\rm res.}(k_{\rm clust.})<\delta v\,, \tag{4.50}$$

are labelled as *unresolved*. This choice guarantees that one is able to compute analytically the contribution of unresolved emissions for an arbitrary rIRC safe observable. For this class of observables, the unresolved clusters can be neglected from the Θ function in Eq. (4.33) since they do not contribute to the observable V up to corrections suppressed by powers of $\delta^p v$, with p being a positive parameter.

To make what we have described more transparent, we will work through the action of the resolution variable on the soft correlated block: first for the case of a single emission and then the case of two emissions. We will see how the momenta are divided into resolved and unresolved. First we introduce the shorthand for the action of the resolution parameter

$$\begin{aligned}\overline{\Theta}_{\delta v}[\{k_i\}]&\equiv\Theta[V_{\rm res.}(\{k_i\})-\delta v]\\ \Theta_{\delta v}[\{k_i\}]&\equiv\Theta[\delta v-V_{\rm res.}(\{k_i\})]\,.\end{aligned} \tag{4.51}$$

We combine the action of the resolution parameter with the observable constraint and making use of the rIRC safety of the observable we can write

$$\begin{aligned}&\Theta[v-V(\{\tilde{p}\},k_1,\ldots,k_n)]\,\Theta_{\delta v}[\{k_1,\ldots,k_l\}]\\ &\qquad=\Theta[V(\{\tilde{p}\},k_{l+1},\ldots,k_n)]\,\Theta[\{k_1,\ldots,k_l\}]+\mathcal{O}(v\,\delta^p)\,,\end{aligned} \tag{4.52}$$

With this shorthand we can write down how the resolution variable divides the momenta

into resolved and unresolved

$$
\begin{aligned}
\int [\mathrm{d}k]\, |\widetilde{\mathcal{M}}(k)|^2 &= \int [\mathrm{d}k]\, |\widetilde{\mathcal{M}}(k)|^2 \left[\Theta_{\delta v}(k) + \overline{\Theta}_{\delta v}(k)\right] \\
&\equiv \int^{\delta v} [\mathrm{d}k]\, |\widetilde{\mathcal{M}}(k)|^2 + \int_{\delta v} [\mathrm{d}k]\, |\widetilde{\mathcal{M}}(k)|^2 \\
&\equiv 16\pi\mu_R^{2\epsilon}\alpha_s(\mu_R) \sum_{(ij)} C_{(ij)} \int [\mathrm{d}k]\, \mathcal{S}_{ij}(k) \times \\
&\qquad \times \left[\Theta\left(V_{\mathrm{sc}}^{(ij)}(k) - \delta v\right) + \Theta\left(\delta v - V_{\mathrm{sc}}^{(ij)}(k)\right)\right] \\
&\equiv 16\pi\mu_R^{2\epsilon}\alpha_s(\mu_R) \sum_{(ij)} C_{(ij)} \left[\int^{\delta v} [\mathrm{d}k]\, \mathcal{S}_{ij}(k) + \int_{\delta v} [\mathrm{d}k]\, \mathcal{S}_{ij}(k)\right], \\
\int [\mathrm{d}k_1][\mathrm{d}k_2]\, |\widetilde{\mathcal{M}}(k_1,k_2)|^2 &= \int [\mathrm{d}k_1][\mathrm{d}k_2]\, |\widetilde{\mathcal{M}}(k_1,k_2)|^2 \left[\Theta_{\delta v}(k_1,k_2) + \overline{\Theta}_{\delta v}(k_1,k_2)\right] \\
&\equiv \int^{\delta v} [\mathrm{d}k_1][\mathrm{d}k_2]\, |\widetilde{\mathcal{M}}(k_1,k_2)|^2 + \int_{\delta v} [\mathrm{d}k_1][\mathrm{d}k_2]\, |\widetilde{\mathcal{M}}(k_1,k_2)|^2 \\
&\equiv (4\pi\mu_R^{2\epsilon}\alpha_s(\mu_R))^2\, C_A \sum_{(ij)} C_{(ij)} \times \\
&\qquad \times \int [\mathrm{d}k_1][\mathrm{d}k_2] \left[2\mathcal{S}_{ij}(k_1,k_2) - \mathcal{S}_{ii}(k_1,k_2) - \mathcal{S}_{jj}(k_1,k_2)\right] \times \\
&\qquad \times \left[\Theta\left(V_{\mathrm{sc}}^{(ij)}(k_1+k_2) - \delta v\right) + \Theta\left(\delta v - V_{\mathrm{sc}}^{(ij)}(k_1+k_2)\right)\right] \\
&\equiv (4\pi\mu_R^{2\epsilon}\alpha_s(\mu_R))^2 C_A \sum_{(ij)} C_{(ij)} \times \\
&\qquad \times \left[\int^{\delta v} [\mathrm{d}k_1][\mathrm{d}k_2] \left[2\mathcal{S}_{ij}(k_1,k_2) - \mathcal{S}_{ii}(k_1,k_2) - \mathcal{S}_{jj}(k_1,k_2)\right]\right. \\
&\qquad \left. + \int_{\delta v} [\mathrm{d}k_1][\mathrm{d}k_2] \left[2\mathcal{S}_{ij}(k_1,k_2) - \mathcal{S}_{ii}(k_1,k_2) - \mathcal{S}_{jj}(k_1,k_2)\right]\right],
\end{aligned}
\tag{4.53}
$$

where again the explicit form of $\mathcal{S}_{ij}$ can be found in Ref. [25]. We can see the same structure as was found for the two-jet case [61], only now acting on each dipole separately.

The above definition of the resolution parameter allows us to exponentiate the contribution of unresolved soft blocks. From the decomposition of Eq. (4.44), we can connect the soft correlated blocks $|\widetilde{\mathcal{M}}_{\mathrm{s}}(k_1,\ldots,k_n)|^2$ to the webs introduced in Eq. (4.38), we find

$$
\sum_{(ij)} C_{ij} w(m^2, (\kappa^{(ij)})^2 + m^2; \epsilon) = \sum_{n=1}^{\infty} S(n) \int \left(\prod_{i=1}^{n} [\mathrm{d}k_i]\right) |\widetilde{\mathcal{M}}_{\mathrm{s}}(k_1,\ldots,k_n)|^2 (2\pi)^d \delta^{(d)}\left(k - \sum_i k_i\right),
\tag{4.54}
$$

Therefore, the contribution of an arbitrary number of soft clusters (and no hard-collinear clusters) gives rise to the following exponential factor

$$
\exp\left\{\sum_{(ij)} C_{(ij)} \int^{Q_{ij}} \frac{\mathrm{d}^d k}{(2\pi)^d}\, w(m^2, (\kappa^{(ij)})^2 + m^2; \epsilon)\, \Theta(\delta v - V_{\mathrm{sc}}^{(ij)}(k))\right\}.
\tag{4.55}
$$

Eq. (4.55) can be combined with the virtual corrections in (4.38) to give

$$\mathcal{V}(\Phi_{\mathcal{B}}) \exp\left\{\sum_{(ij)} C_{(ij)} \int^{Q_{ij}} \frac{\mathrm{d}^d k}{(2\pi)^d} w(m^2, (\kappa^{(ij)})^2 + m^2; \epsilon)\, \Theta(\delta v - V_{\mathrm{sc}}^{(ij)}(k))\right\}$$
$$= H(\Phi_{\mathcal{B}}, \alpha_s(Q)) \exp\left\{-\sum_{(ij)} C_{(ij)}\, R_{\mathrm{s}}^{(ij)}(\delta v)\right\} \exp\left\{-\sum_{\ell=1}^{3} \int^{Q^2} \frac{\mathrm{d}k^2}{k^2} \gamma_\ell(\alpha_s(k,\epsilon))\right\}, \tag{4.56}$$

where we have defined the *soft dipole radiator* $R_{\mathrm{s}}^{(ij)}(\bar{v})$, a function with argument $\bar{v}$, as

$$R_{\mathrm{s}}^{(ij)}(\bar{v}) = \int^{Q_{ij}} \frac{\mathrm{d}^4 k}{(2\pi)^4}\, w(m^2, (\kappa^{(ij)})^2 + m^2)\, \Theta(V_{\mathrm{sc}}^{(ij)}(k) - \bar{v})\,, \tag{4.57}$$

and we have taken the four-dimensional limit of the web since the integral is now finite. We also introduce the complete soft radiator defined as

$$R_{\mathrm{s}}(\bar{v}) \equiv \sum_{(ij)} C_{(ij)}\, R_{\mathrm{s}}^{(ij)}(\bar{v})\,. \tag{4.58}$$

4.5.3 Cancellation of collinear singularities and the structure of resolved radiation

The procedure for the cancellation of the collinear singularities is unchanged with respect to the original considerations made in the derivation of the `ARES` NNLL master equation, however there are new finite terms that appear as compared to the original formulation. We reproduce the discussion of Ref. [61], making clear where there are new contributions.

The next step is to handle the hard-collinear divergences, those present in the integral over γ in Eq. (4.56). Exponentiation of the unresolved hard-collinear emissions is much more delicate than for the soft. Every hard-collinear emission could change the colour charge felt by all subsequent radiation. Fortunately, rIRC safety greatly simplifies the treatment of the hard-collinear radiation, for rIRC safe observables we only need to consider a fixed number of hard-collinear emissions at a given logarithmic order. Therefore, instead of proceeding as in the soft case, we start from the integral over the anomalous dimension γ in the virtual corrections (4.56) and split it into two pieces at the collinear scale of the resolution variable[6], which yields $V_{\mathrm{sc}}(k) \sim k_t^{a+b_\ell}$. Inspired by this, we split the integral over γ at $k = v^{1/(a+b_\ell)} Q$

$$\int^{Q^2} \frac{\mathrm{d}k^2}{k^2} \gamma_\ell(\alpha_s(k,\epsilon)) = \int_{Q^2 v^{\frac{2}{a+b_\ell}}}^{Q^2} \frac{\mathrm{d}k^2}{k^2} \gamma_\ell(\alpha_s(k)) + \int_0^{Q^2 v^{\frac{2}{a+b_\ell}}} \frac{\mathrm{d}k^2}{k^2} \gamma_\ell(\alpha_s(k,\epsilon))\,. \tag{4.59}$$

[6]The collinear scale is found by setting the rapidity $\eta^{(\ell)}$ to its maximum (i.e. $\log(Q/k_t)$) in Eq. (4.30)

Next, we expand the exponential of the second integral on the right hand side of the above equation considering only a fixed number of terms in its expansion

$$\exp\left\{-\int_0^{Q^2 v^{\frac{2}{a+b_\ell}}} \frac{\mathrm{d}k^2}{k^2}\gamma_\ell(\alpha_s(k,\epsilon))\right\} = 1 - \int_0^{Q^2 v^{\frac{2}{a+b_\ell}}} \frac{\mathrm{d}k^2}{k^2}\frac{\alpha_s(k,\epsilon)}{2\pi}\gamma_\ell^{(0)} + \mathcal{O}\Big(\alpha_s^2(Q v^{\frac{1}{a+b_\ell}})\Big)\,. \tag{4.60}$$

The first non-trivial order in the expansion must be included at NNLL, the second at N^{3}LL (together with the squared of the first), and so on and so forth. The divergences in these terms cancel order-by-order in perturbation theory against those of the hard-collinear emissions in the real radiation.

The final step to obtain an NNLL accurate expression for $\Sigma_{\mathcal{B}}(\Phi_{\mathcal{B}}; v)$ is to handle the squared matrix element for resolved real emissions in Eq. (4.33). At NLL accuracy, rIRC safety ensures that resolved radiation contains no hard-collinear emissions, and the real matrix element squared is simply the soft approximation $|\mathcal{M}_{\mathrm{s}}|^2$. In fact it simplifies further, the squared matrix element at this order reduces to the product of n independent, soft-collinear emission probabilities, $[\mathrm{d}k]\,|\mathcal{M}_{\mathrm{s},0}(k)|^2 \simeq [\mathrm{d}k]\,|\mathcal{M}_{\mathrm{sc}}(k)|^2$, where [4]

$$[\mathrm{d}k]\,|\mathcal{M}_{\mathrm{sc}}(k)|^2 \equiv \sum_{(ij)} 2C_{(ij)} \sum_{\ell\in(ij)} \frac{\mathrm{d}\kappa^{(ij)}}{\kappa^{(ij)}}\,\mathrm{d}\eta^{(ij)}\,\frac{\mathrm{d}\phi^{(ij)}}{2\pi}\,\frac{\alpha_s(\kappa^{(ij)})}{\pi}\Theta\left(\log\left(\frac{Q_{ij}}{\kappa^{(ij)}}\right) - \eta_{ij}^{(\ell)}\right)\Theta(\eta_{ij}^{(\ell)})\,. \tag{4.61}$$

In order to achieve NNLL accuracy, it is sufficient to correct the products of independently emitted single-particle clusters with the insertion of a single tree-level correlated cluster of two soft and collinear emissions $|\widetilde{\mathcal{M}}_{\mathrm{s},0}(k_a,k_b)|^2$, and of the one-loop correction to the single-emission cluster $|\widetilde{\mathcal{M}}_{\mathrm{s},1}(k)|^2$.

Moreover, beyond NLL, a finite number of hard-collinear emissions must be considered. In particular, at NNLL, it is sufficient to allow one single emission to be hard and collinear. This single collinear emission factorises as follows

$$|\mathcal{M}(\{\tilde{p}\},k_{\mathrm{hc}},k_1,\ldots,k_n)|^2 \simeq |\mathcal{M}(\Phi_{\mathcal{B}})|^2 |\mathcal{M}_{\mathrm{hc},\ell}(\Phi_{\mathcal{B}},k_{\mathrm{hc}})|^2 \prod_{i=1}^{n} |\widetilde{\mathcal{M}}_{\mathrm{s}}(k_i)|^2\,. \tag{4.62}$$

Note that unlike in the soft case the hard-collinear matrix element can depend on the Born kinematics through spin correlations. When combined with Eq. (4.60), this leads to a finite, logarithmically enhanced, left over, as it will be shown shortly. In such configurations, at NNLL, the remaining soft radiation consists of an arbitrary number of single-emission clusters.

With the above decomposition, the NNLL resummed cross section $\Sigma_{\mathcal{B}}(\Phi_{\mathcal{B}}; v)$ of Eq. (4.33)

takes the form

$$\begin{aligned}
\Sigma_{\mathcal{B}}(\Phi_{\mathcal{B}};v) = H(\Phi_{\mathcal{B}},\alpha_s(Q))\exp\left\{-\sum_{(ij)} C_{(ij)}\, R_{\mathrm{s}}^{(ij)}(\delta v)\right\}\exp\left\{-\sum_{\ell=1}^{3}\int_{Q^2 v^{\frac{2}{a+b_\ell}}}^{Q^2}\frac{\mathrm{d}k^2}{k^2}\gamma_\ell(\alpha_s(k))\right\}\\
\times\left\{\sum_{n=0}^{\infty}\frac{1}{n!}\int\prod_{i=1}^{n}[\mathrm{d}k_i]\,|\mathcal{M}_{\mathrm{s}}(k_1,\ldots,k_n)|^2\,\Theta(v-V(\{\tilde{p}\},\{k_i\}))\prod_{\text{clust.}}\Theta\left(V_{\mathrm{sc}}(k_{\text{clust.}})-\delta v\right)\right.\\
+\sum_{n=0}^{\infty}\frac{1}{n!}\int\prod_{i=1}^{n}[\mathrm{d}k_i]\,|\mathcal{M}_{\mathrm{sc}}(k_i)|^2\,\Theta\left(V_{\mathrm{sc}}(k_i)-\delta v\right)\\
\times\sum_{\ell=1}^{3}\left[\int[\mathrm{d}k_{\mathrm{hc}}]\,|\mathcal{M}_{\mathrm{hc},\ell}(\Phi_{\mathcal{B}},k_{\mathrm{hc}})|^2\,\Theta(v-V(\{\tilde{p}\},\{k_i\},k_{\mathrm{hc}}))\right.\\
\left.\left.-\int_0^{Q^2 v^{\frac{2}{a+b_\ell}}}\frac{\mathrm{d}k^2}{k^2}\frac{\alpha_s(k,\epsilon)}{2\pi}\gamma_\ell^{(0)}\Theta(v-V(\{\tilde{p}\},\{k_i\}))\right]\right\},
\end{aligned}\tag{4.63}$$

where it is understood that when we write $|\mathcal{M}_{\mathrm{sc}}(k_i)|^2\,\Theta\left(V_{\mathrm{sc}}(k_i)-\delta v\right)$, the Θ-function is applied separately to each dipole with the appropriate dipole resolution variable

$$|\mathcal{M}_{\mathrm{sc}}(k_i)|^2\,\Theta\left(V_{\mathrm{sc}}(k_i)-\delta v\right)=\sum_{(ij)}16\pi\alpha_s(\kappa)\,C_{(ij)}\,\mathcal{S}_{ij}(k_i)\,\Theta\left(V_{\mathrm{sc}}^{(ij)}(k_i)-\delta v\right),\tag{4.64}$$

and the squared matrix element $|\mathcal{M}_{\mathrm{s}}(k_1,\ldots,k_n)|^2$ is approximated by

$$\begin{aligned}
|\mathcal{M}_{\mathrm{s}}(k_1,\ldots,k_n)|^2\prod_{\text{clust.}}\Theta\left(V_{\mathrm{sc}}(k_{\text{clust.}})-\delta v\right)\simeq\prod_{i=1}^{n}|\mathcal{M}_{\mathrm{sc}}(k_i)|^2\Theta\left(V_{\mathrm{sc}}(k_i)-\delta v\right)\\
+\sum_{a>b}\prod_{\substack{i=1\\ i\neq a,b}}^{n}|\mathcal{M}_{\mathrm{sc}}(k_i)|^2\Theta\left(V_{\mathrm{sc}}(k_i)-\delta v\right)|\widetilde{\mathcal{M}}_{\mathrm{s},0}(k_a,k_b)|^2\Theta\left(V_{\mathrm{sc}}(k_a+k_b)-\delta v\right)\\
+\frac{\alpha_s(\mu_R)}{2\pi}\sum_{a}\prod_{\substack{i=1\\ i\neq a}}^{n}|\mathcal{M}_{\mathrm{sc}}(k_i)|^2\Theta\left(V_{\mathrm{sc}}(k_i)-\delta v\right)|\widetilde{\mathcal{M}}_{\mathrm{s},1}(k_a)|^2\Theta\left(V_{\mathrm{sc}}(k_a)-\delta v\right)\\
+\ldots,
\end{aligned}\tag{4.65}$$

where $V_{\mathrm{sc}}(k_a+k_b)$ is defined as in Eq. (4.31), and $\kappa^{(ij)},\eta^{(ij)},\phi^{(ij)}$ are the transverse momentum, rapidity and azimuth of the four-vector k_a+k_b with respect to dipole (ij). The cancellation of infrared and collinear divergences in the first term of Eq. (4.63) can be handled with a simple subtraction scheme as outlined in Ref. [4], which allows for a numerical evaluation in $d=4$ dimensions. The cancellation of collinear singularities in the second term still requires the use of dimensional regularisation. In order to make the second term suitable for a numerical evaluation, we add and subtract the following

counter-term

$$
\begin{aligned}
&H(\Phi_{\mathcal{B}},\alpha_s(Q))e^{-R_{\rm s}(\delta v)}\exp\left\{-\sum_{\ell=1}^{3}\int_{Q^2v^{\frac{2}{a+b_\ell}}}^{Q^2}\frac{\mathrm{d}k^2}{k^2}\gamma_\ell(\alpha_s(k,\epsilon))\right\}\\
&\qquad\times\sum_{n=0}^{\infty}\frac{1}{n!}\int\prod_{i=1}^{n}[\mathrm{d}k_i]\,|\mathcal{M}_{\rm sc}(k_i)|^2\,\Theta\left(V_{\rm sc}(k_i)-\delta v\right)\\
&\qquad\times\sum_{\ell=1}^{3}\int[\mathrm{d}k_{\rm hc}]|\mathcal{M}_{{\rm hc},\ell}(k_{\rm hc})|^2\,\Theta(v-V(\{\tilde{p}\},\{k_i\}))\,\Theta(v-V_{\rm sc}(k_{\rm hc}))\,,
\end{aligned}
\tag{4.66}
$$

and recast Eq. (4.63) as follows

$$
\begin{aligned}
&\Sigma(v)=H(\Phi_{\mathcal{B}},\alpha_s(Q))e^{-R_{\rm s}(\delta v)}\exp\left\{-\sum_{\ell=1}^{3}\int_{Q^2v^{\frac{2}{a+b_\ell}}}^{Q^2}\frac{\mathrm{d}k^2}{k^2}\gamma_\ell(\alpha_s(k,\epsilon))\right\}\\
&\times\left\{\sum_{n=0}^{\infty}\frac{1}{n!}\int\prod_{i=1}^{n}[\mathrm{d}k_i]\,|\mathcal{M}_{\rm s}(k_1,\ldots,k_n)|^2\,\Theta(v-V(\{\tilde{p}\},\{k_i\}))\prod_{\rm clust.}\Theta\left(V_{\rm sc}(k_{\rm clust.})-\delta v\right)\right.\\
&+\sum_{n=0}^{\infty}\frac{1}{n!}\int\prod_{i=1}^{n}[\mathrm{d}k_i]\,|\mathcal{M}_{\rm sc}(k_i)|^2\,\Theta\left(V_{\rm sc}(k_i)-\delta v\right)\\
&\times\sum_{\ell=1}^{3}\left[\int[\mathrm{d}k_{\rm hc}]\,|\mathcal{M}_{{\rm hc},\ell}(k_{\rm hc})|^2\right.\\
&\qquad\times\Big(\Theta(v-V(\{\tilde{p}\},\{k_i\}))-\Theta(v-V(\{\tilde{p}\},\{k_i\}))\,\Theta(v-V_{\rm sc}(k_{\rm hc}))\Big)\\
&\qquad+\left(\int[\mathrm{d}k_{\rm hc}]\,|\mathcal{M}_{{\rm hc},\ell}(k_{\rm hc})|^2\Theta(v-V_{\rm sc}(k_{\rm hc}))-\int_0^{Q^2v^{\frac{2}{a+b_\ell}}}\frac{\mathrm{d}k^2}{k^2}\frac{\alpha_s(k,\epsilon)}{2\pi}\gamma_\ell^{(0)}\right)\\
&\left.\left.\qquad\times\Theta(v-V(\{\tilde{p}\},\{k_i\}))\right]\right\}.
\end{aligned}
\tag{4.67}
$$

The integral in round brackets of the last line of the above equation can be evaluated analytically as follows. For each leg $\ell=1,2,3$, we expand the $\Theta(v-V_{\rm sc}(k_{\rm hc}))$ function in the last line of Eq. (4.67) as

$$
\begin{aligned}
\Theta(v-V_{\rm sc}(k_{\rm hc}))&=\Theta\left(v-d_\ell\left(\frac{k_t^{(\ell)}}{Q}\right)^a e^{-b_\ell\eta^{(\ell)}}g_\ell(\phi^{(\ell)})\right)=\Theta\left(v-\left(\frac{k_t^{(\ell)}}{Q}\right)^{a+b_\ell}\frac{d_\ell g_\ell(\phi^{(\ell)})}{(z^{(\ell)})^{b_\ell}}\right)\\
&=\Theta\left(v-\left(\frac{k_t^{(\ell)}}{Q}\right)^{a+b_\ell}\right)-v\,\delta\left(v-\left(\frac{k_t^{(\ell)}}{Q}\right)^{a+b_\ell}\right)\log\frac{d_\ell g_\ell(\phi^{(\ell)})}{(z^{(\ell)})^{b_\ell}}+\ldots
\end{aligned}
\tag{4.68}
$$

where we neglect N^{3}LL corrections in the expansion.

With the expansion Eq. (4.68) it is sufficient to use the azimuthally averaged splitting function in $d=4-2\epsilon$ dimensions to construct the hard-collinear squared matrix element in the subtraction term Eq. (4.66). This is because in Eq. (4.68) the only term that involves

a non-trivial $\phi^{(\ell)}$ dependence is finite in $d = 4$ dimensions. In this approximation, the hard-collinear squared matrix element relative to each leg ℓ is given by

$$[\mathrm{d}k]\,|\mathcal{M}_{\mathrm{hc},\ell}(k)|^2 = 2\frac{e^{\gamma_E\epsilon}}{\Gamma(1-\epsilon)}\frac{\mathrm{d}k_t^{(\ell)}}{k_t^{(\ell)}}\left(\frac{\mu_R}{k_t^{(\ell)}}\right)^{2\epsilon}\mathrm{d}z^{(\ell)}\frac{\mathrm{d}\phi^{(\ell)}}{2\pi}\frac{\alpha_s(k_t^{(\ell)})}{2\pi}\,\langle P_\ell(z;\epsilon)\rangle\,, \tag{4.69}$$

where the running coupling has been renormalised in the $\overline{\mathrm{MS}}$ scheme, and

$$\langle P_q(z;\epsilon)\rangle = \left\langle \hat{P}^{(0)}_{q\to gq}(z;\epsilon)\right\rangle - \frac{2C_F}{z}\,, \tag{4.70}$$

$$\langle P_g(z;\epsilon)\rangle = \left\langle \hat{P}^{(0)}_{g\to gg}(z;\epsilon)\right\rangle + n_F\left\langle \hat{P}^{(0)}_{g\to q\bar{q}}(z;\epsilon)\right\rangle - \frac{2C_A}{z}\,, \tag{4.71}$$

for a (anti)quark and gluon leg respectively. The factor $-2C_\ell/z^{(\ell)}$ eliminates the double counting of the soft singularity which is already accounted for in the first line of Eq. (4.67). After performing the integral in the last line analytically, Eq. (4.67) becomes[7]

$$\begin{aligned}
&\Sigma_{\mathrm{NNLL}}(v) = H(\{\tilde{p}\},\alpha_s(Q))e^{-R_{\mathrm{s}}(v)-R_{\mathrm{hc}}(v)}\\
&\times\frac{e^{-R_{\mathrm{s}}(\delta v)}}{e^{-R_{\mathrm{s}}(v)}}\Bigg\{\sum_{n=0}^{\infty}\frac{1}{n!}\int\prod_{i=1}^{n}[\mathrm{d}k_i]\,|\mathcal{M}_{\mathrm{s}}(k_1,\ldots,k_n)|^2\,\Theta(v-V(\{\tilde{p}\},\{k_i\}))\prod_{\mathrm{clust.}}\Theta\left(V_{\mathrm{sc}}(k_{\mathrm{clust.}})-\delta v\right)\\
&+\sum_{n=0}^{\infty}\frac{1}{n!}\int\prod_{i=1}^{n}[\mathrm{d}k_i]\,|\mathcal{M}_{\mathrm{sc}}(k_i)|^2\,\Theta\left(V_{\mathrm{sc}}(k_i)-\delta v\right)\\
&\times\sum_{\ell=1}^{3}\int[\mathrm{d}k_{\mathrm{hc}}]\,|\mathcal{M}_{\mathrm{hc},\ell}(k_{\mathrm{hc}})|^2\Big(\Theta(v-V(\{\tilde{p}\},\{k_i\},k_{\mathrm{hc}}))-\Theta(v-V(\{\tilde{p}\},\{k_i\}))\,\Theta(v-V_{\mathrm{sc}}(k_{\mathrm{hc}}))\Big)\\
&+\sum_{\ell=1}^{3}\frac{\alpha_s(Qv^{\frac{1}{a+b_\ell}})}{2\pi}C^{(1)}_{\mathrm{hc},\ell}\sum_{n=0}^{\infty}\frac{1}{n!}\int\prod_{i=1}^{n}[\mathrm{d}k_i]\,|\mathcal{M}_{\mathrm{sc}}(k_i)|^2\,\Theta\left(V_{\mathrm{sc}}(k_i)-\delta v\right)\,\Theta(v-V(\{\tilde{p}\},\{k_i\}))\Bigg\}\,,
\end{aligned} \tag{4.72}$$

where we have introduced the hard-collinear radiator defined as

$$R_{\mathrm{hc}}(\bar{v}) = \sum_{\ell=1}^{3}\int_{Q^2\bar{v}^{\frac{2}{a+b_\ell}}}^{Q^2}\frac{\mathrm{d}k^2}{k^2}\gamma_\ell(\alpha_s(k))\,. \tag{4.73}$$

The hard-collinear constant $C^{(1)}_{\mathrm{hc},\ell}$ is given by

$$C^{(1)}_{\mathrm{hc},q} = C_F\left(\frac{7}{2}\frac{b_\ell}{a+b_\ell}+\frac{3}{a+b_\ell}\left(\langle\log d_\ell g_\ell\rangle - b_\ell\log\frac{2E_\ell}{Q}\right)+\frac{1}{2}\right)\,, \tag{4.74}$$

$$C^{(1)}_{\mathrm{hc},g} = \left(\frac{67}{18}C_A-\frac{13}{9}T_R n_F\right)\frac{b_\ell}{a+b_\ell}+\frac{4\pi\beta_0}{a+b_\ell}\left(\langle\log d_\ell g_\ell\rangle - b_\ell\log\frac{2E_\ell}{Q}\right)+\frac{1}{3}T_R n_F\,, \tag{4.75}$$

for hard parton with the flavour of a (anti)quark or gluon respectively, with

$$\langle\log d_\ell g_\ell\rangle = \int_0^{2\pi}\frac{\mathrm{d}\phi^{(\ell)}}{2\pi}\log d_\ell g_\ell(\phi^{(\ell)})\,. \tag{4.76}$$

[7] we abuse notation slightly: in the 4$^{\mathrm{th}}$ line of Eq. (4.72) the hard squared matrix element $|\mathcal{M}_{\mathrm{hc},\ell}(k_{\mathrm{hc}})|^2$ acting of the first Θ-function is the full hard-collinear matrix element with all of the spin dependence, whereas it is the spin averaged hard-collinear matrix element that acts on the second Θ-function.

Finally, the constant part of virtual corrections at NNLL is given by

$$H(\Phi_{\mathcal{B}}, \alpha_s(Q)) = 1 + \frac{\alpha_s(Q)}{2\pi} H^{(1)}(\Phi_{\mathcal{B}}) + \mathcal{O}\big(\alpha_s^2\big), \tag{4.77}$$

where the explicit expression for $H^{(1)}(\Phi_{\mathcal{B}})$ is in general rather long and complicated. However for two-jet events $H^{(1)}$ takes the simple form

$$H^{(1)}(\Phi_{\mathcal{B}}) = C_F \left(-8 + \pi^2\right) , \tag{4.78}$$

in fact in the two-jet case the hard constant is independent of the underlying Born configuration.

For three-jet events $H^{(1)}$ is rather more complicated

$$H^{(1)}(\Phi_{\mathcal{B}}) = \left(\frac{\pi^2}{2}(2C_F + C_A) - 8C_F + \frac{F(y_{12}, y_{13}, y_{23})}{\left|\mathcal{M}(\Phi_{\mathcal{B}})\right|^2} \right) , \tag{4.79}$$

where $F(y_{12}, y_{13}, y_{23})$ is defined in Eq. (2.21) of Ref. [42]. In general $H^{(1)}$ is given by the finite part of the fixed-order one-loop virtual corrections after normalising with the Born level matrix element squared.

4.5.4 The NNLL master formula

Each of the terms in the resolved contribution to Eq. (4.72) can be recast into a finite set of corrections, so that the NNLL cross section $\Sigma_{\mathcal{B}}(\Phi_{\mathcal{B}}; v)$ can be parametrised with the following master formula (we define $\lambda = \alpha_s(Q)\beta_0 \log \frac{1}{v}$)

$$\Sigma_{\mathcal{B}}(\Phi_{\mathcal{B}}; v) = e^{-R_{\rm s}(\lambda) - R_{\rm hc}(\lambda)} \left[\mathcal{F}_{\rm NLL}(\lambda) \left(1 + \frac{\alpha_s(Q)}{2\pi} H^{(1)}(\Phi_{\mathcal{B}}) + \sum_{\ell=1}^{3} \frac{\alpha_s(v^{\frac{1}{a+b_\ell}} Q)}{2\pi} C^{(1)}_{{\rm hc},\ell} \right) + \frac{\alpha_s(Q)}{\pi} \delta\mathcal{F}_{\rm NNLL}(\lambda) \right] , \tag{4.80}$$

where the functions $\mathcal{F}_{\rm NLL}$ and $\delta\mathcal{F}_{\rm NNLL}$ have a general expression for any rIRC safe observable [3, 4, 67] and can be efficiently evaluated numerically in $d = 4$ dimensions. Let us briefly describe the objects in eq. (4.80). First we have the soft radiator $R_{\rm s}$ which includes the contributions due to the *unresolved* soft and optionally collinear radiation, thus the soft radiator contributes terms of LL accuracy and above. The second term is the hard-collinear radiator $R_{\rm hc}$ which includes the contributions due to the *unresolved* hard-collinear radiation, thus the hard-collinear radiator contributes terms of NLL accuracy and above. Next we have $\mathcal{F}_{\rm NLL}$ which includes contributions due to *resolved* soft and collinear radiation, we truncate this term so that its contribution is purely NLL. The

following terms $H^{(1)}$, $C^{(1)}_{\mathrm{hc},\ell}$ and $\delta\mathcal{F}_{\mathrm{NNLL}}$ are the first purely NNLL terms. $H^{(1)}$ and $C^{(1)}_{\mathrm{hc},\ell}$ are constant terms due to the virtual corrections, by multiplying $\mathcal{F}_{\mathrm{NLL}}$ these terms are of order NNLL. Finally there is the $\delta\mathcal{F}_{\mathrm{NNLL}}$ which is due to *resolved* radiation that is soft and/or collinear and is a pure order NNLL term. The NNLL function is decomposed as follows

$$\delta\mathcal{F}_{\mathrm{NNLL}} = \delta\mathcal{F}_{\mathrm{sc}} + \delta\mathcal{F}_{\mathrm{wa}} + \delta\mathcal{F}_{\mathrm{s}} + \delta\mathcal{F}_{\mathrm{correl}} + \delta\mathcal{F}_{\mathrm{clust}} + \delta\mathcal{F}_{\mathrm{rec}} + \delta\mathcal{F}_{\mathrm{hc}}\,, \tag{4.81}$$

where each term has a well-defined physical origin.

- The correction terms $\delta\mathcal{F}_{\mathrm{sc}}$, $\delta\mathcal{F}_{\mathrm{wa}}$, $\delta\mathcal{F}_{\mathrm{s}}$, $\delta\mathcal{F}_{\mathrm{correl}}$ and $\delta\mathcal{F}_{\mathrm{clust}}$ have their origin in soft resolved radiation, the first term in the curly brackets of Eq. (4.72).

  The *soft-collinear* correction function $\delta\mathcal{F}_{\mathrm{sc}}$ accounts for running coupling corrections to the real emissions in the CMW scheme [59] and the correct rapidity boundary for a single soft-collinear emission. For event shapes variables this correction is particularly simple [4] as the rapidity dependence of the observable can always be handled analytically. For observables with a more complicated rapidity dependence, such as jet rates [67], the running coupling correction $\delta\mathcal{F}^{\mathrm{rc}}_{\mathrm{sc}}$ and the correction due to the rapidity boundary $\delta\mathcal{F}^{\mathrm{rap}}_{\mathrm{sc}}$ must be treated separately.

  The *wide-angle* correction function $\delta\mathcal{F}_{\mathrm{wa}}$ accounts for the difference between the observable and its soft-collinear parametrisation for a single soft wide-angle emission accompanied by many soft-collinear gluons.

  The *soft* correction function $\delta\mathcal{F}_{\mathrm{s}}$ accounts for the emission of a soft wide angle gluon at the level of the matrix element squared, but evaluated with the V_{sc}.

  At NLL all *resolved* emissions are strongly ordered in angle, and thus emitted independently. The matrix element used to compute the function $\mathcal{F}_{\mathrm{NLL}}$ is simply given by a product of an arbitrary number of single-gluon emission squared matrix element $|\widetilde{\mathcal{M}}_{\mathrm{sc}}(k_i)|^2$, in the decomposition of Eq. (4.44). Starting from NNLL two or more resolved emissions can become close in angle. In this type of configurations, the squared matrix element is given by an abelian term (defined by the product of n single emission probabilities) and by non-abelian, correlated clusters of two or more particles (see Eq. (4.44)). At NNLL it is sufficient to account for the effect of only two emissions becoming close in angle, while the others can be considered far apart. This induces two types of corrections: $\delta\mathcal{F}_{\mathrm{correl}}$ and $\delta\mathcal{F}_{\mathrm{clust}}$.

  The *correlated* correction function $\delta\mathcal{F}_{\mathrm{correl}}$ accounts for the insertion in the resolved ensemble of soft-collinear, independently emitted gluons of a *single* double-

soft cluster $|\widetilde{\mathcal{M}}_{\mathrm{s},0}(k_1,k_2)|^2$ that is defined as the non-abelian part of the square of the double-soft current [4]. The *clustering* correction function $\delta\mathcal{F}_{\mathrm{clust}}$ (defined in Ref. [67]), on the other hand, accounts for the contribution of two independently emitted gluons that become close in angle. Due to the properties of most event shapes, this correction usually vanishes. It becomes different from zero only when the observable has a non-trivial dependence on the rapidity of the emissions, as for instance in the case of jet rates [67].

- The *hard-collinear* correction $\delta\mathcal{F}_{\mathrm{hc}}$ and *recoil* correction $\delta\mathcal{F}_{\mathrm{rec}}$ originate from the second term in the curly brackets of Eq. (4.72), and have a hard-collinear nature. The emission of a hard collinear parton induces two types of corrections: at the level of the squared matrix element (encoded in $\delta\mathcal{F}_{\mathrm{hc}}$), and at the level of the kinematics, due to the recoil of the whole event against the hard-collinear emission (encoded in $\delta\mathcal{F}_{\mathrm{rec}}$). Note that in general $\delta\mathcal{F}_{\mathrm{rec}}$ contains contributions due to spin correlations and as a result may be dependent on the underlying Born momenta.

- Finally, the term

$$\mathcal{F}_{\mathrm{NLL}}(\lambda)\left(1+\frac{\alpha_s(Q)}{2\pi}H^{(1)}(\Phi_{\mathcal{B}})+\sum_{\ell=1}^{3}\frac{\alpha_s(Qv^{\frac{1}{a+b_\ell}})}{2\pi}C^{(1)}_{\mathrm{hc},\ell}\right), \tag{4.82}$$

  arises from the first and third term in the curly brackets of Eq. (4.72), where N^{3}LL corrections were neglected. The function $\mathcal{F}_{\mathrm{NLL}}$ is purely NLL [3], while the multiplying constants $H^{(1)}$ and $C^{(1)}_{\mathrm{hc},\ell}$ induce NNLL corrections.

Before proceeding, we stress that in the definition of the unresolved soft radiation given in Eq. (4.50) we have some freedom in deciding precisely how we define resolution variable. In particular, instead of V_{sc}, we could use any observable $V_{\mathrm{res.}}$ that shares the same leading logarithms as the full observable V that is being resummed. We choose V_{sc} out of computational convenience, as for an rIRC safe observable this allows us to compute all of the ingredients in the Sudakov radiator analytically. If we were to choose a different resolution variable we would find a different Sudakov radiator, and consequently the different functions $\mathcal{F}_{\mathrm{NLL}}$ and $\delta\mathcal{F}_{\mathrm{NNLL}}$.

A particularly important aspect of the definition of the resolution variable concerns the way V_{sc} in Eq. (4.50) is evaluated on the total momentum $k_{\mathrm{clust.}}$ of a cluster of more than one particle. Although the cluster has a non-zero invariant mass, V_{sc} (4.30) does not depend on the mass, and hence, in the definition of the resolution scale, the cluster is treated as if it were *massless*. This greatly simplifies the calculation of the Sudakov radiator, as we can evaluate the integral over the invariant mass of the web analytically.

4.6 The Sudakov radiator

In this section we explicitly compute the Sudakov radiator defined in Eqs. (4.57) and (4.73) to NNLL.

4.6.1 The soft radiator

With the choice of resolution variable as in Eq. (4.31), the soft dipole radiator reads

$$R_{\rm s}^{(ij)}(v) = \sum_{\ell\in(ij)} \int \frac{\mathrm{d}^4k}{(2\pi)^4}\, w(m^2,(\kappa^{(ij)})^2{+}m^2)\,\Theta\left(d_\ell^{(ij)}\left(\frac{\kappa^{(ij)}}{Q_{ij}}\right)^a e^{-b_\ell\eta_{ij}^{(\ell)}} g_\ell(\phi^{(ij)}) - v\right)\Theta(\eta_{ij}^{(\ell)})\,. \tag{4.83}$$

where the phase space is given in Eq. (4.35). We note that the phase-space measure contains the *massive* rapidity y of the web as defined in Eq. (4.35), whilst the observable is expressed in terms of the rapidity of a massless parton $\eta^{(\ell)}$. This miss-match in the rapidity will give rise to two separate contributions to the soft dipole radiator. We separate out the different contributions to Eq. (4.83) in a way in which LL, NLL and NNLL are each separated. The first step to achieve this is to isolate the dependence on $d_\ell g_\ell(\phi)$ by expanding the observable constraint in Eq. (4.83). This proceeds in the same fashion as we did in Eq. (4.68), we find

$$\begin{aligned}
&\Theta\left(d_\ell^{(ij)}\, g_\ell(\phi^{(ij)})\left(\frac{\kappa^{(ij)}}{Q_{ij}}\right)^a e^{-b_\ell\eta_{ij}^{(\ell)}} - v\right) \simeq \Theta\left(\log\left[\left(\frac{\kappa^{(ij)}}{Q_{ij}}\right)^a e^{-b_\ell\eta_{ij}^{(\ell)}}\right] - \log v\right)\\
&+\delta\left(\log\left[\left(\frac{\kappa^{(ij)}}{Q_{ij}}\right)^a e^{-b_\ell\eta_{ij}^{(\ell)}}\right] - \log v\right)\log\left(d_\ell^{(ij)}\, g_\ell(\phi^{(ij)})\right)\\
&+\delta'\left(\log\left[\left(\frac{\kappa^{(ij)}}{Q_{ij}}\right)^a e^{-b_\ell\eta_{ij}^{(\ell)}}\right] - \log v\right)\frac{1}{2}\log^2\left(d_\ell^{(ij)}\, g_\ell(\phi^{(ij)})\right)\,,
\end{aligned} \tag{4.84}$$

The first term in the above equation starts at LL accuracy, the second at NLL accuracy, and so on. Inserting this expansion into the soft radiator Eq. (4.57) we find

$$R_{\rm s}^{(ij)}(v) \simeq \sum_{\ell\in(ij)}\left(r_\ell(v) + r'_\ell(v)\,\langle\log d_\ell g_\ell\rangle + \frac{1}{2}r''(v)\,\langle\log^2 d_\ell g_\ell\rangle\right)\,, \tag{4.85}$$

with

$$\begin{aligned}
r_\ell(v) &= \int \frac{\mathrm{d}^4k}{(2\pi)^4}\, w(m^2,(\kappa^{(ij)})^2+m^2)\,\Theta\left(\left(\frac{\kappa^{(ij)}}{Q_{ij}}\right)^a e^{-b_\ell\eta_{ij}^{(\ell)}} - v\right)\Theta(\eta_{ij}^{(\ell)})\,,\\
r'_\ell &= \frac{\mathrm{d}r_\ell}{\mathrm{d}\log\frac{1}{v}} = -v\frac{\mathrm{d}r_\ell(v)}{\mathrm{d}v}\,,\\
r''_\ell &= \frac{\mathrm{d}r'_\ell}{\mathrm{d}\log\frac{1}{v}} = -v\frac{\mathrm{d}r'_\ell(v)}{\mathrm{d}v}\,.
\end{aligned} \tag{4.86}$$

We first cast our attention onto $r_\ell(v)$. The kinematic boundary for the rapidity integral is

$\log\left(Q_{ij}/\sqrt{(\kappa^{(ij)})^2+m^2}\right)$, the boundary of the massive emission. Instead of computing directly the integral in Eq. (4.86), we split it into the sum of two terms as

$$r_\ell(v) \simeq r^0_\ell(v) + \delta r_\ell(v)\,, \tag{4.87}$$

where $r^0_\ell(v)$ is defined as in Eq. (4.86) but with a massless rapidity boundary, i.e. $\log\left(Q_{ij}/\kappa^{(ij)}\right)$. This defines a *massless* radiator, in which $\eta^{(\ell)}_{ij}$ coincides with y_{ij}, i.e.

$$r^0_\ell(v) = \int \frac{d^4k}{(2\pi)^4}\, w(m^2,(\kappa^{(ij)})^2{+}m^2)\,\Theta\left(\log\frac{Q_{ij}}{\kappa^{(ij)}} - \eta^{(\ell)}_{ij}\right)\,\Theta\left(\left(\frac{\kappa^{(ij)}}{Q_{ij}}\right)^a e^{-b_\ell\eta^{(\ell)}_{ij}} - v\right)\Theta(\eta^{(\ell)}_{ij})\,. \tag{4.88}$$

The massless radiator beings at LL accuracy. The function $\delta r_\ell(v)$ defines a *mass correction*, which accounts for the correct rapidity bound. By inspecting the phase space constraints due to the physical rapidity bound and the observable, we find that the rapidity integral is bounded by $\log\left(Q_{ij}/\sqrt{(\kappa^{(ij)})^2+m^2}\right)$ only when $\kappa^{(ij)} > v^{\frac{1}{a+b_\ell}}Q_{ij}$. This leads to the following expression for the mass correction to the soft radiator

$$\begin{aligned}\delta r_\ell(v) = \int \frac{\mathrm{d}^4k}{(2\pi)^4}\, w(m^2,(\kappa^{(ij)})^2+m^2)\,\Theta(\kappa^{(ij)} - v^{\frac{1}{a+b_\ell}}Q_{ij})\,\Theta(\eta^{(\ell)}_{ij})\\ \times\left[\Theta\left(\log\sqrt{\frac{Q^2_{ij}}{(\kappa^{(ij)})^2+m^2}} - \eta^{(\ell)}_{ij}\right) - \Theta\left(\log\sqrt{\frac{Q^2_{ij}}{(\kappa^{(ij)})^2}} - \eta^{(\ell)}_{ij}\right)\right]\,.\end{aligned} \tag{4.89}$$

We can justify the separation of the radiator in Eq. (4.87) on physical grounds. If we ignore the running of the coupling constant, then the massless radiator $r^0_\ell(v)$ only contains double logarithmic terms, while the mass correction $\delta r_\ell(v)$ is purely single logarithmic.

Let us now focus of the massless radiator at NNLL. Eq. (4.88) can be evaluated by recalling that the resolution variable was chosen so that it does not depend on the mass of the web. Therefore, in Eq. (4.88) we can freely integrate over the mass of the web. The integral of the web $w(m^2,(\kappa^{(ij)})^2+m^2)$ over its invariant mass defines a generalisation of the physical CMW coupling [59]:

$$\int_0^\infty \mathrm{d}m^2\, w(m^2,(\kappa^{(ij)})^2+m^2) \equiv (4\pi)^2\frac{1}{(\kappa^{(ij)})^2}\alpha_s^{\text{phys.}}(k_t)\,. \tag{4.90}$$

The physical coupling $\alpha_s^{\text{phys.}}$ is related to the $\overline{\text{MS}}$ coupling α_s as follows

$$\alpha_s^{\text{phys.}} = \alpha_s\left(1+\sum_{n=1}^\infty\left(\frac{\alpha_s}{2\pi}\right)^n K^{(n)}\right)\,, \tag{4.91}$$

where the set of constants $K^{(n)}$, are perturbatively calculable and, once identified, the massless radiator $r^0_\ell(v)$ is fully determined for any observable, and given by

$$r^0_\ell(v) = \int\frac{\mathrm{d}\kappa^{(ij)}}{\kappa^{(ij)}}\frac{\alpha_s^{\text{phys.}}(\kappa^{(ij)})}{\pi}\int_0^{\log(Q_{ij}/\kappa^{(ij)})}\mathrm{d}\eta\,\Theta\left(\left(\frac{\kappa^{(ij)}}{Q_{ij}}\right)^a e^{-b_\ell\eta_{ij}} - v\right)\,. \tag{4.92}$$

At NNLL accuracy, in the expression of $\alpha_s^{\text{phys.}}$ we need to include only $K^{(1)}$ and $K^{(2)}$, whose expressions are obtained by integrating the web up to order α_s^3. This requires contributions up to the triple-soft current at tree level [68], the single-soft two loop current [69], and the double-soft current at one loop. We reproduce the explicit expression for $K^{(1)}$ in Eq. (C.6) and $K^{(2)}$ in Eq. (C.7).

For the computation of the mass correction at NNLL, we only need to consider the web up to α_s^2. The only non-vanishing contribution is due to the double-emission soft block, $|\widetilde{\mathcal{M}}_{s,0}(k_a,k_b)|^2$.[8] We reproduce the form of $|\widetilde{\mathcal{M}}_{s,0}(k_a,k_b)|^2$ in Appendix. C.4. Using the rescaled variable $\mu^2 = m^2/(\kappa^{(ij)})^2$, we find

$$\begin{aligned}\delta r_\ell(v) &= \frac{1}{2}\int_{Q_{ij}v^{\frac{1}{a+b_\ell}}}^{Q_{ij}} \frac{\mathrm{d}\kappa^{(ij)}}{\kappa^{(ij)}} \left(\frac{\alpha_s(\kappa^{(ij)})}{\pi}\right)^2 \int_0^\infty \frac{\mathrm{d}\mu^2}{\mu^2(1+\mu)} \times \\ &\quad \times \left(C_A \log\frac{1+\mu^2}{\mu^4} - 2\pi\beta_0\right) \log\left(\sqrt{\frac{1}{1+\mu^2}}\right) \\ &= \pi\beta_0\zeta_2 \frac{1}{2}\int_{Q_{ij}v^{\frac{1}{a+b_\ell}}}^{Q_{ij}} \frac{\mathrm{d}\kappa^{(ij)}}{\kappa^{(ij)}} \left(\frac{\alpha_s(\kappa^{(ij)})}{\pi}\right)^2 .\end{aligned} \tag{4.93}$$

4.6.2 The hard-collinear radiator

The hard-collinear part of the radiator, defined in Eq. (4.73), starts at NLL accuracy. Up to NNLL accuracy, its expression is

$$R_{\text{hc}} = \sum_{\ell=1}^{3} \int_{Q^2 v^{\frac{2}{a+b_\ell}}}^{Q^2} \frac{\mathrm{d}k^2}{k^2} \frac{\alpha_s(k)}{2\pi} \left[\gamma_\ell^{(0)} + \left(\frac{\alpha_s}{2\pi}\right)\gamma_\ell^{(1)}\right] . \tag{4.94}$$

In our case, the coefficients $\gamma_\ell^{(0)}$ and $\gamma_\ell^{(1)}$ are the coefficients of the $\delta(1-x)$ piece of the $P_{\text{qq}}(x)$ splitting functions with an overall minus sign. $\gamma_q^{(0)}$ is given in Eq. (C.8), $\gamma_g^{(0)}$ by Eq. (C.9), $\gamma_q^{(1)}$ by Eq. (C.10) and $\gamma_g^{(1)}$ by Eq. (C.11). These are all of the ingredients necessary to determine the hard-collinear radiator.

4.6.3 The radiator up to NNLL accuracy

The computation of the radiator proceeds by integrating the explicit form of the radiator as defined in the above sections with the running of the coupling. At NNLL accuracy, we must use the following renormalisation group equation

$$\mu_R^2 \frac{\mathrm{d}\alpha_s}{\mathrm{d}\mu_R^2} = -\beta_0\alpha_s^2 - \beta_1\alpha_s^3 - \beta_2\alpha_s^4, \tag{4.95}$$

[8] The virtual corrections to the single-emission soft block are massless.

where β_0, β_1 and β_2 are given by Eqs. (C.2), (C.3) and (C.4) respectively. For resummation purposes, it is sufficient to solve Eq. (4.95) using the following ansatz

$$\alpha_s(\mu_R) = \sum_{n=1}^{\infty} \left(\frac{\alpha_s(Q)}{1+t}\right)^n f_n(t)\,, \qquad t \equiv \alpha_s\beta_0 \log\left(\mu_R^2/Q^2\right). \tag{4.96}$$

Plugging the above in Eq. (4.95), we determine the f_i coefficient functions to be

$$f_1(t) = 1\,, \tag{4.97}$$

$$f_2(t) = -\frac{\beta_1}{\beta_0}\log(1+t)\,, \tag{4.98}$$

$$f_3(t) = -\frac{\beta_2}{\beta_0}t + \left(\frac{\beta_1}{\beta_0}\right)^2 [t + (\log(1+t) - 1)]\log(1+t)\,, \tag{4.99}$$

and we can neglect the contributions of $f_4(t)$ and beyond, as these correspond to N^{3}LL terms.

It is customary to express the radiator in terms of $\lambda = \alpha_s(Q)\beta_0 \log\frac{1}{v}$, and we will do this for the hard-collinear radiator. Note however that each of the soft dipole radiators is instead a function of $\lambda_{ij} = \alpha_s(Q_{ij})\beta_0 \log\frac{1}{v}$. We can expand the soft dipole radiators around $\alpha_s(Q)$ to recover the usual parametrisation in terms of λ. This will be necessary to ensure that our resummation is not contaminated by higher order terms originating in the different scales of the running coupling. We will return to this point when we express the complete resummation. We now parametrise the radiator in terms of functions of λ and λ_{ij}, in such a way as to separate LL, NLL and NNLL contributions:

$$r_\ell(\lambda_{ij}) \simeq r^0_\ell(\lambda_{ij}) + \delta r_\ell(\lambda_{ij})\,, \tag{4.100}$$

$$r^0_\ell(\lambda_{ij}) = -\frac{\lambda_{ij}}{\alpha_s\beta_0} g_1^{(\ell)}(\lambda_{ij}) - g_2^{(\ell)}(\lambda_{ij}) - \frac{\alpha_s}{\pi} g_3^{(\ell)}(\lambda_{ij})\,, \tag{4.101}$$

$$\delta r_\ell(\lambda_{ij}) = -\frac{\alpha_s}{\pi}\delta g_3^{(\ell)}(\lambda_{ij})\,, \tag{4.102}$$

$$R_{\mathrm{hc},\ell}(\lambda) = -h_2^{(\ell)}(\lambda) - \frac{\alpha_s}{\pi} h_3^{(\ell)}(\lambda)\,, \tag{4.103}$$

To ensure that our result is NNLL accurate in terms of the λ variable we must expand each of the soft dipole radiators around λ keeping only the terms up to NNLL accuracy. This procedure is straightforward to carry out and the appropriate replacements are given by Eqs. (C.24,C.25,C.26) for LL, NLL and NNLL accuracy respectively. For the hard-collinear radiator no such replacement must be carried out.

4.7 Resolved radiation at NLL

In this section we will compute the contribution to the observable by the multiple resolved emissions. At NLL accuracy we only need to consider soft-collinear emissions that are

emitted independently. This contribution was originally determined in Ref. [3], we work through the details showing the effects due to the dipole structure.

4.7.1 The NLL correction $\mathcal{F}_{\rm NLL}$

At NLL accuracy the contribution of the resolved radiation is due to an ensemble of soft and collinear gluons that are widely separated in rapidity, this is the first term in the curly brackets in Eq. (4.72) where we take the matrix element to contain only the first term of the clustering Eq. (4.65) (the matrix element is a product of independent soft and collinear emissions). This gives rise to the function

$$\mathcal{F}(v) = \frac{e^{-R_{\rm s}(\delta v)}}{e^{-R_{\rm s}(v)}} \sum_{n=0}^{\infty} \frac{1}{n!} \int_{\delta v} \prod_{i=1}^{n} [{\rm d}k_i] |\mathcal{M}_{\rm sc}(k_i)|^2 \Theta\Big(v - V_{\rm sc}(\{\tilde{p}\}, \{k_i\})\Big)\,, \tag{4.104}$$

at NLL accuracy we can make the replacement

$$\frac{e^{-R_{\rm s}(\delta v)}}{e^{-R_{\rm s}(v)}} = \exp\left(-\int_{\delta v}^{v} [{\rm d}k]\, |\mathcal{M}_{\rm sc}(k)|^2\right)\,, \tag{4.105}$$

and using this expression we can rewrite $\mathcal{F}(v)$ as

$$\mathcal{F}(v) = e^{-\int_{\delta v}^{v} [{\rm d}k]\, |\mathcal{M}_{\rm sc}(k)|^2} \sum_{n=0}^{\infty} \frac{1}{n!} \int_{\delta v} \prod_{i=1}^{n} [{\rm d}k_i]\, |\mathcal{M}_{\rm sc}(k_i)|^2\, \Theta\Big(v - V_{\rm sc}(\{\tilde{p}\}, \{k_i\})\Big)\,. \tag{4.106}$$

Although this expression has all of the terms necessary to achieve NLL accuracy, it also contains subleading effects. We would like to eliminate these to ensure a pure NLL result, with no higher order contamination. We will address each of the NNLL corrections in turn following our computation here.

Before finding the purely NLL approximation to $\mathcal{F}$ we will reparametrise Eq. (4.106) to make it more amenable for numerical evaluation by Monte Carlo methods. In doing so we will reveal what approximations are necessary to achieve a pure NLL result. We begin by transforming k_i to coordinates defined by the triplet $(v_i, \xi_i^{(\ell_i)}, \phi_i^{(\ell_i)})$, there is such a triplet for each dipole that we consider. The members of the triplet are defined as follows

- v_i is the value of the observable in the presence of a single emission k_i

$$v_i^{(ij)} = V_{\rm sc}(\{\tilde{p}\}, k_i) = d_{\ell_i}^{(ij)} \left(\frac{\kappa_i^{(\ell_i)}}{Q_{ij}}\right)^a e^{-b_{\ell_i}\eta_i^{(\ell_i)}} g_{\ell_i}(\phi_i^{(\ell_i)})\,, \tag{4.107}$$

  where all of these variables depend on the dipole we are considering. To avoid the notation becoming too dense we only label v_i with the dipole index.

- $\xi_i^{(\ell_i)}$ is the rapidity fraction defined as the rapidity of the emission divided by the largest available rapidity for a given value of $v_i^{(ij)}$

$$\xi_i^{(\ell_i)} = \frac{\eta_i^{(\ell_i)}}{\eta_{i,\rm max}^{(\ell_i)}}\,, \qquad \eta_{i,\rm max}^{(\ell_i)} = \frac{1}{a + b_{\ell_i}} \log \frac{d_{\ell_i}^{(ij)} g_{\ell_i}(\phi_i^{(\ell_i)})}{v_i^{(ij)}} \tag{4.108}$$

- $\phi_i^{(\ell_i)}$ retains its usual definition, the azimuth of a given emission with respect to the leg ℓ_i.

The relationship between the old variables and the new variables is given explicitly by

$$\log\frac{\kappa_i^{(\ell_i)}}{Q} = \frac{a+(1-\xi^{(\ell_i)})b_{\ell_i}}{a(a+b_{\ell_i})}\log\frac{v_i^{(ij)}}{d_{\ell_i}g_{\ell_i}(\phi_i^{(\ell_i)})}\,, \tag{4.109}$$

$$\eta_i^{(\ell_i)} = \xi_i^{(\ell_i)}\eta_{i,\max}^{(\ell_i)}\,, \tag{4.110}$$

note that ϕ is unchanged between the two coordinate systems. In terms of the new coordinates we can write the probability for a single emission as follows

$$\begin{aligned}\int[\mathrm{d}k_i]\,|\mathcal{M}_{\mathrm{sc}}(k_i)|^2 = \sum_{(ij)}C_{(ij)}\sum_{\ell_i\in(ij)}\int\frac{\mathrm{d}v_i^{(ij)}}{v_i^{(ij)}}\int_0^1\mathrm{d}\xi_i^{(\ell_i)}\int_0^{2\pi}\frac{\mathrm{d}\phi_i^{(\ell_i)}}{2\pi}\times\\ \times 2\frac{\alpha_s^{\mathrm{phys.}}\left(Q_{ij}\left(\frac{v_i^{(ij)}}{d_{\ell_i}^{(ij)}g_{\ell_i}(\phi_i^{(\ell_i)})}\right)^{\frac{a+(1-\xi_i^{(\ell_i)})b_{\ell_i}}{a(a+b_{\ell_i})}}\right)}{\pi}\frac{\log\left(\frac{d_{\ell_i}^{(ij)}g_{\ell_i}(\phi_i^{(\ell_i)})}{v_i^{(ij)}}\right)}{a(a+b_{\ell_i})}\,,\end{aligned} \tag{4.111}$$

now we make some further approximations. The first thing we do is replace $\alpha_s^{\mathrm{phys.}}$ by the explicit running, at NLL accuracy we only need to include the one loop running of the coupling.

$$\begin{aligned}\int[\mathrm{d}k_i]\,|\mathcal{M}_{\mathrm{sc}}(k_i)|^2 = \sum_{(ij)}C_{(ij)}\sum_{\ell_i\in(ij)}\int\frac{\mathrm{d}v_i^{(ij)}}{v_i^{(ij)}}\int_0^1\mathrm{d}\xi_i^{(\ell_i)}\int_0^{2\pi}\frac{\mathrm{d}\phi_i^{(\ell_i)}}{2\pi}\times\\ \times 2\frac{\alpha_s(Q_{ij})}{1+\frac{a+(1-\xi_i^{(\ell_i)})b_{\ell_i}}{a(a+b_{\ell_i})}2\beta_0\alpha_s(Q_{ij})\log\left(\frac{v_i}{d_{\ell_i}^{(ij)}g_{\ell_i}(\phi_i^{(\ell_i)})}\right)}\frac{\log\left(\frac{d_{\ell_i}^{(ij)}g_{\ell_i}(\phi^{(\ell_i)})}{v_i^{(ij)}}\right)}{a(a+b_{\ell_i})}\,.\end{aligned} \tag{4.112}$$

Grouping terms together we see that the we have a complicated integral over the rapidity fraction $\xi_i^{(\ell_i)}$

$$\mathcal{N}(\alpha_s(Q)\log\bar{v}) = \int_0^1\frac{\mathrm{d}\xi^{(\ell)}}{1+\frac{a+(1-\xi^{(\ell)})b_\ell}{a(a+b_\ell)}2\beta_0\,\alpha_s(Q)\log\bar{v}}\,. \tag{4.113}$$

We now choose to normalise this integral, i.e. we would like to change the integration measure to include this extra term. To that end we can multiply the integrand by 1 in a

clever way

$$\int [\mathrm{d}k_i] \left|\mathcal{M}_{\mathrm{sc}}(k_i)\right|^2 = \sum_{(ij)} C_{(ij)} \sum_{\ell_i \in (ij)} \int \frac{\mathrm{d}v_i^{(ij)}}{v_i^{(ij)}} \int_0^1 \mathrm{d}\xi_i'^{(\ell_i)} \int_0^{2\pi} \frac{\mathrm{d}\phi_i^{(\ell_i)}}{2\pi} \times$$
$$\times \frac{\alpha_s(Q_{ij}) \log \frac{1}{v_i^{(ij)}}}{1 + \frac{a+(1-\xi_i'^{(\ell_i)})b_{\ell_i}}{a(a+b_{\ell_i})} 2\beta_0 \alpha_s(Q_{ij}) \log v_i^{(ij)}} \frac{2}{\pi} \frac{1}{a(a+b_{\ell_i})} \times$$
$$\times \frac{1}{\mathcal{N}(\alpha_s(Q_{ij}) \log v_i^{(ij)})} \int_0^1 \frac{\mathrm{d}\xi_i^{(\ell_i)}}{1 + \frac{a+(1-\xi_i^{(\ell_i)})b_{\ell_i}}{a(a+b_{\ell_i})} 2\beta_0 \alpha_s(Q_{ij}) \log v_i^{(ij)}} \quad (4.114)$$

We introduce the variable $\lambda'_{ij} = \alpha_s(Q_{ij})\beta_0 \log \frac{d_\ell^{(ij)} g_\ell(\phi^{(\ell)})}{v_i^{(ij)}}$ (another variant of the usual λ) and focus on the integral over the dummy variable, ξ'_i, that we introduced in our normalisation of the ξ_i integral. This integration can be performed analytically, we find

$$\frac{2}{\pi\beta_0} \frac{1}{a(a+b_\ell)} \int_0^1 \mathrm{d}\xi'^{(\ell)} \frac{\lambda'_{ij}}{1 - 2\frac{a+(1-\xi^{(\ell)})b_\ell}{a(a+b_\ell)} \lambda'_{ij}}$$
$$= \frac{2}{\pi\beta_0} \frac{1}{a(a+b_\ell)} \left[\frac{a(a+b_\ell)}{2b_\ell}\right] \left[\log\left(1 - \frac{2\lambda'_{ij}}{a+b_\ell}\right) - \log\left(1 - \frac{2\lambda'_{ij}}{a}\right)\right]$$
$$= \frac{1}{b_\ell \pi\beta_0} \left[\log\left(1 - \frac{2\lambda'_{ij}}{a+b_\ell}\right) - \log\left(1 - \frac{2\lambda'_{ij}}{a}\right)\right]$$
$$= r'_{\mathrm{NLL},\ell}(\lambda'_{ij}) \,, \quad (4.115)$$

this expression is the derivative of the soft radiator at NLL accuracy. Making this identification we can rewrite the integral as

$$\int [\mathrm{d}k_i] \left|\mathcal{M}_{\mathrm{sc}}(k_i)\right|^2 = \sum_{(ij)} C_{(ij)} \sum_{\ell_i \in (ij)} \int \frac{\mathrm{d}v_i^{(ij)}}{v_i^{(ij)}} \int_0^{2\pi} \frac{\mathrm{d}\phi_i^{(\ell_i)}}{2\pi} \times$$
$$\times \frac{1}{\mathcal{N}(\alpha_s(Q_{ij}) \log\left(\frac{v_i^{(ij)}}{d_{\ell_i} g_{\ell_i}(\phi_i^{(\ell_i)})}\right)} \int_0^1 \frac{\mathrm{d}\xi_i^{(\ell_i)}}{1 + \frac{a+(1-\xi_i^{(\ell_i)})b_{\ell_i}}{a(a+b_{\ell_i})} 2\beta_0 \alpha_s(Q_{ij}) \log\left(\frac{v_i^{(ij)}}{d_{\ell_i} g_{\ell_i}(\phi_i^{(\ell_i)})}\right)} \times$$
$$\times r'_{\mathrm{NLL},\ell_i}\left(\alpha_s(Q_{ij})\beta_0 \log\left(\frac{v_i^{(ij)}}{d_{\ell_i}^{(ij)} g_{\ell_i}(\phi_i^{(\ell_i)})}\right)\right) . \quad (4.116)$$

In fact our choice to perform the running at one loop is what gives us r'_{NLL}, considering a more general running, at an arbitrary loop order, we would instead find the derivative of the full soft radiator. There is one final transformation that we can make to aid our calculation, and that is to introduce

$$\zeta_i^{(ij)} = \frac{v_i^{(ij)}}{v} \,, \quad (4.117)$$

the ratio of the observable's value corresponding to the i^{th} emission to the observable's

actual value v. Performing this change of variables we have our final result

$$\int [\mathrm{d}k_i] \left|\mathcal{M}_{\mathrm{sc}}(k_i)\right|^2 = \sum_{(ij)} C_{(ij)} \sum_{\ell_i \in (ij)} \int \frac{\mathrm{d}\zeta_i^{(ij)}}{\zeta_i^{(ij)}} \int_0^{2\pi} \frac{\mathrm{d}\phi_i^{(\ell_i)}}{2\pi} \times$$
$$\times \frac{1}{\mathcal{N}\left(\alpha_s(Q_{ij}) \log\left(\frac{\zeta_i^{(ij)} v}{d_{\ell_i}^{(ij)} g_{\ell_i}(\phi_i^{(\ell_i)})}\right)\right)} \int_0^1 \frac{\mathrm{d}\xi_i^{(\ell_i)}}{1 + \frac{a+(1-\xi_i^{(\ell_i)})b_{\ell_i}}{a(a+b_{\ell_i})} 2\beta_0 \alpha_s(Q_{ij}) \log\left(\frac{\zeta_i^{(ij)} v}{d_{\ell_i}^{(ij)} g_{\ell_i}(\phi_i^{(\ell_i)})}\right)} \times$$
$$\times R'_{\ell_i}\left(\alpha_s(Q_{ij})\beta_0 \log\left(\frac{\zeta_i^{(ij)} v}{d_{\ell_i}^{(ij)} g_{\ell_i}(\phi_i^{(\ell_i)})}\right)\right), \quad (4.118)$$

where we have replaced r'_{NLL} by the more general result r'.

Now that we have a parametrisation for $\mathcal{F}$ we can start consider the appropriate approximations to make this a purely NLL result. We start by consider the integration over the rapidity, at NLL accuracy we make is the following approximation

$$\frac{1}{\mathcal{N}(\alpha_s(Q)\log v_i)} \int_0^1 \frac{\mathrm{d}\xi_i^{(\ell_i)}}{1 + \frac{a+(1-\xi_i^{(\ell_i)})b_\ell}{a(a+b_\ell)} 2\beta_0 \alpha_s(Q) \log v_i} \to \int_0^1 \mathrm{d}\xi_i^{(\ell_i)}, \quad (4.119)$$

this is legitimate because at NLL accuracy we only need to consider the ordering of the emissions in rapidity. We can replace the complicated integral over ξ by any function monotonic in ξ, so as to preserve the rapidity ordering of the emissions.

Next we see that r' encodes the dependence of the observable on the true rapidity boundaries. However these are NNLL contributions and in fact to ensure we only have NLL terms we must approximate the true boundary by

$$\eta_{i,\max}^{(\ell_i)} = \frac{1}{a+b_{\ell_i}} \log \frac{d_{\ell_i}^{(ij)} g_{\ell_i}(\phi_i^{(\ell_i)})}{v_i^{(ij)}} \to \frac{1}{a+b_{\ell_i}} \log \frac{1}{v_i^{(ij)}}. \quad (4.120)$$

Equivalently we can expand r' as this contains the dependence on the phase space boundary of the observable

$$r'_\ell\left(\alpha_s(Q_{ij})\beta_0 \log\left(\frac{\zeta^{(ij)} v}{d_\ell^{(ij)} g_\ell(\phi)}\right)\right) = r'_\ell\left(\alpha_s(Q_{ij})\beta_0 \log\frac{1}{v}\right) + \mathcal{O}\big(r''_\ell\big). \quad (4.121)$$

There is now no dependence on the d_ℓ, $d_\ell^{(ij)}$ g_ℓ or ϕ. r' also contains subleading contributions, we neglect these by making the further simplification

$$r'_\ell(\lambda_{ij}) = r'_{\mathrm{NLL},\ell}(\lambda_{ij}) + \mathcal{O}(\mathrm{NNLL}). \quad (4.122)$$

We have eliminated the subleading terms due to the functional form of r', but this expression still contains subleading terms due to the running of the coupling. To remove this we must expand $r'(\lambda_{ij})$ around λ

$$r'_{\mathrm{NLL},\ell}(\lambda_{ij}) = r'_{\mathrm{NLL},\ell}(\lambda) + \mathcal{O}(\mathrm{NNLL}). \quad (4.123)$$

Before we proceed to the final statement of $\mathcal{F}$ it is helpful to examine the structure of the sum over dipoles. This double sum is rather cumbersome, so we will work to remove it and express everything that we can as a sum over legs. At this order we observe that

$$\sum_{(ij)} C_{(ij)} \sum_{\ell\in(ij)} r'_{\mathrm{NLL},\ell}(\lambda) = \sum_{\ell=1}^{3} C_\ell \, r'_{\mathrm{NLL},\ell}(\lambda) = R'_{\mathrm{NLL}}(\lambda)\,, \tag{4.124}$$

which allows us to replace the sum over dipoles by a sum over the legs. With these simplifications $\mathcal{F}(v) \simeq \mathcal{F}_{\mathrm{NLL}}(\lambda)$ where

$$\mathcal{F}_{\mathrm{NLL}}(\lambda) = \int \mathrm{d}\mathcal{Z}[\{R'_{\mathrm{NLL},\ell_i}, k_i\}]\, \Theta\left(1 - \lim_{v\to 0} \frac{V_{\mathrm{sc}}(\{\tilde{p}\},\{k_i\})}{v}\right)\,, \tag{4.125}$$

and all of the subleading terms have been neglected. In Eq. (4.125) we have introduced the average of a function $G(\{\tilde{p}\},\{k_i\})$ over the measure $\mathrm{d}\mathcal{Z}[\{R'_{\mathrm{NLL},\ell_i}, k_i\}]$, which we have defined as

$$\begin{aligned}\int \mathrm{d}\mathcal{Z}[\{R'_{\mathrm{NLL},\ell_i}, k_i\}]\, G(\{\tilde{p}\},\{k_i\}) = \\ \delta^{R'_{\mathrm{NLL}}(\lambda)} \sum_{n=0}^{\infty} \frac{1}{n!} \prod_{i=1}^{n} \int_\delta^\infty \frac{\mathrm{d}\zeta_i}{\zeta_i} \sum_{\ell_i=1}^{3} \int_0^1 \mathrm{d}\xi_i^{(\ell_i)} \int_0^{2\pi} \frac{\mathrm{d}\phi_i^{(\ell_i)}}{2\pi} R'_{\mathrm{NLL},\ell_i}(\lambda)\, G(\{\tilde{p}\},\{k_i\})\,.\end{aligned} \tag{4.126}$$

Note that the dependence on the regulator δ cancels in Eq. (4.126). The limit $v \to 0$ in Eq. (4.125) is necessary to remove contributions that are power suppressed in v. The existence of this limit in the Θ-function of Eq. (4.125) is guaranteed by the rIRC safety of the observable, which imply that the quantity $V_{\mathrm{sc}}(\{\tilde{p}\},\{k_i\})/v$ is independent of v, with corrections that scale as a power of v.

Whilst we have considered the full dependence on the rapidity fraction ξ, we will not do so in the following sections. We will specialise to event shape variables, where we can integrate inclusively over ξ. For related variables such as jet rates and jet vetoes we must keep the dependence on ξ.

4.8 Resolved radiation at NNLL

We now will consider the corrections to the NLL multiple emission function that are necessary to achieve NNLL accuracy. The form of $\delta\mathcal{F}_{\mathrm{sc}}$, $\delta\mathcal{F}_{\mathrm{wa}}$, $\delta\mathcal{F}_{\mathrm{correl}}$, $\delta\mathcal{F}_{\mathrm{rec}}$ and $\delta\mathcal{F}_{\mathrm{hc}}$ was first determined in Ref. [4], where they were determined in the case of two-jet events in e^+e^- annihilation. The correction $\delta\mathcal{F}_{\mathrm{clust}}$ was originally determined in Ref. [67] in the context of jet rates. More recently $\delta\mathcal{F}_{\mathrm{correl}}$ was reformulated in Ref. [61]. We will derive all of the NNLL correction function from their basic definitions so as to determine their appropriate form. We have already anticipated a new correction due to the soft in the form of $\delta\mathcal{F}_{\mathrm{s}}$.

4.8.1 The soft-collinear correction $\delta\mathcal{F}_{\rm sc}$

The soft-collinear correction contains two sources of corrections. The first is due to the running of the coupling due to the inclusion of additional terms from Eq. (4.65), and the second from taking into account the exact rapidity boundary for a single emission in the soft-collinear ensemble. For event shape variables we can treat these two corrections simultaneously, by taking Eq. (4.118) and considering the next term in the expansion of r'_ℓ, which takes the following form

$$r'_\ell\left(\frac{\zeta v}{d_\ell g_\ell(\phi)}\right) = r'_{\rm NLL,\ell}(v) + r'_{\rm NNLL,\ell}(v) + r''_{\rm NNLL,\ell}(v)\log\frac{d_\ell g_\ell(\phi)}{\zeta} + \mathcal{O}\big(\mathrm{N^3LL}\big)\,. \tag{4.127}$$

The first term encodes the NLL rapidity boundary, the second term contains the running of the coupling and the third and final term contains the exact rapidity boundary. Including the expansion of r'_ℓ at this order in we find [4]

$$\begin{aligned}\mathcal{F}(v) = \delta^{R'_{\rm NLL}}\Bigg(1 - \sum_{(ij)} C_{(ij)} \sum_{\ell\in(ij)} \Big(r'_{\rm NNLL,\ell}(\lambda_{ij}) + r''_{\rm NNLL,\ell}(\lambda_{ij})\left\langle \log d_\ell^{(ij)} g_\ell\right\rangle\Big)\log\frac{1}{\delta} \\ -\frac{1}{2} r''_{\rm NNLL,\ell}(\lambda_{ij})\log^2\frac{1}{\delta}\Bigg)\times \\ \times \sum_{n=0}^{\infty}\frac{1}{n!}\prod_{i=1}^{n}\sum_{(ij)} C_{(ij)}\int_\delta^\infty \frac{\mathrm{d}\zeta_i^{(ij)}}{\zeta_i^{(ij)}}\sum_{\ell_i\in(ij)}\int\frac{\mathrm{d}\phi_i^{(\ell_i)}}{2\pi}\times \\ \times\left(r'_{\rm NLL,\ell_i}(\lambda_{ij}) + r'_{\rm NNLL,\ell_i}(\lambda_{ij}) + r''_{\rm NNLL,\ell_i}(\lambda_{ij})\log\frac{d_{\ell_i}^{(ij)} g_{\ell_i}(\phi_i^{(\ell_i)})}{\zeta_i^{(ij)}}\right)\times \\ \times\,\Theta\left(1 - \lim_{v\to 0}\frac{V_{\rm sc}(\{\tilde p\},k,\{k_i\})}{v}\right)\,,\end{aligned} \tag{4.128}$$

We can simplify the above equation by keeping only terms in the sum that are linear in $r'_{\rm NNLL,\ell}$ or $r''_{\rm NNLL,\ell}$, i.e. we correct a single emission at a time. This ensures that no contributions beyond NNLL accuracy are included. Next we must expand all of the terms

around λ and separate out the dipole dependence

$$\begin{aligned}\mathcal{F}(v) = \delta^{R'_{\rm NLL}} \Bigg(1 - \sum_{(ij)} C_{(ij)} \sum_{\ell\in(ij)} \Bigg(r'_{{\rm NNLL},\ell}(\lambda) + r''_{{\rm NNLL},\ell}(\lambda) \left(\langle \log d_\ell g_\ell\rangle - b_\ell \log\frac{2E_\ell}{Q}\right)\Bigg) \log\frac{1}{\delta} \\ + r''_{{\rm NNLL},\ell}(\lambda)\,[a + b_\ell - 2\lambda] \log\frac{Q_{ij}}{Q} \log\frac{1}{\delta} - \frac{1}{2} r''_{{\rm NNLL},\ell}(\lambda) \log^2\frac{1}{\delta}\Bigg) \times \\ \times \sum_{n=0}^{\infty} \frac{1}{n!} \prod_{i=1}^{n} \sum_{(ij)} C_{(ij)} \int_\delta^\infty \frac{{\rm d}\zeta_i^{(ij)}}{\zeta_i^{(ij)}} \sum_{\ell_i\in(ij)} \int \frac{{\rm d}\phi_i^{(\ell_i)}}{2\pi} \times \\ \times \Bigg(r'_{{\rm NLL},\ell_i}(\lambda) + r'_{{\rm NNLL},\ell_i}(\lambda) + r''_{{\rm NNLL},\ell_i}(\lambda) \left(\log\frac{d_{\ell_i} g_{\ell_i}(\phi_i^{(\ell_i)})}{\zeta_i} - b_{\ell_i} \log\frac{2E_{\ell_i}}{Q}\right) \\ + r_{{\rm NNLL},\ell_i}(\lambda)\,[a + b_\ell - 2\lambda] \log\frac{Q_{ij}}{Q}\Bigg)\, \Theta\left(1 - \lim_{v\to 0} \frac{V_{\rm sc}(\{\tilde p\}, k, \{k_i\})}{v}\right) \\ \simeq \mathcal{F}_{\rm NLL}(\lambda) + \frac{\alpha_s(Q)}{\pi} \delta\mathcal{F}_{\rm sc}(\lambda) + \frac{\alpha_s(Q)}{\pi} \delta\mathcal{F}_{\rm s}(\lambda)\,, \end{aligned} \tag{4.129}$$

Where we have made the dipole energy scale Q_{ij} explicit in $\mathcal{F}$. In the final line we have separated the expression into terms that are independent of the dipole energy scale and terms with an explicit dependence on the dipole scale. The former make up the soft-collinear correction ($\mathcal{F}_{\rm NLL}$ and $\delta\mathcal{F}_{\rm sc}$) and the latter make up the soft correction ($\delta\mathcal{F}_{\rm s}$). Moreover, we can express the virtual corrections in Eq. (4.129) as the integral over an extra dummy emission as follows

$$\log\frac{1}{\delta} = \int_\delta^1 \frac{{\rm d}\zeta}{\zeta}\,, \frac{1}{2}\log^2\frac{1}{\delta} = \int_\delta^1 \frac{{\rm d}\zeta}{\zeta} \log\frac{1}{\zeta}\,. \tag{4.130}$$

With this representation of the virtual corrections we can write the soft-collinear correction

$$\begin{aligned}\delta\mathcal{F}_{\rm sc}(\lambda) = \frac{\pi}{\alpha_s(Q)} \int_0^\infty \frac{{\rm d}\zeta}{\zeta} \sum_{\ell=1}^{3} \int_0^{2\pi} \frac{{\rm d}\phi^{(\ell)}}{2\pi} \left(R'_{{\rm NNLL},\ell} + R''_{{\rm NNLL},\ell} \left(\log\frac{d_\ell g_\ell(\phi^{(\ell)})}{\zeta} - b_\ell \log\frac{2E_\ell}{Q}\right)\right) \times \\ \times \int {\rm d}\mathcal{Z}[\{R'_{{\rm NLL},\ell_i}, k_i\}] \left[\Theta\left(1 - \lim_{v\to 0} \frac{V_{\rm sc}(\{\tilde p\}, k, \{k_i\})}{v}\right) - \Theta(1-\zeta)\,\Theta\left(1 - \lim_{v\to 0} \frac{V_{\rm sc}(\{\tilde p\}, \{k_i\})}{v}\right)\right], \end{aligned} \tag{4.131}$$

where the average of a function over the measure ${\rm d}\mathcal{Z}[\{R'_{{\rm NLL},\ell_i}, k_i\}]$ is defined in Eq. (4.126). In the first term of Eq. (4.131), $k = k(\zeta, \phi, \ell)$ represents an additional real emission, and the second term corresponds to the virtual corrections. In Eq. (4.131) we have set the ζ lower integration limit to zero, because singular contributions from $\zeta \to 0$ cancel exactly between the real and virtual corrections.

4.8.2 The soft correction $\delta\mathcal{F}_{\rm s}$

The soft correction takes into account the emission of a single soft emission from the correct matrix element and an ensemble of soft-collinear emissions with the soft-collinear

observable definition. Considering the dipole dependent terms in Eq. (4.129) we perform the following manipulations

$$\begin{aligned} r''_{\text{NNLL},\ell}(\lambda)\,[a+b_\ell-2\lambda]\log\frac{Q_{ij}}{Q} &= \frac{\alpha_s(Q)}{\pi}\frac{2}{(a-2\lambda)(a+b_\ell-2\lambda)}[a+b_\ell-2\lambda]\log\frac{Q_{ij}}{Q} \\ &= \frac{2}{a\pi}\frac{\alpha_s(Q)}{1-\frac{2\lambda}{a}}\log\frac{Q_{ij}}{Q} \\ &= \frac{2}{a\pi}\frac{\alpha_s(Q)}{1+\alpha_s(Q)\beta_0\log\frac{Q^2v^{\frac{2}{a}}}{Q^2}}\log\frac{Q_{ij}}{Q} \\ &= \frac{2}{a\pi}\alpha_s(v^{\frac{1}{a}}Q)\log\frac{Q_{ij}}{Q}\,. \end{aligned} \tag{4.132}$$

Which is sufficient to determine the soft correction,

$$\begin{aligned} \delta\mathcal{F}_{\text{s}}(\lambda) = \sum_{(ij)} 2C_{(ij)}\frac{\alpha_s(v^{\frac{1}{a}}Q)}{\alpha_s(Q)}\frac{1}{a}\log\frac{Q_{ij}}{Q}\int_0^\infty\frac{\mathrm{d}\zeta}{\zeta}\int_0^{2\pi}\frac{\mathrm{d}\phi}{2\pi}\int\mathrm{d}\mathcal{Z}[\{R'_{\text{NLL},\ell_i},k_i\}]\times \\ \times\left[\Theta\left(1-\lim_{v\to0}\frac{V_{\text{sc}}(\{\tilde{p}\},k,\{k_i\})}{v}\right)-\Theta(1-\zeta)\,\Theta\left(1-\lim_{v\to0}\frac{V_{\text{sc}}(\{\tilde{p}\},\{k_i\})}{v}\right)\right]. \end{aligned} \tag{4.133}$$

4.8.3 The soft wide angle correction $\delta\mathcal{F}_{\text{wa}}$

This correction arises when one of the soft gluons is emitted at wide angles. We parametrise observable dependence on the momentum of this wide angle gluon k as

$$V^{(ij)}_{\text{wa}}(\{\tilde{p}\},k) = \left(\frac{\kappa^{(ij)}}{Q}\right)^a f^{(ij)}_{\text{wa}}(\eta,\phi)\,. \tag{4.134}$$

In general, when η is close to zero (wide angles), the above expression will differ from the expression of the observable after a soft and collinear emission k

$$\begin{aligned} V^{(ij)}_{\text{sc}}(\{\tilde{p}\},k) &= \left(\frac{\kappa^{(ij)}}{Q}\right)^a f^{(ij)}_{\text{sc}}(\eta,\phi)\,, \\ f^{(ij)}_{\text{sc}}(\eta,\phi) &= d^{(ij)}_i e^{-b_i\eta}g_i(\phi)\Theta(\eta)+d^{(ij)}_j e^{b_j\eta}g_j(\phi)\Theta(-\eta)\,. \end{aligned} \tag{4.135}$$

With fixed values of $(\kappa^{(ij)},\eta,\phi)$ for the extra emission k, we denote with $V_{\text{wa}}(\{\tilde{p}\},k,\{k_i\})$ the observable computed by keeping the full η,ϕ dependence of the emission k, and the the soft-collinear approximation for all the other emissions.

This gives the following correction [4]

$$\begin{aligned} \mathcal{F}_{\text{wa}} = e^{-\int_{\delta v}^v[\mathrm{d}k]\,|\mathcal{M}_{\text{sc}}(k)|^2}\sum_{n=0}^\infty\frac{1}{n!}\int_{\delta v}\prod_{i=1}^n[\mathrm{d}k_i]|\mathcal{M}_{\text{sc}}(k_i)|^{\,2}\sum_{(ij)}2C_{(ij)}\int_0^\infty\frac{\mathrm{d}\kappa^{(ij)}}{\kappa^{(ij)}}\frac{\alpha_s(\kappa^{(ij)})}{\pi}\int_{-\infty}^\infty\mathrm{d}\eta\times \\ \times\int_0^{2\pi}\frac{\mathrm{d}\phi}{2\pi}\left[\Theta\left(1-\lim_{v\to0}\frac{V_{\text{wa}}(\{\tilde{p}\},k,\{k_i\})}{v}\right)-\Theta\left(1-\lim_{v\to0}\frac{V_{\text{sc}}(\{\tilde{p}\},k,\{k_i\})}{v}\right)\right]. \end{aligned} \tag{4.136}$$

Up to corrections beyond NNLL accuracy, we can modify the phase space integration for the extra soft gluon as follows

$$\frac{\mathrm{d}\kappa^{(ij)}}{\kappa^{(ij)}}\frac{\alpha_s(\kappa^{(ij)})}{\pi} = \frac{\mathrm{d}\zeta}{\zeta}\frac{\alpha_s((\zeta v)^{\frac{1}{a}}Q)}{a\pi} \simeq \frac{\mathrm{d}\zeta}{\zeta}\frac{\alpha_s(v^{\frac{1}{a}}Q)}{a\pi}\,, \tag{4.137}$$

where

$$\zeta = \frac{1}{v}\left(\frac{\kappa^{(ij)}}{Q}\right)^a\,. \tag{4.138}$$

This gives $\mathcal{F}_{\rm wa} \simeq (\alpha_s(Q)/\pi)\delta\mathcal{F}_{\rm wa}(\lambda)$, where

$$\begin{aligned}\delta\mathcal{F}_{\rm wa}(\lambda) = \sum_{(ij)} 2C_{(ij)}\frac{\alpha_s(v^{\frac{1}{a}}Q)}{\alpha_s(Q)}\frac{1}{a}\int_0^\infty\frac{\mathrm{d}\zeta}{\zeta}\int_{-\infty}^{\infty}\mathrm{d}\eta\int_0^{2\pi}\frac{\mathrm{d}\phi}{2\pi}\int\mathrm{d}\mathcal{Z}[\{R'_{\mathrm{NLL},\ell_i},k_i\}]\times\\ \times\left[\Theta\left(1-\lim_{v\to0}\frac{V_{\rm wa}(\{\tilde{p}\},k,\{k_i\})}{v}\right)-\Theta\left(1-\lim_{v\to0}\frac{V_{\rm sc}(\{\tilde{p}\},k,\{k_i\})}{v}\right)\right]\,.\end{aligned} \tag{4.139}$$

4.8.4 The correlated correction $\delta\mathcal{F}_{\rm correl}$

The definition of the correlated correction $\delta\mathcal{F}_{\rm correl}$ is given by [4, 61]

$$\begin{aligned}\frac{\alpha_s(Q)}{\pi}\delta\mathcal{F}_{\rm correl}(\lambda) = e^{-\int_{\delta v}^{v}[\mathrm{d}k]\,|\mathcal{M}_{\rm sc}(k)|^2}\sum_{n=0}^{\infty}\frac{1}{n!}\int_{\delta v}\prod_{i=1}^{n}[\mathrm{d}k_i]|\mathcal{M}_{\rm sc}(k_i)|^2\frac{1}{2!}\int[\mathrm{d}k_a][\mathrm{d}k_b]|\widetilde{\mathcal{M}}_{s,0}(k_a,k_b)|^2\times\\ \times\left[\Theta\left(v-V_{\rm sc}(\{\tilde{p}\},k_a,k_b,\{k_i\})\right)-\Theta\left(v-\lim_{m^2\to0}V_{\rm sc}(\{\tilde{p}\},k_a+k_b,\{k_i\})\right)\right]\,,\end{aligned} \tag{4.140}$$

where k_a and k_b are the two soft emissions that are close in angle and collinear to the same leg[9]. The remaining soft-collinear emissions k_i are not close in angle and hence are emitted independently. We denote the invariant mass of the web by $m^2 = (k_a+k_b)^2$.

In the aid of clarity we will reproduce the discussion of Section. 3.4 of Ref. [61], the discussion on how to obtain $\delta\mathcal{F}_{\rm correl}$.

In order to make sense of the difference between the two Θ functions, we should first discuss how the cluster of two soft partons is treated in the `ARES` algorithm.

The two-particle correlated soft block $|\widetilde{\mathcal{M}}_{\rm s,0}(k_a,k_b)|^2$ diverges when k_a and k_b are collinear, i.e. when the invariant mass of the cluster tends to zero. Such a divergence is entirely cancelled by the one-loop correction to the single-emission cluster $|\widetilde{\mathcal{M}}_{\rm s,1}(k)|^2$, that should be included at NNLL. In the evaluation of the Sudakov radiator, the cancellation of the above collinear singularity can be performed analytically. This is because we chose to define a resolution variable that does not depend on the invariant mass of the cluster, and hence the corresponding integral becomes straightforward. This inclusive integration

[9]The configuration in which k_a and k_b are collinear to different Born legs requires the parent gluon to be emitted at wide angles, and hence gives at most a N^{3}LL contribution.

of $|\widetilde{\mathcal{M}}\_\mathrm{s},0(k_a,k_b)|^2$ and $|\widetilde{\mathcal{M}}_{\mathrm{s},1}(k)|^2$ produces the physical coupling in the radiator, see Eq. (4.91).

In the resolved radiation the situation is more complicated, as in the full observable we are not allowed to integrate over the invariant mass of the cluster inclusively. We can, however, define a subtraction scheme to cancel the collinear singularity arising from $|\widetilde{\mathcal{M}}_{\mathrm{s},0}(k_a,k_b)|^2$ in four dimensions. We first treat the $\{k_a,k_b\}$ cluster inclusively, as done in the definition of the radiator. This can be done by considering only the total momentum k_a+k_b when evaluating the contribution of the cluster to the observable, and treat it as if it were a massless (lightlike) momentum in the computation of the observable. This once again allows us to combine it with the one loop correction to the single-emission cluster $|\widetilde{\mathcal{M}}_{\mathrm{s},1}(k)|^2$ analytically. This contribution is captured by $\delta\mathcal{F}_{\mathrm{sc}}$ which features the coefficient $K^{(1)}$ of Eq. (C.6), as explained in refs. [4, 67]. As a second step, we consider the difference between the full observable, where the $\{k_a,k_b\}$ cluster is treated exclusively, and its inclusive approximation that we considered above to cancel the singularity against the virtual correction. This is represented by the difference in the two Θ functions in Eq. (4.140). It is important to bear in mind that in the second Θ function the observable V_{sc} treats the momentum k_a+k_b as if it were *massless*, in order to exactly match our convention for the cancellation of real and virtual corrections in $\delta\mathcal{F}_{\mathrm{sc}}$. This is implemented by the limit in the second Θ function in Eq. (4.140).

There are many ways to parametrise the phase space for k_a and k_b to keep, in $\delta\mathcal{F}_{\mathrm{correl}}$, only NNLL contributions that correspond to configurations in which k_a and k_b are collinear to the same Born leg. We adopt the parametrisation of Ref. [61], we reproduce the details in Appendix. C.4. This is the same parametrisation that we used to compute the NNLL radiator. We define a rescaled invariant mass of the $\{k_a,k_b\}$ cluster $\mu^2=m^2/k_t^2$, and we introduce the *pseudo-parent* parton k of k_a and k_b with transverse momentum k_t and observable fraction ζ defined as

$$\vec{k}_t=\vec{k}_{t,a}+\vec{k}_{t,b}\,,\qquad \zeta\equiv\frac{V_{\mathrm{sc}}(k_a+k_b)}{v}\,. \tag{4.141}$$

Using Eqs. (C.49) and (C.51), the squared amplitude for a double-soft correlated emission reads

$$\frac{1}{2!}[\mathrm{d}k_a][\mathrm{d}k_b]|\widetilde{\mathcal{M}}_{s,0}(k_a,k_b)|^2=[\mathrm{d}k]|\mathcal{M}_{\mathrm{sc}}(k)|^2\frac{\alpha_s(k_t)}{2\pi}\frac{\mathrm{d}\mu^2}{\mu^2(1+\mu^2)}\mathrm{d}z\frac{\mathrm{d}\phi}{2\pi}\frac{1}{2!}C_{ab}(\mu,z,\phi)\,, \tag{4.142}$$

with $C_{ab}(\mu,z,\phi)=C(k_a,k_b)$ given by Eq. (C.52), and $\mu^2\in[0,\infty)$, $z\in[0,1]$, $\phi\in[0,2\pi)$. We understand that this expression must be interpreted as a sum over dipoles. The matrix

element squared and phase space for the pseudo-parent k is given in Eq. (4.61). Actually, due to the fact that the pseudo-parent has a non-zero invariant-mass, the integral over its rapidity $\eta^{(\ell)}$ should have the boundary $|\eta^{(\ell)}| < \log\left(Q/\sqrt{k_t^2+m^2}\right)$. However, following what is done in the computation of the NLL function $\mathcal{F}_{\rm NLL}$ [3], we observe that the exact position of the rapidity integration bound in the resolved radiation enters at one logarithmic order higher. Therefore, in order to neglect all N^{3}LL corrections and obtain a result that is purely NNLL, we replace the actual rapidity integration limit with the massless one, as done in Eq. (4.61).

$$\frac{1}{2!}\int [\mathrm{d}k_a][\mathrm{d}k_b]|\tilde{\mathcal{M}}_{\mathrm{s},0}(k_a,k_b)|^2 = \sum_{(ij)} C_{(ij)} \sum_{\ell\in(ij)} \int \frac{\mathrm{d}\kappa^{(ij)}}{\kappa^{(ij)}} \frac{\mathrm{d}\phi^{(ij)}}{2\pi} \mathrm{d}\eta^{(ij)} \frac{\alpha_s(\kappa^{(ij)})}{\pi} \times \\ \times \frac{\alpha_s(\kappa^{(ij)})}{2\pi} \int_0^\infty \frac{\mathrm{d}\mu^2}{\mu^2(1+\mu^2)} \int_0^1 \mathrm{d}z \int_0^{2\pi} \frac{\mathrm{d}\phi}{2\pi} \frac{1}{2!} C_{ab}(z,\mu,\phi)\,, \tag{4.143}$$

The integral over $\eta^{(ij)}$ can be evaluated analytically [4] and the correlated correction takes the following simple form

$$\frac{1}{2!}\int [\mathrm{d}k_a][\mathrm{d}k_b]|\tilde{\mathcal{M}}_{\mathrm{s},0}(k_a,k_b)|^2 = \sum_{(ij)} C_{(ij)} \sum_{\ell\in(ij)} \frac{\lambda_{ij} r''_{\mathrm{NNLL},\ell}(\lambda_{ij})}{2\pi a\beta_0} \times \\ \times \int_0^\infty \frac{\mathrm{d}\zeta}{\zeta} \int_0^{2\pi} \frac{\mathrm{d}\phi^{(ij)}}{2\pi} \int_0^\infty \frac{\mathrm{d}\mu^2}{\mu^2(1+\mu^2)} \int_0^1 \mathrm{d}z \int_0^{2\pi} \frac{\mathrm{d}\phi}{2\pi} \frac{1}{2!} C_{ab}(z,\mu,\phi)\,. \tag{4.144}$$

Using the fact that k_a and k_b are collinear to the same leg ℓ, we can approximate $\phi^{(ij)} \simeq \phi^{(\ell)}$, and to NNLL accuracy we can replace $\lambda_{ij} r''_{\mathrm{NNLL},\ell}(\lambda_{ij}) \simeq \lambda r''_{\mathrm{NNLL},\ell}(\lambda)$. With these identifications we obtain $\delta\mathcal{F}_{\rm correl}$

$$\delta\mathcal{F}_{\rm correl}(\lambda) = \int_0^\infty \frac{\mathrm{d}\zeta}{\zeta} \sum_{\ell=1}^{3} \int_0^{2\pi} \frac{\mathrm{d}\phi^{(\ell)}}{2\pi} \left(\frac{\lambda}{2a\beta_0} \frac{R''_{\mathrm{NNLL},\ell}(v)}{\alpha_s(Q)}\right) \times \\ \times \int_0^\infty \frac{\mathrm{d}\mu^2}{\mu^2(1+\mu^2)} \int_0^1 \mathrm{d}z \int_0^{2\pi} \frac{\mathrm{d}\phi}{2\pi} \frac{1}{2!} C_{ab}(\mu,z,\phi) \int \mathrm{d}\mathcal{Z}[\{R'_{\mathrm{NLL},\ell_i}, k_i\}] \\ \times \left[\Theta\left(1 - \lim_{v\to 0} \frac{V_{\rm sc}(\{\tilde{p}\}, k_a, k_b, \{k_i\})}{v}\right) - \Theta\left(1 - \lim_{\mu^2\to 0} \lim_{v\to 0} \frac{V_{\rm sc}(\{\tilde{p}\}, k_a+k_b, \{k_i\})}{v}\right)\right]. \tag{4.145}$$

4.8.5 The clustering corrections $\delta\mathcal{F}_{\rm clust}$

Clustering corrections arise when two soft and collinear partons that were emitted independently become close in rapidity, and all other emissions remain strongly ordered. This correction is not present in event shape variables as there is no dependence on the rapidity fraction.

4.8.6 The recoil and hard-collinear corrections $\delta\mathcal{F}_{\rm rec}$ and $\delta\mathcal{F}_{\rm hc}$

The corrections arising due to the correct treatment of hard and collinear emissions is more delicate than the treatment of the soft. Hard-collinear contributions arise when one of the emissions is collinear to any of the legs and hard, namely it carries a sizeable fraction of the emitters longitudinal momentum. The matrix element squared $|\mathcal{M}_\ell(k)|^2$ for the emission of a gluon k collinear to leg ℓ is given by to leg ℓ

$$[\mathrm{d}k]|\mathcal{M}_{\mathrm{hc},\ell}(k)|^2 = C_\ell \frac{\alpha_s^{\rm phys.}(\tilde{k}_t^{(\ell)})}{2\pi}\frac{\mathrm{d}\phi^{(\ell)}}{2\pi}\frac{\mathrm{d}\tilde{k}_t^{(\ell)}}{\tilde{k}_t^{(\ell)}}\mathrm{d}z^{(\ell)}p_\ell(z^{(\ell)})\,. \tag{4.146}$$

The important part is that the collinear singularities are with respect to the emitter, rather than the Born momenta or even the final state momenta. A mapping between the Born momenta and the emitter can be found [4].

We have two NNLL contributions coming from the hard-collinear radiation. we have to take into account the exact expression for the observable when a single emission is hard and collinear

$$\begin{aligned}\mathcal{F}_{\rm rec}(v) = e^{-\int_{\delta v}^{v}[\mathrm{d}k]\,|\mathcal{M}_{\rm sc}(k)|^2}\sum_{n=0}^{\infty}\frac{1}{n!}\int_{\delta v}\prod_{i=1}^{n}[\mathrm{d}k_i]|\mathcal{M}_{\rm sc}(k_i)|^2\times\\ \times\sum_{\ell=1}^{3}\int_0^1\mathrm{d}z\,p_\ell(z,\phi)\int_0^{2\pi}\frac{\mathrm{d}\phi^{(\ell)}}{2\pi}\int\frac{\mathrm{d}k_t'^2}{k_t'^2}\frac{\alpha_s^{\rm phys.}(k_t')}{2\pi}\times\\ \times\left[\Theta\left(v-V_{\rm hc}(\{\tilde{p}\},k[k_t',p_{t,\ell}',z],\{k_i\})\right)-\Theta\left(v-V_{\rm sc}(\{\tilde{p}\},k[k_t',p_{t,\ell}',0],\{k_i\})\right)\right]\,.\end{aligned} \tag{4.147}$$

In the above expression, $V_{\rm hc}(\{\tilde{p}\},k,\{k_i\})$ denotes the observable V where all of the emissions except for k are treated in the soft-collinear approximation. In the second Θ-function we have $V_{\rm sc}(\{\tilde{p}\},k,\{k_i\})$, here k is treated as though it were soft and collinear, so that its transverse momentum with respect to the emitting leg k_t' is equal to k_t. Notice that in Eq. (4.147) we can replace k_t' by k_t because we are integrating over this variable. We make use of the shorthand notation

$$k' = k[k_t,p_{t,\ell}',z]\,,\qquad k = k[k_t,p_{t,\ell}',0]\,. \tag{4.148}$$

To NNLL accuracy we can simplify the phase space for k, by introducing

$$\zeta = \frac{1}{v}\frac{d_\ell g_\ell(\phi)}{z^{b_\ell}}\left(\frac{k_t}{Q}\right)^{a+b_\ell}\,, \tag{4.149}$$

we have, at NNLL accuracy

$$\frac{\mathrm{d}k_t^2}{k_t^2}\frac{\alpha_s(k_t)}{2\pi} = \frac{\alpha_s((z^{b_\ell}\zeta v/(d_\ell g_\ell(\phi)))^{1/(a+b_\ell)}Q)}{\pi(a+b_\ell)}\frac{\mathrm{d}\zeta}{\zeta}\simeq\frac{\alpha_s(v^{\frac{1}{a+b_\ell}}Q)}{\pi(a+b_\ell)}\frac{\mathrm{d}\zeta}{\zeta}\,. \tag{4.150}$$

Making the same approximations to the soft-collinear radiation as we did for $\mathcal{F}_{\rm NLL}$, we eliminate the subleading contributions and obtain $\mathcal{F}_{\rm rec}(v) \simeq (\alpha_s(Q)/\pi)\delta\mathcal{F}_{\rm rec}(\lambda) = (\alpha_s(Q)/\pi)(\delta\mathcal{F}^{\rm avg.}_{\rm rec} + \delta\mathcal{F}^{\rm spins.}_{\rm rec})$, where

$$\delta\mathcal{F}^{\rm avg.}_{\rm rec}(\lambda) = \sum_{\ell=1}^{3} \frac{\alpha_s(v^{\frac{1}{a+b_\ell}}Q)}{\alpha_s(Q)(a+b_\ell)} \int_0^\infty \frac{\mathrm{d}\zeta}{\zeta} \int_0^{2\pi} \frac{\mathrm{d}\phi^{(\ell)}}{2\pi} \int_0^1 \mathrm{d}z\, p_\ell(z) \int \mathrm{d}\mathcal{Z}[\{R'_{\mathrm{NLL},\ell_i}, k_i\}]\times$$
$$\times \left[\Theta\left(1 - \lim_{v\to 0} \frac{V_{\rm hc}(\{\tilde{p}\}, k', \{k_i\})}{v}\right) - \Theta\left(1 - \lim_{v\to 0} \frac{V_{\rm sc}(\{\tilde{p}\}, k, \{k_i\})}{v}\right)\right], \tag{4.151}$$

and

$$\delta\mathcal{F}^{\rm spins.}_{\rm rec}(\lambda) = Sp(\Phi_{\mathcal{B}}) \sum_{\ell=1}^{3} \frac{\alpha_s(v^{\frac{1}{a+b_\ell}}Q)}{\alpha_s(Q)(a+b_\ell)} \int_0^\infty \frac{\mathrm{d}\zeta}{\zeta} \int_0^{2\pi} \frac{\mathrm{d}\phi^{(\ell)}}{2\pi} \int_0^1 \mathrm{d}z\, \Delta p_\ell(z,\phi)\times$$
$$\times \int \mathrm{d}\mathcal{Z}[\{R'_{\mathrm{NLL},\ell_i}, k_i\}]\, \Theta\left(1 - \lim_{v\to 0} \frac{V_{\rm hc}(\{\tilde{p}\}, k', \{k_i\})}{v}\right), \tag{4.152}$$

where $Sp(\Phi_{\mathcal{B}})$ encodes the spins correlations and their dependence on the underlying hard event and $\Delta p_\ell(z,\phi)$ is the spin dependent part of the AP splitting functions.

The second NNLL contribution coming from the hard-collinear radiation is due to the correct hard-collinear matrix element, but with the soft-collinear limit of the observable. This correction is very similar to the soft correction Eq. (4.133), in that we must subtract the double counting due to the inclusion of soft-collinear effects. After removing the double counting we find the expression

$$\delta\mathcal{F}_{\rm hc}(\lambda) = \sum_{\ell=1}^{3} \frac{\alpha_s(v^{\frac{1}{a+b_\ell}}Q)}{\alpha_s(Q)(a+b_\ell)} \int_0^\infty \frac{\mathrm{d}\zeta}{\zeta} \int_0^{2\pi} \frac{\mathrm{d}\phi^{(\ell)}}{2\pi} \int_0^1 \mathrm{d}z \left(p_\ell(z) - \frac{2C_\ell}{z}\right) \int \mathrm{d}\mathcal{Z}[\{R'_{\mathrm{NLL},\ell_i}, k_i\}]\times$$
$$\times \left[\Theta\left(1 - \lim_{v\to 0} \frac{V_{\rm sc}(\{\tilde{p}\}, k, \{k_i\})}{v}\right) - \Theta(1-\zeta)\Theta\left(1 - \lim_{v\to 0} \frac{V_{\rm sc}(\{\tilde{p}\}, \{k_i\})}{v}\right)\right]. \tag{4.153}$$

4.9 Additive observables

Some event shapes have the property that they are additive, meaning that for soft emissions

$$V(\{\tilde{p}\}, \{k_i\}) = \sum_{i=1}^{n} V(\{\tilde{p}\}, k_i) + \mathcal{O}\big(V^2\big), \tag{4.154}$$

while for a hard emission k collinear to leg ℓ, the corresponding $V(\{\tilde{p}\}, k)$ has to be replaced by $V_{\rm hc}$, as defined in Eq. (4.147). For this simpler class of observables, the NNLL corrections can be significantly simplified. We will see that the soft-collinear multiple emission function factorises from the NNLL contribution. For an additive observable the

NLL multiple emission function reads

$$\mathcal{F}_{\rm NLL}(\lambda) = \frac{e^{-\gamma_E R'_{\rm NLL}(\lambda)}}{\Gamma(1+R'_{\rm NLL}(\lambda))}\,. \tag{4.155}$$

4.9.1 The soft-collinear correction

We consider the expression for the soft-collinear contribution $\delta\mathcal{F}_{\rm sc}$ of Eq. (4.131), and use the property of additivity to write the observable as

$$V_{\rm sc}(\{\tilde{p}\},k,\{k_i\}) = \zeta v + V_{\rm sc}(\{\tilde{p}\},\{k_i\})\,. \tag{4.156}$$

With this we can write the expression for $\delta\mathcal{F}_{\rm sc}$ as

$$\begin{aligned}\delta\mathcal{F}_{\rm sc}(\lambda) = \frac{\pi}{\alpha_s(Q)}\int_0^\infty \frac{{\rm d}\zeta}{\zeta}\sum_{\ell=1}^{3}\left(R'_{{\rm NNLL},\ell} + R''_{{\rm NNLL},\ell}\left(\langle \log d_\ell g_\ell\rangle - b_\ell \log\frac{2E_\ell}{Q} + \log\frac{1}{\zeta}\right)\right)\times \\ \times\int {\rm d}\mathcal{Z}[\{R'_{{\rm NLL},\ell_i},k_i\}]\left[\Theta\left(1-\zeta-\lim_{v\to 0}\frac{V_{\rm sc}(\{\tilde{p}\},\{k_i\})}{v}\right) - \Theta(1-\zeta)\,\Theta\left(1-\lim_{v\to 0}\frac{V_{\rm sc}(\{\tilde{p}\},\{k_i\})}{v}\right)\right],\end{aligned} \tag{4.157}$$

where we have used the property of additivity to carry out the $\phi^{(\ell)}$ integrations.

We define rescaled momenta $\{\tilde{k}_1,\ldots,\tilde{k}_n\}$ such that for a single emission $V_{\rm sc}(\{\tilde{p}\},k_i) = (1-\zeta)V_{\rm sc}(\{\tilde{p}\},\tilde{k}_i)$. The recursive IRC safety of V guarantees that when considering an ensemble of emissions the observable will scale in the same way as for a single emission,

$$V_{\rm sc}(\{\tilde{p}\},\{k_i\}) = (1-\zeta)V_{\rm sc}(\{\tilde{p}\},\{\tilde{k}_i\})\,. \tag{4.158}$$

We can apply the momentum rescaling to the first Θ-function of Eq. (4.157), we find

$$\begin{aligned}&\Theta\left(1-\zeta-\lim_{v\to 0}\frac{V_{\rm sc}(\{\tilde{p}\},\{k_i\})}{v}\right)\\ &\quad=\Theta\left(1-\zeta-\lim_{v\to 0}\frac{(1-\zeta)V_{\rm sc}(\{\tilde{p}\},\{\tilde{k}_i\})}{v}\right)\\ &\quad=\Theta\left((1-\zeta)\left(1-\lim_{v\to 0}\frac{V_{\rm sc}(\{\tilde{p}\},\{\tilde{k}_i\})}{v}\right)\right)\\ &\quad=\Theta(1-\zeta)\,\Theta\left(1-\lim_{v\to 0}\frac{V_{\rm sc}(\{\tilde{p}\},\{\tilde{k}_i\})}{v}\right).\end{aligned} \tag{4.159}$$

We make use of the explicit expression for ${\rm d}\mathcal{Z}[\{R'_{{\rm NLL},\ell_i},k_i\}]$ and define $\tilde{\zeta}_i = V_{\rm sc}(\{\tilde{p}\},\tilde{k}_i)/v$,

so that we find

$$\delta\mathcal{F}_{\rm sc}(\lambda) = \frac{\pi}{\alpha_s(Q)}\int_0^\infty \frac{\mathrm{d}\zeta}{\zeta}\sum_{\ell=1}^{3}\left(R'_{\rm NNLL,\ell} + R''_{\rm NNLL,\ell}\left(\langle \log d_\ell g_\ell\rangle - b_\ell \log\frac{2E_\ell}{Q} + \log\frac{1}{\zeta}\right)\right)\times$$
$$\times\delta^{R'_{\rm NLL}}\sum_{n=0}^{\infty}\frac{1}{n!}\prod_{i=1}^{n}\sum_{\ell_i=1}^{3}\int_0^{2\pi}\frac{\mathrm{d}\phi_i^{(\ell_i)}}{2\pi}R'_{\rm NLL,\ell_i}\times$$
$$\times\left[\Theta(1-\zeta)\int_0^\infty\frac{\mathrm{d}\tilde{\zeta}_i}{\tilde{\zeta}_i}\Theta\left(\tilde{\zeta}_i - \frac{\delta}{1-\zeta}\right)\Theta\left(1-\lim_{v\to 0}\frac{V_{\rm sc}(\{\tilde{p}\},\{\tilde{k}_i\})}{v}\right)\right.$$
$$\left.-\Theta(1-\zeta)\int_0^\infty\frac{\mathrm{d}\zeta_i}{\zeta_i}\Theta(\zeta_i-\delta)\Theta\left(1-\lim_{v\to 0}\frac{V_{\rm sc}(\{\tilde{p}\},\{k_i\})}{v}\right)\right]. \tag{4.160}$$

To simplify this expression we would like to reassemble $\mathcal{F}_{\rm NLL}$, factorising the NLL function from the NNLL correction term. This is straightforward to do, we must multiply the first term in the square bracket of Eq. (4.160) by one in a clever way (the second term already reproduces $\mathcal{F}_{\rm NLL}$). The appropriate choice for this factor is

$$\left(\frac{1-\zeta}{1-\zeta}\right)^{R'_{\rm NLL}}. \tag{4.161}$$

Performing the algebra that we have outlined above we find

$$(1-\zeta)^{R'_{\rm NLL}}\left(\frac{\delta}{1-\zeta}\right)^{R'_{\rm NLL}}\sum_{n=0}^{\infty}\frac{1}{n!}\prod_{i=1}^{n}\sum_{\ell_i=1}^{3}\int_0^{2\pi}\frac{\mathrm{d}\phi_i^{(\ell_i)}}{2\pi}R'_{\rm NLL,\ell_i}\times$$
$$\times\left[\Theta(1-\zeta)\int_0^\infty\frac{\mathrm{d}\tilde{\zeta}_i}{\tilde{\zeta}_i}\Theta\left(\tilde{\zeta}_i-\frac{\delta}{1-\zeta}\right)\Theta\left(1-\lim_{v\to 0}\frac{V_{\rm sc}(\{\tilde{p}\},\{\tilde{k}_i\})}{v}\right)\right]$$
$$= (1-\zeta)^{R'_{\rm NLL}}\,\Theta(1-\zeta)\,\mathcal{F}_{\rm NLL}(\lambda)\,. \tag{4.162}$$

Finally we factor out $\mathcal{F}_{\rm NLL}$ and we find for the soft-collinear correction

$$\delta\mathcal{F}_{\rm sc}(\lambda) = \mathcal{F}_{\rm NLL}(\lambda)\frac{\pi}{\alpha_s(Q)}\int_0^\infty\frac{\mathrm{d}\zeta}{\zeta}\sum_{\ell=1}^{3}\left(R'_{\rm NNLL,\ell} + R''_{\rm NNLL,\ell}\left(\langle\log d_\ell g_\ell\rangle - b_\ell\log\frac{2E_\ell}{Q} + \log\frac{1}{\zeta}\right)\right)\times$$
$$\times\left((1-\zeta)^{R'_{\rm NLL}}-1\right)\Theta(1-\zeta)\,, \tag{4.163}$$

we can perform the ζ integration analytically and we find

$$\delta\mathcal{F}_{\rm sc}(\lambda) = -\mathcal{F}_{\rm NLL}(\lambda)\frac{\pi}{\alpha_s(Q)}\sum_{\ell=1}^{3}\left[\left(R'_{\rm NNLL,\ell}\right.\right.$$
$$+R''_{\rm NNLL,\ell}\left(\langle\log d_\ell g_\ell\rangle - b_\ell\log\frac{2E_\ell}{Q}\right)\Big)\left(\psi^{(0)}(1+R'_{\rm NLL})+\gamma_E\right)$$
$$\left.+\frac{R''_{\rm NNLL,\ell}}{2}\left(\left(\psi^{(0)}(1+R'_{\rm NLL})+\gamma_E\right)^2-\psi^{(1)}(1+R'_{\rm NLL})+\frac{\pi^2}{6}\right)\right]. \tag{4.164}$$

4.9.2 The soft correction

We consider the expression for the soft contribution $\delta\mathcal{F}_{\rm s}$ of Eq. (4.133). Using Eq. (4.156) we obtain

$$\delta\mathcal{F}_{\rm s}(\lambda) = \sum_{(ij)} 2C_{(ij)} \frac{\alpha_s(v^{\frac{1}{a}}Q)}{\alpha_s(Q)} \frac{1}{a} \log\frac{Q_{ij}}{Q} \int_0^\infty \frac{\mathrm{d}\zeta}{\zeta} \int_0^{2\pi} \frac{\mathrm{d}\phi}{2\pi} \int \mathrm{d}\mathcal{Z}[\{R'_{\mathrm{NLL},\ell_i}, k_i\}] \times \\ \times \left[\Theta\left(1-\zeta-\lim_{v\to 0}\frac{V_{\rm sc}(\{\tilde{p}\},\{k_i\})}{v}\right) - \Theta(1-\zeta)\,\Theta\left(1-\lim_{v\to 0}\frac{V_{\rm sc}(\{\tilde{p}\},\{k_i\})}{v}\right)\right]. \tag{4.165}$$

Rescaling the momenta in the same way as for the soft-collinear correction we get

$$\begin{aligned}\delta\mathcal{F}_{\rm s}(\lambda) &= \mathcal{F}_{\rm NLL}(\lambda) \sum_{(ij)} 2C_{(ij)} \frac{\alpha_s(v^{\frac{1}{a}}Q)}{\alpha_s(Q)} \frac{1}{a} \log\frac{Q_{ij}}{Q} \int_0^\infty \frac{\mathrm{d}\zeta}{\zeta} \int_0^{2\pi} \frac{\mathrm{d}\phi}{2\pi} \times \\ &\times \left[(1-\zeta)^{R'_{\rm NLL}}\,\Theta(1-\zeta) - \Theta(1-\zeta)\right] \\ &= -\mathcal{F}_{\rm NLL}(\lambda) \sum_{(ij)} 2C_{(ij)} \frac{\alpha_s(v^{\frac{1}{a}}Q)}{\alpha_s(Q)} \frac{1}{a} \log\frac{Q_{ij}}{Q} \left(\psi^{(0)}(1+R'_{\rm NLL}) + \gamma_E\right).\end{aligned} \tag{4.166}$$

4.9.3 The soft wide angle correction

We consider the expression for the soft wide angle contribution $\delta\mathcal{F}_{\rm wa}$ of Eq. (4.139). Consider an emission off of the dipole (ij) and we use the property of additivity to write

$$V_{\rm wa}(\{\tilde{p}\},k,\{k_i\}) = \left(\frac{\kappa^{(ij)}}{Q}\right)^a f_{\rm wa}^{(ij)}(\eta,\phi) + V_{\rm sc}(\{\tilde{p}\},\{k_i\}), \tag{4.167}$$

$$V_{\rm sc}(\{\tilde{p}\},k,\{k_i\}) = \left(\frac{\kappa^{(ij)}}{Q}\right)^a f_{\rm sc}^{(ij)}(\eta,\phi) + V_{\rm sc}(\{\tilde{p}\},\{k_i\}), \tag{4.168}$$

which can be written in terms of the rescaled ζ variable of Eq. (4.138) as follows

$$V_{\rm wa}(\{\tilde{p}\},k,\{k_i\}) = \zeta v f_{\rm wa}^{(ij)}(\eta,\phi) + V_{\rm sc}(\{\tilde{p}\},\{k_i\}), \tag{4.169}$$

$$V_{\rm sc}(\{\tilde{p}\},k,\{k_i\}) = \zeta v f_{\rm sc}^{(ij)}(\eta,\phi) + V_{\rm sc}(\{\tilde{p}\},\{k_i\}). \tag{4.170}$$

$$\delta\mathcal{F}_{\rm wa}(\lambda) = \sum_{(ij)} 2C_{(ij)} \frac{\alpha_s(v^{\frac{1}{a}}Q)}{\alpha_s(Q)} \frac{1}{a} \int_0^\infty \frac{\mathrm{d}\zeta}{\zeta} \int_{-\infty}^\infty \mathrm{d}\eta \int_0^{2\pi} \frac{\mathrm{d}\phi}{2\pi} \int \mathrm{d}\mathcal{Z}[\{R'_{\mathrm{NLL},\ell_i}, k_i\}] \times \\ \times \left[\Theta\left(1-\zeta f_{\rm wa}^{(ij)}(\eta,\phi) - \lim_{v\to 0}\frac{V_{\rm wa}(\{\tilde{p}\},\{k_i\})}{v}\right) - \Theta\left(1-\zeta f_{\rm sc}^{(ij)}(\eta,\phi) - \lim_{v\to 0}\frac{V_{\rm sc}(\{\tilde{p}\},\{k_i\})}{v}\right)\right]. \tag{4.171}$$

We define two sets of rescaled momentum:

- The first rescaling $\{\bar{k}_1, \dots, \bar{k}_n\}$ is of the momenta in the first Θ-function of Eq. (4.171) such that $V_{\rm sc}(\{\tilde{p}\}, k_i) = (1 - \zeta f_{\rm wa}^{(ij)}(\eta, \phi)) V_{\rm sc}(\{\tilde{p}\}, \bar{k}_i)$. The recursive IRC safety of V guarantees that

$$V_{\rm sc}(\{\tilde{p}\}, \{k_i\}) = (1 - \zeta f_{\rm wa}^{(ij)}(\eta, \phi)) V_{\rm sc}(\{\tilde{p}\}, \{\bar{k}_i\}) \,. \tag{4.172}$$

- The second rescaling $\{\tilde{k}_1, \dots, \tilde{k}_n\}$ is of the momenta in the second Θ-function of Eq. (4.171) such that $V_{\rm sc}(\{\tilde{p}\}, k_i) = (1 - \zeta f_{\rm sc}^{(ij)}(\eta, \phi)) V_{\rm sc}(\{\tilde{p}\}, \tilde{k}_i)$. And once again the recursive IRC safety of V guarantees that

$$V_{\rm sc}(\{\tilde{p}\}, \{k_i\}) = (1 - \zeta f_{\rm sc}^{(ij)}(\eta, \phi)) V_{\rm sc}(\{\tilde{p}\}, \{\tilde{k}_i\}) \,. \tag{4.173}$$

We make use of the explicit expression for $\mathrm{d}\mathcal{Z}[\{R'_{{\rm NLL},\ell_i}, k_i\}]$ and define $\bar{\zeta}_i = V_{\rm sc}(\{\tilde{p}\}, \bar{k}_i)/v$ and $\tilde{\zeta}_i = V_{\rm sc}(\{\tilde{p}\}, \tilde{k}_i)/v$. We perform the same manipulation of the Θ-functions as we did in the soft-collinear case, and we find

$$\begin{aligned}
\delta\mathcal{F}_{\rm wa}(\lambda) = \sum_{(ij)} 2C_{(ij)} \frac{\alpha_s(v^{\frac{1}{a}}Q)}{\alpha_s(Q)} \frac{1}{a} \int_0^\infty \frac{\mathrm{d}\zeta}{\zeta} \int_{-\infty}^\infty \mathrm{d}\eta \int_0^{2\pi} \frac{\mathrm{d}\phi}{2\pi} \delta^{R'_{\rm NLL}} \sum_{n=0}^\infty \frac{1}{n!} \prod_{i=1}^n \sum_{\ell_i=1}^2 \int_0^{2\pi} \frac{\mathrm{d}\phi_i^{(\ell_i)}}{2\pi} R'_{{\rm NLL},\ell_i} \times \\
\times \Bigg[\Theta\left(1 - \zeta f_{\rm wa}^{(ij)}(\eta,\phi)\right) \int_0^\infty \frac{\mathrm{d}\bar{\zeta}_i}{\bar{\zeta}_i} \Theta\left(\bar{\zeta}_i - \frac{\delta}{1 - \zeta f_{\rm wa}^{(ij)}(\eta,\phi)}\right) \Theta\left(1 - \lim_{v\to 0} \frac{V_{\rm sc}(\{\tilde{p}\}, \{\bar{k}_i\})}{v}\right) \\
- \Theta\left(1 - \zeta f_{\rm sc}^{(ij)}(\eta,\phi)\right) \int_0^\infty \frac{\mathrm{d}\tilde{\zeta}_i}{\tilde{\zeta}_i} \Theta\left(\tilde{\zeta}_i - \frac{\delta}{1 - \zeta f_{\rm sc}^{(ij)}(\eta,\phi)}\right) \Theta\left(1 - \lim_{v\to 0} \frac{V_{\rm sc}(\{\tilde{p}\}, \{\tilde{k}_i\})}{v}\right) \Bigg] \,.
\end{aligned} \tag{4.174}$$

We can reconstruct $\mathcal{F}_{\rm NLL}$ making similar manipulations to those we made in the soft collinear case, we find

$$\begin{aligned}
\delta\mathcal{F}_{\rm wa}(\lambda) &= \mathcal{F}_{\rm NLL}(\lambda) \sum_{(ij)} 2C_{(ij)} \frac{\alpha_s(v^{\frac{1}{a}}Q)}{\alpha_s(Q)} \frac{1}{a} \int_0^\infty \frac{\mathrm{d}\zeta}{\zeta} \int_{-\infty}^\infty \mathrm{d}\eta \int_0^{2\pi} \frac{\mathrm{d}\phi}{2\pi} \times \\
&\times \left[(1 - \zeta f_{\rm wa}^{(ij)}(\eta,\phi))^{R'_{\rm NLL}} \Theta(1 - \zeta f_{\rm wa}^{(ij)}(\eta,\phi)) - (1 - \zeta f_{\rm sc}^{(ij)}(\eta,\phi))^{R'_{\rm NLL}} \Theta(1 - \zeta f_{\rm sc}^{(ij)}(\eta,\phi)) \right] \\
&= \mathcal{F}_{\rm NLL}(\lambda) \sum_{(ij)} 2C_{(ij)} \frac{\alpha_s(v^{\frac{1}{a}}Q)}{\alpha_s(Q)} \frac{1}{a} \int_{-\infty}^\infty \mathrm{d}\eta \int_0^{2\pi} \frac{\mathrm{d}\phi}{2\pi} \log \frac{f_{\rm sc}^{(ij)}(\eta,\phi)}{f_{\rm wa}^{(ij)}(\eta,\phi)} \,.
\end{aligned} \tag{4.175}$$

4.9.4 The soft correlated correction

We consider the expression for the soft correlated contribution $\delta\mathcal{F}_{\rm correl}$ of Eq. (4.145), and use the property of additivity to write

$$V_{\rm sc}(\{\tilde{p}\}, k_a, k_b, \{k_i\}) = V_{\rm sc}(k_a) + V_{\rm sc}(k_b) + V_{\rm sc}(\{\tilde{p}\}, \{k_i\}) \,, \tag{4.176}$$

$$V_{\rm sc}(\{\tilde{p}\}, k_a + k_b, \{k_i\}) = V_{\rm sc}(k_a + k_b) + V_{\rm sc}(\{\tilde{p}\}, \{k_i\}) \,, \tag{4.177}$$

which can be written in terms of the rescaled ζ variable of Eq. (4.141) as follows

$$V_{\rm sc}(\{\tilde{p}\},k,\{k_i\}) = \zeta v f^{(\ell)}_{\rm correl}(\mu,z,\phi) + V_{\rm sc}(\{\tilde{p}\},\{k_i\})\,, \tag{4.178}$$

$$V_{\rm sc}(\{\tilde{p}\},k,\{k_i\}) = \zeta v + V_{\rm sc}(\{\tilde{p}\},\{k_i\})\,. \tag{4.179}$$

Performing similar manipulations we obtain

$$\begin{aligned}\delta\mathcal{F}_{\rm correl}(\lambda) = \mathcal{F}_{\rm NLL}(\lambda)\int_0^\infty \frac{{\rm d}\zeta}{\zeta}\sum_{\ell=1}^{3}\int_0^{2\pi}\frac{{\rm d}\phi^{(\ell)}}{2\pi}\left(\frac{\lambda}{2a\beta_0}\frac{R''_{{\rm NNLL},\ell}(v)}{\alpha_s(Q)}\right)\times\\ \times\int_0^\infty\frac{{\rm d}\mu^2}{\mu^2(1+\mu^2)}\int_0^1{\rm d}z\int_0^{2\pi}\frac{{\rm d}\phi}{2\pi}\frac{1}{2!}C_{ab}(\mu,z,\phi)\times\\ \times\left[\left(1-\zeta f^{(\ell)}_{\rm correl}(\mu,z,\phi)\right)^{R'_{\rm NLL}}\,\Theta\left(1-\zeta f^{(\ell)}_{\rm correl}(\mu,z,\phi)\right)\right.\\ \left.-(1-\zeta)^{R'_{\rm NLL}}\,\Theta\left(1-\zeta\right)\right]\,,\end{aligned} \tag{4.180}$$

and finally

$$\begin{aligned}\delta\mathcal{F}_{\rm correl}(\lambda) = -\mathcal{F}_{\rm NLL}(\lambda)\sum_{\ell=1}^{3}\int_0^{2\pi}\frac{{\rm d}\phi^{(\ell)}}{2\pi}\left(\frac{\lambda}{2a\beta_0}\frac{R''_{{\rm NNLL},\ell}}{\alpha_s(Q)}\right)\times\\ \times\int_0^\infty\frac{{\rm d}\mu^2}{\mu^2(1+\mu^2)}\int_0^1{\rm d}z\int_0^{2\pi}\frac{{\rm d}\phi}{2\pi}\frac{1}{2!}C_{ab}(\mu,z,\phi)\log f^{(\ell)}_{\rm correl}(\mu,z,\phi)\end{aligned} \tag{4.181}$$

4.9.5 The recoil correction

We consider the expression for the recoil contribution $\delta\mathcal{F}_{\rm rec}$ of Eq. (4.151). We use the property of additivity to write

$$V_{\rm hc}(\{\tilde{p}\},k',\{k_i\}) = \left(\frac{k'_t}{Q}\right)^{(a+b_\ell)} f^{(\ell)}_{\rm hc}(z^{(\ell)},\phi) + V_{\rm sc}(\{\tilde{p}\},\{k_i\})\,, \tag{4.182}$$

$$V_{\rm sc}(\{\tilde{p}\},k,\{k_i\}) = \left(\frac{k_t}{Q}\right)^{(a+b_\ell)} f^{(\ell)}_{\rm sc}(z^{(\ell)},\phi) + V_{\rm sc}(\{\tilde{p}\},\{k_i\})\,, \tag{4.183}$$

where the presence of k', rather than k, denotes that the full recoil has been taken into account in the calculation of the observable. Performing a similar rescaling as for the wide angle correction we find

$$\delta\mathcal{F}^{\rm avg.}_{\rm rec}(\lambda) = \mathcal{F}_{\rm NLL}(\lambda)\sum_{\ell=1}^{3}\frac{\alpha_s(v^{\frac{1}{a+b_\ell}}Q)}{\alpha_s(Q)(a+b_\ell)}\int_0^1{\rm d}z\int_0^{2\pi}\frac{{\rm d}\phi}{2\pi}\,p_\ell(z)\log\frac{f^{(\ell)}_{\rm sc}(z,\phi)}{f^{(\ell)}_{\rm hc}(z,\phi)}\,, \tag{4.184}$$

$$\delta\mathcal{F}^{\rm spins.}_{\rm rec}(\lambda) = -\mathcal{F}_{\rm NLL}(\lambda)\,Sp(\Phi_{\mathcal{B}})\sum_{\ell=1}^{3}\frac{\alpha_s(v^{\frac{1}{a+b_\ell}}Q)}{\alpha_s(Q)(a+b_\ell)}\int_0^1{\rm d}z\int_0^{2\pi}\frac{{\rm d}\phi}{2\pi}\,\Delta p_\ell(z,\phi)\log f^{(\ell)}_{\rm hc}(z,\phi)\,. \tag{4.185}$$

4.9.6 The hard-collinear correction

In a similar way, we can compute the hard-collinear contributing $\delta\mathcal{F}_{\rm hc}$ of Eq. (4.153). Using Eq. (4.156) and performing similar manipulations we obtain

$$\delta\mathcal{F}_{\rm hc}(\lambda) = -\mathcal{F}_{\rm NLL}(\lambda)\sum_{\ell=1}^{3}\frac{\alpha_s(v^{\frac{1}{a+b_\ell}}Q)}{\alpha_s(Q)(a+b_\ell)}\gamma_\ell^{(0)}\left(\psi^{(0)}\left(1+R'_{\rm NLL}\right)+\gamma_E\right). \tag{4.186}$$

4.10 Conclusions

We have repeated the derivations of Ref. [61] allowing for all the possible contributions to a three-jet observable. We stress that the derivation here reproduces exactly that of Ref. [61] when we set the number of legs to 2. We have an extra resolved correction in the form of $\delta\mathcal{F}_{\rm s}$ to account for the mismatch in the treatment of soft wide angle radiation. At NNLL accuracy the other soft corrections remain the same, however we note that this would not be the case at N^{3}LL, where instead we would start to see additional dipole contributions, although it may be possible to absorb these into $\delta\mathcal{F}_{\rm s}$ or a similarly defined soft correction. In the case of collinear corrections we see that the addition of a final-state gluon leads to spin-correlations, and we are no longer able to factorise the Born squared matrix element and the hard-collinear squared matrix element.

We have calculated the main building blocks for a general NNLL resummation of rIRC safe final-state observables with an arbitrary number of hard emitting legs. The only missing ingredient is a general treatment of both initial-state radiation and soft wide-angle corrections for a system with more than three hard emitting legs. Despite the technical difficulties, the philosophy of the `ARES` method remains unchanged. In particular, `ARES` does not depend on the specific factorisation properties of an observable, and gives promise to achieve a fully general solution to the problem of NNLL resummation in the near future.

Chapter 5

The D-parameter at NNLL accuracy

In the previous chapter 4 we extended the ARES method to include the resummation of three-jet event shape variables in e^+e^- annihilation at NNLL accuracy. With the extended ARES method we will examine the phenomenology of the D-parameter (defined in Eq. (3.15)) in near-to-planar three-jet events.

Much like other event-shape distributions, the D-parameter can be used to measure the strong coupling constant α_s and to test models of non-perturbative physics e.g. hadronisation. For details see e.g. [70] and the references therein.

5.1 Observable setup

In order to study event shapes in the near-to-planar limit, we need a procedure to select hadronic events with at least three jets. In our case, we use the Durham algorithm [33] and we select three-jet events if the three-jet resolution variable $y_3(p_1,\ldots,p_n)$ is greater than y_{cut}. Correspondingly, we have a total three-jet cross section given by

$$\sigma_{\mathcal{H}} \equiv \sum_{n=3}^{\infty} \int \mathrm{d}\Phi_n \frac{\mathrm{d}\sigma_n}{\mathrm{d}\Phi_n} \mathcal{H}(p_1,\ldots,p_n) = \sum_{n=3}^{\infty} \int \mathrm{d}\Phi_n \frac{\mathrm{d}\sigma_n}{\mathrm{d}\Phi_n} \Theta\left(y_3(p_1,\ldots,p_n) - y_{\text{cut}}\right) , \tag{5.1}$$

with $\mathrm{d}\Phi_n$ the n-particle phase space. We now consider the cumulative distribution of a three-jet event shape $V(p_1,\ldots,p_n)$, defined as:

$$\begin{aligned} \Sigma_{\mathcal{H}}(v) &\equiv \frac{1}{\sigma_{\mathcal{H}}} \sum_{n=3}^{\infty} \int \mathrm{d}\Phi_n \frac{\mathrm{d}\sigma_n}{\mathrm{d}\Phi_n} \mathcal{H}(p_1,\ldots,p_n) \Theta(v - V(p_1,\ldots,p_n)) \\ &= \frac{1}{\sigma_{\mathcal{H}}} \sum_{n=3}^{\infty} \int \mathrm{d}\Phi_n \frac{\mathrm{d}\sigma_n}{\mathrm{d}\Phi_n} \Theta\left(y_3(p_1,\ldots,p_n) - y_{\text{cut}}\right) \Theta(v - V(p_1,\ldots,p_n)) . \end{aligned} \tag{5.2}$$

In near-to-planar kinematics, i.e. for $v \ll 1$, the cumulative distribution $\Sigma_{\mathcal{H}}(v)$ assumes the factorised form (see e.g. [3])

$$\Sigma_{\mathcal{H}}(v) \simeq \frac{1}{\sigma_{\mathcal{H}}} \int \mathrm{d}\mathcal{B}\, \frac{\mathrm{d}\sigma_3}{\mathrm{d}\mathcal{B}}\, \Sigma_{\mathcal{B}}(v)\, \mathcal{H}(p_1, p_2, p_3)\,, \tag{5.3}$$

where p_1, p_2, p_3 are now the three Born momenta in Eq. (4.21), and $d\mathcal{B}$ their phase space. When $v \ll 1$, the function $\Sigma_{\mathcal{B}}(\Phi_{\mathcal{B}}; v)$ develops large logarithms of v, which we want to resum to all orders up to a given logarithmic accuracy.

5.2 NNLL resummation of the D-parameter in near-to-planar three-jet events

We recall that the D-parameter is defined in terms of the determinant of the linearised spherocity tensor Eq. (3.15). In the case of e^+e^- annihilation we can write a slightly simpler expression

$$\Theta_{\alpha\beta} = \frac{1}{Q} \sum_i \frac{p_{i\alpha} p_{i\beta}}{E_i}\,, \tag{5.4}$$

where the sum runs over all hadron momenta p_i and Q is the centre-of-mass energy of e^+e^- anninilation. The spherocity tensor has three eigenvalues $\lambda_1, \lambda_2, \lambda_3$ satisfying $\lambda_1+\lambda_2+\lambda_3 = \mathrm{Tr}\,\Theta = 1$. Using these eigenvalues we construct the C-parameter

$$C = 3(\lambda_1\lambda_2 + \lambda_1\lambda_3 + \lambda_2\lambda_3)\,, \tag{5.5}$$

and the D-parameter

$$D = 27 \det\Theta = 27\lambda_1\lambda_2\lambda_3\,. \tag{5.6}$$

For an isotropic event all eigenvalues are equal to $1/3$, and hence both the C- and the D-parameter are equal to 1.

The D-parameter can be recast in the form [71]

$$D = \frac{27}{Q^3} \sum_{i<j<k} \frac{[\vec{p}_i \cdot (\vec{p}_j \times \vec{p}_k)]^2}{E_i E_j E_k}\,. \tag{5.7}$$

The above form is very useful to obtain analytic expressions for the D-parameter in the soft and collinear regions, as neeeded for the resummation of large logarithms with the `ARES` method. In particular, in the presence of multiple soft emissions $k_1, \ldots, k_n$, Eq. (5.7) can be approximated as follows:

$$D(\{\tilde{p}\}, k_1, \ldots, k_n) \simeq \frac{27}{Q^3} \sum_{j<k=2}^{3} E_i E_j \sin^2\theta_{ij} \sum_i \frac{k_{ix}^2}{\omega_i}\,, \tag{5.8}$$

where $k_i = (\omega_i, \vec{k})$, and k_{ix} is the component of $\vec{k}_i$ in the direction of $\vec{p}_i \times \vec{p}_j$, i.e. out of the event-plane determined by the three Born momenta p_1, p_2, p_3. Note that, in the presence of soft emissions, the final-state hard momenta $\tilde{p}_1, \tilde{p}_2, \tilde{p}_3$ can be approximated by their Born counterparts p_1, p_2, p_3. Using the fact that, for three particles (see e.g. [71])

$$C = 3\lambda_1\lambda_2 = \frac{3}{Q^2}\sum_{j<k=2}^{3} E_i E_j \sin^2\theta_{ij}\,, \tag{5.9}$$

we obtain the final expression for the D-parameter in the presence of soft emissions:

$$D(\{\tilde{p}\}, k_1, \ldots, k_n) \simeq 27\lambda_1\lambda_2 \sum_i \frac{k_{ix}^2}{Q\omega_i}\,. \tag{5.10}$$

NLL resummation. To compute the NLL resummation of the D-parameter we consider its behaviour after a single soft emission, collinear to leg ℓ. Using Eq. (5.10) and the Sudakov parameterisation in Eq. (4.25) we obtain

$$D(\{\tilde{p}\}, k) \simeq 54\lambda_1\lambda_2 \frac{k_t^{(\ell)}}{Q} e^{-\eta^{(\ell)}} \sin^2\phi^{(\ell)}\,. \tag{5.11}$$

Comparing the above expression with Eq. (4.30) we get:

$$a = 1\,, \quad b^{(\ell)} = 1\,, \quad d_\ell = 54\lambda_1\lambda_2\,, \quad g_\ell(\phi) = \sin^2\phi\,, \quad \ell = 1,2,3\,. \tag{5.12}$$

From this we can determine

$$\langle \log(d_\ell g_\ell)\rangle = \log\frac{d_\ell}{4}\,. \tag{5.13}$$

Furthermore, since for soft and collinear emissions the D-parameter is additive, we recall the NLL accurate multiple emission function is given by Eq. (4.155), which we reproduce here

$$\mathcal{F}_{\rm NLL}(\lambda) = \frac{e^{-\gamma_E R'_{\rm NLL}(\lambda)}}{\Gamma(1 + R'_{\rm NLL}(\lambda))}\,. \tag{5.14}$$

NNLL resummation. In order to use our prescription for the NNLL radiator, we first compute $d_\ell^{(ij)}$ for each dipole by combining Eq. (5.12) with Eq. (4.32). Once we have $d_\ell^{(ij)}$, we can compute the soft NNLL radiator using Eq. (4.85). This gives

$$d_\ell^{(ij)} = 54\lambda_1\lambda_2 \left(\frac{Q}{2E_\ell}\right)\left(\frac{Q_{ij}}{Q}\right)^2\,. \tag{5.15}$$

In particular

$$\langle \log^2(d_\ell g_\ell)\rangle = \log^2\frac{d_\ell}{4} + \frac{\pi^2}{3}\,. \tag{5.16}$$

The hard-collinear coefficients $C^{(1)}_{\mathrm{hc},\ell}$ can be computed by replacing $\langle \log(d_\ell g_\ell)\rangle$ in eqs. (4.74) and (4.75) with the appropriate expression in Eq. (4.76).

We now consider the various real-emission NNLL corrections. The functions $\delta\mathcal{F}_{\mathrm{sc}}$, $\delta\mathcal{F}_{\mathrm{s}}$ and $\delta\mathcal{F}_{\mathrm{hc}}$ are the ones for additive observables, as there is no specific observable dependent input needed. Their expressions can be found in Eqs. (4.164), (4.166) and (4.186) respectively.

To compute the function $\delta\mathcal{F}_{\mathrm{rec}}$ we need to obtain the expression for the D-parameter after a single hard splitting of leg ℓ. This produces an emission k with a fraction $z^{(\ell)}$ of the energy E_ℓ of the parent momentum p_ℓ, and a final-state momentum $\tilde{p}$ carrying the remaining energy fraction $1-z^{(\ell)}$. Both particles carry equal and opposite out of plane momenta, $\tilde{p}_x = -k_x$. From Eq. (5.7), labelling the remaining two hard partons with the indexes $\ell_1, \ell_2 \neq \ell$, we have

$$D(\{p\},k) = \frac{27}{Q^3} E_{\ell_1} E_{\ell_2} \sin^2\theta_{\ell_1\ell_2} \left(\frac{k_x^2}{z^{(\ell)}E_\ell} + \frac{k_x^2}{(1-z^{(\ell)})E_\ell}\right) \simeq 54\lambda_1\lambda_2 \frac{k_x^2}{2z^{(\ell)}(1-z^{(\ell)})E_\ell Q}\,. \tag{5.17}$$

If we add an arbitrary number of soft and collinear emissions $k_1,\ldots,k_n$, their transverse momenta are much smaller than that of the hard collinear emission, which is the only one that effectively recoils agains hard parton $\tilde{p}_\ell$. Therefore, k_x is the out-of-event-plane component of the transverse momentum with respect to the emitter p_ℓ. This gives

$$D_{\mathrm{hc}}(\{p\},k,k_1,\ldots,k_n) = \frac{k_t^2}{Q^2} f^{(\ell)}_{\mathrm{hc}}(z^{(\ell)},\phi^{(\ell)}) + D_{\mathrm{sc}}(\{p\},k_1,\ldots,k_n) \tag{5.18}$$

with

$$f^{(\ell)}_{\mathrm{hc}}(z,\phi) = \frac{54\lambda_1\lambda_2\, Q}{2z(1-z)E_\ell} \sin^2\phi\,. \tag{5.19}$$

This means that the D-parameter is additive also in the presence of an extra hard and collinear emission. For $z \to 0$ we have

$$f^{(\ell)}_{\mathrm{hc}}(z,\phi) \simeq \frac{54\lambda_1\lambda_2\, Q}{2zE_\ell} \sin^2\phi \equiv f^{(\ell)}_{\mathrm{sc}}(z,\phi)\,. \tag{5.20}$$

Using eqs. (5.19) and (5.20), as well as the additivity of the D-parameter, we can compute $\delta\mathcal{F}_{\mathrm{rec}}$ using Eq. (4.151) as follows:

$$\begin{aligned}\delta\mathcal{F}^{\mathrm{avg.}}_{\mathrm{rec}}(\lambda) &= \mathcal{F}_{\mathrm{NLL}}(\lambda) \sum_{\ell=1}^{3} \frac{\alpha_s(\sqrt{D}Q)}{2\,\alpha_s(Q)} \int_0^{2\pi} \frac{\mathrm{d}\phi}{2\pi} \int_0^1 \mathrm{d}z\, p_\ell(z) \log(1-z) \\ &= \mathcal{F}_{\mathrm{NLL}}(\lambda) \frac{\alpha_s(\sqrt{D}Q)}{2\,\alpha_s(Q)} \left(2C_F\left(\frac{5}{4} - \frac{\pi^2}{3}\right) + C_A\left(\frac{67}{36} - \frac{\pi^2}{3}\right) - T_R n_F \frac{13}{18}\right)\,.\end{aligned} \tag{5.21}$$

Using Eq. (5.19) we can also compute $\delta\mathcal{F}_{\rm rec}^{\rm spins.}$ from Eq. (4.185), as follows:

$$\begin{aligned}\delta\mathcal{F}_{\rm rec}^{\rm spins.}(\lambda) &= -\mathcal{F}_{\rm NLL}(\lambda)\, Sp(\Phi_{\mathcal{B}})\frac{\alpha_s\left(\sqrt{D}\,Q\right)}{2\,\alpha_s(Q)}\left(\frac{1}{2!}C_A - T_R n_F\right)\times \\ &\times\int_0^1 \mathrm{d}z\, 4z(1-z)\int_0^{2\pi}\frac{\mathrm{d}\phi}{2\pi}\left(2\cos^2\phi - 1\right)\log\left(\sin^2\phi\right) \\ &= \mathcal{F}_{\rm NLL}(\lambda)\frac{\alpha_s\left(\sqrt{D}\,Q\right)}{3\,\alpha_s(Q)}\left(\frac{C_A}{2} - T_R n_F\right) Sp(\Phi_{\mathcal{B}})\,,\end{aligned} \tag{5.22}$$

where $Sp(\Phi_{\mathcal{B}})$ for $e^+e^-\to q\bar{q}g$ events is

$$Sp(\Phi_{\mathcal{B}}) \equiv Sp(x_1,x_2) = \frac{x_1+x_2-1}{x_1^2+x_2^2}\,, \tag{5.23}$$

where the details of the x_1 and x_2 variables are explained in Appendix. C.5.

The next NNLL correction we need to compute is $\delta\mathcal{F}_{\rm wa}$. According to Eq. (5.10), for soft emissions the D-parameter is additive, so we can make use of the general expression in Eq. (4.175). In order to do this, we need to recast the expression of the D-parameter with a single soft wide-angle emission in the form of Eq. (4.167). Using the Sudakov decomposition in Eq. (4.22), we obtain

$$f_{\rm wa}^{(ij)}(\eta,\phi) = 27\lambda_1\lambda_2\sin^2\phi\frac{\sin(\theta_{ij}/2)}{\cosh\left(\eta+\eta_0^{(ij)}\right)+\cos(\theta_{ij}/2)\cos\phi}\,,\qquad \eta_0^{(ij)}\equiv\frac{1}{2}\log\frac{E_i}{E_j}\,. \tag{5.24}$$

From the above expression, taking the limit $|\eta|\to\infty$, we obtain

$$f_{\rm sc}^{(ij)}(\eta,\phi) = 54\lambda_1\lambda_2\sin\frac{\theta_{ij}}{2}\left[e^{-(\eta+\eta_0^{(ij)})}\,\Theta(\eta) + e^{\eta+\eta_0^{(ij)}}\,\Theta(-\eta)\right]\sin^2\phi\,. \tag{5.25}$$

Inserting the above expressions in Eq. (4.175) we obtain

$$\begin{aligned}\delta\mathcal{F}_{\rm wa}(\lambda) &= \mathcal{F}_{\rm NLL}(\lambda)\sum_{(ij)}C_{ij}\frac{\alpha_s(DQ)}{\alpha_s(Q)}\int_0^{2\pi}\frac{\mathrm{d}\phi}{2\pi}\int_{-\infty}^{\infty}\mathrm{d}\eta\times \\ &\times\left(\log\left[2e^{-(\eta+\eta_0^{(ij)})}\left(\cosh\left(\eta+\eta_0^{(ij)}\right)+\cos\frac{\theta_{ij}}{2}\cos\phi\right)\right]\Theta(\eta)\right. \\ &\left.+\log\left[2e^{\eta+\eta_0^{(ij)}}\left(\cosh\left(\eta+\eta_0^{(ij)}\right)+\cos\frac{\theta_{ij}}{2}\cos\phi\right)\right]\Theta(-\eta)\right) \\ &= \mathcal{F}_{\rm NLL}(\lambda)\sum_{(ij)}C_{ij}\frac{\alpha_s(DQ)}{\alpha_s(Q)}\times \\ &\times\left((\eta_0^{(ij)})^2 + 2\int_0^{\infty}\mathrm{d}\eta\,\log\left[e^{-\eta}\left(\cosh\eta+\sqrt{\cosh^2\eta-\cos^2\frac{\theta_{ij}}{2}}\right)\right]\right)\,,\end{aligned} \tag{5.26}$$

the final term must be evaluated numerically, and it depends on the configuration of the Born event through the term θ_{ij}.

The last contribution we need to compute is $\delta\mathcal{F}_{\rm correl}$. Since the D-parameter is additive, we can again use the general formula for additive observables in Eq. (4.181). In order to

do this we need to recast the D-parameter with two soft and collinear emissions in the form of Eq. (4.176). This gives

$$f^{(\ell)}_{\rm correl}(\mu, z, \phi, \phi^{(\ell)}) = 1 + \mu^2 \frac{\sin^2(\phi + \phi^{(\ell)})}{\sin^2 \phi^{(\ell)}}\,, \tag{5.27}$$

the same for all three legs. This gives

$$\delta\mathcal{F}_{\rm correl}(\lambda) = -\mathcal{F}_{\rm NLL}(\lambda) \frac{\lambda R''_{\rm NNLL}}{2\beta_0 \alpha_s(Q)} \left(C_A \langle \log f_{\rm correl}\rangle_{C_A} + 2T_R n_F \langle \log f_{\rm correl}\rangle_{n_F}\right)\,, \tag{5.28}$$

where

$$\begin{aligned}
\langle \log f_{\rm correl}\rangle_{C_A} &= \frac{1}{2!}\int_0^{2\pi} \frac{{\rm d}\phi^{(\ell)}}{2\pi} \int_0^\infty \frac{{\rm d}\mu^2}{\mu^2(1+\mu^2)} \int_0^1 {\rm d}z \int_0^{2\pi} \frac{{\rm d}\phi}{2\pi} (2\mathcal{S} + \mathcal{H}_g) \log f_{\rm correl}(\mu, z, \phi, \phi^{(\ell)})\,,\\
\langle \log f_{\rm correl}\rangle_{n_F} &= \frac{1}{2!}\int_0^{2\pi} \frac{{\rm d}\phi^{(\ell)}}{2\pi} \int_0^\infty \frac{{\rm d}\mu^2}{\mu^2(1+\mu^2)} \int_0^1 {\rm d}z \int_0^{2\pi} \frac{{\rm d}\phi}{2\pi} \mathcal{H}_q \log f_{\rm correl}(\mu, z, \phi, \phi^{(\ell)})\,,
\end{aligned} \tag{5.29}$$

We evaluate these expressions numerically and find,

$$\langle \log f_{\rm correl}\rangle_{C_A} = 1.8139\,, \qquad \langle \log f_{\rm correl}\rangle_{n_F} = 1.1562\,. \tag{5.30}$$

With these corrections we and the Sudakov radiator we have all of the ingredients necessary to perform the resummation of the D-parameter.

5.3 Phenomenology

In order to provide a suitable cumulative distribution that paves the way for phenomenological studies, one has to match the resummation to fixed order. Matching is required to provide results across all values of the observable. The basic idea is to combine the results of both the resummation and fixed order, while making sure to get rid of contributions that are double counted. There are two generic conditions that the matching procedure must satisfy. First, based on physical grounds the matched total cross section should go to zero as $v \to 0$. Second, the matched distribution, or likewise the total cross section, must reproduce the fixed order at the kinematic endpoint $v \to v_{\rm max}$.

The two most popular matching schemes for e^+e^- annihilation are the R and log-R schemes [44, 46]. In other contexts, multiplicative matching schemes are used [72, 73]. Adopting one over the other is a choice that depends on the problem at hand. In our case, we could not achieve a stable matched distribution using the R and log-R schemes, given that the available data sets for the D-parameter forces us to use low values of $y_{\rm cut}$. The problem with both schemes is that, given that the various components of the resummed cross section contain powers of $\log y_{\rm cut}$, the resummation does not switch off quickly enough

and ends up substantially contributing to the tail of the matched distribution. This situation might be expected given that the K-factor NLO/LO is very large, approximately 100%. This is similar to the case of resumming the distribution in the Higgs transverse momentum $p_{t,H}$ where the K-factor is also known to be large [74]. Therefore, we supplement our matching scheme with a factor that effectively damps the resummation at large values of D.

Based on the above discussion, we use the multiplicative matching scheme designed in ref. [74]. The goal of that scheme is precisely to suppress the large terms, present in the resummation, which emerge outside the resummation region. This enables us to control the tail of the distribution and achieve a stable matching. In this scheme, matching is performed on the level of the total cross section. Given that NLOJet++ simulates the *inclusive* cross section, i.e. integrated over Born kinematics with the three-jet selection cut, we have to match on the same level. Explicitly, we have

$$\Sigma_{\mathcal{H}}^{\text{Mat.}}(v) = \left(\Sigma_{\mathcal{H}}^{\text{Res.}}(v)\right)^{Z} \frac{\Sigma_{\mathcal{H}}^{\text{FO.}}(v)}{\left(\Sigma_{\mathcal{H}}^{\text{Exp.}}(v)\right)^{Z}}\,, \tag{5.31}$$

where

$$Z = \left(1 - \left(\frac{v}{v_0}\right)^{u}\right)^{h} \Theta(v - v_0)\,, \tag{5.32}$$

is a damping factor that controls how quickly the logarithms are shut down outside the resummation region. In eq. (5.31), $\Sigma_{\mathcal{H}}^{\text{Res.}}$ is the resummed cross section, $\Sigma_{\mathcal{H}}^{\text{FO.}}$ is the corresponding fixed-order quantity and $\Sigma_{\mathcal{H}}^{\text{Exp.}}$ denotes the expansion of the resummation to NLO. The details of the matching can be found in appendix C.6 and the expanded version of eq. (5.31) is given in full in eq. (C.64). We carry out the matching using the values $u = 1$, $h = 3$ and $v_0 = 1/2$.

As is customary in resummed calculations, we need to probe the size of sub-leading logarithmic terms. This is done using two simultaneous variations. The first introduces a rescaling x_V as follows

$$\log\frac{1}{v} = \log\frac{x_V}{v} - \log x_V\,, \quad x_V \equiv X \cdot X_V \quad . \tag{5.33}$$

In the above, X is a variable choice to define the resummation scale, i.e. the logarithms being practically resummed, while X_V controls the scale variation. We expand the total cross section around $\log(x_V/v)$ neglecting sub-leading terms. Furthermore, the resummed logarithm, $\log(x_V/v)$, must be modified in order to impose that the total cross section is reproduced at the kinematic endpoint v_{max} [73]

$$\log\frac{x_V}{v} \to \tilde{L} \equiv \frac{1}{p}\log\left(\left(\frac{x_V}{v}\right)^{p} - \left(\frac{x_V}{v_{\text{max}}}\right)^{p} + 1\right) \quad , \tag{5.34}$$

where p denotes a positive number that controls how quickly the logarithms are switched off close to the endpoint. The parameter p is free, but is only constrained by the behaviour of the fixed order distribution near the endpoint [73]. In our case, we set $p = 1$, as is customary in event-shape studies.

Another estimate for the uncertainty in our matched distribution comes from varying the renormalisation scale, μ_R, around a central scale that we take to be the centre-of-mass energy of the hard scattering, Q. For LEP-1 energies, $Q = M_Z$ corresponding to $\alpha_s(M_Z) = 0.118$ while for FCC-ee energies, $Q = 500\,\text{GeV}$ corresponding to $\alpha_s(500\,\text{GeV}) = 0.094$.

We implement two different choices for X in eq. (5.33). The first is referred to as the X_{const} scheme which corresponds to setting $X = 1$ in eq. (5.33), while the second is the X_{prod} scheme which corresponds to setting

$$X = \frac{3}{2C_F + C_A} \log \frac{27\lambda_1\lambda_2}{2}\,, \tag{5.35}$$

which is a function of the Born kinematics. Finally, we construct the uncertainty bands by varying μ_R by a factor of two in either direction and X_V by a factor of three-halves in either direction.

In figs. 5.1 and 5.2 we plot the matched distribution for $Q = M_Z$ using the two resummation schemes and for two different values of y_{cut}, namely $y_{\text{cut}} = 0.1$ and $y_{\text{cut}} = 0.05$. We immediately notice the following features:

- The uncertainty bands are not drastically reduced when increasing the logarithmic accuracy of the resummation, at least when compared to the typical situation with two-jet observables.
- The position of the peak is stable under varying y_{cut}.
- For NLL, the uncertainty bands remain almost unchanged with decreasing y_{cut}. In contrast, the uncertainty bands for NNLL are noticeably enhanced as we increase y_{cut}.

The fact that the uncertainty does not reduce significantly from NLL to NNLL might be due to the fact that not all possible sources of theoretical uncertainties have been explored. In fact, varying the renormalisation scale probes the typical scale of hard QCD radiation, whereas the sensitivity to soft and collinear physics is probed by varying the parameter X_V. By doing so, we vary the typical scales of soft radiation ($\sim Qv^{1/a}$) and collinear radiation ($\sim Qv^{1/(a+b_\ell)}$) in a correlated way. One way to decorrelate the two regions might be that

of introducing a "jet scale" Q_J that probes variation of the collinear scale only, as done in SCET, see e.g. [75]. Since in our formalism all the scales introduced have a definite physical meaning, the only place where we can introduce a new scale is in eq. (4.60). There we can split virtual corrections at the scale $Q_J v^{1/(a+b_\ell)}$. As a consequence, $R_{\rm hc}$ has to be evaluated at $v(Q_J/Q)^{a+b_\ell}$, and this change is compensated, up to sub-leading corrections, by the following change in the coefficients $C_{{\rm hc},\ell}(1)$ in Eqs. (4.74) and (4.75):

$$C^{(1)}_{{\rm hc},\ell} \to C^{(1)}_{{\rm hc},\ell} + \gamma^{(0)}_\ell \log\left(\frac{Q^2}{Q_J^2}\right) \ ,. \tag{5.36}$$

An equivalent procedure up to N^{3}LL corrections is to vary the quantity X_V introduced in eq. (5.33) in the hard collinear radiator only by a factor $(Q_J/Q)^{a+b_\ell}$. Note that, for the D-parameter, since $a + b_\ell = 2$, changing Q_J by a factor of two around Q means changing X_V by a factor of four around $X_V = 1$. This is way beyond the range of X_V that is customary explored in event-shape studies, that involves variation at most by a factor of two (see e.g. [4]). As a check, we have indeed varied X_V for the hard-collinear radiator only, in the range $1/4 < X_V < 4$. Although we have observed that the corresponding uncertainty band increases, reaching deviations up to 40% from the central value in the peak region, the size of the band does not decrease in moving from NLL to NNLL. This issue definitely calls for further studies. However, we believe that choosing an appropriate range for the variation of Q_J requires at least a comprehensive re-analysis of two-jet event shapes, as well as another three-jet event-shape for comparison. Therefore, we leave this investigation to future work.

We believe that the issues we have with theory uncertainties can partly be traced to the fact that jet selection generates terms that go as $\log^2 y_{\rm cut}$, for each power of α_s relative to the Born cross section. The largest *transverse* momentum of soft-collinear emissions, at fixed value of D, is of the order of $\sqrt{D}Q$. Our resummation is strictly defined when the largest momentum is much smaller than the largest transverse momentum available, the latter being of the order of $\sqrt{y_{\rm cut}}Q$. Essentially, our resummation is formally correct, as $D \ll 1$, but phenomenologically viable only in the limit $D \ll y_{\rm cut} \ll 1$. Inspection of figs. 5.1 and 5.2 shows that the most probable value of D, which corresponds to the position of the peak of differential distributions, is of the same order as $y_{\rm cut}$ and that is why we see the features described above. This is also reflected in the sensitivity of the uncertainty bands of the NNLL distribution to the variation of $y_{\rm cut}$ in comparison to NLL. Simply, the NNLL pieces in the cross section, e.g. $\delta\mathcal{F}_{\rm s}$, contain extra powers of $\log y_{\rm cut}$ compared to NLL. These logarithms are large, for $y_{\rm cut} = 0.05 - 0.1$, and thus we observe this behaviour of the uncertainty bands.

The situation becomes better at FCC-ee energies, as we see clearly in figs. 5.3 and 5.4. Noticeably the position of the peak tends towards smaller values of D, and we start approaching the strict resummation regime $D \ll y_{\text{cut}} \ll 1$. Simultaneously we see a reduction in the uncertainty by almost 50%. To conclude, for this observable, and depending on the value of y_{cut}, we expect large sub-leading corrections that are not under control in any resummation formalism. This calls for a joint resummation of both types of logarithms, the observable and y_{cut}, along the line of the presented resummation of both $p_{\text{t,H}}$ and the transverse momentum of the leading jet [76].

Leaving these caveats aside, we note that NNLL corrections generically yield harder D-parameter distributions. The effect is larger using the X_{prod} scheme, because the resummed logarithms in the latter scheme are typically larger than the X_{const} scheme. Indeed, this is one of the reasons why the NNLL uncertainty bands get larger when we use the X_{prod} scheme, while their counterparts at NLL remain virtually the same. Note that in the X_{prod} scheme the resummation scale is effectively of the order $\sqrt{y_{\text{cut}}}Q$ which is the appropriate upper bound for transverse momenta. Therefore, this scheme automatically captures some of the terms which are enhanced by logarithms of y_{cut}.

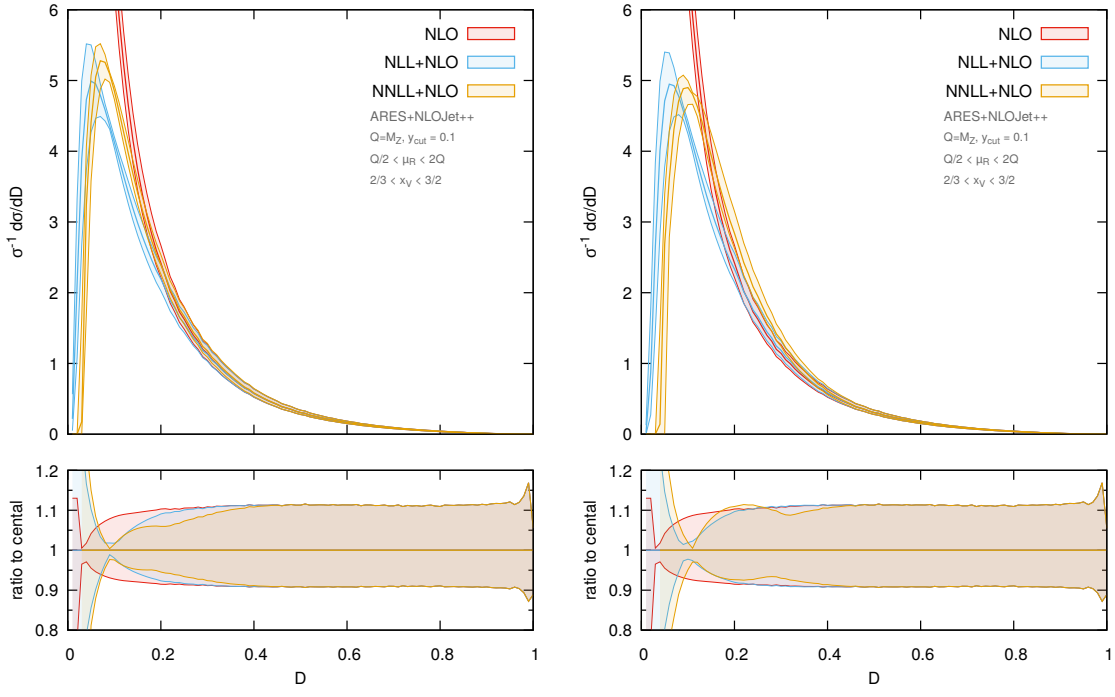

Figure 5.1: The matched distribution for $y_{\text{cut}} = 0.1$ and $Q = M_Z$. The left plot using the X_{const} scheme and the right using the X_{prod} scheme.

Last, we compare our predictions to existing LEP-1 data [77–79]. In order to do so, we need to supplement our perturbative resummation with some estimate of non-perturbative

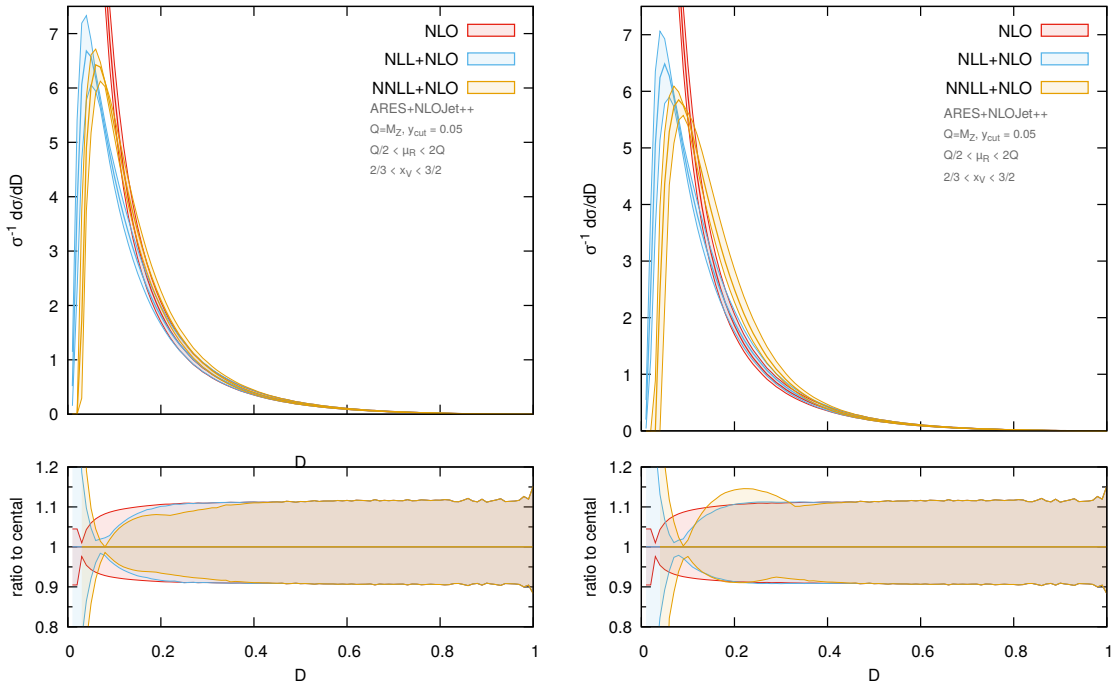

Figure 5.2: The matched distribution for $y_{\text{cut}} = 0.05$ and $Q = M_Z$. The left plot using the X_{const} scheme and the right using the X_{prod} scheme.

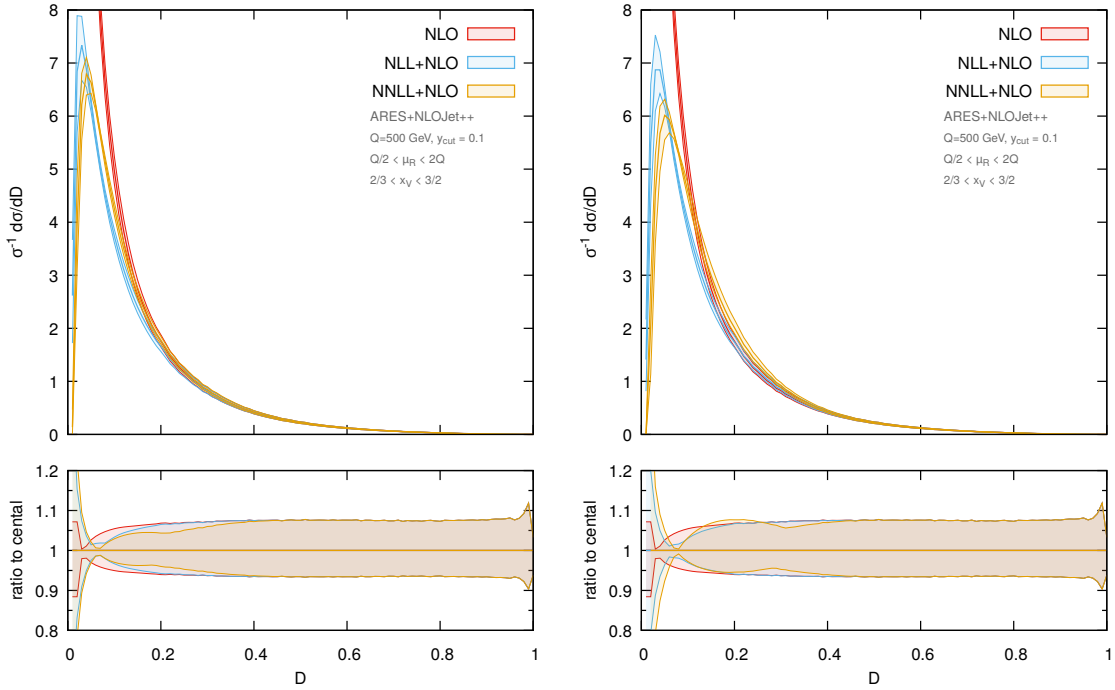

Figure 5.3: The matched distribution for $y_{\text{cut}} = 0.1$ and $Q = 500\text{GeV}$. The left plot using the X_{const} scheme and the right using the X_{prod} scheme.

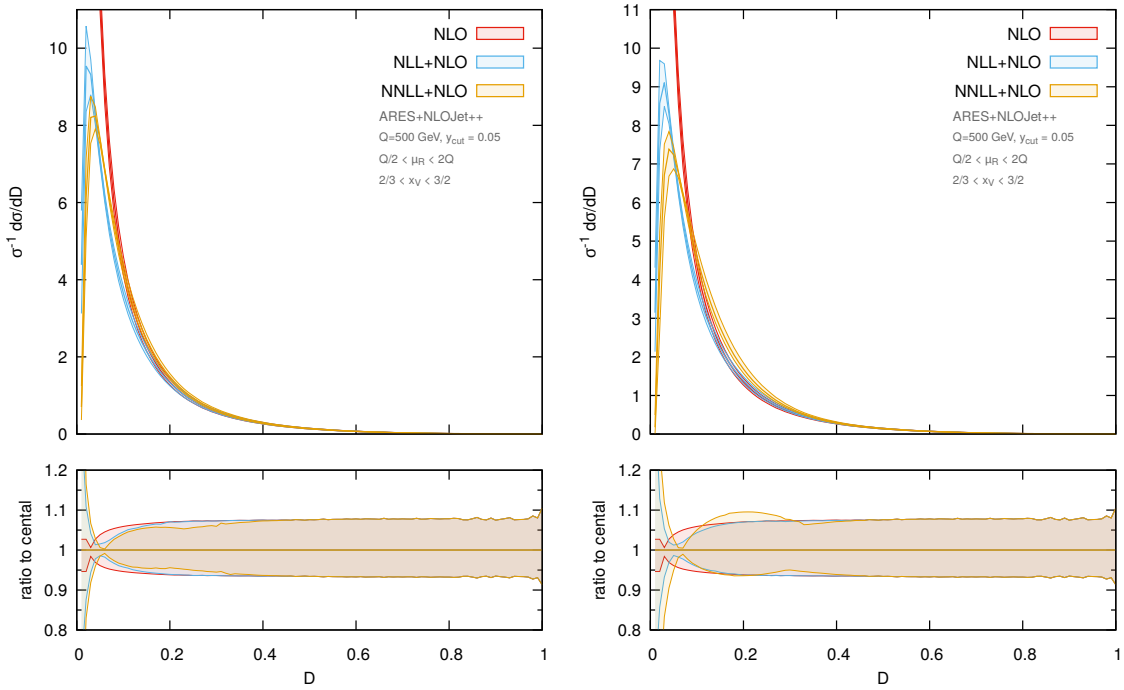

Figure 5.4: The matched distribution for $y_{\rm cut} = 0.05$ and $Q = 500$GeV. The left plot using the $X_{\rm const}$ scheme and the right using the $X_{\rm prod}$ scheme.

hadronisation corrections. Before we do this, we need to choose whether to use $X_{\rm const}$ or $X_{\rm prod}$ as our default choice for the resummation scale. We have observed that NNLL distributions obtained with $X_{\rm prod}$ are not very stable with respect to the choice of the matching parameter v_0, which points to the fact that such a choice brings in numerically large sub-leading corrections, which we cannot control within our framework. Therefore, we decide to present non-perturbative plots using $X_{\rm const}$ as our resummation scale, and $v_0 = 1/2$. We have checked that using other values of v_0 does not change considerably our findings. We include hadronisation corrections in the dispersive approach of ref. [80], where leading hadronisation corrections result in a shift of the corresponding perturbative distributions. In our case, we use the non-perturbative shift computed in ref. [81], and define

$$\Sigma^{\rm NP}_{\mathcal{H}}(D) = \frac{1}{\sigma_{\mathcal{H}}} \int {\rm d}\Phi_3 \frac{{\rm d}\sigma_3}{{\rm d}\Phi_3} \Sigma_{\mathcal{B}}\left(\{p_1,p_2,p_3\}, D - Z_{\rm NP}\,\delta D\left(\{p_1,p_2,p_3\}\right)\right) \mathcal{H}(p_1,p_2,p_3)\,, \tag{5.37}$$

where

$$\delta D(\{p_1,p_2,p_3\}) = \frac{a_{\rm NP}}{Q} 27\lambda_1\lambda_2 \sum_{(ij)} C_{(ij)}\, g_{ij}\left(\theta_{ij}\right)\,. \tag{5.38}$$

In the above equation, the geometry dependent functions g_{ij} are those of ref. [81], which

we rewrite using our own notation and conventions as follows:

$$g_{ij}(\theta_{ij}) = \sin\frac{\theta_{ij}}{2}\int_0^{2\pi}\frac{\mathrm{d}\phi}{2\pi}\int_{-\infty}^{\infty}\mathrm{d}\eta\frac{\sin^2\phi}{\cosh\eta+\cos(\theta_{ij}/2)\cos\phi}\,. \tag{5.39}$$

The non-perturbative parameter a_{NP} is given by

$$a_{\mathrm{NP}} = \frac{4\mu_I}{\pi^2}\mathcal{M}\left(\alpha_0(\mu_I) - \alpha_s(Q) - 2\beta_0\alpha_s^2(Q)\left(\log\frac{Q}{\mu_I} + \frac{K^{(1)}}{4\pi\beta_0} + 1\right)\right)\,, \tag{5.40}$$

where

$$\alpha_0(\mu_I) = \int_0^{\mu_I}\frac{\mathrm{d}k}{\mu_I}\alpha_s(k)\,, \tag{5.41}$$

and $\alpha_s(k)$ is the dispersive coupling defined in ref. [80], and $\mathcal{M} \simeq 1.49$ is the Milan factor [82–85] corresponding to three light flavours, as appropriate for non-perturbative corrections in the dispersive model [82, 83]. As in previous non-perturbative studies, we set $\mu_I = 2\,\mathrm{GeV}$. In eq. (5.37), we have also introduced the factor

$$Z_{\mathrm{NP}} = 1 - \left(\frac{D}{D_{\mathrm{max}}}\right)^q\,, \tag{5.42}$$

that ensures that the shift vanishes at the endpoint of the distribution. Also, to ensure that the distribution vanishes at its endpoint, we replace $\tilde{L}$ defined in eq. (5.34) with

$$\tilde{L}_{\mathrm{NP}} \equiv \frac{1}{p}\log\left(\left(\frac{x_D}{D-\delta D}\right)^p - \left(\frac{x_D}{D_{\mathrm{max}}-\delta D}\right)^p + 1\right)\,. \tag{5.43}$$

Specifically, we have set $q = 2$ and $p = 1$. Last, in order to produce matched non-perturbative distributions, we compute $\delta D_{\mathcal{H}}$ defined by

$$\Sigma_{\mathcal{H}}(D - \delta D_{\mathcal{H}}) = \Sigma_{\mathcal{H}}^{\mathrm{NP}}(D)\,, \tag{5.44}$$

and define our matched non-perturbative distribution as $\Sigma_{\mathcal{H}}^{\mathrm{Mat.}}(D - \delta D_{\mathcal{H}})$. In Fig. 5.5 we produce plots for non-perturbative matched distributions, with central scales, corresponding to NLL and NNLL accuracy. The non-perturbative shift corresponds to a value of $\alpha_0(2\,\mathrm{GeV})$ that is inside the range favoured by existing fits to event-shape data [86]. We see that, for this value of α_0, namely $\alpha_0 = 0.5$, the NNLL resummation has a shape that resembles the data more closely than NLL resummation. This trend persists irrespective of the value of y_{cut}. Note that this value of α_0 is similar to the central value of a fit obtained with the NNLL thrust distribution [87]. We also observe that increasing the value of v_0 up to D_{max} does not change the distributions close to the peak, but gives a better agreement with the data in the tails.

Despite the fact that our choice of the NP parameter α_0 provides a good description of the D-parameter distributions for intermediate values of D, the peak region is not

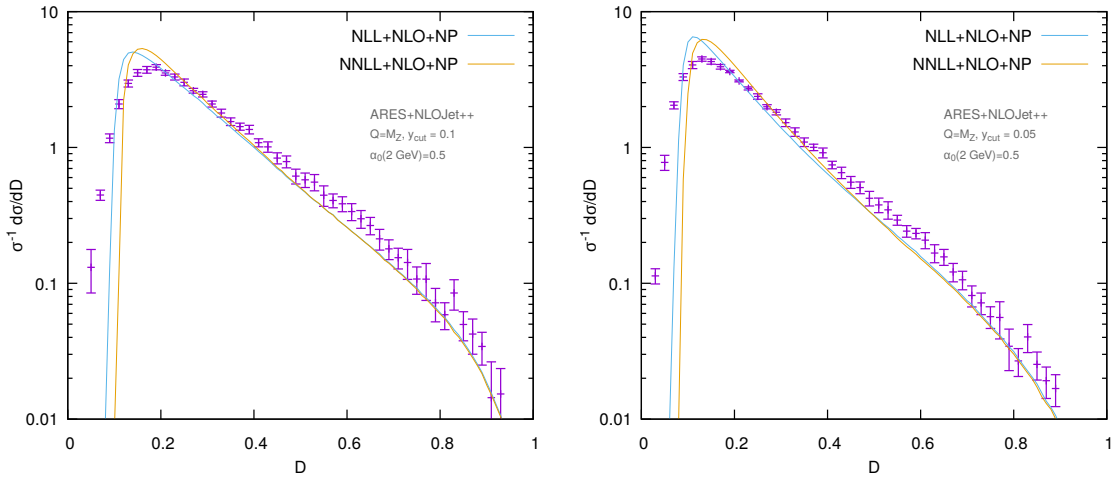

Figure 5.5: The matched distribution, including the non-perturbative corrections, is compared to data from LEP-1 for the two values of y_{cut} we adopt in this article.

well described. However, this is hardly surprising, given that including hadronisation corrections as a shift is strictly valid only for $\delta D \ll D$, i.e to the right of the peak of the D-parameter distributions. Due to an extra radiating gluon, the shift for three-jet event shapes is roughly twice as big as that for two-jet event shapes. Therefore, at LEP energies, we expect that a shift alone is not enough to accurately describe the peak of three-jet event-shape distributions, as was generally the case for two-jet event shapes [86]. To obtain a good description of the peak, one needs to upgrade the shift to a shape function, as done for instance in refs. [88–91].

5.4 Conclusions

We have applied the `ARES` method for three-jet events, derived in chapter 4, to the D-parameter to NNLL accuracy. Since this is an additive observable, we are able to compute most of the NNLL functions analytically, with only a couple of integrals that must be computed numerically. We have performed phenomenological studies by matching our resummation to exact fixed-order and presenting predictions for LEP-1 and future colliders. We have seen that using the LEP-1 cuts to select three-jet events gives rise to large sub-leading effects at LEP-1 energies, the situation is somewhat improved at FCC-ee. Nevertheless, we envisage that, to improve phenomenological studies of the D-parameter, one should attempt a joint resummation of logarithms of the D-parameter and of the variable determining the three-jet selection. A similar procedure to that used for the case of angularities, or for the transverse momentum of a colour singlet and an accompanying

leading jet.

A comparison with LEP-1 data requires the inclusion of non-perturbative hadronisation corrections. We have added the leading hadronisation corrections evaluated in the dispersive model to our NNLL resummation. In general, the NNLL distribution has a shape that is similar to data. And, for values of the D-parameter larger than those at the peak of distribution, hadronisation corrections are compatible with a shift of the perturbative distribution. We find that, in order to describe the data in the region following the peak, we can set the non-perturbative parameter α_0, that determining the size of the shift, to a value that is comparable to the one obtained from fits of NLL event shape distributions. A very interesting piece of future work would be to perform a comprehensive simultaneous fit of α_s and α_0 using NNLL resummations for different event shapes.

Chapter 6

BSM WW production with a jet veto

In chapters 4 & 5 we extended the ARES method to observables with higher multiplicity. In this chapter we apply the ARES method to the resummation of jet-veto effects at hadron colliders. Jet-veto effects for colourless final states have already been resummed up to NNLL accuracy within the ARES framework [92, 93]. These resummations were implemented in the code JetVHeto, for the production of Z and Higgs bosons at threshold. In this chapter we take these resummations and re-implement them as a extension to the Monte Carlo integrator MCFM. This implementation resums jet-veto for *all* colourless final states[1] and is differential (exclusive) in the kinematics of the Born.

We examine the possibility of using the di-boson channels to constrain new physics models, in particular the WW channel is challenging to model correctly due to presence of a jet-veto on the final state. We use this new implementation of ARES inside MCFM to make projections for constraining power of the WW channel relative to the ZZ channel.

6.1 Introduction

Di-boson production at the Large Hadron Collider constitutes a promising window into physics beyond the SM. This is particularly true for di-boson pairs with high invariant mass, which have been already probed by a number of recent experimental analyses [94–104]. On the one hand, their production through gluon fusion receives contributions from an off-shell Higgs boson [105–107]. In particular, the interference of the contribution of an off-shell Higgs boson and di-boson continuum background makes it possible to access the

[1] Naturally we can only resum those processes that are implemented in MCFM.

Higgs width in a model-independent way [108]. On the other hand, contact interactions arising from higher-dimensional effective field theory operators [109–113] could give rise to spectacular effects in the tails of di-boson differential distributions, due to the fact that some of their contribution increases with energy. Technically, in the SM, di-boson production via gluon fusion is a loop-induced process. At low di-boson invariant masses, top quarks in the loops behave as very heavy particles, thus giving rise to effective contact interactions. At high invariant masses, the two bosons probe virtualities that are much larger than the masses of the top quarks running in the loops, hence suppressing their contribution and enhancing the effect of BSM contact interactions. Such a feature has been already used to constrain the coefficient of a number of higher-dimensional operators, see e.g. [114] for a recent study.

We restrict ourselves to considering the unique dimension-six operator coupling gluons to the Higgs boson, given by [110]

$$\mathcal{L} \supset \frac{c_{gg}}{\Lambda^2} G^a_{\mu\nu} G^{a,\mu\nu} \phi^\dagger \phi, \tag{6.1}$$

with $G^a_{\mu\nu}$ the gluon field strength and ϕ the Higgs field. This operator can be used to represent contributions to SM Higgs production from particles with mass of order $\Lambda \gg m_H$. This operator has previously been considered in high-invariant-mass ZZ production with a fully leptonic final state in [115, 116]. However, the leptonic final state for WW has larger cross section and so WW could give complementary or better sensitivity than leptonic final states for ZZ. However, in WW production, a tight jet veto is employed by experiments to suppress the background from top-pair production. Such a veto "forbids" the radiation of jets from the initial-state partons, with the effect of suppressing not only the background, but also the operator-mediated signal. In the present case, the signal occurs through gluon fusion, whereas WW production is mainly driven by quark-antiquark annihilation. Since gluons radiate more than quarks, one expects the suppression due to a jet veto to be stronger for the signal than for the background. It is therefore important to address the general question of how BSM searches with WW production compare to ZZ in the presence of a jet veto.[2]

We wish to quantify in a simple way how the significance of such a BSM signal is affected by the presence of a jet veto. The same procedure can be applied to any BSM scenario that modifies the production rate of a colour singlet, for instance dimension-8 operators [125]. A similar study [126] investigates the impact of a jet veto in the

[2] In fact, a supposed discrepancy of the total WW cross section from SM predictions [117–119] could be partly ascribed to mismodelling of jet-veto effects [120–124].

determination of the Higgs width using interference. To be more specific, we veto all jets that have a transverse momentum (with respect to the beam axis) above $p_{\mathrm{t,veto}}$. First we observe that, at the level of the matrix element squared, a generic BSM signal mediated by a single higher-dimensional operator consists of an interference piece and a quadratic piece:

$$|M_{\mathrm{SM}}|^2 + 2\mathrm{Re}(M^*_{\mathrm{SM}} M_{\mathrm{BSM}}) + |M_{\mathrm{BSM}}|^2. \tag{6.2}$$

The last piece is of higher order $1/\Lambda^4$. Therefore, if the interference piece is not suppressed or vanishing for some reason, then, to a first approximation, we can neglect it relative to the $1/\Lambda^2$ interference piece.[3] The presence of a jet veto induces large logarithms of the ratio of $p_{\mathrm{t,veto}}$ and the invariant mass of the WW pair M_{WW}. Such logarithms arise at all orders in QCD, and originate from vetoing soft-collinear parton emissions. Considering just the leading logarithms, and neglecting the quadratic piece $|M_{\mathrm{BSM}}|^2$, the deviation of a BSM signal that proceeds from gluon fusion from the SM prediction is approximately given by

$$\mathcal{L}_{gg}(M_{WW}) \times 2\mathrm{Re}(M^*_{\mathrm{SM}} M_{\mathrm{BSM}})\, e^{-2C_A \frac{\alpha_s}{\pi} \log^2\left(\frac{M_{WW}}{p_{\mathrm{t,veto}}}\right)}, \tag{6.3}$$

where $C_A = 3$, α_s is the strong coupling, and $\mathcal{L}_{gg}(M_{WW})$ is the gluon-gluon luminosity corresponding to a partonic centre-of-mass energy equal to M_{WW}. The effect of the jet veto is an exponential (Sudakov) suppression with respect to a naive Born-level estimate. Note also that, for fixed $p_{\mathrm{t,veto}}$, such a suppression becomes more and more important, the higher the invariant mass of the WW pair. This is precisely where the contribution of the BSM operator in eq. (6.1) has the most impact on the signal. For the SM background, dominated by quark-antiquark annihilation, we have instead a contribution proportional to

$$\mathcal{L}_{q\bar{q}}(M_{WW}) \times |M_{\mathrm{SM}}|^2\, e^{-2C_F \frac{\alpha_s}{\pi} \log^2\left(\frac{M_{WW}}{p_{\mathrm{t,veto}}}\right)}, \tag{6.4}$$

with $C_F = 4/3$ and $\mathcal{L}_{q\bar{q}}(M_{WW})$ the quark-antiquark luminosity. The relative deviation from the SM can be obtained by integrating eqs. (6.3) and (6.4) over the appropriate phase space. Note that, for a fixed value of M_{WW}, the exponential encoding jet-veto effects factorise completely. Therefore, the relative deviation from the SM in the presence of the jet-veto is different from that obtained with a Born-level calculation by a factor

$$e^{-2(C_A - C_F) \frac{\alpha_s}{\pi} \log^2\left(\frac{M_{WW}}{p_{\mathrm{t,veto}}}\right)}. \tag{6.5}$$

[3] Note that, if we consider more than one higher-dimensional operator, there are possibly other BSM effects of order $1/\Lambda^3$ or $1/\Lambda^4$ in the interference piece in general, which might still compete with or dominate over the quadratic piece.

For $\alpha_s = 0.1, M_{WW} = 1\,\text{TeV}, p_{\text{t,veto}} = 20\,\text{GeV}$, the above factor is about 0.2. Therefore, despite the gain in the number of events one has in WW production with respect to ZZ, the significance of the signal might be reduced due to jet-veto effects. This is why it is crucial to have an estimate of jet-veto effects that is as accurate as possible.

The first question we address is what accuracy we can aim for in the description of a BSM signal and a QCD background involving the production of a colour singlet. In the absence of large jet-veto corrections, a generic BSM signal can be predicted at Born-level, or leading order (LO), in QCD, whereas any QCD background is nowadays known at least at next-to-leading order (NLO). In the presence of a jet veto, the production of a system of invariant mass M is affected by logarithms of the ratio $p_{\text{t,veto}}/M$, which make fixed-order predictions unreliable. After the all-order resummation of $\log(p_{\text{t,veto}}/M)$, the differential cross-section $\mathrm{d}\sigma(p_{\text{t,veto}})/\mathrm{d}M^2$ with no jets with a transverse momentum above $p_{\text{t,veto}}$ can be written in the form[4]

$$\frac{\mathrm{d}\sigma(p_{\text{t,veto}})}{\mathrm{d}M^2} = \frac{\mathrm{d}\sigma_0}{\mathrm{d}M^2}\, e^{Lg_1(\alpha_s L)} \left(G_2(\alpha_s L) + \alpha_s G_3(\alpha_s L) + \dots\right), \quad L \equiv \log\frac{M}{p_{\text{t,veto}}}. \tag{6.6}$$

with $\mathrm{d}\sigma_0/\mathrm{d}M^2$ the corresponding LO cross section. The above expression is meaningful for $\alpha_s \log(M/p_{\text{t,veto}}) \sim 1$ and misses terms that vanish as powers of $p_{\text{t,veto}}/M$ (possibly enhanced by logarithms). The leading logarithmic (LL) contributions exponentiate giving rise to the function $g_1(\alpha_s L)$, with α_s evaluated at a renormalisation scale of order M. Next-to-leading logarithmic terms (NLL) factorise from LL ones, and are embedded in the function $G_2(\alpha_s L)$. Next-to-next-to-leading logarithmic (NNLL) contributions, resummed by $G_3(\alpha_s L)$, are of relative order α_s with respect to NLL ones, and similarly one can define higher logarithmic accuracy. The knowledge of NLO corrections to a QCD background process gives access to all ingredients to compute G_3, i.e. to achieve NNLL accuracy, whereas the lack of knowledge of corrections of relative order α_s to a generic BSM process implies that the best accuracy one can aim at for such processes is NLL. Therefore, from the point of view of the accuracy of the resummation, having LO makes it possible to reach NLL accuracy, whereas NLO gives access to NNLL accuracy.

The most widely used method to estimate jet-veto effects are Monte Carlo event generators, which simulate the contribution of multiple soft-collinear QCD emissions. Although very flexible, these tools cannot formally guarantee more than LL accuracy, and at the moment require a considerable amount of tuning to reliably describe observables, like the cross section with a jet-veto in eq. (6.6), sensitive to QCD radiation from the initial state

[4]The general expression in eq. (6.6) holds because the transverse momentum of the leading jet has the property of recursive infrared and collinear (rIRC) safety [3].

(see e.g. [127] for a recent study). In order to have more accurate predictions, one needs to consider analytical resummations.

Jet-veto effects in the production of a colour singlet have been computed at NNLL accuracy in QCD [93] and in soft-collinear effective theory (SCET) [128, 129]. The calculation of [93] is implemented for Higgs and Z-boson production, inclusive in all decay products, in the program `JetVHeto` [130]. The calculation of [128] has been implemented in `aMC@NLO` for the production of a generic colour singlet, fully exclusive in its decay products [122]. This implementation has been used to estimate jet-veto effects in WW production [122] in the SM, and for hypothetical Z' and W' bosons [131]. The specificity of this SCET calculation is the presence of beam functions, that are precomputed and replace traditional parton distribution functions. We discuss an alternative approach that implements the QCD resummation of ref. [93], fully exclusive in the decay products of the colour singlet, in a way that is not tied to a specific event generator (e.g. `aMC@NLO`), but that requires minimal and simple modifications of the setup that is already available in any NLO QCD program. The starting point is to observe that, in eq. (6.6), the factor multiplying leading logarithms is in fact a new perturbative series, whose coefficients are functions of $\alpha_s L$. As stated previously, NLL corrections have the same structure as Born-level contributions, while NNLL corrections closely resemble NLO contributions. Therefore, NLL resummation could just be obtained by an event-by-event reweighting of a Born-level generator by keeping only the functions g_1 and G_2 in eq. (6.6). This is enough to estimate jet-veto effects to the BSM production of a colour singlet. Including NNLL corrections, needed for a precise estimate of the corresponding SM background, is also possible in a general way. In fact, resummation effects originate from soft and/or collinear emissions in such a way that NNLL corrections share the same phase space with Born-level contributions, but are of relative order α_s. In all NLO calculations there is always a contribution that lives in the same phase space as the Born, and is of relative order α_s. This is the subtraction term that cancels the infrared singularities of virtual corrections. Therefore, to implement NNLL effects, we can just modify the appropriate subtraction term in the NLO event generator. Having done this, all other NNLL effects factorise, and can be accounted for by an event-by-event reweighting, so as to reproduce eq. (6.6). The whole procedure requires generating Born-level events only, and hence is much faster than a full NLO calculation.

In the following two sections we give a detailed description of this procedure for the specific case of BSM effects induced by the operator in eq. (6.1). In section 6.2, we study

the effect of such an operator on WW production with a jet veto. As discussed above, this operator induces a modification of the cross section of WW production through gluon fusion. We denote the (differential) cross section for gluon fusion, potentially including an additional BSM contribution, with $\mathrm{d}\sigma_{gg}$. The main result of this section is a recipe to compute cross sections for WW production with a jet veto at NLL accuracy, fully exclusive in the decay products of the W bosons. In section 6.3 we compute the cross section for the dominant contribution to the SM background, which is WW production via quark-antiquark annihilation, again in the presence of a jet veto. We denote the cross-section for this process with $\mathrm{d}\sigma_{q\bar{q}}$, and compute exclusive cross sections in the decay products of the W bosons, while resumming $\log(M_{WW}/p_{\mathrm{t,veto}})$ at NNLL accuracy. The main result of this section is a general recipe to modify a NLO event generator for the production of any colour singlet so that it produces resummed cross-section with a jet veto at NNLL accuracy. In section 6.4 we present some numerical results for a simplified model derived from the Lagrangian in eq. (6.1), corresponding to a realistic experimental setup. We compare our resummed predictions with parton-shower event generators, and assess the size of effects, such as limited detector acceptances, hadronisation and the underlying event, that are not included in our resummation. In section 6.5 we perform some basic sensitivity studies to investigate the exclusion potential of the HL-LHC for the parameters of the simplified model of section 6.4. Finally, section 6.6 presents our conclusions.

6.2 Gluon fusion (including BSM effects)

Let us first consider WW production via gluon fusion, possibly with a modification of the amplitude induced by the BSM operator in eq. (6.1). For simplicity, we consider here the decays $WW \to e^+\nu_e\mu^-\bar{\nu}_\mu$ and $WW \to e^-\bar{\nu}_e\mu^+\nu_\mu$. As explained in the introduction, if we impose that all jets have a transverse momentum below a threshold value $p_{\mathrm{t,veto}}$, the distribution in M_{WW}^2, differential in the phase space of the leptons, is affected by the presence of large logarithms $\log(M_{WW}/p_{\mathrm{t,veto}})$, that have to be resummed to all orders to obtain sensible theoretical predictions. Specifically, we consider jets obtained by applying the anti-k_t algorithm [37] with a given radius R. At NLL accuracy, the best we can achieve for gluon fusion, the aforementioned observable is given by [92, 93]

$$\frac{\mathrm{d}\sigma_{gg}^{\mathrm{NLL}}(p_{\mathrm{t,veto}})}{\mathrm{d}\Phi_{\mathrm{leptons}}\mathrm{d}M_{WW}^2} = \mathcal{L}_{gg}^{(0)}(L, M_{WW})\, e^{Lg_1(\alpha_s L)+g_2(\alpha_s L)}\,, \tag{6.7}$$

where $L = \log(M_{WW}/p_{\mathrm{t,veto}})$, $\alpha_s = \alpha_s(M_{WW})$, and explicit expressions for the functions $g_1(\alpha_s L)$ and $g_2(\alpha_s L)$ can be found, for instance, in ref. [93]. In particular, they are the

same for any colour singlet that is produced via gluon fusion (e.g. Higgs production). Note that, at NLL accuracy, the resummed distribution in eq. (6.7) does not depend on the radius R of the jets [92].

The phase space of the leptons is given by

$$\mathrm{d}\Phi_{\text{leptons}} = \frac{\mathrm{d}^3\vec{p}_e}{(2\pi)^3 2E_e}\frac{\mathrm{d}^3\vec{p}_{\nu_e}}{(2\pi)^3 2E_{\nu_e}}\frac{\mathrm{d}^3\vec{p}_\mu}{(2\pi)^3 2E_\mu}\frac{\mathrm{d}^3\vec{p}_{\nu_\mu}}{(2\pi)^3 2E_{\nu_\mu}}(2\pi)^4\delta\left(p_e + p_\mu + p_{\nu_e} + p_{\nu_\mu} - p_1 - p_2\right) , \tag{6.8}$$

with $p_\ell = (E_\ell, \vec{p}_\ell)$ is the four-momentum of lepton $\ell = e, \mu, \nu_e, \nu_\mu$, and $p_i = x_i P_i, i = 1, 2$ are the momenta of the incoming partons, carrying each a fraction x_i of the incoming proton momentum P_i.

Last, we have a process dependent "luminosity" factor $\mathcal{L}_{gg}^{(0)}$, given by[5]

$$\mathcal{L}_{gg}^{(0)}(L, M_{WW}) = \int \mathrm{d}x_1\mathrm{d}x_2\, |M_{\text{SM}}^{(gg)} + M_{\text{BSM}}^{(gg)}|^2\, \delta(x_1 x_2 s - M_{WW}^2)\times \\ \times\, f_g(x_1, p_{\text{t,veto}})\, f_g(x_2, p_{\text{t,veto}}) \, . \tag{6.9}$$

The two main ingredients entering $\mathcal{L}_{gg}^{(0)}$ are:

- the SM amplitude $M_{\text{SM}}^{(gg)}$ for the production of a WW pair (and its decay products) through gluon fusion, which can be supplemented with an additional contribution $M_{\text{BSM}}^{(gg)}$ accounting for BSM effects;

- the gluon density in the proton $f_g(x, \mu_F)$ at the factorisation scale $\mu_F = p_{\text{t,veto}}$. This value of μ_F reflects the fact that the factorisation scale is the highest scale up to which the considered observable is inclusive with respect to multiple collinear emissions from the initial-state partons. Since all collinear emissions with a transverse momentum above $p_{\text{t,veto}}$ are vetoed, the factorisation scale has to be $p_{\text{t,veto}}$ (see e.g. [3] for a formal derivation).

By comparing eq. (6.7) to eq. (6.6), $G_2(\alpha_s L)$ resumming all NLL contributions:

$$G_2(\alpha_s L) = \frac{\mathcal{L}_{gg}^{(0)}(L, M_{WW})}{\mathcal{L}_{gg}^{(0)}(0, M_{WW})}\, e^{g_2(\alpha_s L)} \, . \tag{6.10}$$

So far, with the exception of ref. [122], such resummations have been obtained by devising process-dependent codes that produce numerical results for $\mathcal{L}_{gg}^{(0)}(L, M_{WW})$. For

[5] Note that, since jet-veto measurements do not keep track of any correlation between the angle of the jet and the outgoing leptons, the logarithmically enhanced contributions due to the helicity of incoming gluons described in [132] are not present in our case, so eq. (6.9) is valid as is.

instance, the program `JetVHeto` [130] returns NNLL resummations integrated over the full phase space of the decay products of a Higgs or a Z boson. However, the luminosity in eq. (6.9) can be obtained by running any Born-level event generator. In fact, any such program will compute a Born-level cross-section in WW production via gluon fusion (possibly with BSM contributions) starting from the formula:

$$\frac{\mathrm{d}\sigma^{(0)}_{gg}}{\mathrm{d}\Phi_{\text{leptons}}\mathrm{d}M^2_{WW}} = \int \mathrm{d}x_1\mathrm{d}x_2\,|M^{(gg)}_{\text{SM}} + M^{(gg)}_{\text{BSM}}|^2\,\delta(x_1x_2s - M^2_{WW})\times \\ \times\, f_g(x_1,\mu_F)\,f_g(x_2,\mu_F) = \mathcal{L}^{(0)}_{gg}(0, M_{WW})\,, \quad (6.11)$$

where μ_F here is the default factorisation scale in the considered Born-level generator. Therefore, to obtain the differential distribution in eq. (6.7), it is enough to set that factorisation scale μ_F to $p_{\text{t,veto}}$, and multiply the weight of each phase-space point by $\exp[Lg_1(\alpha_sL) + g_2(\alpha_sL)]$. Note that, if the programs returns event files with information on M_{WW} for each event, or if one produces histograms binned in M_{WW}, the reweighting can be performed without any need to touch the Born-level generator code.

6.3 Quark-antiquark annihilation (SM only)

Since SM background processes are typically known at least to NLO, in the presence of a jet veto, the SM cross-section for WW production can be computed at NNLL accuracy. The corresponding NNLL resummed expression is given by

$$\frac{\mathrm{d}\sigma^{\text{NNLL}}_{q\bar{q}}(p_{\text{t,veto}})}{\mathrm{d}\Phi_{\text{leptons}}\mathrm{d}M^2_{WW}} = \left(\mathcal{L}^{(0)}_{q\bar{q}}(L, M_{WW}) + \mathcal{L}^{(1)}_{q\bar{q}}(L, M_{WW})\right)\times \\ \times\,(1 + \mathcal{F}_{\text{clust}}(R) + \mathcal{F}_{\text{correl}}(R))\times e^{Lg_1(\alpha_sL)+g_2(\alpha_sL)+\frac{\alpha_s}{\pi}g_3(\alpha_sL)}\,, \quad (6.12)$$

where again $L = \log(M_{WW}/p_{\text{t,veto}})$, $\alpha_s = \alpha_s(M_{WW})$, and $d\Phi_{\text{leptons}}$ is the lepton phase space defined in eq. (6.8). The functions g_1, g_2 and g_3 are reported in [93], and are the same as for Drell-Yan production. The dependence on the jet radius R appears for the first time at NNLL accuracy in the functions $\mathcal{F}_{\text{clust}}(R)$, $\mathcal{F}_{\text{correl}}(R)$, whose explicit expressions can be found in [92].

At NNLL accuracy we have two process-dependent "luminosities" $\mathcal{L}^{(0)}_{q\bar{q}}$ and $\mathcal{L}^{(1)}_{q\bar{q}}$. The luminosity $\mathcal{L}^{(0)}_{q\bar{q}}$ is the analogue of $\mathcal{L}^{(0)}_{gg}$ of eq. (6.9), this time for a $q\bar{q}$ initiated process:

$$\mathcal{L}^{(0)}_{q\bar{q}}(L, M_{WW}) = \sum_{i,j}\int \mathrm{d}x_1\mathrm{d}x_2|M^{(q\bar{q})}_{ij}|^2\delta(x_1x_2s - M^2_{WW})f_i(x_1, p_{\text{t,veto}})\,f_j(x_2, p_{\text{t,veto}})\,. \quad (6.13)$$

The only difference with respect to $\mathcal{L}^{(0)}_{gg}$ is the LO SM amplitude $M^{(q\bar{q})}_{ij}$, which is different from zero only if i, j is a quark-antiquark pair with the same flavour.

At NNLL accuracy we need to add the luminosity $\mathcal{L}^{(1)}_{q\bar{q}}$, which is of relative order α_s with respect to $\mathcal{L}^{(0)}_{q\bar{q}}$, and is given by

$$\mathcal{L}^{(1)}_{q\bar{q}}(L, M_{WW}) = \sum_{i,j} \int \mathrm{d}x_1 \mathrm{d}x_2 |M^{(q\bar{q})}_{ij}|^2 \delta(x_1 x_2 s - M^2_{WW}) \times \tag{6.14}$$

$$\times \left[f_i(x_1, p_{\mathrm{t,veto}})\, f_j(x_2, p_{\mathrm{t,veto}})\, \frac{\alpha_s(M_{WW})}{2\pi} \mathcal{H}^{(1)} + \right.$$

$$\left. \frac{\alpha_s(p_{\mathrm{t,veto}})}{2\pi} \sum_k \left(\int_{x_1}^1 \frac{\mathrm{d}z}{z} C^{(1)}_{ik}(z) f_k\Big(\frac{x_1}{z}, p_{\mathrm{t,veto}}\Big)\, f_j(x_2, p_{\mathrm{t,veto}}) + \{(x_1, i) \leftrightarrow (x_2, j)\} \right) \right]. \tag{6.15}$$

Here new ingredients appear:

- one-loop virtual corrections to WW production. They are included in the term $\mathcal{H}^{(1)}$, the coefficient of $\alpha_s(M_{WW})$;
- coefficient constants arising from real collinear radiation. They are included in the terms $C^{(1)}_{ik}(z)$, whose explicit expressions can be found in ref. [93], and are the same as for Drell-Yan production. They multiply $\alpha_s(p_{\mathrm{t,veto}})$, which reflects the fact that the characteristic scale of collinear radiation in jet-veto cross sections is $p_{\mathrm{t,veto}}$.

With reference to eq. (6.6), the function G_2 resumming NLL contributions is

$$G_2(\alpha_s L) = \frac{\mathcal{L}^{(0)}_{q\bar{q}}(L, M_{WW})}{\mathcal{L}^{(0)}_{q\bar{q}}(0, M_{WW})}\, e^{g_2(\alpha_s L)}\,, \tag{6.16}$$

whereas the function G_3 resumming NNLL contributions is

$$G_3(\alpha_s L) = \frac{e^{g_2(\alpha_s L)}}{\alpha_s \mathcal{L}^{(0)}_{q\bar{q}}(0, M_{WW})} \left[\mathcal{L}^{(1)}_{q\bar{q}}(L, M_{WW}) \right.$$

$$\left. + \mathcal{L}^{(0)}_{q\bar{q}}(L, M_{WW}) \left(\mathcal{F}_{\mathrm{clust}}(R) + \mathcal{F}_{\mathrm{correl}}(R) + \frac{\alpha_s}{\pi} g_3(\alpha_s L) \right) \right]. \tag{6.17}$$

As explained in the previous section, the function $\mathcal{L}^{(0)}_{q\bar{q}}$ can be obtained from an appropriate Born-level program. The function $\mathcal{L}^{(1)}_{q\bar{q}}$ instead represents a correction to $\mathcal{L}^{(0)}_{q\bar{q}}$ of relative order α_s, that cannot be obtained from a LO calculation. A viable possibility to perform NNLL resummation would be to modify eq. (6.9) so that it includes the convolutions over the variable z in eq. (6.14), and implement the modification in a Born-level generator. This is the approach taken in ref. [122], and in some way underlying the current implementation of the `JetVHeto` program [130]. Here we want to present an alternative

procedure. First, let us consider how the NLO WW cross section is calculated in a NLO event generator:

$$\frac{\mathrm{d}\sigma^{\mathrm{NLO}}_{q\bar{q}}(p_{\mathrm{t,veto}})}{\mathrm{d}\Phi_{\mathrm{leptons}}\mathrm{d}M^2_{WW}} = \frac{\mathrm{d}\sigma^{(0)}_{q\bar{q}}}{\mathrm{d}\Phi_{\mathrm{leptons}}\mathrm{d}M^2_{WW}} + \frac{\mathrm{d}\sigma^{(1)}_{q\bar{q},v+ct}}{\mathrm{d}\Phi_{\mathrm{leptons}}\mathrm{d}M^2_{WW}} + \frac{\mathrm{d}\sigma^{(1)}_{q\bar{q},r}}{\mathrm{d}\Phi_{\mathrm{leptons}}\mathrm{d}M^2_{WW}}\,. \tag{6.18}$$

The first term in the sum is the LO SM cross section $\mathrm{d}\sigma^{(0)}_{q\bar{q}}/\mathrm{d}\Phi_{\mathrm{leptons}}\mathrm{d}M^2_{WW} = \mathcal{L}^{(0)}_{q\bar{q}}(0, M_{WW})$. The last term, $\mathrm{d}\sigma^{(1)}_{q\bar{q},r}/\mathrm{d}\Phi_{\mathrm{leptons}}\mathrm{d}M^2_{WW}$, represents NLO corrections coming from the emission of an extra parton. They include the counterterms needed to ensure their finiteness in four space-time dimensions. The second term, $\mathrm{d}\sigma^{(1)}_{q\bar{q},v+ct}/\mathrm{d}\Phi_{\mathrm{leptons}}\mathrm{d}M^2_{WW}$, gives NLO corrections arising from the sum of virtual corrections, and the counterterms integrated over the full extra-parton phase space. This contribution lives in the same phase-space as the Born contribution, and is of relative order α_s. It has the form

$$\begin{aligned}\frac{\mathrm{d}\sigma^{(1)}_{q\bar{q},v+ct}}{\mathrm{d}\Phi_{\mathrm{leptons}}\mathrm{d}M^2_{WW}} = \frac{\alpha_s(\mu_R)}{2\pi}\sum_{i,j}\int \mathrm{d}x_1\mathrm{d}x_2 |M^{(q\bar{q})}_{ij}|^2 \delta(x_1x_2s - M^2_{WW})\Bigg[f_i(x_1,\mu_F)\, f_j(x_2,\mu_F)\,\tilde{\mathcal{H}}^{(1)} + \\ \sum_k\left(\int_{x_1}^1 \frac{\mathrm{d}z}{z}\tilde{C}^{(1)}_{ik}(z) f_k\Big(\frac{x_1}{z},\mu_F\Big) f_j(x_2,\mu_F) + \{(x_1,i) \leftrightarrow (x_2,j)\}\right)\Bigg]\,.\end{aligned} \tag{6.19}$$

In the above equation, μ_R, μ_F are the renormalisation and factorisation scales used by the NLO generator, $\tilde{\mathcal{H}}^{(1)}$ represents virtual corrections to $q\bar{q} \to WW$, and $\tilde{C}^{(1)}_{ik}(z)$ the integrated counterterms. The explicit expressions of $\tilde{\mathcal{H}}^{(1)}$ and $\tilde{C}^{(1)}_{ik}(z)$ depend on their actual implementation in the NLO generator, in particular on the employed subtraction scheme. However, the form of eq. (6.19) is the same as that of the NNLL luminosity $\mathcal{L}^{(1)}_{q\bar{q}}(L, M_{WW})$ in eq. (6.14). Therefore, by comparing eqs. (6.14) and (6.19), we find that $\mathcal{L}^{(1)}_{q\bar{q}}(L, M_{WW})$ can be implemented in a NLO event generator by performing the replacements

$$\begin{aligned}\frac{\alpha_s(\mu_R)}{2\pi}\tilde{\mathcal{H}}^{(1)} &\to \frac{\alpha_s(M_{WW})}{2\pi}\mathcal{H}^{(1)}\,,\\ \frac{\alpha_s(\mu_R)}{2\pi}\tilde{C}^{(1)}_{ik}(z) &\to \frac{\alpha_s(p_{\mathrm{t,veto}})}{2\pi}C^{(1)}_{ik}(z)\,,\end{aligned} \tag{6.20}$$

and by evaluating the parton distribution functions at the factorisation scale $\mu_F = p_{\mathrm{t,veto}}$. Finally, in order to obtain the resummed distribution in eq. (6.12), we need to reweight each phase space point by

$$(1 + \mathcal{F}_{\mathrm{clust}}(R) + \mathcal{F}_{\mathrm{correl}}(R))\, e^{Lg_1(\alpha_s L) + g_2(\alpha_s L) + \frac{\alpha_s}{\pi}g_3(\alpha_s L)}\,. \tag{6.21}$$

This rescaling can also be performed when constructing histograms, as long as one has access to M_{WW} for each bin, or for each event in an event record.

We have implemented this procedure in the code `MCFM-RE` [133], a suitable modification of the NLO program `MCFM` [134]. The actual implementation is richer than what has been discussed so far, because it allows a user to change the default renormalisation and factorisation scales, and contains additional features. Since these details are not relevant for a general discussion, we have omitted them here. The interested reader is referred to appendix D.1 for the actual formulae we implement, and to appendix D.2 for a short manual of the code.

In the following two sections, we use this implementation to produce numerical results and sensitivity studies for an explicit BSM model.

6.4 Numerical results

Let us discuss first our results for WW production via $q\bar{q}$ annihilation. We consider W pairs produced at the LHC with $\sqrt{s} = 13\,\text{TeV}$, specifically $W^+W^- \to e^+\nu_e\mu^-\bar{\nu}_\mu$ and $W^+W^- \to \mu^+\nu_\mu e^-\bar{\nu}_e$, and select the final state according to a simplified version of the experimental cuts of ref. [96], reported in table 6.1. Jets are reconstructed according to the anti-k_t algorithm [37] with a jet radius $R = 0.4$. In table 6.1 we encounter the newly

Fiducial selection requirement	Cut value
p_T^ℓ	$> 25\,\text{GeV}$
$\lvert y_\ell \rvert$	< 2.5
$M_{e\mu}$	$> 10\,\text{GeV}$
Number of jets with $p_T > 30\,\text{GeV}$	0
$\not{E}_{\text{T,Rel}}$	$> 15\,\text{GeV}$
$\not{E}_{\text{T}}$	$> 20\,\text{GeV}$

Table 6.1: Definition of the $WW \to e\mu$ fiducial phase space, where p_T^ℓ, y_ℓ are the transverse momentum and rapidity of either an electron or a muon, $M_{e\mu}$ is the invariant mass of the electron-muon pair, $\not{E}_{\text{T}}$ is the missing transverse energy, and $\not{E}_{\text{T,Rel}}$ is defined in eq. (6.22).

introduced observable $\not{E}_{\text{T,Rel}}$, which is defined as follows [135]:

$$\not{E}_{\text{T,Rel}} = \begin{cases} \not{E}_{\text{T}} \sin\Delta\phi\,, & \text{if } \Delta\phi \leq \frac{\pi}{2} \\ \not{E}_{\text{T}}\,, & \text{if } \Delta\phi > \frac{\pi}{2} \end{cases} \tag{6.22}$$

with $\Delta\phi = \min\left(|\phi_e - \phi_{\text{MET}}|, |\phi_\mu - \phi_{\text{MET}}|\right)$, and ϕ_e, ϕ_μ and ϕ_{MET} the azimuthal angle of the electron, the muon and the missing transverse energy respectively.

In our analysis, we omit b quark-initiated contributions to $pp \to WW$. At LO, the $b\bar{b}$ scattering subprocess contributes only 1% to the cross section. The gb and $g\bar{b}$ subprocesses, which enter at NLO QCD increase the NLO cross section by a factor 1.5. This large increase is due to graphs like $gb \to W^-(t \to W^+b)$. Such graphs feature a resonant top quark propagator, which effects an enhancement of $\mathcal{O}(m_t/\Gamma_t) = \mathcal{O}(10^2)$, which compensates the $\mathcal{O}(1\%)$ suppression due to the b PDF, and altogether an $\mathcal{O}(1)$ contribution is obtained. This contribution is commonly attributed to Wt production and decay (at LO QCD) [136], and hence has to be omitted in the NLO QCD corrections to WW production, which we consider here. We note that this treatment is somewhat ad-hoc, the most consistent way to perform this calculation would be to use the four-flavour scheme, where there are only four massless flavours of quark. In such a scheme the resonant top diagrams are explicitly absent at this order in perturbation theory. However `MCFM` makes use of the five-flavour scheme for di-boson production leading to the above prescription.

We now produce both NLO, NNLL resummed, and matched NLO+NNLL (with the matching procedure explained in appendix D.1.3) predictions for the differential distribution $\mathrm{d}\sigma/\mathrm{d}M_{WW}$ using `PDF4LHC15` parton distribution functions (PDFs) at NLO [137], accessed through `LHAPDF6` [138], corresponding to $\alpha_s(M_Z) = 0.118$, and we set both renormalisation and factorisation scales at $M_{WW}/2$, as customary in Higgs precision studies [139]. We note that the observable $\mathrm{d}\sigma/\mathrm{d}M_{WW}$ is of theoretical interest only, because we do not have access to the momenta of the neutrinos. We will consider related observables that are experimentally accessible after our discussion of M_{WW}. Fig. 6.1 shows the differential cross section in the invariant mass M_{WW} of the WW pair. We first note that both NLO and NNLL+NLO are both smaller than the LO, as expected due to the presence of a jet veto, with the suppression with respect to LO increasing with M_{WW}. This implies that, in this situation, a naive Born-level calculation fails to capture this effect and that, in the absence of a resummation, one should use at least a NLO prediction. NNLL+NLO gives a mild extra suppression with respect to NLO, revealing that logarithms are not particularly large in the considered kinematical region. However, we note that the difference between pure NNLL resummed and matched NNLL+NLO (the so-called "remainder"), which contains the part of the NLO which is not enhanced by logarithms, is basically negligible. This means that the resummation alone is very close to the best prediction we have at this order. This is remarkable in view of the fact that to obtain NNLL predictions we need to perform a calculation with Born-level kinematics. On the contrary, the computational cost of the NLO calculation is larger due to the presence of an extra emission,

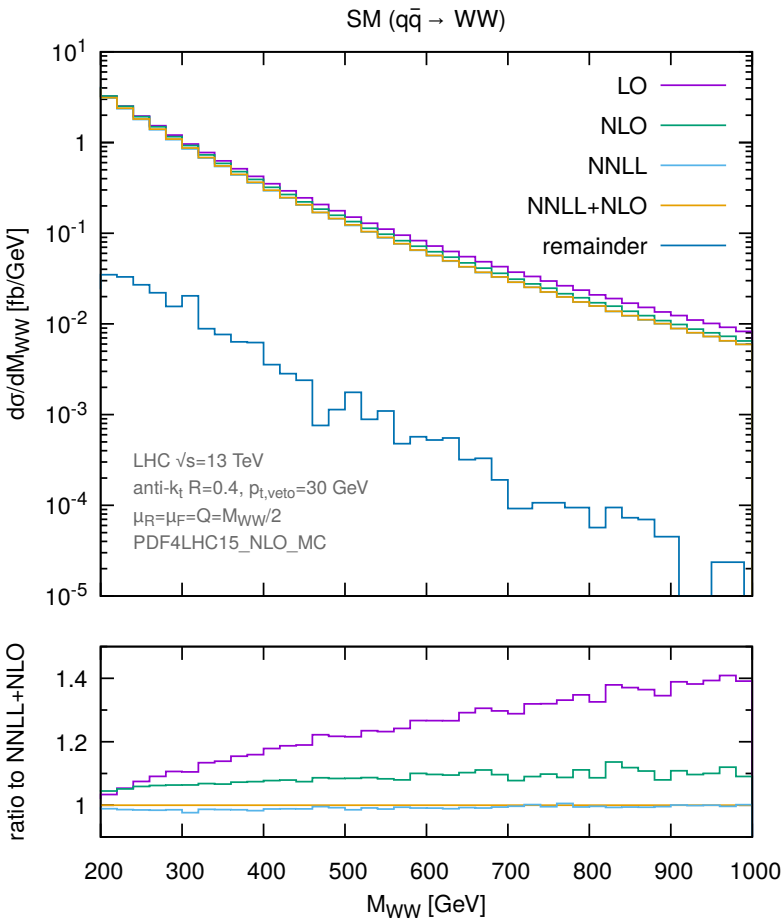

Figure 6.1: The differential distribution $\mathrm{d}\sigma/\mathrm{d}M_{WW}$ in the Standard Model, computed at different accuracies, and for the cuts described in the main text.

without any significant gain in accuracy compared to the NNLL prediction.

To complete our discussion of the $q\bar{q}$ channel, we compare our predictions to those obtained from SCET via the program `aMC@NLO-SCET` of ref. [122]. The comparison is shown in Fig. 6.2. Our results contains theoretical uncertainties evaluated both with the

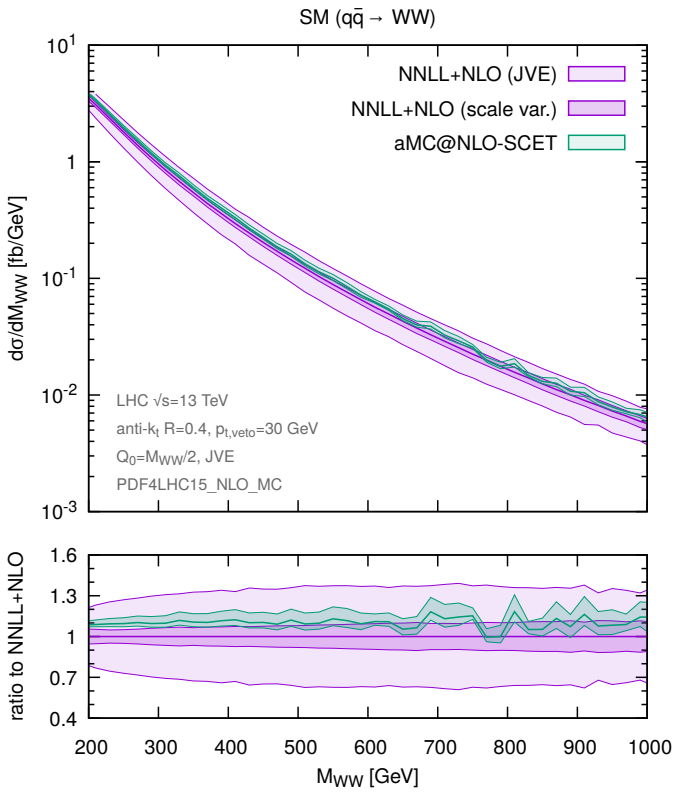

Figure 6.2: The differential distribution $\mathrm{d}\sigma/\mathrm{d}M_{WW}$ in the Standard Model, computed with our method, and with the program `aMC@NLO-SCET` [122]. See the main text for details.

most recent jet-veto efficiency (JVE) method [140] at the relevant accuracy (the wider, lighter band), and pure scale variations (the tighter, darker band). The details of both prescriptions can be found in appendix D.1. The SCET prediction corresponds to the default scale choices, and is at the boundary of scale variation uncertainties and well within JVE uncertainties. We remark that we do not expect perfect agreement, because, although both methods share the same formal accuracy, they differ in the treatment of subleading effects.

A last comment on uncertainties is in order here. Within `MCFM`, we do not have access to NNLO calculations for di-boson production, so we cannot match our resummed predictions to NNLO. As a result of this, the JVE method may be overly conservative, due to the largish (~ 1.5) K-factor of the WW inclusive total cross-section, which propagates in the evaluation of the uncertainty according to the JVE method. If we were to match to NNLO,

the JVE uncertainty would be reduced, and, as happens for Higgs production [93], would probably be much closer to plain scale uncertainties.

In order to have a specific example of a BSM theory that implements the effective operator of eq. (6.1), we consider the following modification of the SM Lagrangian [141]:

$$\mathcal{L} \supset -\kappa_t \frac{m_t}{v} h\bar{t}t + \kappa_g \frac{\alpha_s}{12\pi}\frac{h}{v} G^a_{\mu\nu} G_a^{\mu\nu} \,, \tag{6.23}$$

with t, h, $G^a_{\mu\nu}$ the top field, the SM Higgs field, and the gluon field strength respectively. The SM corresponds to $(\kappa_t, \kappa_g) = (1, 0)$, and in this section we will only explore BSM scenarios such that $\kappa_t + \kappa_g = 1$, which ensures that the Higgs total cross section stays unchanged (modulo quark-mass effects, which give a correction of a few percent [140]). Such modifications of the SM Lagrangian has only an appreciable affect the gluon-fusion contribution to di-boson production. Their effect has been investigated before for the case of ZZ production [116], where one does not need to impose a jet veto to suppress unwanted background. Here we wish to study how the presence of a jet veto, required for studies of WW production, affects the relative size of a BSM contribution with respect to the SM background. We consider the three benchmark scenarios studied in ref. [116], i.e.

$$(\kappa_t, \kappa_g)_{\rm SM} = (1, 0)\,, \quad (\kappa_t, \kappa_g)_{\rm BSM_1} = (0.7, 0.3)\,, \quad (\kappa_t, \kappa_g)_{\rm BSM_2} = (0, 1)\,. \tag{6.24}$$

First, in Fig. 6.3 we compare the loop-induced gluon fusion contribution to the M_{WW} distribution at LO, which is what is given by default by any automated Born-level event generator, with the NLL analytic resummation, which gives the best modelling of jet-veto effects at the currently available accuracy. Our best $q\bar{q}$ prediction is also shown for comparison. We see that, if we include resummation effects, the cross section for each

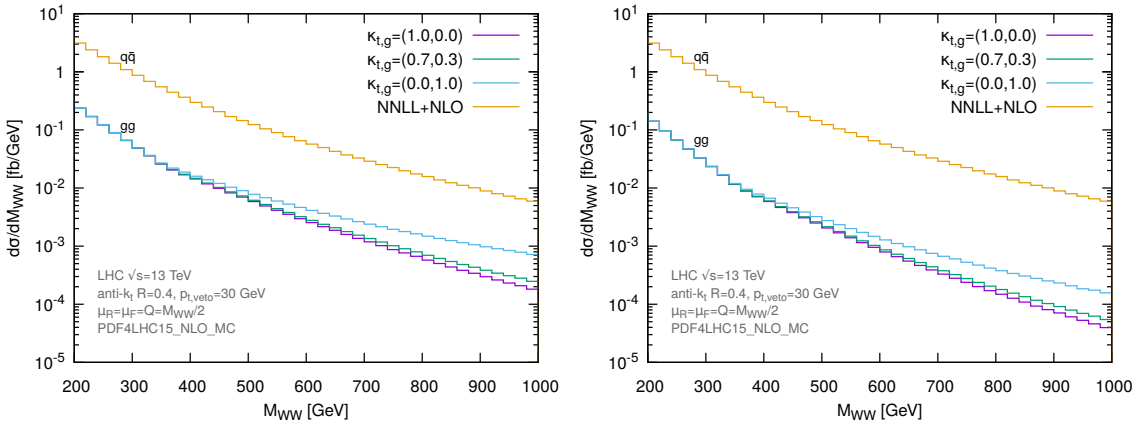

Figure 6.3: The differential cross section $\mathrm{d}\sigma/\mathrm{d}M_{WW}$ for the three benchmark scenarios of eq. (6.24), at LO (left) and at NLL (right) accuracy.

benchmark point is reduced by almost an order of magnitude in the tail of the distribution, where BSM effects start to become important. We then investigate more quantitatively how this impacts the deviations we might observe with respect to the SM, by plotting the quantity

$$\delta(M_{WW}) = \frac{\mathrm{d}\sigma_{gg}^{\mathrm{BSM}}/\mathrm{d}M_{WW} - \mathrm{d}\sigma_{gg}^{\mathrm{SM}}/\mathrm{d}M_{WW}}{\mathrm{d}\sigma_{q\bar{q}}/\mathrm{d}M_{WW}} \,. \tag{6.25}$$

In the above equation, $\mathrm{d}\sigma_{gg}^{\mathrm{BSM}}$ is computed according to eq. (6.7), $\mathrm{d}\sigma_{gg}^{\mathrm{SM}}$ differs from $\mathrm{d}\sigma_{gg}^{\mathrm{BSM}}$ by the fact that the BSM contribution to the amplitude (M_{gg}^{BSM} in eq. (6.9)) is set to zero, and $\mathrm{d}\sigma_{q\bar{q}}$ follows from eq. (6.12). Fig. 6.4 (left) shows $\delta(M_{WW})$ for the benchmark point $(0.7, 0.3)$. We first note the growth of this quantity with energy, as expected from the effective nature of the ggH vertex. Fortunately, the growth persists after including jet-veto effects through NLL resummation, however the deviation from the SM reduces from the 1% that one would obtain using fixed-order calculations (see fig. 6.3) to fractions of a percent. The same quantity shown in the right panel of fig. 6.4 for the benchmark point $(0.0, 1.0)$ displays qualitatively the same behaviour, although the deviation is a factor ten bigger. We see that, in the presence of jet-veto restrictions such as the one in the ATLAS cuts [96], one is bound to use a theoretical tool that resums large logarithms. This could be either resummed predictions, or simulations with parton-shower event generators. We will first consider resummed predictions and then the predictions of parton-shower event generators.

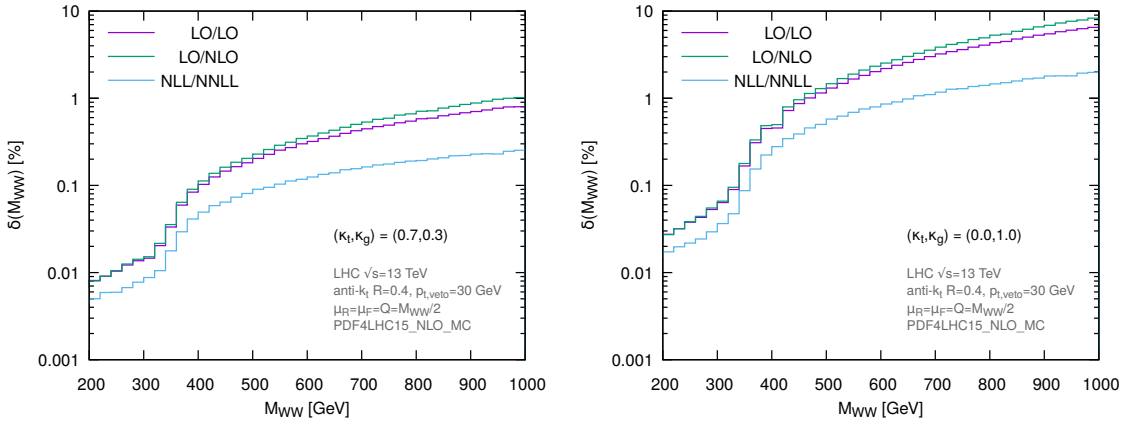

Figure 6.4: The relative difference between BSM and SM $\mathrm{d}\sigma/\mathrm{d}M_{WW}$ defined in eq. (6.25) for the two benchmark scenarios $(\kappa_t, \kappa_g)_{\mathrm{BSM}_1}$ (left) and $(\kappa_t, \kappa_g)_{\mathrm{BSM}_2}$ (right). The labels refer to the accuracy employed in the calculation of numerator and denominator in eq. (6.25).

The variable $\delta(M_{WW})$ is of theoretical interest only, because, as mentioned above, we

do not have access to the momenta of the neutrinos. To have experimentally accessible observables, we consider differential distributions in M_{T1} [142], M_{T2} [143] and M_{T3} [142], three measurable variables that are strongly correlated with M_{WW}

$$M_{T1} = \sqrt{(M_{\mathrm{T,e}\mu} + \not{p}_{\mathrm{T}})^2 - (\vec{p}_{\mathrm{T,e}\mu} + \vec{\not{p}}_{\mathrm{T}})^2}\,, \quad M_{\mathrm{T,e}\mu} = \sqrt{p^2_{\mathrm{T,e}\mu} + M^2_{e\mu}}\,, \tag{6.26a}$$

$$M_{T2} = \sqrt{2p_{\mathrm{T,e}\mu}\not{p}_{\mathrm{T}}(1 - \cos\Delta\phi_{e\mu,\mathrm{miss}})}\,, \tag{6.26b}$$

$$M_{T3} = \sqrt{(M_{\mathrm{T,e}\mu} + \not{M}_{\mathrm{T}})^2 - (\vec{p}_{\mathrm{T,e}\mu} + \vec{\not{p}}_{\mathrm{T}})^2}\,, \quad \not{M}_{\mathrm{T}} = \sqrt{\not{p}^2_{\mathrm{T}} + M^2_{e\mu}}\,. \tag{6.26c}$$

In the above equations, $\vec{p}_{\mathrm{T,e}\mu} = \vec{p}_{T,e} + \vec{p}_{T,\mu}$, and $M^2_{e\mu} = (p_e + p_\mu)^2$. The vector $\vec{\not{p}}_{\mathrm{T}}$ is the missing transverse momentum, defined as minus the vector sum of all detectable particles. Note that, if no jets are present, as at Born-level and in NNLL resummed predictions, $\vec{\not{p}}_{\mathrm{T}} = -\vec{p}_{\mathrm{T,e}\mu}$. Last, $\Delta\phi_{e\mu,\mathrm{miss}}$ is the azimuthal angle between $\vec{p}_{\mathrm{T,e}\mu}$ and $\vec{\not{p}}_{\mathrm{T}}$. The corresponding results for δ are shown in Fig. 6.5. We note that M_{T2} gives rise to

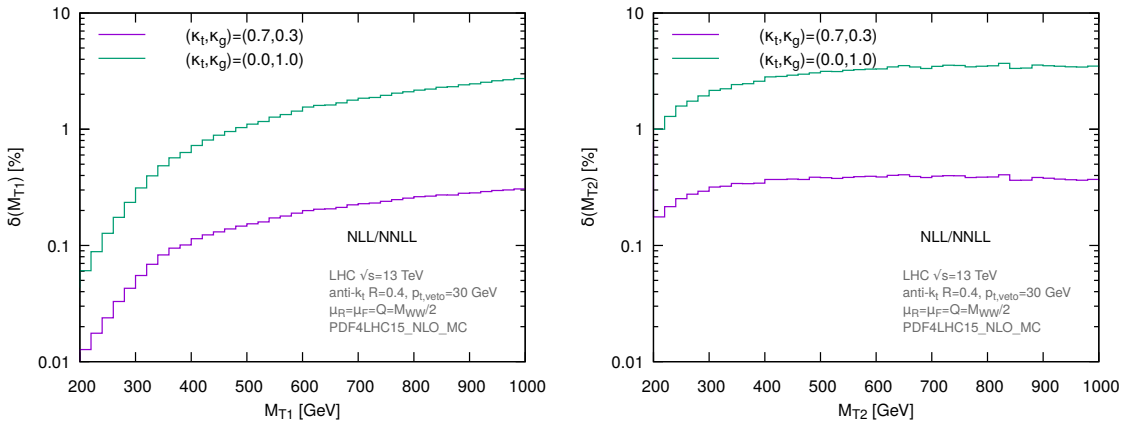

Figure 6.5: The relative difference between BSM and Standard Model WW production, differential in M_{T1} (left) and M_{T2} (right).

considerably larger deviations with respect to M_{T1}. This is because low values of M_{T2} are correlated to larger values of M_{WW}, so M_{T2} effectively probes the M_{WW} distribution in the high-mass tail, where BSM effects are appreciable. However, this also means that the differential cross section in M_{T2} is much smaller than that in M_{T1}, as can be seen from Fig. 6.6. Therefore, the discriminatory power of M_{T2} is only of use if we have a very large number of events. We have also studied the variable M_{T3} defined again in ref. [143] and first devised in ref. [144]. The distribution in this variable looks very similar to that of $2M_{T1}$, so the same discussion as for M_{T1} applies here.

We now compare our results to parton-level predictions from parton-shower event generators, using existing tunes. In particular, for $q\bar{q}$ we consider `POWHEG` [145–148]

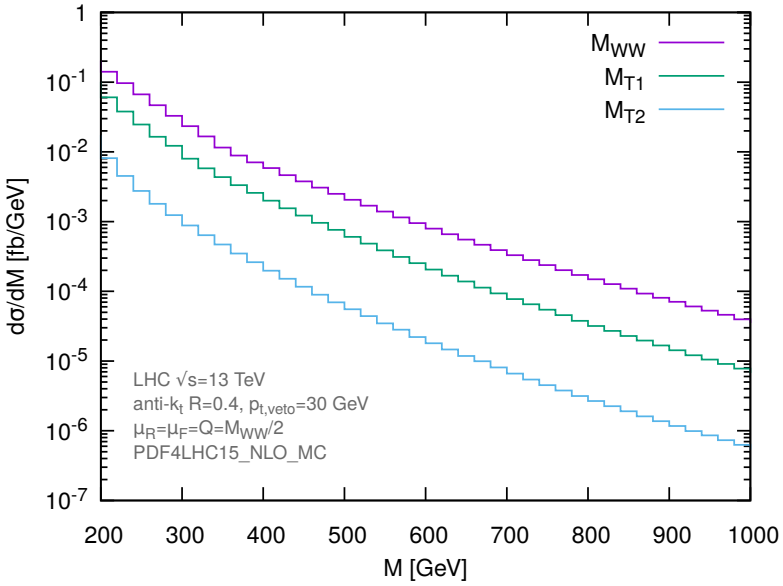

Figure 6.6: The distributions in $M = M_{WW}, M_{T1}, M_{T2}$ for the gg incoming channel.

matched to the `AZNLO` [127] tune of `PYTHIA v8.230` [149], and `aMC@NLO` [150–154] matched to `PYTHIA`, this time with the default parameters. To investigate the dependence on the shower algorithm, we also consider the parton shower `HERWIG v7.1.0` [155, 156] matched as `POWHEG+HERWIG`, and `aMC@NLO+HERWIG`, both with the default parameters. For `POWHEG+PYTHIA`, we use the PDF set by the `AZNLO` tune, i.e. `CT10` [157] for `POWHEG` and `CTEQ6L1` [158] for the parton shower. For consistency, we use `CT10` everywhere for `POWHEG+HERWIG`. For `POWHEG+HERWIG`, we also performed runs with default shower PDFs, and noted no significance difference in the resulting distributions. For all the `aMC@NLO` runs we use `PDF4LHC15` PDFs, both for the generation of the hard configurations and the shower.

The comparison of resummation with event generators is shown in Fig. 6.7 for the SM (for $q\bar{q} \to WW$ and $gg \to WW$ separately), and in Fig. 6.8 for the two BSM scenarios considered above. Resummed predictions include an estimate of theory uncertainties at the appropriate accuracy, as explained in appendix D.1.3. Note that, due to the missing NLO total cross-section for the incoming gg channel, JVE and scale uncertainties for $gg \to WW$ are of comparable size, with the JVE ones slightly larger. We first observe that, both for $q\bar{q}$- and for gg-initiated WW production, all event generators agree with the resummation within its uncertainties. For $q\bar{q}$, where we can match parton-shower predictions to NLO, `POWHEG+PYTHIA` shows a remarkable agreement with the resummation, but other event generators give comparable results. We note that predictions obtained with `aMC@NLO` show a slightly different trend with M_{WW}. In particular `aMC@NLO+PYTHIA` is slightly above our

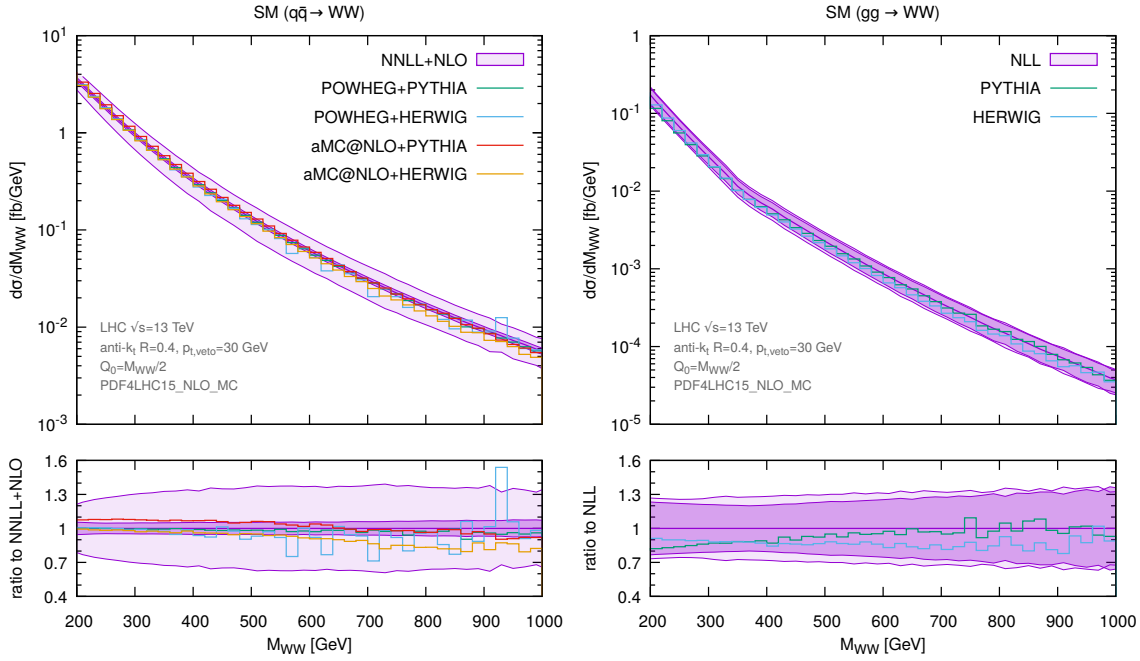

Figure 6.7: Analytical predictions for the SM distribution in the invariant mass of a WW pair, compared to results from various parton-shower event generators, corresponding to the details given in the main text.

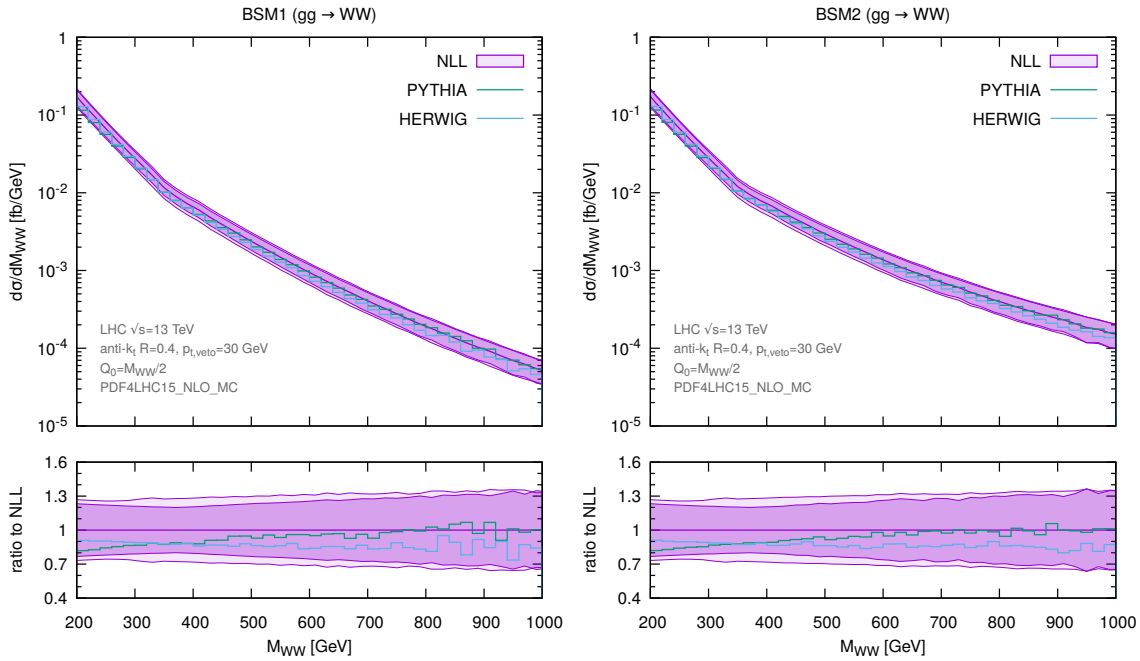

Figure 6.8: The same distribution as in Fig. 6.7 for the two BSM scenarios considered in the main text.

central prediction at low M_{WW}, and a bit lower at high M_{WW}, whereas aMC@NLO+HERWIG shows the same trend but is everywhere lower than our predictions.

In the gg case, both for the SM and the considered BSM scenarios, we can only compare to unmatched parton-showers results, as no NLO calculation is available. We observe that PYTHIA is in better agreement with our predictions at large values of M_{WW}, whereas HERWIG's predictions have the same shape as ours, but are systematically lower by about 10%. Overall, there is agreement between our predictions and parton showers within uncertainty bands, so the latter can be reliably used for this process. We remark that parton-shower predictions not only have lower formal accuracy, but are also much more expensive computationally. Hence it might be lengthy to assess with those tools if a range of BSM parameters leads to sizeable deviations from the SM, whereas with our numerical implementation such analyses could be performed at the cost of an unshowered Born-level calculation.

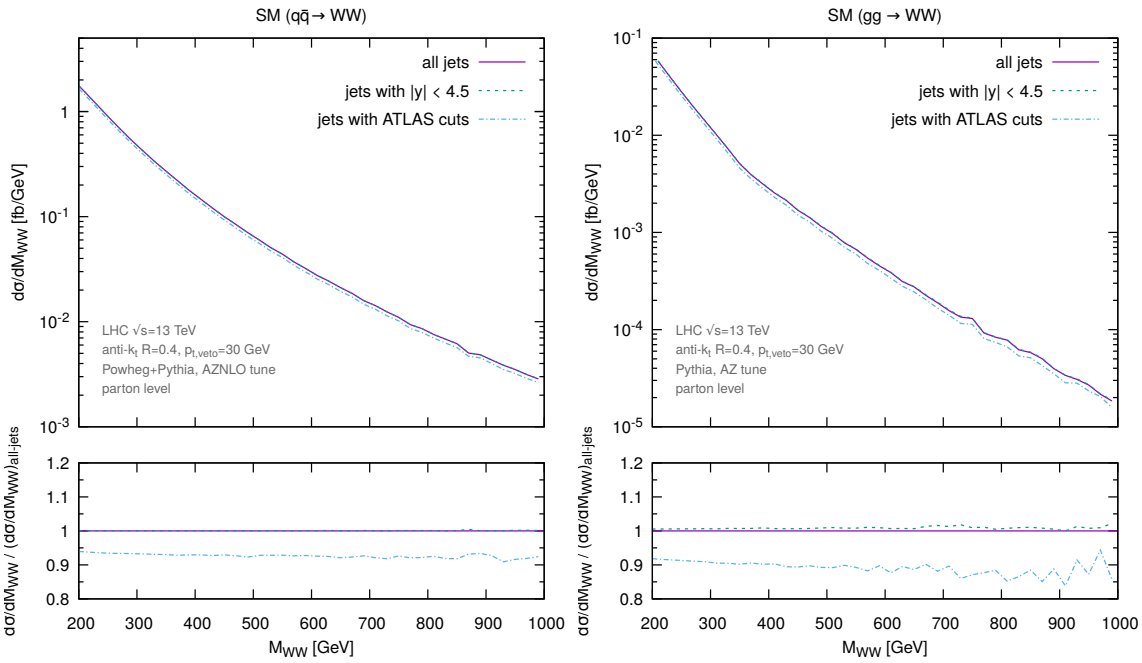

Figure 6.9: Impact of different cuts on the jets on $\mathrm{d}\sigma/\mathrm{d}M_{WW}$ in the SM for $q\bar{q}$ (left) modelled with POWHEG+PYTHIA and gg (right) modelled with plain PYTHIA.

We now investigate the impact of actual ATLAS cuts on the jets with respect to the simplified cuts in table 6.1. First, ATLAS vetoes only jets with $|y| < 4.5$. This does not cause problems for our resummed calculation because, according to the arguments in ref. [159], it just limits its validity to the range $\log(M_{WW}/p_{\mathrm{t,veto}}) < 4.5$, which is within the region we consider. However, ATLAS employs an additional cut on the jets, vetoing

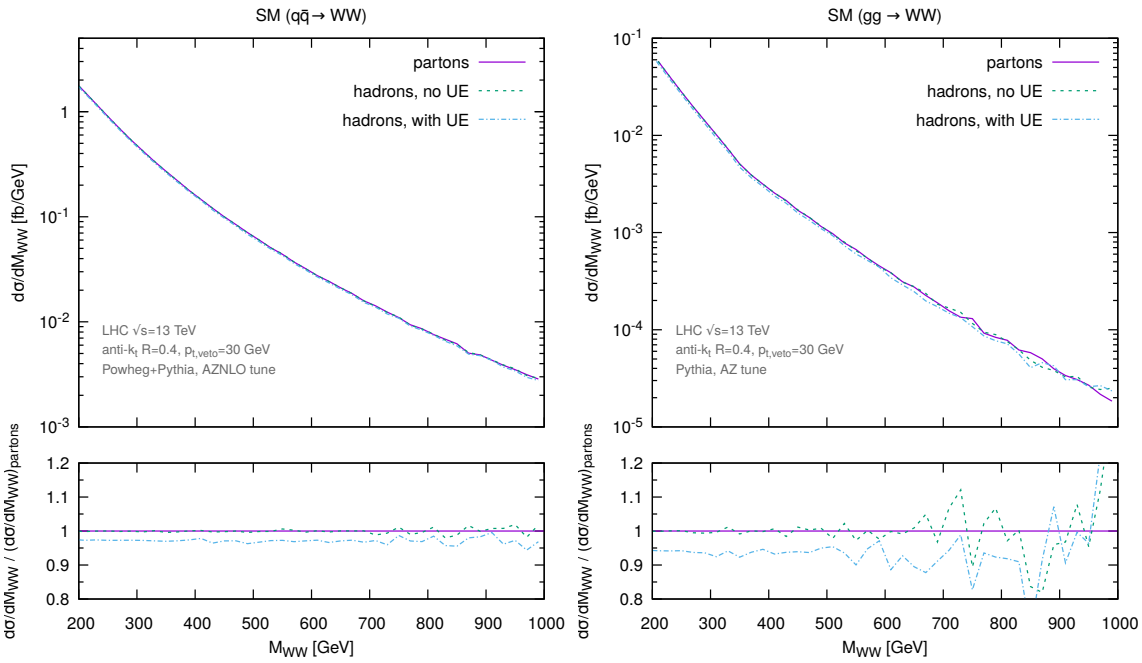

Figure 6.10: Impact of hadronisation and underlying event on $\mathrm{d}\sigma/\mathrm{d}M_{WW}$ in the SM for $q\bar{q}$ (left) modelled with `POWHEG+PYTHIA` and gg (right) modelled with plain `PYTHIA`. The fluctuations in the right plot are due to statistical uncertainties in the Monte Carlo samples.

also jets with $p_T > 25\,\text{GeV}$ and $|y| < 2.5$. If we compute $\mathrm{d}\sigma/\mathrm{d}M_{WW}$ with the cuts in table 6.1, we miss a contribution of order $\exp[-C(\alpha_s/\pi)\Delta y \log(30\,\text{GeV}/25\,\text{GeV})]$[6], with $C = C_F$ or $C = C_A$ according to whether we have quarks or gluons in the initial state and Δy the size of rapidity region in which the jet veto cuts differ, in this case $\Delta y = 5$. This contribution is formally NNLL, because the rapidity region where ATLAS applies a more stringent jet-veto cut does not increase with increasing M_{WW}, for fixed $p_{\text{t,veto}}$. Last, the definition of $\not{E}_{\text{T,Rel}}$ used to define the cuts in table 6.1 considers only leptons, whereas ATLAS considers all reconstructed particles, including jets. This leads to small NNLL corrections that depend on the area in the y-ϕ plane occupied by the rejected jets. We study these effects using parton-shower event generators. In particular, in fig. 6.9 we assess the impact of different cuts on the jets on $\mathrm{d}\sigma/\mathrm{d}M_{WW}$, using parton shower event generators at parton level, in particular we use `POWHEG+PYTHIA` for $q\bar{q}$ and plain `PYTHIA` for gg. We observe that the rapidity cut $|y| < 4.5$ has essentially no effect. On the contrary, implementing the full ATLAS cuts gives a sizeable but constant extra suppression. This is reasonable given that the jet veto cut imposed by ATLAS in the central region $|y| < 2.5$ is tighter than the one corresponding to our simplified cuts. Although the contribution we miss is formally NNLL, for the values of M_{WW} we consider here, the rapidity region in which $p_{\text{t,veto}} = 25\,\text{GeV}$ is larger than that where $p_{\text{t,veto}} = 30\,\text{GeV}$. Therefore, using our simplified cuts to mimic the ATLAS cuts we miss a potentially large contribution. In the case of gg, the suppression is larger with respect to $q\bar{q}$ due to the larger colour factor of the initial-state gluons with respect to the quarks.

Last, in fig. 6.10 we investigate the impact on $\mathrm{d}\sigma/\mathrm{d}M_{WW}$ of non-perturbative corrections due to hadronisation and underlying event, using parton shower event generators. Again we make use of `POWHEG+PYTHIA` for $q\bar{q}$ and plain `PYTHIA` for gg. We observe that hadronisation corrections are essentially negligible, which is expected since they scale like inverse powers of the hard scale, in this case M_{WW}. Corrections arising from the underlying event are a few percent, smaller than the typical theoretical uncertainties of our predictions.

To summarise, the effect with the greatest impact is the different jet-veto procedure employed by ATLAS. This could be modelled more accurately, either by making use of an effective $p_{\text{t,veto}}$, or even better by performing a resummation of jet-veto effects with rapidity cuts, as done in [161]. Both improvements are beyond the scope of the present work.

[6] This naive estimate neglects the so-called non-global logarithms [160].

6.5 Sensitivity studies

In this section, we compare the sensitivity of WW and ZZ production at HL-LHC ($\sqrt{s} = 14\,\text{TeV}$, with $3\,\text{ab}^{-1}$ of integrated luminosity) to the BSM operator considered in eq. (6.1). Here we consider only the decay $ZZ \to e^+e^-\mu^+\mu^-$. First we present the best predictions that could be obtained with the theoretical tools considered here, for a given choice of observables for the two processes. For WW we choose M_{T1} in eq. (6.26a), and our best prediction is NNLL for $q\bar{q} \to WW$ and NLL for $gg \to WW$. For ZZ we consider M_{ZZ}, and our best prediction is NLO for $q\bar{q} \to ZZ$ and LO for $gg \to ZZ$. Note that the accuracy of the predictions for $q\bar{q}$ annihilation for both WW and ZZ production can be improved to include the most recent NNLO calculations of refs. [162–166]. For gluon fusion, full NLO corrections have yet to be calculated, although approximate results are available [167–173] [7]. While the inclusion of NNLO corrections to ZZ is straightforward, and can be obtained by running the code `MATRIX` [163, 164, 166, 174–176], the use of NNLO corrections to WW requires matching of fixed-order predictions to the NNLL resummation. Although this can be achieved by interfacing the NNLL resummation to `MATRIX`, it is technically more involved than the simple procedure described in section 6.3. Therefore, we leave matching to NNLO to future work. The differential distributions in M_{T1} and M_{ZZ} are shown in figure 6.11. We observe that, in the $q\bar{q}$ channel, the cross section $\mathrm{d}\sigma/\mathrm{d}M_{T1}$ with a jet-veto

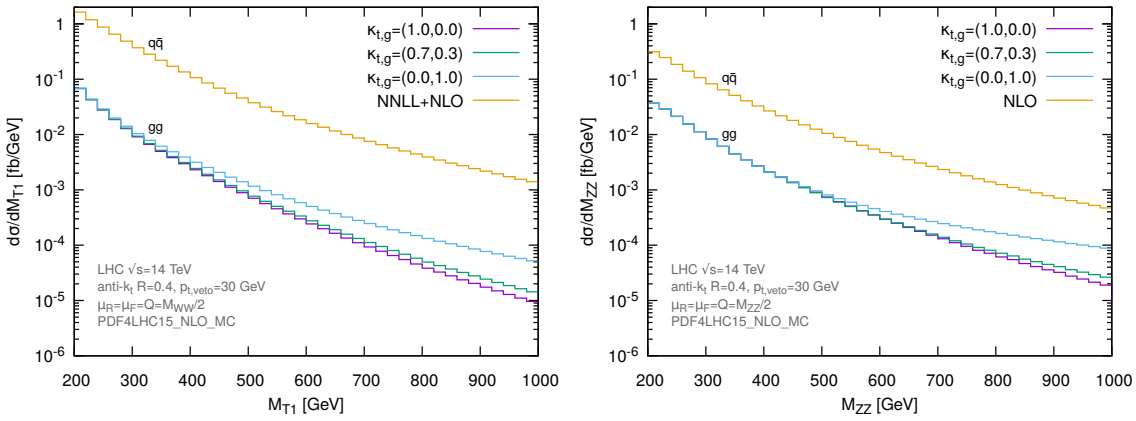

Figure 6.11: Our best predictions for the differential distributions $\mathrm{d}\sigma/\mathrm{d}M_{T1}$ for WW production with the experimental cuts in table 6.1 (left) and $\mathrm{d}\sigma/\mathrm{d}M_{ZZ}$ for ZZ production with the cuts in ref. [177] (right) for $q\bar{q}$ and gg processes.

[7] The two-loop diagrams with internal masses have not yet been calculated. Thus the contribution of third generation quarks to the $gg \to W^+W^-$ matrix element must either be neglected or approximated by another massless generation.

is comparable to the cross section $\mathrm{d}\sigma/\mathrm{d}M_{ZZ}$ where no jet veto is applied. We note that, even with a jet veto, the $q\bar{q}$ background is much larger in the WW case. Therefore, we naively expect WW to perform slightly worse than ZZ for exclusion of BSM effects.

To be more quantitative, we generate exclusion plots for a range of values of the parameters κ_t and κ_g entering the Lagrangian of eq. (6.23). To do this we ask ourselves how likely it is that predictions corresponding to different values of (κ_t, κ_g) are compatible with data that agree with the SM. Quantitatively, given a value of (κ_t, κ_g), we compute $n_i(\kappa_t, \kappa_g)$, the expected number of events in bin i of the distribution in a suitable leptonic observable. Specifically, we choose M_{T1} for WW production and M_{ZZ} for ZZ. Given a set of data points $\{n_i\}_{i=1,\ldots,N}$, and a given value of (κ_t, κ_g), we define

$$\chi^2(\kappa_t, \kappa_g) \equiv \sum_i \frac{(n_i(\kappa_t, \kappa_g) - n_i)^2}{n_i}\,, \tag{6.27}$$

and from that we construct our test statistic

$$\Delta\chi^2(\kappa_t, \kappa_g) \equiv \chi^2(\kappa_t, \kappa_g) - \chi^2(\hat{\kappa}_t, \hat{\kappa}_g)\,, \tag{6.28}$$

where $(\hat{\kappa}_t, \hat{\kappa}_g)$ are the values of (κ_t, κ_g) that minimise $\chi^2(\kappa_t, \kappa_g)$. This test statistic is a good approximation to the usual log-likelihood ratio for counting experiments [70] in the limit of a large number of events, and in the assumption that there are no correlations between bins. Assuming $n_i(\kappa_t, \kappa_g)$ is the expected number of events, in the denominator of eq. (6.27) we can approximate $n_i \simeq n_i(\kappa_t, \kappa_g)$. Therefore, $\Delta\chi^2(\kappa_t, \kappa_g)$ is asymptotically distributed according to a chi-squared distribution with two degrees of freedom (see e.g. [178]), which we denote by $f(\Delta\chi^2(\kappa_t, \kappa_g) \mid \kappa_t, \kappa_g)$.

We now consider data $\{n_i\}_{i=1,\ldots,N}$ generated in such a way that the expected number of events in each bin is the "central" SM prediction, corresponding to $\mu_R = \mu_F = Q = M_{WW}/2$ for WW and $\mu_R = \mu_F = M_{ZZ}/2$ for ZZ, which we denote with $\bar{n}_i(1, 0)$. This constitutes our "background-only" hypothesis. We now set exclusion limits in the (κ_t, κ_g) plane using the median significance [70, 179], assuming those data, with which one reject the hypothesis corresponding to each value of (κ_t, κ_g) (our "signal" hypothesis). More precisely, for each value of (κ_t, κ_g), we construct the distribution in $\Delta\chi^2(\kappa_t, \kappa_g)$ under the assumption of the background-only hypothesis, which we denote by $f(\Delta\chi^2(\kappa_t, \kappa_g) \mid 1, 0)$. We then compute the median of that distribution, which we denote with $\Delta\chi^2_{\text{med}}(\kappa_t, \kappa_g)$. The p-value for each (κ_t, κ_g) is given by

$$p(\kappa_t, \kappa_g) = \int_{\Delta\chi^2_{\text{med}}(\kappa_t,\kappa_g)}^{\infty} f(\Delta\chi^2 \mid \kappa_t, \kappa_g)\, \mathrm{d}\big(\Delta\chi^2\big)\,, \tag{6.29}$$

and we exclude at the 95% confidence level all (κ_t, κ_g) such that $p(\kappa_t, \kappa_g) < 0.05$. In practice, we have binned the variables M_{T1} and M_{ZZ} in such a way that, when computing

$\Delta\chi^2_{\rm med}(\kappa_t,\kappa_g)$, in the denominator of eq. (6.27) we can always approximate n_i with $\bar{n}_i^{q\bar{q}}$, the number of events obtained using central scales and the $q\bar{q}$ subprocess only.

We first consider the case in which the expected number of events for the signal hypothesis corresponds to $\bar{n}_i(\kappa_t,\kappa_g)$. We have examined two cases, both corresponding to di-boson invariant masses above the Higgs mass, so as to ensure to have complementary information with respect to Higgs cross sections. In one case, we have considered only two bins, a low-mass bin ($200\,\text{GeV} < M_{T1}, M_{ZZ} < 400\,\text{GeV}$) and a high-mass bin containing the rest of the distributions. The low-mass bin is more sensitive to κ_t, and the high-mass bin to κ_g. The corresponding exclusion regions in the (κ_t,κ_g) plane are bounded by the dashed contours in Fig. 6.12. We see that WW is complementary to ZZ for low values

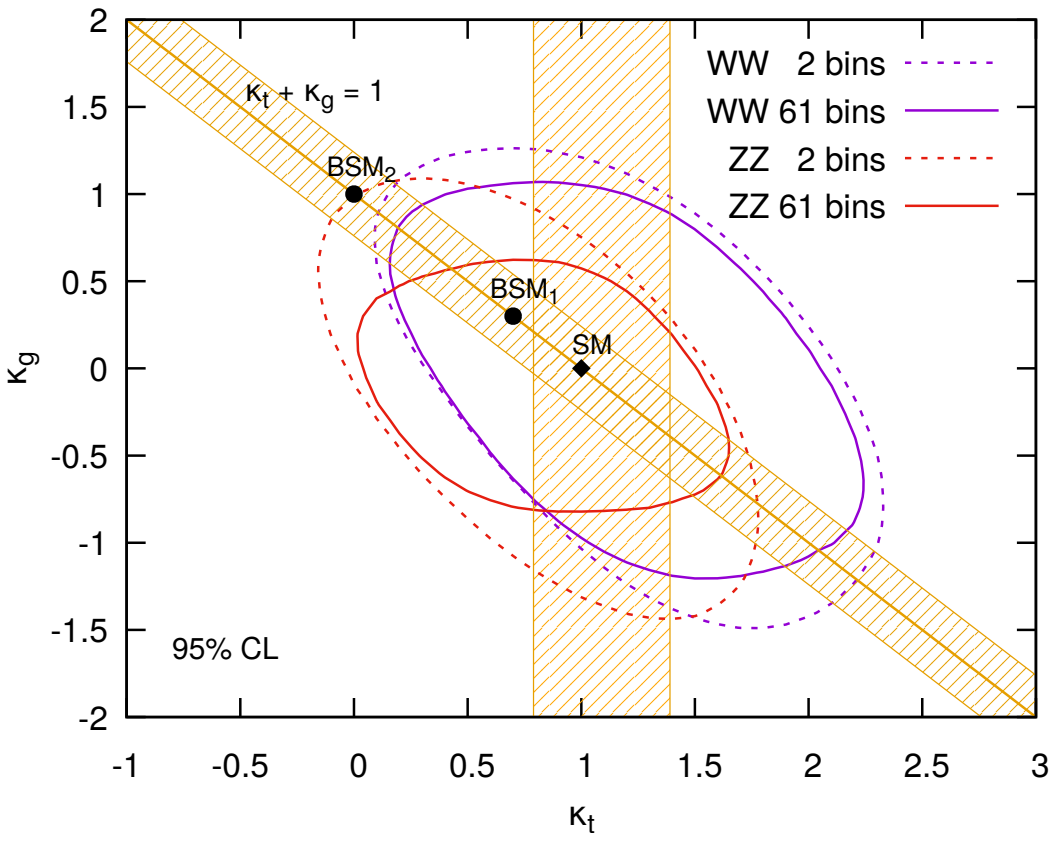

Figure 6.12: Exclusion contours at 95% level for WW and ZZ production. See the main text for details.

of κ_t, whereas the sensitivity to κ_g of ZZ is larger. This can be understood from figure 6.11. Note that, despite the fact that the WW cross-section is larger, the presence of the jet veto kills a good fraction of the gg signal, with the net effect that its cross-section decreases with increasing M_{T1}. In the ZZ case, where there is no suppression due to a

jet veto, the contact interaction driven by κ_g is fully effective, and makes the gg signal flatter with respect to the $q\bar{q}$ background, thus giving a larger sensitivity to κ_g. We gain sensitivity by considering a greater number of bins. For instance, we have considered 60 bins equally spaced from 200 GeV to 1400 GeV, and an extra bin containing the distribution with larger values of M_{T1} or M_{ZZ}. The corresponding exclusion contours are the solid lines in Fig. 6.12. For reference, we also plot the line $\kappa_t + \kappa_g = 1$, and three points corresponding to the SM, and the scenarios BSM_1 and BSM_2 considered in the previous section. We also draw bands corresponding to 95% confidence-level bounds on $\kappa_t + \kappa_g$ and κ_t obtained from ref. [180]. These give more stringent constraints than our observables, which have nevertheless complementary sensitivity, since the analysis of ref. [180] probes regions of di-boson invariant masses that we do not consider here. Also, having full control of theoretical predictions for both the signal and the background, our procedure is suitable for optimisation of both the observables and the binning procedure, and is open to improvements of the theoretical predictions.

The exclusion contours we have obtained so far do not take into account theoretical uncertainties. Including theoretical uncertainties, the true theory value $n_i(\kappa_t, \kappa_g)$ will differ from its central prediction $\bar{n}_i(\kappa_t, \kappa_g)$ by some theoretical error δ_i, taken to lie in some interval Δ_i. In every bin, $n_i(\kappa_t, \kappa_g)$ will be the sum of a contribution $n_i^{(q\bar{q})}$ arising from quark-antiquark annihilation, and a contribution $n_i^{(gg)}(\kappa_t, \kappa_g)$ arising from gluon fusion. Denoting by $\Delta_i^{(gg)}(\kappa_t, \kappa_g)$ and $\Delta_i^{(q\bar{q})}$ the theoretical uncertainties on (respectively) $n_i^{(gg)}(\kappa_t, \kappa_g)$ and $n_i^{(q\bar{q})}$, and considering the fact that these predictions correspond to completely uncorrelated processes, we take the theoretical uncertainty on $n_i(\kappa_t, \kappa_g)$ to be given by

$$\Delta_i(\kappa_t, \kappa_g) = \sqrt{\left(\Delta_i^{(gg)}(\kappa_t, \kappa_g)\right)^2 + \left(\Delta_i^{(q\bar{q})}\right)^2}\,. \tag{6.30}$$

Therefore, the χ^2 corresponding to a given value of $(\kappa_t, \kappa_g, \vec{\delta} \equiv \{\delta_1, \delta_2, \dots\})$ is given by

$$\chi^2_{\mathrm{exp}}(\kappa_t, \kappa_g, \vec{\delta}) \equiv \sum_i \frac{(\bar{n}_i(\kappa_t, \kappa_g) + \delta_i - n_i)^2}{n_i}\,. \tag{6.31}$$

In order to estimate the impact of theoretical uncertainties on our sensitivity contours, we adopt the approach of ref. [178], and add to χ^2_{exp} a Gaussian "theory term", with a width $\Delta_i(\kappa_t, \kappa_g)/2$, as follows:

$$\chi^2_{\mathrm{th}}(\kappa_t, \kappa_g, \vec{\delta}) \equiv \sum_i \frac{\delta_i^2}{\left(\Delta_i(\kappa_t, \kappa_g)/2\right)^2}\,. \tag{6.32}$$

The test statistic corresponding to (κ_t, κ_g) is then obtained by profiling with respect to $\vec{\delta}$, i.e. computing

$$\chi^2(\kappa_t, \kappa_g) \equiv \min_{\vec{\delta}} \left[\chi^2_{\mathrm{exp}}(\kappa_t, \kappa_g, \vec{\delta}) + \chi^2_{\mathrm{th}}(\kappa_t, \kappa_g, \vec{\delta})\right]. \tag{6.33}$$

For $\chi^2_{\rm exp}$ and $\chi^2_{\rm th}$ as in (6.31) and (6.32) this gives

$$\chi^2(\kappa_t,\kappa_g) = \sum_i \frac{(\bar{n}_i(\kappa_t,\kappa_g) - n_i)^2}{n_i + (\Delta_i(\kappa_t,\kappa_g)/2)^2}. \tag{6.34}$$

In other words, for a Gaussian theory term our treatment is equivalent to the common prescription to combine theoretical and experimental errors in quadrature.[8] With our choice of bins, we can approximate $\Delta_i(\kappa_t,\kappa_g) \simeq \Delta_i^{(q\bar{q})}$.

Before presenting sensitivity contours including theory uncertainties, it is worth comparing the impact of statistical and theoretical uncertainties. In the case of WW production, theory uncertainties differ according to whether we use the efficiency method described in appendix D.1.3, or we just perform 9-point scale variations in the resummed cross section. In the former case, as can be seen from Fig. 6.7, relative theory uncertainties are of order 40%, whereas in the latter they are of order 10%, with a mild dependence on M_{WW}. In both cases then $\Delta_i^{(q\bar{q})}$ roughly scales like n_i. Therefore, by looking at the denominator of eq. (6.34), we see that in the bins with larger n_i, theory uncertainties will dominate over statistical uncertainties ($\sim \sqrt{n_i}$), and hence these bins have very little power to constrain (κ_t,κ_g). In the case of ZZ, theory uncertainties are smaller, around 5%, so all bins retain their constraining power. This is illustrated in Fig. 6.13. All contours have been obtained with 61 bins, as explained above. The outer contour (dotted) corresponds to WW production with theory uncertainties estimated with the JVE method. As explained in sec. 6.4, the method is probably overly conservative, and the corresponding contour cannot compete with the constraints from ZZ production. Note in particular that large theoretical uncertainties affect mostly the bins with lowest values of M_{T1}, which are the most sensitive to κ_t. This explains why the JVE contour is so wide compared to the others. The solid contours correspond to uncertainties obtained with the appropriate scale variations, both for WW and for ZZ. Based on previous works on Higgs production with a jet-veto [92, 93, 140], we believe that scale variations for WW give a realistic estimate of the best theoretical uncertainties that could be obtained with a matching to NNLO with the JVE method. We see that, taking into account theory uncertainties at the currently achievable accuracy, WW does not have complementary constraining power with respect to ZZ. However, the dashed curves, corresponding to all predictions fixed at their central value without theory uncertainties, show that WW might compete with ZZ. We have

[8] In fact, (6.32) itself can similarly be obtained as follows: (i) introduce separate $\delta_i^{(gg)}$ and $\delta_i^{(q\bar{q})}$ parameters for the two components of $n_i(\kappa_t,\kappa_g)$, (ii) add separate Gaussian theory terms for the former, of respective widths $\Delta_i^{(gg)}/2$ and $\Delta_i^{(q\bar{q})}/2$, (iii) define $\delta_i = \delta_i^{(gg)} + \delta_i^{(q\bar{q})}$ and rewrite the χ^2 in terms of δ and $\delta_i^{(q\bar{q})}$, (iv) profile (minimise) the χ^2 with respect to $\delta_i^{(q\bar{q})}$. This again gives the expression (6.34).

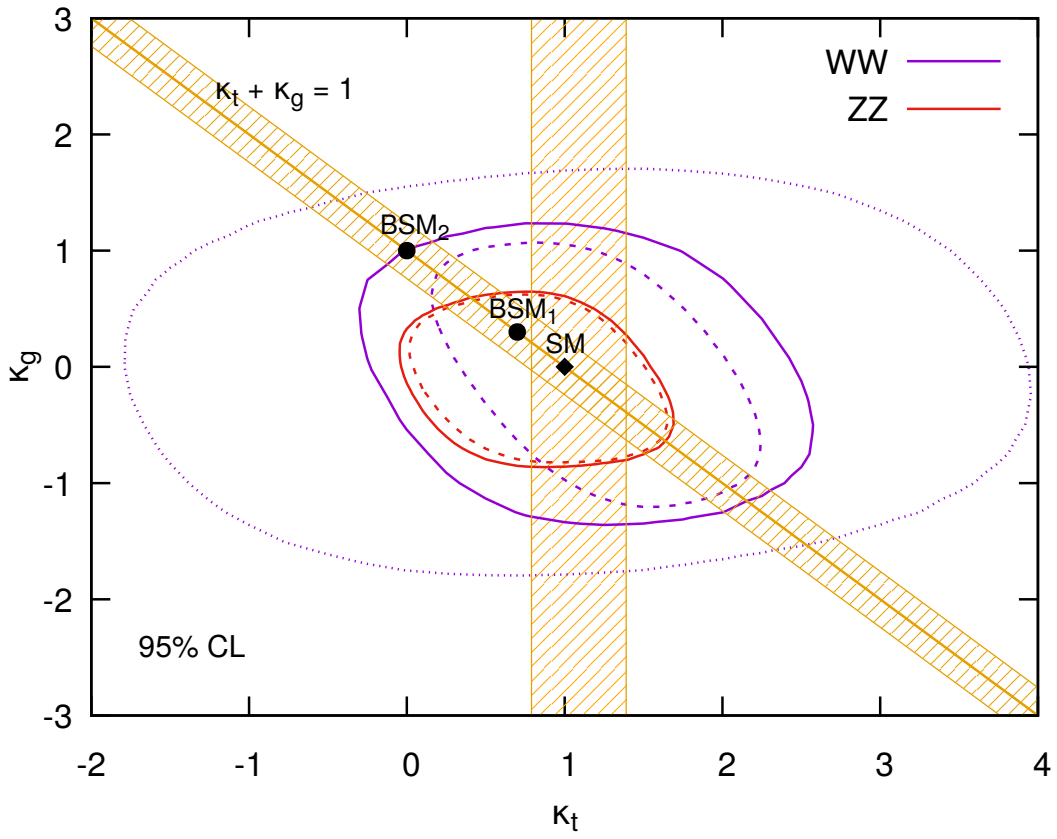

Figure 6.13: Exclusion contours at 95% level for WW and ZZ production, corresponding to different ways of estimating theoretical uncertainties, see the main text for details.

therefore determined the necessary accuracy on WW production such that one obtains a comparable sensitivity with ZZ. First, we have observed that, in the case of ZZ, adding the NNLO contribution to $q\bar{q}$ does not improve the overall theory accuracy, due to missing higher orders in the gg channel. So we assume that the uncertainties on ZZ production will remain the NLO ones, i.e. around 5%. The solid contour for WW in Fig. 6.14 corres-

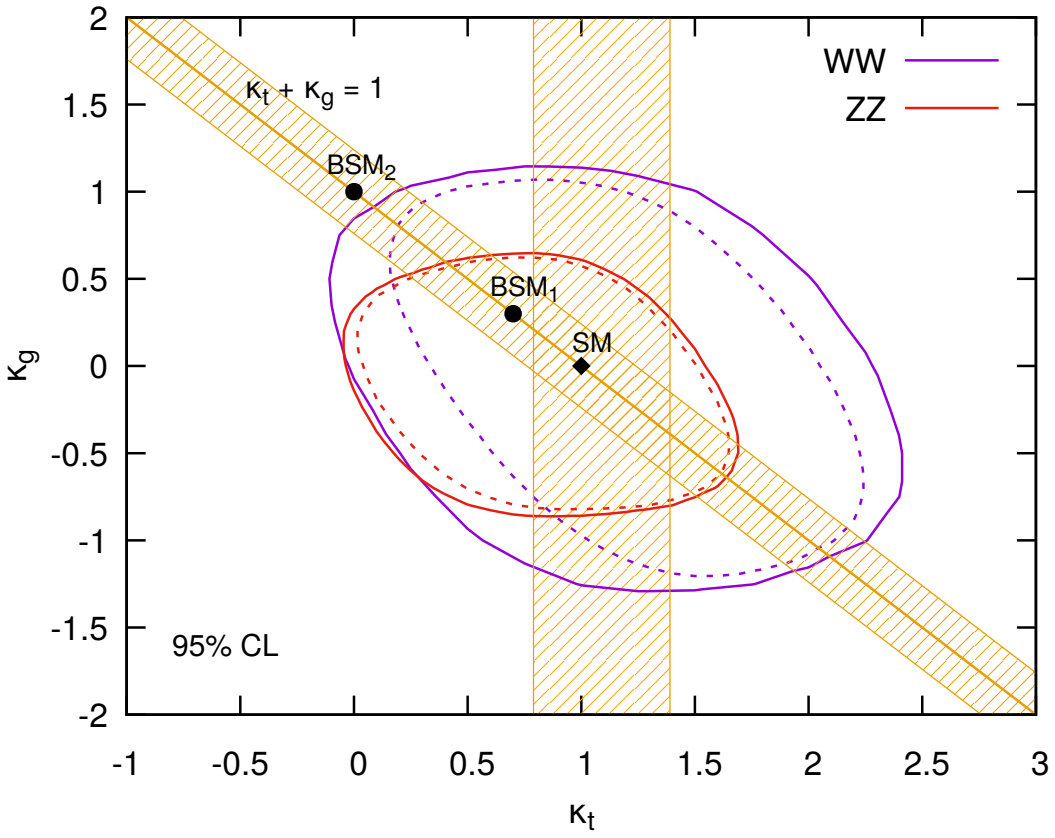

Figure 6.14: Exclusion contours at 95% level for WW and ZZ production, corresponding to an optimistic reduction of theoretical uncertainties, see the main text for details.

ponds to an estimated theoretical uncertainty of 3% in every bin, which is approximately the one you need for WW to be competitive with current ZZ predictions. Based again on previous work on Higgs production [140], such an uncertainty could be reached by matching NNLL resummation to a future NNLO calculation for WW plus one jet, and maybe even further decreased after an N^{3}LL resummation. We note that improving ZZ predictions hardly offers any stronger constraint. However, improved predictions for the gg channel, both for WW and ZZ, might move the central prediction, and may open up further space for constraints.

We conclude this section with a comment on the actual implementation of the calculation of $\chi^2(\kappa_t, \kappa_g)$. If we consider the numerator of $\chi^2(\kappa_t, \kappa_g)$ in eqs. (6.27) and (6.34),

we see that it involves $n_i^{(gg)}(\kappa_t, \kappa_g)$. This quantity is a second-order polynomial in κ_t and κ_g, arising from the square of the matrix element

$$M_{\rm SM}^{(gg)} + M_{\rm BSM}^{(gg)} = \kappa_t M_t^{(gg)} + \kappa_g M_g^{(gg)} + M_c^{(gg)}\,, \tag{6.35}$$

where $M_t^{(gg)}$ and $M_g^{(gg)}$ are the contributions of the Higgs produced via a top loop and a contact interaction respectively, and $M_c^{(gg)}$ the remaining contributions, giving rise to the so-called "continuum" background. The fact that we have full control over $M^{(gg)}$ allows us to compute the coefficient of each power of κ_t and κ_g separately, and once and for all. This is crucial for an accurate calculation of $\chi^2(\kappa_t, \kappa_g)$, because a naive implementation of this quantity might involve cancellations between large numbers, whose control requires Monte Carlo samples with large statistics.

6.6 Conclusion

We have studied the impact of a veto on additional jets on setting limits on the coupling of a dimension-6 operator affecting WW production. In the presence of such a veto, large logarithms of the ratio of the maximum allowed jet transverse momentum $p_{\rm t,veto}$ and the invariant mass of the WW pair M_{WW} have to be resummed at all orders in QCD. These logarithmically enhanced contributions give rise to the so-called Sudakov suppression of cross sections with respect to naive Born-level predictions. The dimension-6 operator we considered affects WW production via gluon fusion, but does not affect WW production via quark-antiquark annihilation, which stays unchanged with respect to the SM. At Born level, the effect of this operator amounts to a growth of the cross section at large values of M_{WW}. Unfortunately, the suppression due to the jet-veto gets larger with increasing M_{WW}. Also, such suppression affects gluon fusion more than quark-antiquark annihilation due to the fact that gluons radiate roughly twice as much as quarks, so vetoing radiation off gluons cuts a larger portion of cross sections. Therefore, enhancement due to a contact interaction and Sudakov suppression are in competition.

To investigate quantitatively the impact of a jet veto on WW production, we have devised a new method to interface the most accurate resummed predictions for the gg and $q\bar{q}$ channels to fixed-order QCD event generators. This procedure provides events that are fully differential in the decay products of the WW pair, so that suitable acceptance cuts can be applied. The method involves minimal modifications of the ingredients already present in fixed-order event generators, and can be applied to the production of any colour singlet. In particular, we have implemented the procedure in the fixed-order program `MCFM`,

which resulted in the code we called `MCFM-RE`, a Resummation Edition of `MCFM`.

Our program `MCFM-RE` has been used to produce differential cross sections for WW production with a simplified version of the ATLAS acceptance cuts, both in the SM, and including BSM effects induced by the aforementioned dimension-6 contact interaction. The main message is that, with the value of $p_{\mathrm{t,veto}}$ used in current analyses, Sudakov suppression effects dominate over the enhancement produced by a contact interaction, so that deviations from the Standard Model are in general quite small for reasonable values of the strength of the contact interaction.

We have compared our results with those obtained from a number of parton-shower event generators, and we have found very good agreement. We have used parton-shower event generators to estimate effects that cannot be not be taken into account by our analytical calculation, and found that they have a small impact, well within our theory uncertainties. We emphasise that our predictions have the computational cost of a Born-level event generator, and provide full analytical control of theoretical uncertainties. Our predictions are also in agreement, within uncertainties, with those obtained by interfacing a SCET calculation with the same formal accuracy with `aMC@NLO`.

We produced projections for the sensitivity to the considered BSM effects for HL-LHC, and compared with what could be obtained using ZZ production, which is not affected by the presence of a jet veto. We have found that WW has complementary sensitivity, provided it is possible to reduce theory uncertainties below 3%. This could be achieved by both matching current resummed predictions with a future calculation of WW plus one jet at NNLO, and improving the resummation to achieve $\mathrm{N^3LL}$ accuracy. We hope this work encourages further theoretical work in both directions. We remark that the main advantage of using `MCFM-RE` for such studies compared to parton-shower event generators is that we have access to amplitudes, so we can compute separately all terms contributing to square matrix elements, in particular interference terms which can be computed separately with an arbitrary numerical accuracy.

We have found that, with the current acceptance cuts, the observables we have considered are not yet competitive with Higgs total cross sections, although they do provide additional information. However, our code does provide an accurate and fast tool to explore different choices of cuts and observables, so could be used for further studies in this direction. Also, it makes it possible to implement other models of new physics affecting the production of a colour singlet.

Last, our code is the only implementation of the jet-veto resummation of ref. [140]

that is fully exclusive in the decay products of a colour singlet, so it can be used for precision determinations of Standard Model parameters, notably those characterising the Higgs boson.

Chapter 7

Conclusion

The quest for ever increasing precision in elementary particle physics is a never ending one, the discovery of new physics at higher energy scales demands that we know the QCD background at the sub-percent level. We have contributed to this quest through our study of the soft and collinear behaviour of QCD. We have provided better predictions of the QCD background at the LHC for the study of processes that require a jet veto. And we have been able to study at NNLL accuracy the D-parameter, a three-jet event-shape, measured during the LEP era for the first time. The extension we have made to the `ARES` framework offer new opportunities to study the phenomenology of interesting observables at present and future colliders.

In Chapter. 4 we extended the `ARES` method to the calculation of three-jet event-shapes in e^+e^- annihilation. We kept the presentation as general as possible so that any rIRC safe observable can be computed. To account for additional sources of NNLL corrections we introduced a new correction function $\delta\mathcal{F}_{\rm s}$ to account for the emission of soft wide angle radiation. We encountered spin-correlations in the final-state for the first time, due to the presence of a gluon in the final state of three-jet events. We were able to account for this correlation by extending the definition of $\delta\mathcal{F}_{\rm rec}$ and for the case of $e^+e^- \to q\bar{q}g$ we were able to factorise the spin correlations into a terms that depends onto on the momentum of the hard-collinear gluon Δp_ℓ and a single function that depends on the Born configuration $Sp(\Phi_{\mathcal{B}})$. We re-derived the remaining multiple emission functions from first principles, and were able to, for the most part, retain their previous definitions.

Following the considerations made in Chapter. 4, in Chapter. 5 we made use of the newly extended `ARES` method to resum the D-parameter in near-to-planar three-jet events at NNLL accuracy for the first time. The D-parameter is an additive observable and as a result of this we were able to determine most of the ingredients for the resummation

analytically, for the remaining pieces we determined their numerical value with simple Monte Carlo methods. We were able to produce predictions that can be compared to data taken by the ALEPH detector at LEP-1. And we made predictions for a future e^+e^- collider. The commonly used log-R matching scheme does not work particularly well for this observable and more aggressive matching schemes are needed to perform comprehensive phenomenology.

In Chapter. 6 we took the results of the jet veto resummation of Ref. [92, 93] and extended them to be differential in the leptonic final state. We devised a completely general procedure to allow the interface of resummation and fixed-order event-generators. We rely only on elements that must be present in all event-generators. We produced a code, `MCFM-RE`, that demonstrates the method. The code interfaces the `JetVHeto` code [93] with the fixed-order event-generator `MCFM`. This greatly extends the code of `JetVHeto`, it can now be used to resum jet veto effects for any colour singlet final state at NNLL accuracy, provided that the virtual corrections to the process are implemented in `MCFM`. And we gain access to the phase space generation of `MCFM`, so we are able to produce predictions that are differential in the leptonic final-states. Then we used the `MCFM-RE` code to constrain the BSM operator Eq. (6.1). With the jet veto under control we are able to examine how the WW channel impacts constrains on the operator. Previous studies had only been able to consider ZZ, as there was no way to correctly account for the jet veto effects. We discovered that WW, while somewhat complementary to constraints coming from ZZ, is not particularly competitive. The situation is however dominated by the error on the background prediction, with an N^{3}LL resummation of the jet veto and matching to N^{3}LO fixed-order the bound could be made competitive. As an aside to this, using `MCFM` as a matrix element provider gives us full control over the amplitudes. Using this technique we were able to compute only the coefficients of the different contributions. This makes our constraints very cheap to compute, as there is no need to run a parton-shower event-generator for every parameter value of interest.

Looking to the future, our extension of the `ARES` framework to three-jet observables encapsulates the majority of the work necessary for predictions of n-jet observables. The opening of three-jet event phenomenology gives us access to new precision observables that contribute to the precise determination of α_s. Further, the D-parameter is not the only three-jet event shape for which there exists interesting data, at ALEPH data for thrust-minor was taken, and further work with `ARES` will enable us to study it for the first time at NNLL accuracy.

By making use of fixed-order event-generators as we have done in Chapter. 6 we gain access to matrix elements and phase space generation. These can be interfaced with resummed calculation, only now we can easily make these calculations differential in the leptonic final-states, and we are able to consider many underlying hard processes for any given observable provided that associated virtual corrections are includes in the event-generator. We can use the well tested event-generation frameworks as a base for our predictions, this way we need only concern ourselves with the performing resummation, and the implementation follows very simply.

These extensions we have made to the `ARES` framework pave the way for interesting studies on the phenomenology of multi-jet events and for increasingly exclusive resummation predictions.

Bibliography

[1] Luke Arpino, Andrea Banfi and Basem Kamal El-Menoufi. 'Near-to-planar three-jet events at NNLL accuracy'. In: *JHEP* 07 (2020), p. 171. DOI: 10.1007/JHEP07(2020)171. arXiv: 1912.09341 [hep-ph].

[2] Luke Arpino et al. 'BSM WW production with a jet veto'. In: (2019). arXiv: 1905.06646 [hep-ph].

[3] Andrea Banfi, Gavin P. Salam and Giulia Zanderighi. 'Principles of general final-state resummation and automated implementation'. In: *JHEP* 03 (2005), p. 073. DOI: 10.1088/1126-6708/2005/03/073. arXiv: hep-ph/0407286 [hep-ph].

[4] Andrea Banfi et al. 'A general method for the resummation of event-shape distributions in e^+e annihilation'. In: *JHEP* 05 (2015), p. 102. DOI: 10.1007/JHEP05(2015)102. arXiv: 1412.2126 [hep-ph].

[5] Murray Gell-Mann. 'A Schematic Model of Baryons and Mesons'. In: *Phys. Lett.* 8 (1964), pp. 214–215. DOI: 10.1016/S0031-9163(64)92001-3.

[6] G. Zweig. 'An SU(3) model for strong interaction symmetry and its breaking. Version 1'. In: (1964).

[7] G. Zweig. 'An SU(3) model for strong interaction symmetry and its breaking. Version 2'. In: *DEVELOPMENTS IN THE QUARK THEORY OF HADRONS. VOL. 1. 1964 - 1978*. Ed. by D.B. Lichtenberg and Simon Peter Rosen. 1964, pp. 22–101.

[8] Chen-Ning Yang and Robert L. Mills. 'Conservation of Isotopic Spin and Isotopic Gauge Invariance'. In: *Phys. Rev.* 96 (1954). [,150(1954)], pp. 191–195. DOI: 10.1103/PhysRev.96.191.

[9] Steven Weinberg. 'Current algebra and gauge theories. 1.' In: *Phys. Rev.* D8 (1973), pp. 605–625. DOI: 10.1103/PhysRevD.8.605.

[10] Steven Weinberg. 'Current algebra and gauge theories. 2. NonAbelian gluons'. In: *Phys. Rev.* D8 (1973), pp. 4482–4498. DOI: 10.1103/PhysRevD.8.4482.

[11] H. Lehmann, K. Symanzik and W. Zimmermann. 'On the formulation of quantized field theories'. In: *Nuovo Cim.* 1 (1955), pp. 205–225. DOI: 10.1007/BF02731765.

[12] H. Lehmann, K. Symanzik and W. Zimmermann. 'On the formulation of quantized field theories. II'. In: *Nuovo Cim.* 6 (1957), pp. 319–333. DOI: 10.1007/BF02832508.

[13] L. D. Faddeev and V. N. Popov. 'Feynman Diagrams for the Yang-Mills Field'. In: *Phys. Lett.* 25B (1967). [,325(1967)], pp. 29–30. DOI: 10.1016/0370-2693(67)90067-6.

[14] Gerard 't Hooft and M.J.G. Veltman. 'Regularization and Renormalization of Gauge Fields'. In: *Nucl. Phys. B* 44 (1972), pp. 189–213. DOI: 10.1016/0550-3213(72)90279-9.

[15] C.G. Bollini and J.J. Giambiagi. 'Dimensional Renormalization: The Number of Dimensions as a Regularizing Parameter'. In: *Nuovo Cim. B* 12 (1972), pp. 20–26. DOI: 10.1007/BF02895558.

[16] J.F. Ashmore. 'A Method of Gauge Invariant Regularization'. In: *Lett. Nuovo Cim.* 4 (1972), pp. 289–290. DOI: 10.1007/BF02824407.

[17] T. Kinoshita. 'Mass singularities of Feynman amplitudes'. In: *J. Math. Phys.* 3 (1962), pp. 650–677. DOI: 10.1063/1.1724268.

[18] T. D. Lee and M. Nauenberg. 'Degenerate Systems and Mass Singularities'. In: *Phys. Rev.* 133 (1964). [,25(1964)], B1549–B1562. DOI: 10.1103/PhysRev.133.B1549.

[19] S. Catani and M. H. Seymour. 'A General algorithm for calculating jet cross-sections in NLO QCD'. In: *Nucl. Phys.* B485 (1997). [Erratum: Nucl. Phys.B510,503(1998)], pp. 291–419. DOI: 10.1016/S0550-3213(96)00589-5,10.1016/S0550-3213(98)81022-5. arXiv: hep-ph/9605323 [hep-ph].

[20] Gabor Somogyi, Zoltan Trocsanyi and Vittorio Del Duca. 'Matching of singly- and doubly-unresolved limits of tree-level QCD squared matrix elements'. In: *JHEP* 06 (2005), p. 024. DOI: 10.1088/1126-6708/2005/06/024. arXiv: hep-ph/0502226 [hep-ph].

[21] Gabor Somogyi, Zoltan Trocsanyi and Vittorio Del Duca. 'A Subtraction scheme for computing QCD jet cross sections at NNLO: Regularization of doubly-real emissions'. In: *JHEP* 01 (2007), p. 070. DOI: 10.1088/1126-6708/2007/01/070. arXiv: hep-ph/0609042 [hep-ph].

[22] Zoltan Nagy, Gabor Somogyi and Zoltan Trocsanyi. 'Separation of soft and collinear infrared limits of QCD squared matrix elements'. In: (2007). arXiv: hep-ph/0702273 [HEP-PH].

[23] D. Amati, R. Petronzio and G. Veneziano. 'Relating Hard QCD Processes Through Universality of Mass Singularities'. In: *Nucl. Phys.* B140 (1978), pp. 54–72. DOI: 10.1016/0550-3213(78)90313-9.

[24] D. Amati, R. Petronzio and G. Veneziano. 'Relating Hard QCD Processes Through Universality of Mass Singularities. 2.' In: *Nucl. Phys.* B146 (1978), pp. 29–49. DOI: 10.1016/0550-3213(78)90430-3.

[25] Stefano Catani and Massimiliano Grazzini. 'Infrared factorization of tree level QCD amplitudes at the next-to-next-to-leading order and beyond'. In: *Nucl. Phys.* B570 (2000), pp. 287–325. DOI: 10.1016/S0550-3213(99)00778-6. arXiv: hep-ph/9908523 [hep-ph].

[26] A. Bassetto, M. Ciafaloni and G. Marchesini. 'Jet Structure and Infrared Sensitive Quantities in Perturbative QCD'. In: *Phys. Rept.* 100 (1983), pp. 201–272. DOI: 10.1016/0370-1573(83)90083-2.

[27] George F. Sterman and Steven Weinberg. 'Jets from Quantum Chromodynamics'. In: *Phys. Rev. Lett.* 39 (1977), p. 1436. DOI: 10.1103/PhysRevLett.39.1436.

[28] T. Gleisberg et al. 'Event generation with SHERPA 1.1'. In: *JHEP* 02 (2009), p. 007. DOI: 10.1088/1126-6708/2009/02/007. arXiv: 0811.4622 [hep-ph].

[29] John E. Huth et al. 'Toward a standardization of jet definitions'. In: *1990 DPF Summer Study on High-energy Physics: Research Directions for the Decade (Snowmass 90) Snowmass, Colorado, June 25-July 13, 1990*. 1990, pp. 0134–136. URL: http://lss.fnal.gov/cgi-bin/find_paper.pl?conf-90-249.

[30] Gavin P. Salam. 'Towards Jetography'. In: *Eur. Phys. J.* C67 (2010), pp. 637–686. DOI: 10.1140/epjc/s10052-010-1314-6. arXiv: 0906.1833 [hep-ph].

[31] S. Bethke et al. 'Experimental Investigation of the Energy Dependence of the Strong Coupling Strength'. In: *Phys. Lett.* B213 (1988), pp. 235–241. DOI: 10.1016/0370-2693(88)91032-5.

[32] Andrea Banfi. *Hadronic Jets*. 2053-2571. Morgan & Claypool Publishers, 2016. ISBN: 978-1-6817-4073-7. DOI: 10.1088/978-1-6817-4073-7. URL: http://dx.doi.org/10.1088/978-1-6817-4073-7.

[33] S. Catani et al. 'New clustering algorithm for multi - jet cross-sections in e+ e- annihilation'. In: *Phys. Lett.* B269 (1991), pp. 432–438. DOI: 10.1016/0370-2693(91)90196-W.

[34] S. Catani et al. 'Longitudinally invariant K_t clustering algorithms for hadron hadron collisions'. In: *Nucl. Phys.* B406 (1993), pp. 187–224. DOI: 10.1016/0550-3213(93)90166-M.

[35] Stephen D. Ellis and Davison E. Soper. 'Successive combination jet algorithm for hadron collisions'. In: *Phys. Rev.* D48 (1993), pp. 3160–3166. DOI: 10.1103/PhysRevD.48.3160. arXiv: hep-ph/9305266 [hep-ph].

[36] Yuri L. Dokshitzer et al. 'Better jet clustering algorithms'. In: *JHEP* 08 (1997), p. 001. DOI: 10.1088/1126-6708/1997/08/001. arXiv: hep-ph/9707323 [hep-ph].

[37] Matteo Cacciari, Gavin P. Salam and Gregory Soyez. 'The anti-k_t jet clustering algorithm'. In: *JHEP* 04 (2008), p. 063. DOI: 10.1088/1126-6708/2008/04/063. arXiv: 0802.1189 [hep-ph].

[38] Edward Farhi. 'A QCD Test for Jets'. In: *Phys. Rev. Lett.* 39 (1977), pp. 1587–1588. DOI: 10.1103/PhysRevLett.39.1587.

[39] J. D. Bjorken and Stanley J. Brodsky. 'Statistical Model for electron-Positron Annihilation Into Hadrons'. In: *Phys. Rev.* D1 (1970), pp. 1416–1420. DOI: 10.1103/PhysRevD.1.1416.

[40] G. Parisi. 'Super Inclusive Cross-Sections'. In: *Phys. Lett.* 74B (1978), pp. 65–67. DOI: 10.1016/0370-2693(78)90061-8.

[41] John F. Donoghue, F. E. Low and So-Young Pi. 'Tensor Analysis of Hadronic Jets in Quantum Chromodynamics'. In: *Phys. Rev.* D20 (1979), p. 2759. DOI: 10.1103/PhysRevD.20.2759.

[42] R. Keith Ellis, D. A. Ross and A. E. Terrano. 'The Perturbative Calculation of Jet Structure in e+ e- Annihilation'. In: *Nucl. Phys.* B178 (1981), pp. 421–456. DOI: 10.1016/0550-3213(81)90165-6.

[43] John C. Collins, Davison E. Soper and George F. Sterman. 'Transverse Momentum Distribution in Drell-Yan Pair and W and Z Boson Production'. In: *Nucl. Phys.* B250 (1985), pp. 199–224. DOI: 10.1016/0550-3213(85)90479-1.

[44] S. Catani et al. 'Resummation of large logarithms in e+ e- event shape distributions'. In: *Nucl. Phys.* B407 (1993), pp. 3–42. DOI: 10.1016/0550-3213(93)90271-P.

[45] Roberto Bonciani et al. 'Sudakov resummation of multiparton QCD cross-sections'. In: *Phys. Lett.* B575 (2003), pp. 268–278. DOI: 10.1016/j.physletb.2003.09.068. arXiv: hep-ph/0307035 [hep-ph].

[46] S. Catani et al. 'Thrust distribution in e+ e- annihilation'. In: *Phys. Lett.* B263 (1991), pp. 491–497. DOI: 10.1016/0370-2693(91)90494-B.

[47] S. Catani, G. Turnock and B. R. Webber. 'Heavy jet mass distribution in e+ e- annihilation'. In: *Phys. Lett.* B272 (1991), pp. 368–372. DOI: 10.1016/0370-2693(91)91845-M.

[48] S. Catani and B. R. Webber. 'Resummed C parameter distribution in e+ e- annihilation'. In: *Phys. Lett.* B427 (1998), pp. 377–384. DOI: 10.1016/S0370-2693(98)00359-1. arXiv: hep-ph/9801350 [hep-ph].

[49] Yuri L. Dokshitzer et al. 'On the QCD analysis of jet broadening'. In: *JHEP* 01 (1998), p. 011. DOI: 10.1088/1126-6708/1998/01/011. arXiv: hep-ph/9801324 [hep-ph].

[50] Thomas Becher and Matthew D. Schwartz. 'A precise determination of α_s from LEP thrust data using effective field theory'. In: *JHEP* 07 (2008), p. 034. DOI: 10.1088/1126-6708/2008/07/034. arXiv: 0803.0342 [hep-ph].

[51] Yang-Ting Chien and Matthew D. Schwartz. 'Resummation of heavy jet mass and comparison to LEP data'. In: *JHEP* 08 (2010), p. 058. DOI: 10.1007/JHEP08(2010)058. arXiv: 1005.1644 [hep-ph].

[52] Thomas Becher and Matthias Neubert. 'Factorization and NNLL Resummation for Higgs Production with a Jet Veto'. In: *JHEP* 07 (2012), p. 108. DOI: 10.1007/JHEP07(2012)108. arXiv: 1205.3806 [hep-ph].

[53] André H. Hoang et al. 'C-parameter distribution at N^{3}LL including power corrections'. In: *Phys. Rev.* D91.9 (2015), p. 094017. DOI: 10.1103/PhysRevD.91.094017. arXiv: 1411.6633 [hep-ph].

[54] Thomas Becher and Matthias Neubert. 'Drell-Yan Production at Small q_T, Transverse Parton Distributions and the Collinear Anomaly'. In: *Eur. Phys. J.* C71 (2011), p. 1665. DOI: 10.1140/epjc/s10052-011-1665-7. arXiv: 1007.4005 [hep-ph].

[55] Iain W. Stewart, Frank J. Tackmann and Wouter J. Waalewijn. 'The Beam Thrust Cross Section for Drell-Yan at NNLL Order'. In: *Phys. Rev. Lett.* 106 (2011), p. 032001. DOI: 10.1103/PhysRevLett.106.032001. arXiv: 1005.4060 [hep-ph].

[56] Thomas Becher, Xavier Garcia i Tormo and Jan Piclum. 'Next-to-next-to-leading logarithmic resummation for transverse thrust'. In: *Phys. Rev.* D93.5 (2016). [Erratum: Phys. Rev.D93,no.7,079905(2016)], p. 054038. DOI: 10.1103/PhysRevD.93.054038,10.1103/PhysRevD.93.079905. arXiv: 1512.00022 [hep-ph].

[57] A. Banfi, G. P. Salam and G. Zanderighi. 'Semi-numerical resummation of event shapes'. In: *JHEP* 01 (2002), p. 018. DOI: 10.1088/1126-6708/2002/01/018. arXiv: hep-ph/0112156 [hep-ph].

[58] Gionata Luisoni and Simone Marzani. 'QCD resummation for hadronic final states'. In: *J. Phys.* G42.10 (2015), p. 103101. DOI: 10.1088/0954-3899/42/10/103101. arXiv: 1505.04084 [hep-ph].

[59] S. Catani, B. R. Webber and G. Marchesini. 'QCD coherent branching and semi-inclusive processes at large x'. In: *Nucl. Phys.* B349 (1991), pp. 635–654. DOI: 10.1016/0550-3213(91)90390-J.

[60] Yuri L. Dokshitzer et al. *Basics of perturbative QCD*. 1991.

[61] Andrea Banfi, Basem Kamal El-Menoufi and Pier Francesco Monni. 'The Sudakov radiator for jet observables and the soft physical coupling'. In: *JHEP* 01 (2019), p. 083. DOI: 10.1007/JHEP01(2019)083. arXiv: 1807.11487 [hep-ph].

[62] Eric Laenen, George F. Sterman and Werner Vogelsang. 'Recoil and threshold corrections in short distance cross-sections'. In: *Phys. Rev.* D63 (2001), p. 114018. DOI: 10.1103/PhysRevD.63.114018. arXiv: hep-ph/0010080 [hep-ph].

[63] Lance J. Dixon, Lorenzo Magnea and George F. Sterman. 'Universal structure of subleading infrared poles in gauge theory amplitudes'. In: *JHEP* 08 (2008), p. 022. DOI: 10.1088/1126-6708/2008/08/022. arXiv: 0805.3515 [hep-ph].

[64] J. Frenkel and J. C. Taylor. 'NONABELIAN EIKONAL EXPONENTIATION'. In: *Nucl. Phys.* B246 (1984), pp. 231–245. DOI: 10.1016/0550-3213(84)90294-3.

[65] J. G. M. Gatheral. 'Exponentiation of Eikonal Cross-sections in Nonabelian Gauge Theories'. In: *Phys. Lett.* 133B (1983), pp. 90–94. DOI: 10.1016/0370-2693(83)90112-0.

[66] Stefano Catani and Massimiliano Grazzini. 'The soft gluon current at one loop order'. In: *Nucl. Phys.* B591 (2000), pp. 435–454. DOI: 10.1016/S0550-3213(00)00572-1. arXiv: hep-ph/0007142 [hep-ph].

[67] Andrea Banfi et al. 'The two-jet rate in e^+e^- at next-to-next-to-leading-logarithmic order'. In: *Phys. Rev. Lett.* 117.17 (2016), p. 172001. DOI: 10.1103/PhysRevLett.117.172001. arXiv: 1607.03111 [hep-ph].

[68] Frits A. Berends and W. T. Giele. 'Multiple Soft Gluon Radiation in Parton Processes'. In: *Nucl. Phys.* B313 (1989), pp. 595–633. DOI: 10.1016/0550-3213(89)90398-2.

[69] Ye Li and Hua Xing Zhu. 'Single soft gluon emission at two loops'. In: *JHEP* 11 (2013), p. 080. DOI: 10.1007/JHEP11(2013)080. arXiv: 1309.4391 [hep-ph].

[70] M. Tanabashi et al. 'Review of Particle Physics'. In: *Phys. Rev.* D98.3 (2018), p. 030001. DOI: 10.1103/PhysRevD.98.030001.

[71] Andrew J. Larkoski and Aja Procita. 'New Insights on an Old Problem: Resummation of the D-parameter'. In: *JHEP* 02 (2019), p. 104. DOI: 10.1007/JHEP02(2019)104. arXiv: 1810.06563 [hep-ph].

[72] Vito Antonelli, Mrinal Dasgupta and Gavin P. Salam. 'Resummation of thrust distributions in DIS'. In: *JHEP* 02 (2000), p. 001. DOI: 10.1088/1126-6708/2000/02/001. arXiv: hep-ph/9912488 [hep-ph].

[73] M. Dasgupta and G. P. Salam. 'Resummation of the jet broadening in DIS'. In: *Eur. Phys. J.* C24 (2002), pp. 213–236. DOI: 10.1007/s100520200915. arXiv: hep-ph/0110213 [hep-ph].

[74] Wojciech Bizon et al. 'Momentum-space resummation for transverse observables and the Higgs $p_\perp$ at N^{3}LL+NNLO'. In: *JHEP* 02 (2018), p. 108. DOI: 10.1007/JHEP02(2018)108. arXiv: 1705.09127 [hep-ph].

[75] Leandro G. Almeida et al. 'Comparing and counting logs in direct and effective methods of QCD resummation'. In: *JHEP* 04 (2014), p. 174. DOI: 10.1007/JHEP04(2014)174. arXiv: 1401.4460 [hep-ph].

[76] Pier Francesco Monni, Luca Rottoli and Paolo Torrielli. 'Higgs transverse momentum with a jet veto: a double-differential resummation'. In: (2019). arXiv: 1909.04704 [hep-ph].

[77] http://aleph.web.cern.ch/aleph/aleph_general/analysis/QCD/evsh/dat/91/lep1.html.

[78] R Barate et al. 'Studies of quantum chromodynamics with the ALEPH detector'. In: *Phys. Rep.* 294.CERN-PPE-96-186 (Dec. 1996), 1–165. 166 p. DOI: 10.1016/S0370-1573(97)00045-8. URL: http://cds.cern.ch/record/317674.

[79] A Heister et al. 'Studies of QCD at e^+e^- Centre-of-Mass Energies between 91 and 209 GeV'. In: *Eur. Phys. J. C* 35.CERN-EP-2003-084 (Dec. 2003), 457–486. 46 p. DOI: 10.1140/epjc/s2004-01891-4. URL: http://cds.cern.ch/record/690637.

[80] Yuri L. Dokshitzer, G. Marchesini and B. R. Webber. 'Dispersive approach to power behaved contributions in QCD hard processes'. In: *Nucl. Phys.* B469 (1996), pp. 93–142. DOI: 10.1016/0550-3213(96)00155-1. arXiv: hep-ph/9512336 [hep-ph].

[81] A. Banfi et al. 'QCD analysis of D-parameter in near to planar three jet events'. In: *JHEP* 05 (2001), p. 040. DOI: 10.1088/1126-6708/2001/05/040. arXiv: hep-ph/0104162 [hep-ph].

[82] Yuri L. Dokshitzer et al. 'Universality of 1/Q corrections to jet-shape observables rescued'. In: *Nucl. Phys.* B511 (1998). [Erratum: Nucl. Phys.B593,729(2001)], pp. 396–418. DOI: 10.1016/S0550-3213(97)00650-0,10.1016/S0550-3213(00)00646-5. arXiv: hep-ph/9707532 [hep-ph].

[83] Yuri L. Dokshitzer et al. 'On the universality of the Milan factor for 1 / Q power corrections to jet shapes'. In: *JHEP* 05 (1998), p. 003. DOI: 10.1088/1126-6708/1998/05/003. arXiv: hep-ph/9802381.

[84] Mrinal Dasgupta, Lorenzo Magnea and Graham Smye. 'Universality of 1/Q corrections revisited'. In: *JHEP* 11 (1999), p. 025. DOI: 10.1088/1126-6708/1999/11/025. arXiv: hep-ph/9911316.

[85] Graham E. Smye. 'On the 1/Q correction to the C - parameter at two loops'. In: *JHEP* 05 (2001), p. 005. DOI: 10.1088/1126-6708/2001/05/005. arXiv: hep-ph/0101323.

[86] G. P. Salam and D. Wicke. 'Hadron masses and power corrections to event shapes'. In: *JHEP* 05 (2001), p. 061. DOI: 10.1088/1126-6708/2001/05/061. arXiv: hep-ph/0102343 [hep-ph].

[87] Thomas Gehrmann, Gionata Luisoni and Pier Francesco Monni. 'Power corrections in the dispersive model for a determination of the strong coupling constant from the thrust distribution'. In: *Eur. Phys. J.* C73.1 (2013), p. 2265. DOI: 10.1140/epjc/s10052-012-2265-x. arXiv: 1210.6945 [hep-ph].

[88] Gregory P. Korchemsky and George F. Sterman. 'Nonperturbative corrections in resummed cross-sections'. In: *Nucl. Phys. B* 437 (1995), pp. 415–432. DOI: 10.1016/0550-3213(94)00006-Z. arXiv: hep-ph/9411211.

[89] Gregory P. Korchemsky and George F. Sterman. 'Power corrections to event shapes and factorization'. In: *Nucl. Phys. B* 555 (1999), pp. 335–351. DOI: 10.1016/S0550-3213(99)00308-9. arXiv: hep-ph/9902341.

[90] Andrei V. Belitsky, G.P. Korchemsky and George F. Sterman. 'Energy flow in QCD and event shape functions'. In: *Phys. Lett. B* 515 (2001), pp. 297–307. DOI: 10.1016/S0370-2693(01)00899-1. arXiv: hep-ph/0106308.

[91] Christopher Lee and George F. Sterman. 'Momentum Flow Correlations from Event Shapes: Factorized Soft Gluons and Soft-Collinear Effective Theory'. In: *Phys. Rev. D* 75 (2007), p. 014022. DOI: 10.1103/PhysRevD.75.014022. arXiv: hep-ph/0611061.

[92] Andrea Banfi, Gavin P. Salam and Giulia Zanderighi. 'NLL+NNLO predictions for jet-veto efficiencies in Higgs-boson and Drell-Yan production'. In: *JHEP* 06 (2012), p. 159. DOI: 10.1007/JHEP06(2012)159. arXiv: 1203.5773 [hep-ph].

[93] Andrea Banfi et al. 'Higgs and Z-boson production with a jet veto'. In: *Phys. Rev. Lett.* 109 (2012), p. 202001. DOI: 10.1103/PhysRevLett.109.202001. arXiv: 1206.4998 [hep-ph].

[94] Morad Aaboud et al. 'Measurements of gluon-gluon fusion and vector-boson fusion Higgs boson production cross-sections in the $H \to WW^* \to e\nu\mu\nu$ decay channel in pp collisions at $\sqrt{s} = 13$ TeV with the ATLAS detector'. In: *Phys. Lett.* B789 (2019), pp. 508–529. DOI: 10.1016/j.physletb.2018.11.064. arXiv: 1808.09054 [hep-ex].

[95] Morad Aaboud et al. 'Search for heavy resonances decaying into WW in the $e\nu\mu\nu$ final state in pp collisions at $\sqrt{s} = 13$ TeV with the ATLAS detector'. In: *Eur. Phys. J.* C78.1 (2018), p. 24. DOI: 10.1140/epjc/s10052-017-5491-4. arXiv: 1710.01123 [hep-ex].

[96] Morad Aaboud et al. 'Measurement of the W^+W^- production cross section in pp collisions at a centre-of-mass energy of $\sqrt{s} = 13$ TeV with the ATLAS experiment'. In: *Phys. Lett.* B773 (2017), pp. 354–374. DOI: 10.1016/j.physletb.2017.08.047. arXiv: 1702.04519 [hep-ex].

[97] Morad Aaboud et al. 'Constraints on off-shell Higgs boson production and the Higgs boson total width in $ZZ \to 4\ell$ and $ZZ \to 2\ell 2\nu$ final states with the ATLAS detector'. In: *Phys. Lett.* B786 (2018), pp. 223–244. DOI: 10.1016/j.physletb.2018.09.048. arXiv: 1808.01191 [hep-ex].

[98] Morad Aaboud et al. 'Searches for heavy ZZ and ZW resonances in the $\ell\ell qq$ and $\nu\nu qq$ final states in pp collisions at $\sqrt{s} = 13$ TeV with the ATLAS detector'. In: *JHEP* 03 (2018), p. 009. DOI: 10.1007/JHEP03(2018)009. arXiv: 1708.09638 [hep-ex].

[99] Morad Aaboud et al. 'Search for diboson resonances with boson-tagged jets in pp collisions at $\sqrt{s} = 13$ TeV with the ATLAS detector'. In: *Phys. Lett.* B777 (2018), pp. 91–113. DOI: 10.1016/j.physletb.2017.12.011. arXiv: 1708.04445 [hep-ex].

[100] Morad Aaboud et al. 'Search for WW/WZ resonance production in $\ell\nu qq$ final states in pp collisions at $\sqrt{s} = 13$ TeV with the ATLAS detector'. In: *JHEP* 03 (2018), p. 042. DOI: 10.1007/JHEP03(2018)042. arXiv: 1710.07235 [hep-ex].

[101] Morad Aaboud et al. 'Measurement of the four-lepton invariant mass spectrum in 13 TeV proton-proton collisions with the ATLAS detector'. In: (2019). arXiv: 1902.05892 [hep-ex].

[102] Albert M Sirunyan et al. 'Measurements of the $pp \to ZZ$ production cross section and the $Z \to 4\ell$ branching fraction, and constraints on anomalous triple gauge couplings at $\sqrt{s} = 13\,\text{TeV}$'. In: *Eur. Phys. J.* C78 (2018). [Erratum: Eur. Phys. J.C78,no.6,515(2018)], p. 165. DOI: 10.1140/epjc/s10052-018-5567-9,10.1140/epjc/s10052-018-5769-1. arXiv: 1709.08601 [hep-ex].

[103] Albert M. Sirunyan et al. 'Measurements of properties of the Higgs boson decaying to a W boson pair in pp collisions at $\sqrt{s} = 13$ TeV'. In: *Phys. Lett.* B791 (2019), p. 96. DOI: 10.1016/j.physletb.2018.12.073. arXiv: 1806.05246 [hep-ex].

[104] Albert M Sirunyan et al. 'Measurements of the Higgs boson width and anomalous HVV couplings from on-shell and off-shell production in the four-lepton final state'. In: (2019). arXiv: 1901.00174 [hep-ex].

[105] E. W. Nigel Glover and J. J. van der Bij. 'Vector Boson Pair Production via Gluon Fusion'. In: *Phys. Lett.* B219 (1989), pp. 488–492. DOI: 10.1016/0370-2693(89)91099-X.

[106] Nikolas Kauer and Giampiero Passarino. 'Inadequacy of zero-width approximation for a light Higgs boson signal'. In: *JHEP* 08 (2012), p. 116. DOI: 10.1007/JHEP08(2012)116. arXiv: 1206.4803 [hep-ph].

[107] Nikolas Kauer. 'Interference effects for H → WW/ZZ → $\ell\bar{\nu}_\ell\bar{\ell}\nu_\ell$ searches in gluon fusion at the LHC'. In: *JHEP* 12 (2013), p. 082. DOI: 10.1007/JHEP12(2013)082. arXiv: 1310.7011 [hep-ph].

[108] Fabrizio Caola and Kirill Melnikov. 'Constraining the Higgs boson width with ZZ production at the LHC'. In: *Phys. Rev.* D88 (2013), p. 054024. DOI: 10.1103/PhysRevD.88.054024. arXiv: 1307.4935 [hep-ph].

[109] W. Buchmuller and D. Wyler. 'Effective Lagrangian Analysis of New Interactions and Flavor Conservation'. In: *Nucl. Phys.* B268 (1986), pp. 621–653. DOI: 10.1016/0550-3213(86)90262-2.

[110] B. Grzadkowski et al. 'Dimension-Six Terms in the Standard Model Lagrangian'. In: *JHEP* 10 (2010), p. 085. DOI: 10.1007/JHEP10(2010)085. arXiv: 1008.4884 [hep-ph].

[111] G. F. Giudice et al. 'The Strongly-Interacting Light Higgs'. In: *JHEP* 06 (2007), p. 045. DOI: 10.1088/1126-6708/2007/06/045. arXiv: hep-ph/0703164 [hep-ph].

[112] J. Elias-Miro et al. 'Higgs windows to new physics through d=6 operators: constraints and one-loop anomalous dimensions'. In: *JHEP* 11 (2013), p. 066. DOI: 10.1007/JHEP11(2013)066. arXiv: 1308.1879 [hep-ph].

[113] Robert V. Harlander and Tobias Neumann. 'Probing the nature of the Higgs-gluon coupling'. In: *Phys. Rev.* D88 (2013), p. 074015. DOI: 10.1103/PhysRevD.88.074015. arXiv: 1308.2225 [hep-ph].

[114] John Ellis et al. 'Updated Global SMEFT Fit to Higgs, Diboson and Electroweak Data'. In: *JHEP* 06 (2018), p. 146. DOI: 10.1007/JHEP06(2018)146. arXiv: 1803.03252 [hep-ph].

[115] Aleksandr Azatov et al. 'Taming the off-shell Higgs boson'. In: *Zh. Eksp. Teor. Fiz.* 147 (2015). [J. Exp. Theor. Phys.120,354(2015)], pp. 410–425. DOI: 10.1134/S1063776115030140,10.7868/S0044451015030039. arXiv: 1406.6338 [hep-ph].

[116] Malte Buschmann et al. 'Mass Effects in the Higgs-Gluon Coupling: Boosted vs Off-Shell Production'. In: *JHEP* 02 (2015), p. 038. DOI: 10.1007/JHEP02(2015)038. arXiv: 1410.5806 [hep-ph].

[117] Georges Aad et al. 'Measurement of W^+W^- production in pp collisions at $\sqrt{s} = 7\,\text{TeV}$ with the ATLAS detector and limits on anomalous WWZ and $WW\gamma$ couplings'. In: *Phys. Rev.* D87.11 (2013). [Erratum: Phys. Rev.D88,no.7,079906(2013)],

p. 112001. DOI: 10.1103/PhysRevD.87.112001,10.1103/PhysRevD.88.079906. arXiv: 1210.2979 [hep-ex].

[118] Serguei Chatrchyan et al. 'Measurement of the W^+W^- Cross Section in pp Collisions at $\sqrt{s} = 7$ TeV and Limits on Anomalous $WW\gamma$ and WWZ Couplings'. In: *Eur. Phys. J.* C73.10 (2013), p. 2610. DOI: 10.1140/epjc/s10052-013-2610-8. arXiv: 1306.1126 [hep-ex].

[119] Serguei Chatrchyan et al. 'Measurement of W^+W^- and ZZ Production Cross Sections in pp Collisions at $\sqrt{s} = 8TeV$'. In: *Phys. Lett.* B721 (2013), pp. 190–211. DOI: 10.1016/j.physletb.2013.03.027. arXiv: 1301.4698 [hep-ex].

[120] Prerit Jaiswal and Takemichi Okui. 'Explanation of the WW excess at the LHC by jet-veto resummation'. In: *Phys. Rev.* D90.7 (2014), p. 073009. DOI: 10.1103/PhysRevD.90.073009. arXiv: 1407.4537 [hep-ph].

[121] Pier Francesco Monni and Giulia Zanderighi. 'On the excess in the inclusive $W^+W^- \to l^+l^-\nu\overline{\nu}$ cross section'. In: *JHEP* 05 (2015), p. 013. DOI: 10.1007/JHEP05(2015)013. arXiv: 1410.4745 [hep-ph].

[122] Thomas Becher et al. 'Automated NNLL + NLO resummation for jet-veto cross sections'. In: *Eur. Phys. J.* C75.4 (2015), p. 154. DOI: 10.1140/epjc/s10052-015-3368-y. arXiv: 1412.8408 [hep-ph].

[123] Emanuele Re, Marius Wiesemann and Giulia Zanderighi. 'NNLOPS accurate predictions for W^+W^- production'. In: *JHEP* 12 (2018), p. 121. DOI: 10.1007/JHEP12(2018)121. arXiv: 1805.09857 [hep-ph].

[124] Prerit Jaiswal, Patrick Meade and Harikrishnan Ramani. 'Precision diboson measurements and the interplay of pT and jet-veto resummations'. In: *Phys. Rev.* D93.9 (2016), p. 093007. DOI: 10.1103/PhysRevD.93.093007. arXiv: 1509.07118 [hep-ph].

[125] Johannes Bellm et al. 'Anomalous coupling, top-mass and parton-shower effects in W^+W^- production'. In: *JHEP* 05 (2016), p. 106. DOI: 10.1007/JHEP05(2016)106. arXiv: 1602.05141 [hep-ph].

[126] Ian Moult and Iain W. Stewart. 'Jet Vetoes interfering with $H \to WW$'. In: *JHEP* 09 (2014), p. 129. DOI: 10.1007/JHEP09(2014)129. arXiv: 1405.5534 [hep-ph].

[127] Georges Aad et al. 'Measurement of the transverse momentum and ϕ^*_η distributions of Drell–Yan lepton pairs in proton–proton collisions at $\sqrt{s} = 8$ TeV with the ATLAS detector'. In: *Eur. Phys. J.* C76.5 (2016), p. 291. DOI: 10.1140/epjc/s10052-016-4070-4. arXiv: 1512.02192 [hep-ex].

[128] Thomas Becher, Matthias Neubert and Lorena Rothen. 'Factorization and N^3LL_p+NNLO predictions for the Higgs cross section with a jet veto'. In: *JHEP* 10 (2013), p. 125. DOI: 10.1007/JHEP10(2013)125. arXiv: 1307.0025 [hep-ph].

[129] Iain W. Stewart et al. 'Jet p_T resummation in Higgs production at $NNLL' + NNLO$'. In: *Phys. Rev.* D89.5 (2014), p. 054001. DOI: 10.1103/PhysRevD.89.054001. arXiv: 1307.1808 [hep-ph].

[130] https://jetvheto.hepforge.org/.

[131] Benjamin Fuks and Richard Ruiz. 'A comprehensive framework for studying W' and Z' bosons at hadron colliders with automated jet veto resummation'. In: *JHEP* 05 (2017), p. 032. DOI: 10.1007/JHEP05(2017)032. arXiv: 1701.05263 [hep-ph].

[132] Stefano Catani and Massimiliano Grazzini. 'QCD transverse-momentum resummation in gluon fusion processes'. In: *Nucl. Phys.* B845 (2011), pp. 297–323. DOI: 10.1016/j.nuclphysb.2010.12.007. arXiv: 1011.3918 [hep-ph].

[133] Available on request.

[134] https://mcfm.fnal.gov/.

[135] The ATLAS collaboration. 'Measurement of the W^+W^- production cross section in proton-proton collisions at $\sqrt{s} = 8$ TeV with the ATLAS detector'. In: (2014).

[136] John M. Campbell and Francesco Tramontano. 'Next-to-leading order corrections to Wt production and decay'. In: *Nucl. Phys.* B726 (2005), pp. 109–130. DOI: 10.1016/j.nuclphysb.2005.08.015. arXiv: hep-ph/0506289 [hep-ph].

[137] Jon Butterworth et al. 'PDF4LHC recommendations for LHC Run II'. In: *J. Phys.* G43 (2016), p. 023001. DOI: 10.1088/0954-3899/43/2/023001. arXiv: 1510.03865 [hep-ph].

[138] Andy Buckley et al. 'LHAPDF6: parton density access in the LHC precision era'. In: *Eur. Phys. J.* C75 (2015), p. 132. DOI: 10.1140/epjc/s10052-015-3318-8. arXiv: 1412.7420 [hep-ph].

[139] S. Dittmaier et al. 'Handbook of LHC Higgs Cross Sections: 1. Inclusive Observables'. In: (2011). DOI: 10.5170/CERN-2011-002. arXiv: 1101.0593 [hep-ph].

[140] Andrea Banfi et al. 'Jet-vetoed Higgs cross section in gluon fusion at N^{3}LO+NNLL with small-R resummation'. In: *JHEP* 04 (2016), p. 049. DOI: 10.1007/JHEP04(2016)049. arXiv: 1511.02886 [hep-ph].

[141] Christophe Grojean et al. 'Very boosted Higgs in gluon fusion'. In: *JHEP* 05 (2014), p. 022. DOI: 10.1007/JHEP05(2014)022. arXiv: 1312.3317 [hep-ph].

[142] Georges Aad et al. 'Search for the Standard Model Higgs boson in the $H \to$ WW(*) $\to \ell\nu\ell\nu$ decay mode with 4.7 fb of ATLAS data at $\sqrt{s} = 7$ TeV'. In: *Phys. Lett.* B716 (2012), pp. 62–81. DOI: 10.1016/j.physletb.2012.08.010. arXiv: 1206.0756 [hep-ex].

[143] Serguei Chatrchyan et al. 'Search for the standard model Higgs boson decaying to W^+W^- in the fully leptonic final state in pp collisions at $\sqrt{s} = 7$ TeV'. In: *Phys. Lett.* B710 (2012), pp. 91–113. DOI: 10.1016/j.physletb.2012.02.076. arXiv: 1202.1489 [hep-ex].

[144] David L. Rainwater and D. Zeppenfeld. 'Observing $H \to W^*W^* \to e^\pm\mu\mp \not{p}_T$ in weak boson fusion with dual forward jet tagging at the CERN LHC'. In: *Phys. Rev.* D60 (1999). [Erratum: Phys. Rev.D61,099901(2000)], p. 113004. DOI: 10.1103/PhysRevD.61.099901,10.1103/PhysRevD.60.113004. arXiv: hep-ph/9906218 [hep-ph].

[145] Simone Alioli et al. 'A general framework for implementing NLO calculations in shower Monte Carlo programs: the POWHEG BOX'. In: *JHEP* 06 (2010), p. 043. DOI: 10.1007/JHEP06(2010)043. arXiv: 1002.2581 [hep-ph].

[146] Stefano Frixione, Paolo Nason and Carlo Oleari. 'Matching NLO QCD computations with Parton Shower simulations: the POWHEG method'. In: *JHEP* 11 (2007), p. 070. DOI: 10.1088/1126-6708/2007/11/070. arXiv: 0709.2092 [hep-ph].

[147] Paolo Nason. 'A New method for combining NLO QCD with shower Monte Carlo algorithms'. In: *JHEP* 11 (2004), p. 040. DOI: 10.1088/1126-6708/2004/11/040. arXiv: hep-ph/0409146 [hep-ph].

[148] Paolo Nason and Giulia Zanderighi. 'W^+W^- , WZ and ZZ production in the POWHEG-BOX-V2'. In: *Eur. Phys. J.* C74.1 (2014), p. 2702. DOI: 10.1140/epjc/s10052-013-2702-5. arXiv: 1311.1365 [hep-ph].

[149] Torbjörn Sjöstrand et al. 'An Introduction to PYTHIA 8.2'. In: *Comput. Phys. Commun.* 191 (2015), pp. 159–177. DOI: 10.1016/j.cpc.2015.01.024. arXiv: 1410.3012 [hep-ph].

[150] J. Alwall et al. 'The automated computation of tree-level and next-to-leading order differential cross sections, and their matching to parton shower simulations'. In: *JHEP* 07 (2014), p. 079. DOI: 10.1007/JHEP07(2014)079. arXiv: 1405.0301 [hep-ph].

[151] Stefano Frixione et al. 'NLO QCD corrections in Herwig++ with MC@NLO'. In: *JHEP* 01 (2011), p. 053. DOI: 10.1007/JHEP01(2011)053. arXiv: 1010.0568 [hep-ph].

[152] Stefano Frixione and Bryan R. Webber. 'Matching NLO QCD computations and parton shower simulations'. In: *JHEP* 06 (2002), p. 029. DOI: 10.1088/1126-6708/2002/06/029. arXiv: hep-ph/0204244 [hep-ph].

[153] S. Frixione. 'A General approach to jet cross-sections in QCD'. In: *Nucl. Phys.* B507 (1997), pp. 295–314. DOI: 10.1016/S0550-3213(97)00574-9. arXiv: hep-ph/9706545 [hep-ph].

[154] S. Frixione, Z. Kunszt and A. Signer. 'Three jet cross-sections to next-to-leading order'. In: *Nucl. Phys.* B467 (1996), pp. 399–442. DOI: 10.1016/0550-3213(96)00110-1. arXiv: hep-ph/9512328 [hep-ph].

[155] M. Bahr et al. 'Herwig++ Physics and Manual'. In: *Eur. Phys. J.* C58 (2008), pp. 639–707. DOI: 10.1140/epjc/s10052-008-0798-9. arXiv: 0803.0883 [hep-ph].

[156] Johannes Bellm et al. 'Herwig 7.0/Herwig++ 3.0 release note'. In: *Eur. Phys. J.* C76.4 (2016), p. 196. DOI: 10.1140/epjc/s10052-016-4018-8. arXiv: 1512.01178 [hep-ph].

[157] Hung-Liang Lai et al. 'New parton distributions for collider physics'. In: *Phys. Rev.* D82 (2010), p. 074024. DOI: 10.1103/PhysRevD.82.074024. arXiv: 1007.2241 [hep-ph].

[158] J. Pumplin et al. 'New generation of parton distributions with uncertainties from global QCD analysis'. In: *JHEP* 07 (2002), p. 012. DOI: 10.1088/1126-6708/2002/07/012. arXiv: hep-ph/0201195 [hep-ph].

[159] Andrea Banfi, Gavin P. Salam and Giulia Zanderighi. 'Resummed event shapes at hadron - hadron colliders'. In: *JHEP* 08 (2004), p. 062. DOI: 10.1088/1126-6708/2004/08/062. arXiv: hep-ph/0407287 [hep-ph].

[160] M. Dasgupta and G. P. Salam. 'Resummation of nonglobal QCD observables'. In: *Phys. Lett.* B512 (2001), pp. 323–330. DOI: 10.1016/S0370-2693(01)00725-0. arXiv: hep-ph/0104277 [hep-ph].

[161] Johannes K. L. Michel, Piotr Pietrulewicz and Frank J. Tackmann. 'Jet Veto Resummation with Jet Rapidity Cuts'. In: *JHEP* 04 (2019), p. 142. DOI: 10.1007/JHEP04(2019)142. arXiv: 1810.12911 [hep-ph].

[162] F. Cascioli et al. 'ZZ production at hadron colliders in NNLO QCD'. In: *Phys. Lett.* B735 (2014), pp. 311–313. DOI: 10.1016/j.physletb.2014.06.056. arXiv: 1405.2219 [hep-ph].

[163] Massimiliano Grazzini, Stefan Kallweit and Dirk Rathlev. 'ZZ production at the LHC: fiducial cross sections and distributions in NNLO QCD'. In: *Phys. Lett.* B750 (2015), pp. 407–410. DOI: 10.1016/j.physletb.2015.09.055. arXiv: 1507.06257 [hep-ph].

[164] Stefan Kallweit and Marius Wiesemann. 'ZZ production at the LHC: NNLO predictions for $2\ell 2\nu$ and 4ℓ signatures'. In: *Phys. Lett.* B786 (2018), pp. 382–389. DOI: 10.1016/j.physletb.2018.10.016. arXiv: 1806.05941 [hep-ph].

[165] T. Gehrmann et al. 'W^+W^- Production at Hadron Colliders in Next to Next to Leading Order QCD'. In: *Phys. Rev. Lett.* 113.21 (2014), p. 212001. DOI: 10.1103/PhysRevLett.113.212001. arXiv: 1408.5243 [hep-ph].

[166] Massimiliano Grazzini et al. 'W^+W^- production at the LHC: fiducial cross sections and distributions in NNLO QCD'. In: *JHEP* 08 (2016), p. 140. DOI: 10.1007/JHEP08(2016)140. arXiv: 1605.02716 [hep-ph].

[167] Fabrizio Caola et al. 'Two-loop helicity amplitudes for the production of two off-shell electroweak bosons in gluon fusion'. In: *JHEP* 06 (2015), p. 129. DOI: 10.1007/JHEP06(2015)129. arXiv: 1503.08759 [hep-ph].

[168] Andreas von Manteuffel and Lorenzo Tancredi. 'The two-loop helicity amplitudes for $gg \to V_1V_2 \to 4$ leptons'. In: *JHEP* 06 (2015), p. 197. DOI: 10.1007/JHEP06(2015)197. arXiv: 1503.08835 [hep-ph].

[169] Fabrizio Caola et al. 'QCD corrections to ZZ production in gluon fusion at the LHC'. In: *Phys. Rev.* D92.9 (2015), p. 094028. DOI: 10.1103/PhysRevD.92.094028. arXiv: 1509.06734 [hep-ph].

[170] Fabrizio Caola et al. 'QCD corrections to W^+W^- production through gluon fusion'. In: *Phys. Lett.* B754 (2016), pp. 275–280. DOI: 10.1016/j.physletb.2016.01.046. arXiv: 1511.08617 [hep-ph].

[171] Fabrizio Caola et al. 'QCD corrections to vector boson pair production in gluon fusion including interference effects with off-shell Higgs at the LHC'. In: *JHEP* 07 (2016), p. 087. DOI: 10.1007/JHEP07(2016)087. arXiv: 1605.04610 [hep-ph].

[172] John M. Campbell et al. 'Two loop correction to interference in $gg \to ZZ$'. In: *JHEP* 08 (2016), p. 011. DOI: 10.1007/JHEP08(2016)011. arXiv: 1605.01380 [hep-ph].

[173] Massimiliano Grazzini et al. 'ZZ production at the LHC: NLO QCD corrections to the loop-induced gluon fusion channel'. In: *JHEP* 03 (2019), p. 070. DOI: 10.1007/JHEP03(2019)070. arXiv: 1811.09593 [hep-ph].

[174] Massimiliano Grazzini, Stefan Kallweit and Marius Wiesemann. 'Fully differential NNLO computations with MATRIX'. In: *Eur. Phys. J.* C78.7 (2018), p. 537. DOI: 10.1140/epjc/s10052-018-5771-7. arXiv: 1711.06631 [hep-ph].

[175] Massimiliano Grazzini et al. '$W^\pm Z$ production at hadron colliders in NNLO QCD'. In: *Phys. Lett.* B761 (2016), pp. 179–183. DOI: 10.1016/j.physletb.2016.08.017. arXiv: 1604.08576 [hep-ph].

[176] Massimiliano Grazzini et al. '$W^\pm Z$ production at the LHC: fiducial cross sections and distributions in NNLO QCD'. In: *JHEP* 05 (2017), p. 139. DOI: 10.1007/JHEP05(2017)139. arXiv: 1703.09065 [hep-ph].

[177] Vardan Khachatryan et al. 'Measurement of differential and integrated fiducial cross sections for Higgs boson production in the four-lepton decay channel in pp collisions at $\sqrt{s} = 7$ and 8 TeV'. In: *JHEP* 04 (2016), p. 005. DOI: 10.1007/JHEP04(2016)005. arXiv: 1512.08377 [hep-ex].

[178] Andreas Hocker et al. 'A New approach to a global fit of the CKM matrix'. In: *Eur. Phys. J.* C21 (2001), pp. 225–259. DOI: 10.1007/s100520100729. arXiv: hep-ph/0104062 [hep-ph].

[179] Glen Cowan et al. 'Asymptotic formulae for likelihood-based tests of new physics'. In: *Eur. Phys. J.* C71 (2011). [Erratum: Eur. Phys. J.C73,2501(2013)], p. 1554. DOI: 10.1140/epjc/s10052-011-1554-0,10.1140/epjc/s10052-013-2501-z. arXiv: 1007.1727 [physics.data-an].

[180] The ATLAS collaboration. 'Combined measurements of Higgs boson production and decay using up to 80 fb^{-1} of proton–proton collision data at $\sqrt{s} = 13$ TeV collected with the ATLAS experiment'. In: (2018).

[181] R. Keith Ellis, W. James Stirling and B. R. Webber. 'QCD and collider physics'. In: *Camb. Monogr. Part. Phys. Nucl. Phys. Cosmol.* 8 (1996), pp. 1–435.

[182] Michael E. Peskin and Daniel V. Schroeder. *An Introduction to quantum field theory*. Reading, USA: Addison-Wesley, 1995. ISBN: 9780201503975. URL: http://www.slac.stanford.edu/~mpeskin/QFT.html.

[183] Howard Georgi. 'Lie algebras in particle physics'. In: *Front. Phys.* 54 (1999), pp. 1–320.

[184] Matthew D. Schwartz. *Quantum Field Theory and the Standard Model*. Cambridge University Press, 2014. ISBN: 9781107034730. URL: http://www.cambridge.org/us/academic/subjects/physics/theoretical-physics-and-mathematical-physics/quantum-field-theory-and-standard-model.

[185] N. Brown and W. James Stirling. 'Finding jets and summing soft gluons: A New algorithm'. In: *Z. Phys.* C53 (1992), pp. 629–636. DOI: 10.1007/BF01559740.

[186] John M. Campbell and R. Keith Ellis. 'Radiative corrections to Z b anti-b production'. In: *Phys. Rev.* D62 (2000), p. 114012. DOI: 10.1103/PhysRevD.62.114012. arXiv: hep-ph/0006304 [hep-ph].

Appendix A

The $SU(N_c)$ Lie Algebra

The $SU(N_c)$ Lie group can be represented by $N_c \times N_c$ complex unitary matrices $\mathbf{U}$, meaning that $\mathbf{U}$ must satisfy $\mathbf{U}^\dagger\mathbf{U} = \mathbf{I}$ and $\det \mathbf{U} = 1$ where $\mathbf{I}$ is the identity matrix. An infinitesimal group element $\mathbf{U}(\vec{\theta})$ can be written as

$$\mathbf{U}(\vec{\theta}) = \mathbf{I} + i\theta^A T^A + \mathcal{O}(\theta^2)\,, \tag{A.1}$$

where we adopt the convention that $\mathbf{U}(\vec{0}) = \mathbf{I}$, θ^A are the parameters of the transformation and the set of matrices T^A are called the *generators* of the Lie group. The vector space, $\mathfrak{su}(N_c)$, spanned by the generators is referred to as a *Lie algebra*[1]. We can construct the elements of the Lie group from the Lie algebra by making use of the *exponential map*

$$\mathbf{U}(\vec{\theta}) = \exp\left(i\theta^A T^A\right)\,. \tag{A.2}$$

For a finite dimensional representation, the generators of $\mathfrak{su}(N_c)$ are a set of traceless Hermitian matrices. For a generic representation of $\mathfrak{su}(N_c)$ we will denote the generators by the matrix T_r^A. The generators satisfy the Lie bracket

$$[T_r^A, T_r^B] = if^{ABC}T_r^C\,, \tag{A.3}$$

where f^{ABC} are the *structure constants* of the Lie algebra. The structure constants are unique to a given Lie algebra, irrespective of the chosen representation of the generators. The uppercase indices run over $A, B, \ldots = \{1, \ldots, N_c^2 - 1\}$. The Lie bracket of Eq. (A.3) must also satisfy the *Jacobi identity*

$$[T_r^A, [T_r^B, T_r^C]] + [T_r^B, [T_r^C, T_r^A]] + [T_r^C, [T_r^A, T_r^B]] = 0\,. \tag{A.4}$$

[1] Strictly a Lie algebra is a vector space $\mathfrak{g}$, together with a Lie bracket that satisfies the Jacobi identity. So really, on its own, $\mathfrak{su}(N_c)$ is just a vector space.

However, in our case, we are only interested in two specific representations, the so called *fundamental* (or defining representation) and the *adjoint* representation. These representations correspond to the quarks and gluons respectively. For these specific representations of $\mathfrak{su}(N_c)$, we denote the generators by the matrices $(t^A)_{bc}$ and $(T^A)_{BC}$ for the fundamental and the adjoint respectively. Here we make the connection between the case of the indices and the associated representations. Uppercase indices are associated with the adjoint and lowercase indices are associated with the fundamental and run over $a, b, \ldots = \{1, \ldots, N_c\}$.

The generators of the fundamental representation, t^A are provided by the eight Gell-Mann matrices, $t^A = \frac{1}{2}\lambda^A$. And we construct the generators of the adjoint representation from the structure constants, $(T^A)_{BC} = -if^{ABC}$. The conventional normalisation for the generators of $\mathfrak{su}(N_c)$ is chosen to be

$$\mathrm{Tr}\left(t^A t^B\right) = T_R\,\delta^{AB}\,, \quad T_R = \frac{1}{2}\,. \tag{A.5}$$

Certain combinations of generators can yield quantities that are invariant under the action of the Lie algebra. The simplest, and most useful of these comes from considering an operator $T_r^2 \equiv T_r^A T_r^A$. This operator is an invariant and so it commutes with all the generators of the Lie algebra, it is therefore proportional to the identity. We then write this operator as $T_r^2 = C_r\mathbf{I}$, where C_r is the *quadratic Casimir*. For the fundamental and adjoint representations we have

$$(t^A)_{ab}(t^A)_{bc} = C_F\,\delta_{ac}\,, \qquad \text{with} \qquad C_F = \frac{N_c^2 - 1}{2N_c}\,, \tag{A.6}$$

$$(T^A)_{BC}(T^A)_{CD} = C_A\,\delta_{BD}\,, \qquad \text{with} \qquad C_A = N_c\,. \tag{A.7}$$

This is all of the background on Lie groups and Lie algebras that is necessary to construct the theory of the strong force. A more pedagogical review on the application of Lie groups and Lie algebras to elementary particle physics can be found in any of the standard textbooks on QFT, for example Refs. [181–184].

Appendix B

The QCD Feynman Rules

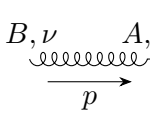

$$= i\frac{-g^{\mu\nu} + (1-\xi)\frac{p^\mu p^\nu}{p^2}}{p^2 + i\epsilon}\delta^{AB} \tag{B.1}$$

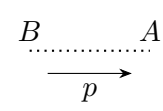

$$= \frac{i\delta^{AB}}{p^2 + i\epsilon} \tag{B.2}$$

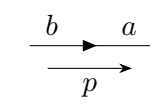

$$= \frac{i\delta^{ab}}{\not{p} - m + i\epsilon} \tag{B.3}$$

$$\Gamma^A_\mu = \qquad = -ig_s(t^A)_{bc}\gamma_\mu \tag{B.4}$$

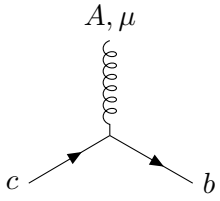

$$\Gamma^{ABC}_{\mu\nu\rho}(p,q,r) = \qquad = -ig_s(T^A)_{BC}V_{\mu\nu\rho}(p,q,r) \tag{B.5}$$

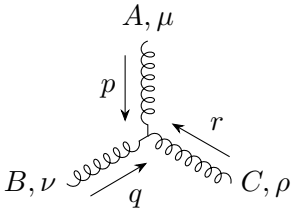

$$\Gamma^{ABCD}_{\mu\nu\rho\sigma} = \qquad = -ig_s^2 \begin{bmatrix} +f^{EAC}f^{EBD}(g_{\mu\nu}g_{\rho\sigma} - g_{\mu\sigma}g_{\nu\rho}) \\ +f^{EAD}f^{EBC}(g_{\mu\nu}g_{\rho\sigma} - g_{\mu\rho}g_{\nu\sigma}) \\ +f^{EAB}f^{ECD}(g_{\mu\rho}g_{\nu\sigma} - g_{\mu\sigma}g_{\nu\rho}) \end{bmatrix} \tag{B.6}$$

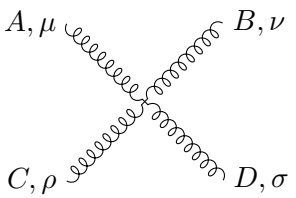

$$\Gamma^{ABC}_\mu = \qquad = -ig_s(T^A)_{BC}r_\mu \tag{B.7}$$

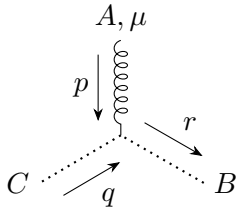

$$V_{\mu\nu\rho}(p,q,r) = (p-q)_\rho\, g_{\mu\nu} + (q-r)_\mu\, g_{\nu\rho} + (r-p)_\nu\, g_{\mu\rho}\,, \quad p+q+r = 0\,. \tag{B.8}$$

Appendix C

Resummation coefficients

C.1 Radiator

The renormalisation group equation for the QCD coupling constant is

$$\frac{\mathrm{d}\alpha_s(\mu^2)}{\mathrm{d}\log\mu^2} = -\alpha_s^2(\mu^2)\sum_{n=0}^{\infty}\beta_n\alpha_s^n(\mu^2)\,, \tag{C.1}$$

where the coefficients of $\beta(\alpha_s)$ are given by

$$\beta_0 = \frac{11C_A - 4T_R n_F}{12\pi}\,, \tag{C.2}$$

$$\beta_1 = \frac{17C_A - T_R n_F(10C_A + 6C_F)}{24\pi^2}\,, \tag{C.3}$$

$$\beta_2 = \frac{2857C_A^3 + 2T_R n_F(54C_F^2 - 615C_F C_A - 1415C_A^2) + (2T_R n_F)^2(66C_F + 79C_A)}{3456\pi^3}\,. \tag{C.4}$$

The physical coupling $\alpha_s^{\text{phys.}}$ is related to the $\overline{\text{MS}}$ coupling $\alpha_s^{\overline{\text{MS}}}$ as follows

$$\alpha_s^{\text{phys.}} = \alpha_s^{\overline{\text{MS}}}\left(1 + \sum_{n=1}^{\infty}\left(\frac{\alpha_s^{\overline{\text{MS}}}}{2\pi}\right)^n K^{(n)}\right)\,, \tag{C.5}$$

where the set of coefficients $K^{(n)}$ are given by

$$K^{(1)} = C_A\left(\frac{67}{18} - \frac{\pi^2}{6}\right) - \frac{10}{9}T_R n_F\,, \tag{C.6}$$

$$\begin{aligned} K^{(2)} = {} & C_A^2\left(\frac{245}{24} - \frac{67}{9}\zeta_2 + \frac{11}{6}\zeta_3 + \frac{11}{5}\zeta_2^2\right) + 2T_R n_F C_F\left(-\frac{55}{24} + 2\zeta_3\right) \\ & + C_A T_R n_F\left(-\frac{209}{54} + \frac{20}{9}\zeta_2 - \frac{14}{3}\zeta_3\right) - \frac{4}{27}(T_R n_F)^2 \\ & + \frac{\pi\beta_0}{2}\left(C_A\left(\frac{808}{27} - 28\zeta_3\right) - 2T_R n_F\frac{224}{54}\right)\,. \end{aligned} \tag{C.7}$$

Minus the coefficient of $\delta(1-x)$ in the AP splitting functions is given by

$$\gamma_q^{(0)} = -\frac{3}{2}C_F\,, \tag{C.8}$$

$$\gamma_g^{(0)} = -2\pi\beta_0\,, \tag{C.9}$$

$$\begin{aligned}\gamma_q^{(1)} = -\frac{C_F}{2}\Bigg(&C_F\left(\frac{4}{3}-\pi^2+12\zeta_3\right)+C_A\left(\frac{17}{12}+\frac{11\pi^2}{9}-6\zeta_3\right)\\&-2T_R n_F\left(\frac{1}{6}+\frac{2\pi^2}{9}\right)\Bigg)\,,\end{aligned} \tag{C.10}$$

$$\gamma_g^{(1)} = 2T_R n_F\left(\frac{1}{2}C_F+\frac{2}{3}C_A\right)-C_A^2\left(\frac{8}{3}+3\zeta_3\right)\,. \tag{C.11}$$

The massless radiator r_ℓ^0 is composed of the $g_i^{(\ell)}$ functions that are defined in Eq. (4.101), and the massive radiator δr_ℓ is determined solely by $\delta g^{(\ell)}$. Their explicit expressions are given by

$$g_1^{(\ell)}(\lambda) = \frac{1}{2}\frac{(a+b_\ell-2\lambda)\log\left(1-\frac{2\lambda}{a+b_\ell}\right)-(a-2\lambda)\log\left(1-\frac{2\lambda}{a}\right)}{\pi b_\ell\beta_0\lambda}\,, \tag{C.12}$$

$$\begin{aligned}g_2^{(\ell)}(\lambda) = \frac{1}{2}\Bigg[&\frac{K^{(1)}\left(a\log\left(1-\frac{2\lambda}{a}\right)-(a+b_\ell)\log\left(1-\frac{2\lambda}{a+b_\ell}\right)\right)}{2\pi^2 b_\ell\beta_0^2}\\&+\frac{\beta_1(a+b_\ell)\log^2\left(1-\frac{2\lambda}{a+b_\ell}\right)}{2\pi b_\ell\beta_0^3}+\frac{\beta_1(a+b_\ell)\log\left(1-\frac{2\lambda}{a+b_\ell}\right)}{\pi b_\ell\beta_0^3}\\&-\beta_1\frac{a\log\left(1-\frac{2\lambda}{a}\right)\left(\log\left(1-\frac{2\lambda}{a}\right)+2\right)}{2\pi b_\ell\beta_0^3}\Bigg]\,,\end{aligned} \tag{C.13}$$

$$\begin{aligned}g_3^{(\ell)}(\lambda) = \frac{1}{2}\Bigg[&K^{(1)}\frac{\beta_1\left(a^2(a+b_\ell+2\lambda)\log\left(1-\frac{2\lambda}{a}\right)-(a+b_\ell)^2(a-2\lambda)\log\left(1-\frac{2\lambda}{a+b_\ell}\right)+6b_\ell\lambda^2\right)}{2\pi b_\ell\beta_0^3(a-2\lambda)(a+b_\ell-2\lambda)}\\&+\frac{\left(\beta_1^2(a+b_\ell)^2(a-2\lambda)\log^2\left(1-\frac{2\lambda}{a+b_\ell}\right)-4b_\ell\lambda^2\left(\beta_0\beta_2+\beta_1^2\right)\right)}{2b_\ell\beta_0^4(a-2\lambda)(a+b_\ell-2\lambda)}\\&-\frac{a\log\left(1-\frac{2\lambda}{a}\right)\left(2\beta_0\beta_2(a-2\lambda)+a\beta_1^2\log\left(1-\frac{2\lambda}{a}\right)+4\beta_1^2\lambda\right)}{2b_\ell\beta_0^4(a-2\lambda)}\\&+\frac{(a+b_\ell)\log\left(1-\frac{2\lambda}{a+b_\ell}\right)\left(\beta_0\beta_2(a+b_\ell-2\lambda)+2\beta_1^2\lambda\right)}{b_\ell\beta_0^4(a+b_\ell-2\lambda)}\\&-K^{(2)}\frac{2\lambda^2}{4\pi^2(a-2\lambda)(a+b_\ell-2\lambda)\beta_0^2}\Bigg]\,,\end{aligned} \tag{C.14}$$

$$\delta g_3^{(\ell)}(\lambda) = -\zeta_2\frac{\lambda}{(a+b_\ell-2\lambda)}\,, \tag{C.15}$$

note that compared to the functions defined in Ref. [61], we have stripped away the colour factor.

Similarly we provide explicit expressions for the derivative of the soft radiator

$$r'_{\mathrm{NLL},\ell}(\lambda) = \frac{1}{b_\ell \pi \beta_0}\left(\log\left(1-\frac{2\lambda}{a+b_\ell}\right)-\log\left(1-\frac{2\lambda}{a}\right)\right), \tag{C.16}$$

$$\begin{aligned} r'_{\mathrm{NNLL},\ell}(\lambda) = \frac{\alpha_s(Q)}{b_\ell \pi^2 \beta_0^2 (a-2\lambda)(a+b_\ell-2\lambda)}\Bigg[& b_\ell \beta_0 \lambda K^{(1)} - 2\pi b_\ell \beta_1 \lambda \\ & - \pi a (a+b_\ell-2\lambda)\beta_1 \ln\left(1-\frac{2\lambda}{a}\right) \\ & + \pi (a+b_\ell)(a-2\lambda)\beta_1 \ln\left(1-\frac{2\lambda}{a+b_\ell}\right)\Bigg], \end{aligned} \tag{C.17}$$

$$r''_{\mathrm{NNLL},\ell}(\lambda) = \frac{\alpha_s(Q)}{\pi}\frac{2}{(a-2\lambda)(a+b_\ell-2\lambda)}. \tag{C.18}$$

We note that we can build the derivatives of the radiator for each leg by restoring the colour factors

$$R'_{\mathrm{NLL},\ell}(\lambda) = C_\ell\, r'_{\mathrm{NLL},\ell}(\lambda), \tag{C.19}$$

$$R'_{\mathrm{NNLL},\ell}(\lambda) = C_\ell\, r'_{\mathrm{NNLL},\ell}(\lambda), \tag{C.20}$$

$$R''_{\mathrm{NNLL},\ell}(\lambda) = C_\ell\, r''_{\mathrm{NNLL},\ell}(\lambda). \tag{C.21}$$

The hard-collinear radiator is composed of $h_i^{(\ell)}$ functions that are defined in Eq. (4.103). Their explicit expressions are given by

$$h_2^{(\ell)}(\lambda) = \frac{\gamma_\ell^{(0)}}{2\pi\beta_0}\log\left(1-\frac{2\lambda}{a+b_\ell}\right), \tag{C.22}$$

$$h_3^{(\ell)}(\lambda) = \gamma_\ell^{(0)}\frac{\beta_1\left((a+b_\ell)\left(\log\left(1-\frac{2\lambda}{a+b_\ell}\right)\right)+2\lambda\right)}{2\beta_0^2\,(a+b_\ell-2\lambda)} - \gamma_\ell^{(1)}\frac{\lambda}{2\pi\beta_0(a+b_\ell-2\lambda)}. \tag{C.23}$$

C.2 Scale variations

To vary the renormalisation scale we must expand all of the terms in the radiator, which are functions of $\lambda = \alpha_s(Q)\beta_0 \log\frac{1}{v}$, around $\bar{\lambda} = \alpha_s(\mu_R)\beta_0\log\frac{1}{v}$. Keeping terms only up to NNLL accuracy we find that in the soft radiator we must make the following replacements for the $g_i^{(\ell)}$ functions

$$g_1(\lambda) \to g_1(\bar{\lambda}, \mu_R^2) = g_1(\bar{\lambda}), \tag{C.24}$$

$$g_2(\lambda) \to g_2(\bar{\lambda}, \mu_R^2) = g_2(\bar{\lambda}) + \bar{\lambda}^2 g_1'(\bar{\lambda}) \log\frac{\mu_R^2}{Q^2}, \tag{C.25}$$

$$\begin{aligned} g_3(\lambda) \to g_3(\bar{\lambda}, \mu_R^2) = g_3(\bar{\lambda}) & + \pi\left(\beta_0\bar{\lambda} g_2'(\bar{\lambda}) + \frac{\beta_1}{\beta_0}\bar{\lambda}^2 g_1'(\bar{\lambda})\log\frac{\mu_R^2}{Q^2}\right) \\ & + \pi\left(\beta_0\bar{\lambda}^2 g_1'(\bar{\lambda}) + \frac{\beta_0}{2}\bar{\lambda}^3 g_1''(\bar{\lambda})\right)\log^2\frac{\mu_R^2}{Q^2}. \end{aligned} \tag{C.26}$$

For the derivative terms that appear in the soft radiator, we must make the following replacements

$$r'_{\mathrm{NLL},\ell}(\lambda) \to r'_{\mathrm{NLL},\ell}(\bar{\lambda},\mu_R^2) = r'_{\mathrm{NLL},\ell}(\bar{\lambda})\,, \tag{C.27}$$

$$r'_{\mathrm{NNLL},\ell}(\lambda) \to r'_{\mathrm{NNLL},\ell}(\bar{\lambda},\mu_R^2) = r'_{\mathrm{NNLL},\ell}(\bar{\lambda}) + \bar{\lambda} r''_{\mathrm{NNLL},\ell}(\bar{\lambda}) \log\frac{\mu_R^2}{Q^2}\,, \tag{C.28}$$

$$r''_{\mathrm{NNLL},\ell}(\lambda) \to r''_{\mathrm{NNLL},\ell}(\bar{\lambda},\mu_R^2) = r''_{\mathrm{NNLL},\ell}(\bar{\lambda})\,. \tag{C.29}$$

For the hard-collinear radiator we must make the following replacements

$$h_2(\lambda) \to h_2(\bar{\lambda},\mu_R^2) = h_2(\bar{\lambda})\,, \tag{C.30}$$

$$h_3(\lambda) \to h_3(\bar{\lambda},\mu_R^2) = h_3(\bar{\lambda}) + \pi\beta_0\bar{\lambda}h'_2(\bar{\lambda}) \log\frac{\mu_R^2}{Q^2}\,. \tag{C.31}$$

Note that the ratio $\log\mu_R^2/Q^2$ is a feature of using λ and $\bar{\lambda}$, if we were to use λ_{ij} we would pick up a term $\log\mu_R^2/Q_{ij}^2$ instead.

Similar to the variation of μ_R we would also like to probe the dependence of the observable on x_V. We must perform similar set of replacements as we did for the renormalisation scale. This time we wish to expand $\lambda = \alpha_s(Q)\beta_0\log\frac{1}{v}$ around $\hat{\lambda} = \alpha_s(Q)\beta_0\log\frac{x_V}{v}$. Keeping terms only up to NNLL accuracy we find that in the soft radiator we must make the following replacements for the $g_i^{(\ell)}$ functions

$$g_1(\lambda) \to g_1(\hat{\lambda},x_V) = g_1(\hat{\lambda})\,, \tag{C.32}$$

$$g_2(\lambda) \to g_2(\hat{\lambda},x_V) = g_2(\hat{\lambda}) + \Big(g_1(\hat{\lambda}) + \hat{\lambda}g'_1(\hat{\lambda})\Big)\,(-\log x_V)\,, \tag{C.33}$$

$$\begin{aligned} g_3(\lambda) \to g_3(\hat{\lambda},x_V) &= g_3(\hat{\lambda}) + \pi\beta_0 g'_2(\hat{\lambda})\,(-\log x_V) \\ &\quad - \pi\beta_0\left(g'_1(\hat{\lambda}) + \frac{1}{2}g''_1(\hat{\lambda})\right)(-\log x_V)^2\,. \end{aligned} \tag{C.34}$$

For the derivative terms that appear in the soft radiator, we must make the following replacements

$$r'_{\mathrm{NLL},\ell}(\lambda) \to r'_{\mathrm{NLL},\ell}(\hat{\lambda},x_V) = r'_{\mathrm{NLL},\ell}(\hat{\lambda})\,, \tag{C.35}$$

$$r'_{\mathrm{NNLL},\ell}(\lambda) \to r'_{\mathrm{NNLL},\ell}(\hat{\lambda},x_V) = r'_{\mathrm{NNLL},\ell}(\hat{\lambda}) + r''_{\mathrm{NNLL},\ell}(\hat{\lambda})\,(-\log x_V)\,, \tag{C.36}$$

$$r''_{\mathrm{NNLL},\ell}(\lambda) \to r''_{\mathrm{NNLL},\ell}(\hat{\lambda},x_V) = r''_{\mathrm{NNLL},\ell}(\hat{\lambda})\,. \tag{C.37}$$

For the hard-collinear radiator we must make the following replacements

$$h_2(\lambda) \to h_2(\hat{\lambda},x_V) = h_2(\hat{\lambda})\,, \tag{C.38}$$

$$h_3(\lambda) \to h_3(\hat{\lambda},x_V) = h_3(\hat{\lambda}) + \pi\beta_0 h_2(\hat{\lambda})\,(-\log x_V)\,. \tag{C.39}$$

C.3 Expansion coefficients

$$\begin{aligned}\Sigma_{\rm NNLL}(v) = &\left[\mathcal{F}_{\rm NLL}(\lambda)\left(1+\frac{\alpha_s(Q)}{2\pi}H^{(1)}+\sum_\ell \frac{\alpha_s(v^{\frac{1}{a+b_\ell}}Q)}{2\pi}C^{(1)}_{{\rm hc},\ell}\right)+\frac{\alpha_s(Q)}{\pi}\delta\mathcal{F}_{\rm NNLL}(\lambda)\right]\times\\ &\times\exp\left[\sum_{n=1}^{\infty}\sum_{m=0}^{n+1}\mathscr{G}_{nm}\bar\alpha_s^n L^m\right]\\ =&\sum_{n=1}^{\infty}\sum_{m=0}^{n+1}\mathscr{H}_{nm}\bar\alpha_s^n L^m\,.\end{aligned} \tag{C.40}$$

$$\mathscr{G}_{nm}=\sum_{(ab)}G^{(ab)}_{nm}+\sum_\ell H^{(\ell)}_{nm}\,. \tag{C.41}$$

$$G_{12}=-\sum_{(ab)}C_{ab}\sum_{\ell\in(ab)}\frac{1}{a(a+b_\ell)}\,, \tag{C.42a}$$

$$G_{11}=-\sum_{(ab)}C_{ab}\sum_{\ell\in(ab)}\frac{2}{a(a+b_\ell)}\left\langle\log d_\ell g_\ell\right\rangle\,, \tag{C.42b}$$

$$G_{10}=-\sum_{(ab)}C_{ab}\sum_{\ell\in(ab)}\frac{1}{a(a+b_\ell)}\left\langle\log^2 d_\ell g_\ell\right\rangle\,, \tag{C.42c}$$

$$G_{23}=-\sum_{(ab)}C_{ab}\sum_{\ell\in(ab)}\frac{4\pi\beta_0}{3a^2}\frac{(2a+b_\ell)}{(a+b_\ell)^2}\,, \tag{C.42d}$$

$$\begin{aligned}G_{22}=&-\sum_{(ab)}C_{ab}\sum_{\ell\in(ab)}\frac{4\pi\beta_0}{a^2}\frac{(2a+b_\ell)}{(a+b_\ell)^2}\left\langle\log d_\ell g_\ell\right\rangle\\ &-\sum_{(ab)}C_{ab}\sum_{\ell\in(ab)}\frac{K^{(1)}}{a(a+b_\ell)}\,,\end{aligned} \tag{C.42e}$$

$$\begin{aligned}G_{21}=&-\sum_{(ab)}C_{ab}\sum_{\ell\in(ab)}\frac{\pi^3\beta_0}{3}\frac{1}{a+b_\ell}\\ &-\sum_{(ab)}C_{ab}\sum_{\ell\in(ab)}\frac{2K^{(1)}}{a(a+b_\ell)}\left\langle\log d_\ell g_\ell\right\rangle\\ &-\sum_{(ab)}C_{ab}\sum_{\ell\in(ab)}\frac{4\pi\beta_0}{a^2}\frac{(2a+b_\ell)}{(a+b_\ell)^2}\left\langle\log^2 d_\ell g_\ell\right\rangle\,.\end{aligned} \tag{C.42f}$$

$$H_{12} = 0\,, \tag{C.43a}$$

$$H_{11} = -\sum_{\ell} \frac{2\gamma_\ell^{(0)}}{(a+b_\ell)}\,, \tag{C.43b}$$

$$H_{10} = 0\,, \tag{C.43c}$$

$$H_{23} = 0\,, \tag{C.43d}$$

$$H_{22} = -\sum_{\ell} 4\pi\beta_0 \frac{\gamma_\ell^{(0)}}{(a+b_\ell)^2}\,, \tag{C.43e}$$

$$H_{21} = -\sum_{\ell} \frac{2\gamma_\ell^{(1)}}{a+b_\ell}\,. \tag{C.43f}$$

C.4 Correlated two-parton emission

In the interest of completeness we reproduce Appendix. A of Ref. [61], the definition of the double-soft block and the decomposition of the two-particle phase space into that of a pseudo-parent and internal variables.

We start by decomposing the momenta of the two partons k_a and k_b as in Eq. (4.25). We then introduce relative variables to parameterise the two-parton phase space, as follows

$$\begin{aligned} z_a^{(\ell)} &= z\, z^{(\ell)}\,, \quad z_b^{(\ell)} = (1-z)\, z^{(\ell)}\,, \\ \vec{q}_a &= \frac{\vec{k}_{ta}}{z}\,, \quad \vec{q}_b = \frac{\vec{k}_{tb}}{1-z}\,, \end{aligned} \tag{C.44}$$

in terms of which the Lorentz invariant phase-space in $4-2\epsilon$ dimensions becomes

$$[\mathrm{d}k_a][\mathrm{d}k_b] = \frac{1}{(4\pi)^2}\frac{\mathrm{d}z^{(\ell)}}{z^{(\ell)}}\mathrm{d}z[z(1-z)]^{1-2\epsilon}\frac{\mathrm{d}^{2-2\epsilon}q_a}{(2\pi)^{2-2\epsilon}}\frac{\mathrm{d}^{2-2\epsilon}q_b}{(2\pi)^{2-2\epsilon}}\,. \tag{C.45}$$

Another useful change of variables is

$$\vec{k}_t = \vec{k}_{ta} + \vec{k}_{tb}\,, \qquad \vec{q} = \vec{q}_a - \vec{q}_b\,, \tag{C.46}$$

in terms of which the phase-space becomes

$$[\mathrm{d}k_a][\mathrm{d}k_b] = \frac{1}{(4\pi)^2}\frac{\mathrm{d}z^{(\ell)}}{z^{(\ell)}}\frac{\mathrm{d}^{2-2\epsilon}k_t}{(2\pi)^{2-2\epsilon}}\mathrm{d}z[z(1-z)]^{1-2\epsilon}\frac{\mathrm{d}^{2-2\epsilon}q}{(2\pi)^{2-2\epsilon}} = [\mathrm{d}k]\frac{\mathrm{d}z[z(1-z)]^{1-2\epsilon}}{4\pi}\frac{\mathrm{d}^{2-2\epsilon}q}{(2\pi)^{2-2\epsilon}}\,, \tag{C.47}$$

where we have been able to factor out the phase space $[\mathrm{d}k]$ defined in Eq. (4.37). Last, we can isolate the integration over ϕ, the angle between $\vec{k}_t$ and $\vec{q}$, and introduce

$$m^2 \equiv (k_a+k_b)^2 = z(1-z)q^2\,, \tag{C.48}$$

to obtain yet another expression for the two-body phase space

$$[\mathrm{d}k_a][\mathrm{d}k_b] = [\mathrm{d}k]\frac{\mathrm{d}z[z(1-z)]^{-\epsilon}}{(4\pi)^2}\frac{\mathrm{d}m^2}{(m^2)^\epsilon}\frac{\mathrm{d}\Omega_{2-2\epsilon}}{(2\pi)^{1-2\epsilon}}\,. \tag{C.49}$$

The factor $\mathrm{d}\Omega_{2-2\epsilon}$ is the azimuthal phase space for the vector $\vec{q}$ with respect to $\vec{k}_t$. Explicitly, this is given by

$$\mathrm{d}\Omega_{2-2\epsilon} = \frac{(4\pi)^\epsilon}{\sqrt{\pi}\Gamma(\frac{1}{2}-\epsilon)}\mathrm{d}\phi(\sin^2\phi)^{-\epsilon}\,. \tag{C.50}$$

where the relative angle ϕ in the range $0 < \phi < \pi$.

In terms of these variables, the correlated matrix element $|\widetilde{\mathcal{M}}_{s,0}(k_a,k_b)|^2$ is given by

$$|\widetilde{\mathcal{M}}_{s,0}(k_a,k_b)|^2 = (4\pi\alpha_s\mu_R^{2\epsilon})^2\frac{8C_\ell}{m^2(m^2+k_t^2)}C_{ab}(k_a,k_b)\,, \tag{C.51}$$

where μ_R is the renormalisation scale, C_ℓ is the colour factor associated with the emitting leg, and

$$C_{ab}(k_a,k_b) = C_A(2\mathcal{S}+\mathcal{H}_g) + 2T_R n_F\mathcal{H}_q\,. \tag{C.52}$$

The contribution due to two final-state quarks in Eq. (C.52) has been multiplied by two, to compensate for the overall 1/2! factor. The three functions $\mathcal{S}$, $\mathcal{H}_g$ and $\mathcal{H}_q$ are the $4-2\epsilon$ dimensional counterparts of the homonymous terms defined in Ref. [82]. They depend only on the dimensionless variables z, ϕ and $\mu^2 \equiv m^2/k_t^2$. It is also useful to introduce the rescaled momenta $\vec{u}_i = \vec{q}_i/k_t$, such that

$$u_a^2 = 1 + 2\sqrt{\frac{1-z}{z}}\mu\cos\phi + \frac{1-z}{z}\mu^2\,, \qquad u_b^2 = 1 - 2\sqrt{\frac{z}{1-z}}\mu\cos\phi + \frac{z}{1-z}\mu^2\,. \tag{C.53}$$

In terms of these variables, we have

$$2\mathcal{S} = \frac{1}{z(1-z)}\left[\frac{1-(1-z)\mu^2/z}{u_a^2} + \frac{1-z\mu^2/(1-z)}{u_b^2}\right] \tag{C.54a}$$

$$\begin{aligned}\mathcal{H}_g = {} & -4 + (1-\epsilon)\frac{z(1-z)}{1+\mu^2}\left(2\cos\phi + \frac{(1-2z)\mu}{\sqrt{z(1-z)}}\right)^2 \\ & + \frac{1}{2(1-z)}\left[1 - \frac{1-(1-z)\mu^2/z}{u_a^2}\right] + \frac{1}{2z}\left[1 - \frac{1-z\mu^2/(1-z)}{u_b^2}\right]\end{aligned} \tag{C.54b}$$

$$\mathcal{H}_q = 1 - \frac{z(1-z)}{1+\mu^2}\left(2\cos\phi + \frac{(1-2z)\mu}{\sqrt{z(1-z)}}\right)^2\,. \tag{C.54c}$$

Note that, in the limit $\mu^2 \to 0$, we recover the azimuthally unaveraged splitting functions, in particular

$$2\mathcal{S} + \mathcal{H}_g \to 2\left[\frac{1}{z(1-z)} - 2 + 2(1-\epsilon)z(1-z)\cos^2\phi\right]\,, \tag{C.55a}$$

$$\mathcal{H}_q \to 1 - 4z(1-z)\cos^2\phi\,. \tag{C.55b}$$

C.5 Three-parton kinematics

We consider three momenta p_1, p_2, p_3, with $p_1+p_2+p_3 = q = (Q, 0, 0, 0)$. Using a flavour-based labelling, p_1 is a quark, p_2 an antiquark and p_3 a gluon. We define the dimensionless variables $x_i = 2(p_i \cdot q)/Q^2 < 1$, satisfying $x_1 + x_2 + x_3 = 2$. In terms of these variables,

$$E_i = x_i \frac{Q}{2}\,, \qquad 2(p_i \cdot p_j) = (x_i + x_j - 1)Q^2\,. \tag{C.56}$$

This makes it possible to write the angles between pairs of momenta in terms of the x_i's.

The three-parton cross section, differential in x_1 and x_2, in four dimensions reads

$$\frac{\mathrm{d}\sigma}{\mathrm{d}x_1 \mathrm{d}x_2} = \sigma_0 C_F \frac{\alpha_s}{2\pi} \frac{x_1^2 + x_2^2}{(1-x_1)(1-x_2)}\,, \tag{C.57}$$

with σ_0 the Born cross section for producing a quark-antiquark pair in e^+e^- annihilation.

To obtain the Born three-jet cross section $\sigma_0(y_{\mathrm{cut}})$ with the Durham algorithm [33] we need to integrate the differential cross section in Eq. (C.57) with the constraint $y_3(p_1, p_2, p_3) = \min\{y_{12}, y_{13}, y_{23}\} > y_{\mathrm{cut}}$, where y_{ij} is the "distance" between pairs of partons defined by

$$y_{ij} \equiv 2\frac{\min\{E_i^2, E_j^2\}}{Q^2}(1 - \cos\theta_{ij}) = \min\left\{\frac{x_i}{x_j}, \frac{x_j}{x_i}\right\}(x_i + x_j - 1)\,. \tag{C.58}$$

The Durham algorithm defines a six-sided region in the (x_1, x_2) plane, as shown in Fig. C.1.

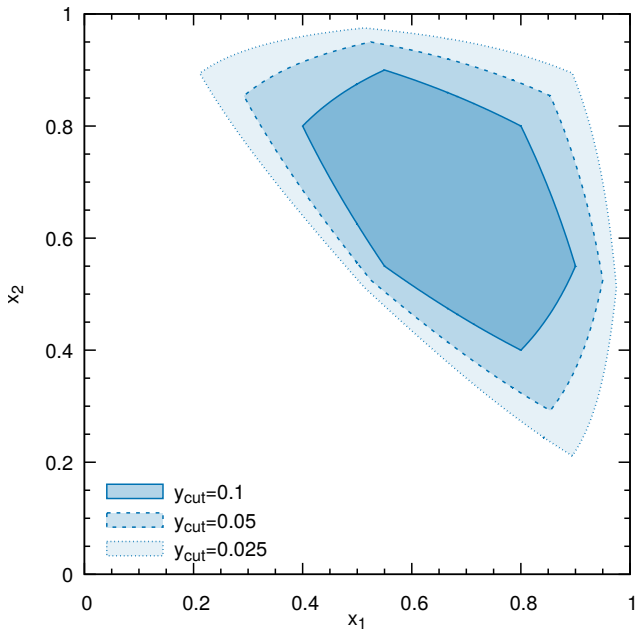

Figure C.1: Durham algorithm three jet region

The corresponding Born cross section $\sigma_{\mathcal{H}}^{(0)}$ is

$$\sigma_{\mathcal{H}}^{(0)} = \sigma_0 C_F \frac{\alpha_s}{2\pi} \int_0^1 \mathrm{d}x_1 \int_0^1 \mathrm{d}x_2 \frac{x_1^2 + x_2^2}{(1-x_1)(1-x_2)} \Theta(x_1 + x_2 - 1)\, \Theta\left(\min\{y_{12}, y_{13}, y_{23}\} - y_{\mathrm{cut}}\right) . \tag{C.59}$$

This cross section can be computed analytically. Its expression, not particularly illuminating, can be found in [185].

C.6 Full matching formulae

In our matching formulae $\Sigma_{\mathcal{H}}^{\mathrm{Mat.}}(v)$ we normalise all of the distributions to the total cross section $\sigma_{\mathcal{H}}$. However this is not what is provided by NLOjet++, instead it provides the un-normalised differential distribution for the D-parameter. We can transform the output of NLOjet++ into our conventions as follows. First we compute the un-normalised, *barred*, total cross section

$$\bar{\Sigma}_{\mathrm{NLOJet}}^{(i)} = -\int_v^{v_{\max}} \mathrm{d}v' \frac{\mathrm{d}\Sigma_{\mathrm{NLOJet}}^{(i)}(v')}{\mathrm{d}v'} , \tag{C.60}$$

where i refers to the power of α_s in perturbation theory. To transform this result into our conventions we perform the following manipulations

$$\begin{aligned} \bar{\Sigma}_{\mathrm{FO.}}^{(1)}(v) &= \frac{\bar{\Sigma}_{\mathrm{NLOJet}}^{(1)}(v)}{\sigma_{\mathcal{H}}^{(0)}} , \\ \bar{\Sigma}_{\mathrm{FO.}}^{(2)}(v) &= \frac{\bar{\Sigma}_{\mathrm{NLOJet}}^{(2)}(v)}{\sigma_{\mathcal{H}}^{(0)}} - \frac{\sigma_{\mathcal{H}}^{(1)}}{\sigma_{\mathcal{H}}^{(0)}} \bar{\Sigma}_{\mathrm{FO.}}^{(1)}(v) . \end{aligned} \tag{C.61}$$

In terms of the barred variables we have

$$\begin{aligned} \Sigma_{\mathrm{FO.}}(v) &= \sum_{i=0}^{2} \Sigma_{\mathrm{FO.}}^{(i)}(v) \\ &= 1 + \sum_{i=1}^{2} \bar{\Sigma}_{\mathrm{FO.}}^{(i)}(v) , \end{aligned} \tag{C.62}$$

and analogously for the expansion of the resummation

$$\Sigma_{\mathrm{Exp.}}(v) = \sum_{i=0}^{2} \Sigma_{\mathrm{Exp.}}^{(i)}(v) . \tag{C.63}$$

Finally we can present the explicit form of our matched distribution in eq. (5.31)

$$\begin{aligned} \Sigma_{\mathrm{Mat.}}(v) = \left(\Sigma_{\mathrm{Res.}}(v)\right)^Z \Big[& 1 + \bar{\Sigma}_{\mathrm{FO.}}^{(1)}(v) - Z\Sigma_{\mathrm{Exp.}}^{(1)}(v) + \\ & + \bar{\Sigma}_{\mathrm{FO.}}^{(2)}(v) - Z\Sigma_{\mathrm{Exp.}}^{(2)}(v) - Z\Sigma_{\mathrm{Exp.}}^{(1)}(v) \left(\Sigma_{\mathrm{FO.}}^{(1)}(v) - \frac{Z+1}{2} \Sigma_{\mathrm{Exp.}}^{(1)}(v) \right) \Big] . \end{aligned} \tag{C.64}$$

Appendix D

MCFM-RE

D.1 Collection of relevant formulae

In this appendix we report the explicit expressions that we have implemented in `MCFM` to achieve NLL and NNLL resummation of the cross section for the production of a colour singlet with a jet-veto. This discussion is of a technical nature, and we assume that the reader is familiar with the details of the jet-veto resummations performed in refs. [92, 93, 140].

In general, we consider the production of a colour singlet of invariant mass M, for instance a Higgs, a Z boson, or a pair of W bosons. At Born-level, this proceeds via either $q\bar{q}$ annihilation or gluon fusion. We then compute the cross section $\mathrm{d}\sigma_{\text{i.s.}}/(\mathrm{d}M^2\mathrm{d}\Phi_n)$, with i.s. $= q\bar{q}, gg$, fully differential in the phase space of the decay products of the colour singlet. Given their momenta $q_1, q_2, \ldots, q_n$, and incoming momenta p_1 and p_2, the phase space $\mathrm{d}\Phi_n$ is defined as

$$\mathrm{d}\Phi_n = \prod_{i=1}^{n} \frac{\mathrm{d}^3\vec{q}_i}{(2\pi)^3 2E_i} (2\pi)^4 \delta\left(p_1 + p_2 - \sum_{i=1}^{n} q_i\right) , \tag{D.1}$$

with E_i and $\vec{q}_i$ the energy and three-momentum of particle q_i.

Any prediction for $\mathrm{d}\sigma_{\text{i.s.}}/(\mathrm{d}M^2\mathrm{d}\Phi_n)$ depends on the renormalisation scale μ_R at which we evaluate the strong coupling α_s, as well as the factorisation scale μ_F at which we evaluate the PDFs. Both scales are typically set at values of order M. Furthermore, in the presence of a jet-veto, $\mathrm{d}\sigma_{(\text{i.s.})}/(\mathrm{d}M^2\mathrm{d}\Phi_n)$ is affected by large logarithms $L \equiv \log(M/p_{\text{t,veto}})$, with $p_{\text{t,veto}}$ the maximum allowed transverse momentum of the observed jets. When resumming such logarithms at all orders, our predictions become functions of $\tilde{L}$, defined as

$$\tilde{L} = \frac{1}{p} \log\left(\left(\frac{Q}{p_{\text{t,veto}}}\right)^p + 1\right) . \tag{D.2}$$

The quantity $\tilde{L}$ is such that for large $p_{\text{t,veto}}$, $\tilde{L} \to 0$, which implements the fact that, in this regime, there are no large logarithms to be resummed. Also, at small $p_{\text{t,veto}}$, $\tilde{L} \simeq \log(Q/p_{\text{t,veto}})$, so in fact we resum logarithms of the ratio of $p_{\text{t,veto}}$ and the so-called resummation scale Q. The three scales μ_R, μ_F, Q are handles that we will use to estimate theoretical uncertainties, as explained in app. D.1.3. The power p determines how fast the resummation switches off at large $p_{\text{t,veto}}$. We choose $p = 5$, as in refs. [92, 93, 140].

D.1.1 NLL resummation

At NLL accuracy, the distribution $\mathrm{d}\sigma_{\text{i.s.}}/(\mathrm{d}M^2\mathrm{d}\Phi_n)$ is given by

$$\frac{\mathrm{d}\sigma^{\text{NLL}}_{\text{i.s.}}}{\mathrm{d}M^2\mathrm{d}\Phi_n} = \mathcal{L}^{(0)}_{\text{i.s.}}(\tilde{L}, M)\, e^{\tilde{L}g_1(\alpha_s\tilde{L})+g_2(\alpha_s\tilde{L})}\,, \qquad \alpha_s = \alpha_s(\mu_R)\,. \tag{D.3}$$

Explicit expressions for the functions g_1, g_2 can be found in the supplemental material of ref. [93]. The NLL "luminosity" $\mathcal{L}^{(0)}_{\text{i.s.}}(L, M)$ is given by

$$\mathcal{L}^{(0)}_{\text{i.s.}}(L, M) \equiv \sum_{i,j} \int \mathrm{d}x_1 \mathrm{d}x_2 \left|M^{(\text{i.s.})}_{ij}\right|^2 \delta(x_1x_2s - M^2) f_i\left(x_1, \mu_F e^{-L}\right) f_j\left(x_2, \mu_F e^{-L}\right)\,. \tag{D.4}$$

In the above expression, $M^{(\text{i.s.})}_{ij}$ is the Born-level amplitude for the production of the colour singlet via annihilation of the two partons i and j, and $f_{i,j}$ is the density of parton i, j in the proton.

Given any Born-level event generator, the recipe to implement the NLL resummation of eq. (D.3) is straightforward:

1. change the factorisation scale μ_F provided by the generator to $\mu_F e^{-\tilde{L}}$;
2. multiply the weight of every event by a factor $\exp\left[\tilde{L}g_1(\alpha_s\tilde{L}) + g_2(\alpha_s\tilde{L})\right]$.

Note that, if $p_{\text{t,veto}}$ is fixed, and we do not integrate over different values of M^2, both operations can be performed without touching the Born-level generator code. In fact, many programs allow a change in the factorisation scale by a constant factor. Also, the rescaling of the weight can be performed by the analysis routines that produce histograms for physical distributions. In our implementation, since we do want to integrate over M^2, we have implemented the change in factorisation scale inside the `MCFM` code.

Another advantage we have in using `MCFM` is that it gives us access to the matrix elements in a form that is human readable. This is particularly useful in case one wishes to separate contributions from different parts of the matrix element, for instance a possible BSM contribution from that of the SM background. We consider here the case of WW production via gluon fusion, but the argument applies to other processes as well. There,

the Born-level matrix element has the form $M^{(gg)} = M^{(gg)}_{\rm SM} + M^{(gg)}_{\rm BSM}$, where $M^{(gg)}_{\rm SM}$ is the SM amplitude, and $M^{(gg)}_{\rm BSM}$ a BSM contribution. For each phase space point, we can then isolate individual contributions to the luminosity by computing separately each term in the square

$$|M^{(gg)}|^2 = |M^{(gg)}_{\rm SM}|^2 + |M^{(gg)}_{\rm BSM}|^2 + 2{\rm Re}\left[M^{(gg)}_{\rm SM}\left(M^{(gg)}_{\rm BSM}\right)^*\right] . \tag{D.5}$$

In the specific case, given the expression of $M^{(gg)}$ in eq. (6.35), we compute the luminosity $\mathcal{L}^{(0)}_{gg}(L, M)$ as follows

$$\begin{aligned}\mathcal{L}^{(0)}_{gg}(L,M) = \kappa_t^2\,\mathcal{L}^{(t^2)}_{gg}(L,M) + \kappa_g^2\,\mathcal{L}^{(g^2)}_{gg}(L,M) + \kappa_t\kappa_g\,\mathcal{L}^{(tg)}_{gg}(L,M) + \\ + \kappa_t\,\mathcal{L}^{(tc)}_{gg}(L,M) + \kappa_g\,\mathcal{L}^{(gc)}_{gg}(L,M) + \mathcal{L}^{(c^2)}_{gg}(L,M)\,,\end{aligned} \tag{D.6}$$

where we have used the notation

$$\mathcal{L}^{(i^2)}_{gg}(L,M) = \int {\rm d}x_1{\rm d}x_2\,\left|M^{(gg)}_i\right|^2\,\delta(x_1x_2s - M^2) f_g\left(x_1,\mu_F e^{-L}\right) f_g\left(x_2,\mu_F e^{-L}\right)\,, \tag{D.7}$$

with $i = t, g, c$, and

$$\begin{aligned}\mathcal{L}^{(ij)}_{gg}(L,M) = \int {\rm d}x_1{\rm d}x_2\,2{\rm Re}\left[M^{(gg)}_i\left(M^{(gg)}_j\right)^*\right]\,\delta(x_1x_2s - M^2)\times \\ \times f_g\left(x_1,\mu_F e^{-L}\right) f_g\left(x_2,\mu_F e^{-L}\right)\,,\end{aligned} \tag{D.8}$$

with $ij = tg, tc, gc$. Using these luminosities we can interpret $\mathcal{L}^{(0)}_{gg}$ as a polynomial in the various κ_i, and compute each coefficient separately. All one has to do then is to reweight each phase-space point using the Sudakov exponent $\exp\left[\tilde{L}g_1(\alpha_s\tilde{L}) + g_2(\alpha_s\tilde{L})\right]$. In doing so, we have used the fact that the Sudakov exponent depends only on the colour and kinematics of the incoming partons, and therefore is the same for every single contribution to the luminosity.

D.1.2 NNLL resummation

At NNLL accuracy, the cross section ${\rm d}\sigma_{\rm i.s.}/({\rm d}M^2{\rm d}\Phi_n)$ with a jet veto is given by

$$\begin{aligned}\frac{{\rm d}\sigma^{\rm NNLL}_{\rm i.s.}(p_{\rm t,veto})}{{\rm d}M^2{\rm d}\Phi_n} = \left(\mathcal{L}^{(0)}_{\rm i.s.}(\tilde{L},M) + \mathcal{L}^{(1)}_{\rm i.s.}(\tilde{L},M)\right)\times \\ \times\left(1 + \mathcal{F}_{\rm clust}(R) + \mathcal{F}_{\rm correl}(R)\right)\times e^{\tilde{L}g_1(\alpha_s\tilde{L}) + g_2(\alpha_s\tilde{L}) + \frac{\alpha_s}{\pi}g_3(\alpha_s\tilde{L})}\,,\end{aligned} \tag{D.9}$$

where the function g_3 can be found in ref. [93]. The functions $\mathcal{F}_{\rm clust}(R), \mathcal{F}_{\rm correl}(R)$ depend on the jet radius R. Their expressions can be found in ref. [92]. As for the NLL resummation, $\alpha_s = \alpha_s(\mu_R)$. The remaining new ingredient for NNLL resummation is the

luminosity $\mathcal{L}^{(1)}_{\text{i.s.}}(L,M)$, defined as

$$\mathcal{L}^{(1)}_{\text{i.s.}}(L,M) = \sum_{i,j}\int \mathrm{d}x_1\mathrm{d}x_2 |M^{(\text{i.s.})}_{ij}|^2 \delta(x_1x_2s-M^2)\frac{\alpha_s}{2\pi}\left[\mathcal{H}^{(1)}_{\text{i.s.}} f_i\big(x_1,\mu_F e^{-L}\big)\, f_j\big(x_2,\mu_F e^{-L}\big)\right.$$
$$\left. + \frac{1}{1-2\alpha_s\beta_0 L}\sum_k\left(\int_{x_1}^1 \frac{\mathrm{d}z}{z} C^{(1)}_{ik}(z) f_k\Big(\frac{x_1}{z},\mu_F e^{-L}\Big)\, f_j\big(x_2,\mu_F e^{-L}\big) + \{(x_1,i)\leftrightarrow(x_2,j)\}\right)\right], \tag{D.10}$$

with $\beta_0 = (11C_A - 4T_R n_F)/(12\pi)$. Using the conventions of ref. [93], we have

$$\begin{aligned}\mathcal{H}^{(1)}_{q\bar{q}} &= H^{(1)} - 2C_F\left(\frac{3}{2}+\log\frac{M^2}{Q^2}\right)\log\frac{M^2}{Q^2}\,,\\ \mathcal{H}^{(1)}_{gg} &= H^{(1)} - 2C_A\left(2\pi\beta_0+\log\frac{M^2}{Q^2}\right)\log\frac{M^2}{Q^2}\,.\end{aligned} \tag{D.11}$$

with $H^{(1)}$ the finite part of one-loop virtual corrections to the process in question, e.g. WW production through $q\bar{q}$ annihilation. The coefficients $C^{(1)}_{ij}$ depend on whether incoming partons i and j are quarks/antiquarks (q) or gluons (g), and are given by:

$$\begin{aligned}C^{(1)}_{qq}(z) &= C_F\left[(1-z) - \frac{\pi^2}{12}\delta(1-z) + \left(\frac{1+z^2}{1-z}\right)_+\log\frac{Q^2}{\mu_F^2}\right],\\ C^{(1)}_{qg}(z) &= \frac{1}{2}\left[2z(1-z) + (1-2z(1-z))\log\frac{Q^2}{\mu_F^2}\right],\\ C^{(1)}_{gq}(z) &= C_F\left[z + \left(\frac{1+(1-z)^2}{z}\right)\log\frac{Q^2}{\mu_F^2}\right],\\ C^{(1)}_{gg}(z) &= C_A\left[\left(2\pi\beta_0 - \frac{\pi^2}{12}\right)\delta(1-z) + 2\left(\frac{z}{(1-z)_+} + \frac{1-z}{z} + z(1-z)\right)\log\frac{Q^2}{\mu_F^2}\right].\end{aligned} \tag{D.12}$$

As explained in the previous section, the NLL luminosity $\mathcal{L}^{(0)}_{\text{i.s.}}$ can be obtained from a Born-level event generator. The function $\mathcal{L}^{(1)}_{\text{i.s.}}$ represents a correction to $\mathcal{L}^{(0)}_{\text{i.s.}}$ of relative order α_s. Therefore, its implementation requires at least a NLO generator. Any NLO event generator includes the calculation of virtual corrections, as well as integrated counterterms. This contribution, which we denote by $\mathrm{d}\sigma^{(1)}_{\text{i.s.},v+ct}/(\mathrm{d}\Phi_n \mathrm{d}M^2)$, has the same form as the luminosity $\mathcal{L}^{(1)}_{\text{i.s.}}$, but with PDFs evaluated at a different factorisation scale, and different functions replacing $\mathcal{H}^{(1)}_{\text{i.s.}}$ and $C^{(1)}_{ij}(z)$. Its expression in general depends on the way each process is implemented in the NLO event generator. For instance, the implementation of WW production in the NLO program `MCFM` follows from the general coding of the production of a colour singlet, whose details can be found in ref. [186]. Schematically,

$$\left(\frac{\mathrm{d}\sigma^{(1)}_{\text{i.s.},v+ct}}{\mathrm{d}\Phi_n\mathrm{d}M^2}\right)_{\texttt{MCFM}} = \sum_{i,j}\int \mathrm{d}x_1\mathrm{d}x_2 |M^{(\text{i.s.})}_{ij}|^2 \delta(x_1x_2s-M^2)\frac{\alpha_s}{2\pi}\left[\mathcal{H}^{(1)}_{\texttt{MCFM},\text{i.s.}}\, f_i(x_1,\mu_F)\, f_j(x_2,\mu_F)\right.$$
$$\left. + \sum_k\left(\int_{x_1}^1 \frac{\mathrm{d}z}{z} C^{(1)}_{\texttt{MCFM},ik}(z) f_k\Big(\frac{x_1}{z},\mu_F\Big)\, f_j(x_2,\mu_F) + \{(x_1,i)\leftrightarrow(x_2,j)\}\right)\right]. \tag{D.13}$$

After direct inspection of the MCFM code, we realised that the term $\mathcal{H}^{(1)}_{\texttt{MCFM,i.s.}}$ does not contain just the finite part of the virtual corrections $H^{(1)}$, but also the terms $-(\pi^2/12)\,\delta(1-z)$ in the coefficients $C^{(1)}_{qq}(z)$ and $C^{(1)}_{gg}(z)$, as well as terms containing $\log\big(M^2/\mu_R^2\big)$. Keeping this in mind, to compute the luminosity $\mathcal{L}^{(1)}_{\text{i.s.}}$ through MCFM, we had to perform the following changes to the MCFM code:

1. replace $\mathcal{H}^{(1)}_{\texttt{MCFM,i.s.}}$ as follows

$$\begin{aligned}
\mathcal{H}^{(1)}_{\texttt{MCFM},q\bar{q}} &\to \mathcal{H}^{(1)}_{\texttt{MCFM},q\bar{q}} + 2C_F\left(\frac{\pi^2}{12} + \frac{3}{2}\log\frac{Q^2}{\mu_R^2} + \frac{1}{2}\log\frac{M^2}{\mu_R^2} - \log^2\frac{M^2}{Q^2}\right), \\
\mathcal{H}^{(1)}_{\texttt{MCFM},gg} &\to \mathcal{H}^{(1)}_{\texttt{MCFM},gg} + 2C_A\left(\frac{\pi^2}{12} + 2\pi\beta_0\log\frac{Q^2}{\mu_R^2} + \frac{1}{2}\log\frac{M^2}{\mu_R^2} - \log^2\frac{M^2}{Q^2}\right);
\end{aligned} \tag{D.14}$$

2. modify the integrated counterterms as follows

$$C^{(1)}_{\texttt{MCFM},ij}(z) \to \frac{1}{1-2\alpha_s\beta_0\tilde{L}}\,C^{(1)}_{ij}(z)\,; \tag{D.15}$$

3. change the factorisation scale in all PDFs from μ_F to $\mu_F\,e^{-\tilde{L}}$.

Last, to implement the full NNLL resummation, we just rescale the weight of each event by the factor

$$\big(1+\mathcal{F}_{\text{clust}}(R)+\mathcal{F}_{\text{correl}}(R)\big)\;e^{\tilde{L}g_1(\alpha_s\tilde{L})+g_2(\alpha_s\tilde{L})+\frac{\alpha_s}{\pi}g_3(\alpha_s\tilde{L})}\,. \tag{D.16}$$

D.1.3 Matching to fixed order and theoretical uncertainties

Our MCFM implementation includes the matching of resummed predictions with NLO calculations. In particular, we have implemented the relevant contributions to the two multiplicative matching schemes introduced in refs. [93, 140]. At NLO, the total cross section σ_{NLO} for the production of a colour singlet, satisfying a set of kinematical cuts for its decay products, is given by

$$\sigma_{\text{NLO}} = \sigma^{(0)} + \sigma^{(1)}\,, \tag{D.17}$$

with $\sigma^{(0)}$ its Born-level contribution, and $\sigma^{(1)}$ a correction of relative order α_s. Similarly, at NLO, the corresponding cross section with a jet-veto $\Sigma_{\text{NLO}}(p_{\text{t,veto}})$ is given by

$$\Sigma_{\text{NLO}}(p_{\text{t,veto}}) = \sigma^{(0)} + \Sigma^{(1)}(p_{\text{t,veto}})\,. \tag{D.18}$$

For computational convenience, it is customary to introduce

$$\bar{\Sigma}^{(1)}(p_{\text{t,veto}}) = \Sigma^{(1)}(p_{\text{t,veto}}) - \sigma^{(1)}\,, \tag{D.19}$$

which implies $\Sigma_{\rm NLO}(p_{\rm t,veto}) = \sigma_{\rm NLO} + \bar{\Sigma}^{(1)}(p_{\rm t,veto})$. We also denote by $\Sigma_{\rm N^kLL}(p_{\rm t,veto})$ the resummed jet-veto cross section at N^{k}LL accuracy, again satisfying the chosen set of kinematical cuts for the decay products of the considered colour singlet. At this order, it has the following expansion in powers of α_s:

$$\Sigma_{\rm N^kLL}(p_{\rm t,veto}) = \sigma_0 + \Sigma^{(1)}_{\rm N^kLL}(p_{\rm t,veto})\,. \tag{D.20}$$

As in refs. [93, 140], the matching is performed at the level of the jet-veto efficiency $\epsilon(p_{\rm t,veto})$, the fraction of events that survives the jet veto. This quantity is matched to exact NLO, as follows:

$$\epsilon^{(a)}(p_{\rm t,veto}) = \frac{\Sigma_{\rm N^kLL}(p_{\rm t,veto})}{\sigma_{\rm NLO}}\left[1 + \frac{\Sigma^{(1)}(p_{\rm t,veto}) - \Sigma^{(1)}_{\rm N^kLL}(p_{\rm t,veto})}{\sigma_0\,(1+\delta\mathcal{L}_{\rm N^kLL}(p_{\rm t,veto}))}\right], \tag{D.21a}$$

$$\epsilon^{(b)}(p_{\rm t,veto}) = \frac{\Sigma_{\rm N^kLL}(p_{\rm t,veto})}{\sigma_0}\left[1 + \frac{\bar{\Sigma}^{(1)}(p_{\rm t,veto}) - \Sigma^{(1)}_{\rm N^kLL}(p_{\rm t,veto})}{\sigma_0\,(1+\delta\mathcal{L}_{\rm N^kLL}(p_{\rm t,veto}))}\right]. \tag{D.21b}$$

At NLL accuracy, $\delta\mathcal{L}_{\rm NLL} = 0$. At NNLL accuracy, if we define $\langle\mathcal{L}^{(0)}\rangle$ and $\langle\mathcal{L}^{(1)}\rangle$ as the integral of the luminosities $\mathcal{L}^{(0)}$ and $\mathcal{L}^{(1)}$ in eqs. (D.4) and (D.10) respectively over the appropriate configurations of the decay products of the colour singlet, we have $\delta\mathcal{L}_{\rm N^kLL}(p_{\rm t,veto}) \equiv \langle\mathcal{L}^{(1)}\rangle / \langle\mathcal{L}^{(0)}\rangle$. Both matched efficiencies reduce to $\Sigma_{\rm N^kLL}(p_{\rm t,veto})/\sigma_{\rm NLO}$ for $p_{\rm t,veto} \ll M$, up to N^{3}LL corrections. On the other hand, for $p_{\rm t,veto} \sim M$, we have

$$\epsilon^{(a)}(p_{\rm t,veto}) \simeq \frac{\Sigma_{\rm NLO}(p_{\rm t,veto})}{\sigma_{\rm NLO}}\,, \qquad \epsilon^{(b)}(p_{\rm t,veto}) \simeq 1 - \frac{\bar{\Sigma}^{(1)}(p_{\rm t,veto})}{\sigma_0}\,. \tag{D.22}$$

Note also that, for $p_{\rm t,veto} \to \infty$, both efficiencies tend to one, as is physically sensible.

In order to estimate the theoretical uncertainties on jet-veto cross sections, we adapt the jet-veto efficiency method of ref. [140] to the present situation. First, our "central" prediction is $\epsilon^{(a)}(p_{\rm t,veto})$ with $\mu_R = \mu_F = Q = Q_0$, with $Q_0 = M/2$. Then, we vary renormalisation and factorisation scale for $\epsilon^{(a)}(p_{\rm t,veto})$ in the range

$$\frac{1}{2} \le \frac{\mu_{R,F}}{Q_0} \le 2\,, \qquad \frac{1}{2} \le \frac{\mu_R}{\mu_F} \le 2\,. \tag{D.23}$$

Then, we vary the resummation scale Q for $\epsilon^{(a)}(p_{\rm t,veto})$ in the range $2/3 \le Q/Q_0 \le 3/2$, with $\mu_R = \mu_F = Q_0$. In practice, we do not vary the scales continuously, but we consider only $\mu_{R,F} = \{1/2, 1, 2\}Q_0$ and $Q = \{2/3, 1, 3/2\}Q_0$. Our uncertainty band is the envelope of the curves obtained by fixing the considered scales at the boundaries of the allowed range (i.e. 9-point scale variation), plus $\epsilon^{(b)}(p_{\rm t,veto})$ with all scales set to Q_0.

We then compute the total cross section $\sigma_{\rm NLO}$ by choosing as our central prediction the one with both renormalisation and factorisation scales set at Q_0. We then perform

renormalisation and factorisation scale variations in the range (D.23), and constructing an uncertainty band as for the efficiency, i.e. using the values of the scales at the boundaries of the allowed region (7-point scale variation).

Last, the central value for the jet-veto cross section is defined as the product of the central prediction for $\sigma_{\rm NLO}$ and $\epsilon^{(a)}(p_{\rm t,veto})$, and the corresponding uncertainty band is obtained by adding the uncertainties of the total cross section and the efficiency in quadrature.

If the total cross section is only available at leading-order, we perform the resummation at NLL accuracy. Since we cannot normalise resummed cross sections using $\sigma_{\rm NLO}$, $\epsilon^{(a)}(p_{\rm t,veto}) = \epsilon^{(b)}(p_{\rm t,veto})$. Once we have the efficiency, we evaluate theoretical uncertainties by adding in quadrature the uncertainties on $\sigma_{\rm LO}$ and the jet-veto efficiency.

D.2 Numerical implementation in `MCFM`

In this section we give the details of the implementation of the resummation of jet-veto effects for colour singlets in `MCFM`. We assume that the reader can successfully compile and run the `MCFM` code, in all its operation modes. If not, the interested reader should consult the `MCFM` manual [134].

D.2.1 Overview

`MCFM-RE` (an acronym for Resummation Edition) is a modification of `MCFM-8.0` to include the resummation of jet-veto effects in colour-singlet processes up to NNLL+LL$_R$ accuracy. The modifications are modular, as most of the resummation effects are included through an interface to the code `JetVHeto` [130], suitably modified to become a library linkable to `MCFM`. Although a small number of modifications require us to directly change the `MCFM` code, these do not interfere with its usual modes of operation. The program is available at [133]. Included in the package are a README file and an example input card.

To run `MCFM-RE`, one must simply provide a suitably modified `MCFM` input card. We list here the new parameters we have added or changes made to existing parameters, described with the same conventions and terminology as the `MCFM` manual.

- `file version number`. This should match the version number that is printed when `mcfm` is executed.

{blank line}

`[Flags to specify the mode in which MCFM is run]`

- `part`
  - `ll`. Jet-veto resummation at LL accuracy, i.e. each event produced by `MCFM` is reweighted with $\exp\left[\tilde{L}g_1(\alpha_s\tilde{L})\right]$.
  - `nll`. Jet-veto resummation at NLL accuracy, see eq. (D.3).
  - `nnll`. Jet-veto resummation at NNLL accuracy, with or without the inclusion of small jet radius resummation (LL_R), see eq. (D.9).
  - `lumi0`. Calculation of the luminosity $\mathcal{L}^{(0)}$ in eq. (D.4)
  - `lumi1`. Calculation of the luminosity $\mathcal{L}^{(1)}$ in eq. (D.10)
  - `nllexp1`. Expansion of the NLL resummation at order α_s (for matching).
  - `nnllexp1`. Expansion of the NNLL resummation at order α_s (for matching).

{blank line}

`[JetVHeto resummation options]`

- `observable`.
  - `ptj`. The default mode of the resummation, resum logarithms of the jet-veto.
  - `ptj+small-r`. Available for NNLL resummations only. Include the effect of resumming the jet radius at leading logarithmic accuracy.
- `Qscale`. This parameter may be used to adjust the value of the *resummation scale* Q introduced in eq. (D.2). It behaves in the same way as the `MCFM` parameters `scale` and `facscale` do, i.e. if `dynamicscale` is `.false.`, Q is set to `Qscale`, otheerwise $Q =$ `Qscale` $\times \mu_0$, with μ_0 the dynamic scale specified by the parameter `dynamicscale`.
- `Rscale`. This parameter may be used to adjust the value of the jet-radius resummation scale.
- `ptjveto`. The value of the jet-veto cut $p_{\mathrm{t,veto}}$ in units of GeV.

{blank line}

`[Coupling rescaling in the kappa formalism]`

- `kappa_t`. The parameter κ_t of the Lagrangian in eq. (6.23), a.k.a the anomalous top Yukawa coupling.

- `kappa_b`. Anomalous bottom Yukawa coupling.
- `kappa_g`. The parameter κ_g of the Lagrangian in eq. (6.23).
- `interference only`. Flag to control whether to compute just the interference terms, e.g. the coefficient of $\kappa_t\kappa_g$ arising from squaring the amplitude in eq. (6.35). All other coefficients can be determined by setting a single $\kappa_i, i = t, g, b$ to zero.

Normally, `MCFM` identifies whether a process is $q\bar{q}$- or gg-initiated, and running `MCFM-RE` in resummation mode does not lead to any problems. However, in cases like process 61, in fact WW production, `MCFM` includes in the NLO correction to a $q\bar{q}$-initiated process formally higher-order gg-initiated contribution. As a consequence, not specifying the colour of the initial state leads to an ambiguity that is impossible to resolve. To avoid such problems, we have decided that, when running `MCFM-RE` in any resummation mode for ambiguous processes, the user must impose that a process is either $q\bar{q}$- or gg-initiated, by making use of the `MCFM` flags `omitgg` and `ggonly`. Failure of doing so will result in `MCFM-RE` stopping and returning an error message.

D.2.2 Details of `MCFM` implementation

We modify `MCFM` version 8.0 to include the resummation of jet-veto effects. To this end there are two pieces that we must include, the computation of the luminosities $\mathcal{L}^{(0)}_{\text{i.s.}}, \mathcal{L}^{(1)}_{\text{i.s.}}$, and the Sudakov form factor combined with the functions $\mathcal{F}_{\text{clust}}, \mathcal{F}_{\text{correl}}$. The computation of the luminosities requires structural changes to `MCFM` whereas we are able to include the Sudakov form factor through an interface in `src/User/usercode.f90`.

The inclusion of the Sudakov form factor is the simplest change. The reweighting is included through the subroutine `userplotter`,

```
interface
  function sudakov(proc, M, muR, muF, Q, as, p, jet_radius, &
       &observable, small_r, small_r_R0, ptj_veto, order)

    ....

  end function
end interface
```

The user should not normally make changes to this function. The reweighting is applied to all histograms, including the default `MCFM` ones, as `wt` and `wt2` are `intent(inout)`, so our reweighting is applied globally. The cost of doing the reweighting here is that the

cross section returned by the main MCFM program is wrong, or rather it includes only the contribution of the luminosities and not the Sudakov exponent. To that end we include the extra histogram xsec, a single-bin histogram to record the correct total cross section for runs with the jet-veto.

To include the luminosities we have to modify the factorisation scales of the PDFs. Instead of adding lots of switches to the default MCFM integration routines, we create our own special routines resmNLL.f (based on lowint.f) and resmNNLL.f (based on virtint.f), which we include in the src/Procdep directory along with the other default integration routines. The changes made in resmNLL.f are modest with respect to lowint.f, schematically

```
function resmNLL(r,wgt)
use rad_tools, only: Ltilde
implicit none
include `types.f'
real(dp):: resmNLLint

! resummation
include `jetvheto.f'
real(dp) :: facscaleLtilde
real(dp) :: L_tilde_arr(1)

L_tilde_arr = Ltilde((/ptj_veto/q_scale/), p_pow)
L_tilde = L_tilde_arr(1)
if (do_lumi) then
  facscaleLtilde = facscale*exp(-L_tilde)
else
  facscaleLtilde = facscale
end if

call fdist(ih1,xx(1),facscaleLtilde,fx1)
call fdist(ih2,xx(2),facscaleLtilde,fx2)

end
```

At the beginning of each event we determine $\tilde{L}$, and the modified facscale which we call facscaleLtilde. We then use this scale in the computation of the PDFs. The simplicity here is that at NLL accuracy all we need to do is change the factorisation scale and reweight, so these changes are very modest.

To perform the same calculation at NNLL is much more involved, since there are three

separate actions that must be performed to compute the luminosity. First, we need to cast the virtual matrix element into the correct form for the resummation. We do this with a utility function in the file `src/Procdep/virtfin.f`, which performs the replacement detailed in eq. (D.14). This is carried out by the subroutine

```
subroutine virtfin(p,msq,msqv)
real(dp) :: p(mxpart, 4)
real(dp) :: msq(-nf:nf,-nf:nf), msqv(-nf:nf,-nf:nf)
end subroutine virtfin
```

where one must provide the array of momenta `p(mxpart,4)`, the tree level matrix element squared `msq(-nf:nf)` and the matrix element of the virtual corrections `msqv(-nf:nf)` (using the conventions of `MCFM`).

The second contribution to the luminosities comes from the convolution of the coefficient functions. To include this coefficient function we modify the integrated dipole functions located inside `src/Need/dipoles.f`, adding switches to choose between the different types of "dipoles" that we have added as well as the default `MCFM` subtraction dipole.

The third and final piece is performed in the new integration routine `src/Procdep/resmNNLL.f`. This calls the previous two routines, and then performs the convolutions of all coefficient functions with the PDFs.

```
function resmNNLL(r,wgt)
use rad_tools, only: Ltilde
implicit none
include `types.f'
real(dp):: resmNNLLint

! resummation
include `jetvheto.f'
real(dp) :: facscaleLtilde
real(dp) :: L_tilde_arr(1)

L_tilde_arr = Ltilde((/ptj_veto/q_scale/), p_pow)
L_tilde = L_tilde_arr(1)
if (do_lumi) then
  facscaleLtilde = facscale*exp(-L_tilde)
else
  facscaleLtilde = facscale
end if

!! Move contribution of collinear counterterm into the ``dipoles''
! AP(q,q,1)=+ason2pi*Cf*1.5_dp*epcorr
```

```
! AP(q,q,2)=+ason2pi*Cf*(-1._dp-z)*epcorr
! AP(q,q,3)=+ason2pi*Cf*2._dp/omz*epcorr
!! all AP terms are removed, those displayed here are just schematic

! extract the finite part of the virtual and modify for resummation
! must come before subtraction to get coefficient correct in checks
call virtfin(p, msq, msqv)

call fdist(ih1,xx(1),facscaleLtilde,fx1)
call fdist(ih2,xx(2),facscaleLtilde,fx2)
call fdist(ih1,x1onz,facscaleLtilde,fx1z)
call fdist(ih2,x2onz,facscaleLtilde,fx2z)

end
```

In addition, we can perform the matching with fixed-order using the same method we have used in computing the resummation. We modify the dipoles, this time to include the terms from the expansion of the resummation. With these one can then compute the matched distribution up to NNLL+NLO accuracy.